Contents

13th International Workshop on Optimization and Inverse Problems in Electromagnetism
September 10 – 12, 2014, Delft, The Netherlands

MULTISCALE MODELING IN ELECTROTECHNICS: HOMOGENIZATION TECHNIQUES

Ruth V. Sabariego

*KU Leuven, Research Institute EnergyVille, Belgium

E-mail: ruth.sabariego@esat.kuleuven.be

ABSTRACT

The behavior and performance of electromagnetic AC devices may be considerably altered by the eddy currents in its laminated iron cores as well as by skin and proximity effect in its windings. This is the case in e.g. power electronic applications where working frequencies and harmonic distortion are constantly increasing. Neglecting these effects in the resolution stage of the FE modeling of e.g. an electrical machine, possibly followed by an a posteriori loss estimation, may then be insufficient for certain design aspects. The eddy-current effects should be accounted for in the early stages of the design. For real-life machine geometries, the 2D or 3D modeling of the individual laminations and turns is normally excluded because of the huge computational cost. Alternative methods are thus indispensable. Homogenization methods are then a viable alternative.

Many techniques have been successfully applied for dealing with lamination stacks in finite-element models: non-conducting and homogeneous stacked core with *a posteriori* loss estimation, anisotropic surrogate material laws, embedded lower dimensional models, multiscale computational homogenization techniques, ... We will pay particular attention to so-called one-step homogenization techniques, accounting for nonlinear and hysteretical material laws. They are based on a polynomial expansion of the variation of the induction throughout the thickness of an individual lamination and further embedded in a magnetodynamic finite-element formulation. Multiscale computational homogenization techniques will be considered as well. The multiscale approach presented in is built up within the heterogeneous multiscale method framework. It couples: 1) a macroscale problem that captures the slow variations of the overall solution; 2) many microscale problems that allow determining the macroscale constitutive law. Particular attention will be paid to local data.

As for windings, skin and proximity effects are accounted for by adopting a complex impedance in the electrical circuit and a complex reluctivity in the homogenized winding domain, respectively. The frequency dependence of these complex quantities is obtained either analytically or using an elementary FE model. Round conductors with rectangular packing are mostly studied. We consider a more general approach, i.e. a multiturn winding of periodically spaced conductors of arbitrary but symmetric cross section. Furthermore, the frequency-domain skin and proximity coefficients are converted into time-domain equations, where again a certain order has to be fixed considering the relevant frequency interval.

MODELING AND SIZING BY OPTIMIZATION OF A BRUSHLESS DOUBLY-FED RELUCTANCE MACHINE

Tiago STAUDT*, Laurent GERBAUD*, Frédéric WURTZ*, Adrien COUSSY*, Nelson Jhoe BATISTELA** and Patrick KUO-PENG**

*Université de Grenoble, G2ELab (CNRS UMR5269, Grenoble INP, UJF), ENSE3, F-38142 Cedex, France

**Federal University of Santa Catarina, Grucad, PO-Box 476, CEP 88040-970, Florianopolis, Brazil

E-mail: staudt@ieee.org

Abstract. The paper proposes an optimization approach to address the modeling and sizing complexities of Brushless Doubly-Fed Reluctances Machines. A semi-analytical model and a reluctance network model are coupled to a deterministic optimization algorithm where several inputs and outputs parameters can be constrained to solve system equations iteratively by maximizing or minimizing an objective function. A Pareto Front strategy is used to illustrate the model capabilities, highlighting the trade-offs on the design of this kind of electrical machines. The optimization model provides fast results to define an initial design, reducing the number of unknown parameters of early development stages. This saves computation time and computer resources in the design process compared to Finite Element Analysis.

Keywords: Design Optimization, Brushless machines, Electromagnetic analysis, Wind energy.

BDFRM SIZING COMPLEXITY - OPTIMIZATION AS A SOLUTION

The Brushless Doubly-Fed Reluctance Machine (BDFRM) is being considered as a viable alternative for the Doubly-Fed Induction Generator (DFIG) in wind power applications. Although many works have presented advances along last years [1], [2], there is still a lack of researches to define a procedure on its electromagnetic design mostly due to its complex electromagnetic field interaction occasioned by rotor modulation. Aiming to contribute in this sense, the paper presents a design procedure based on an optimization approach to (pre) design a BDFRM.

Roughly, optimization may be used in all machine development phases. However, every stage has its constraints and must have a model adapted for its purpose. As an example, one may consider a new machine design, where most parameters are unknown and must be deduced from a few specifications. Although possible, it is harder to use Finite Element Analysis (FEA) associated to optimization to find the best machine because the number of uncertainties are huge. On the contrary, FEA coupled to optimization may be very useful in final stages, where only a few parameters could be optimized to refine and find the best solution for a specific application. In early design stages, usually analytical methods allied to designer's expertise are used to define an initial machine. They are fast to calculate and the results fall within an acceptable precision for a pre-design model. In order to take advantage of these characteristics and at the same time using a fast deterministic optimization algorithm to solve a constrained input/output problem iteratively, the paper presents a methodology to pre-design a BDFRM based on semi-analytical approaches.

DESIGN PROCESS AND RESULTS OBTAINED WITH OPTIMIZATION APPROACH

The procedure is based on three modeling levels: *(i)* a Semi-Analytical Model - SAM, defined by using an equivalent electric circuit of the BDFRM [3]; *(ii)* a Reluctance Network Model - RNM, which relies on the electrical circuit analogy applied to electromagnetism to calculate machines fluxes, whereas torque is estimated by using the system coenergy variation; and *(iii)* a FEA model, used to validate calculations and refine results. The SAM and RNM are built by using the software package CADES/Reluctool [4]. It generates a Java library containing external functions to calculate outputs and the Jacobian matrix with the respective partial derivatives between output and input parameters giving a global analysis of the model sensitivity for optimization purpose.

The SAM is very useful for initial designs because it is fast and allows testing many different design variations in order to define a first design. In a former work [5], a BDFRM SAM, which relies on the air gap flux density determination to calculate the equivalent circuit inductances, has been presented. In this work, this SAM is transformed into an optimization model (OM) and coupled to a deterministic optimization algorithm (SQP – Sequential Quadratic Programming) for system solution. In general, the results are very fast, typically from some seconds to a few minutes, offering to the designer an extra degree of freedom to test many different machine configurations. The OM computes symbolically the partial derivatives between output and input parameters giving a global analysis of the model sensitivity. The most important feature on this approach is that several parameters can be constrained (16 out of 40 inputs and 72 out of 422 outputs in this OM) leading to an optimized design which satisfies specifications. To illustrate the model capabilities, Fig. 1 presents an optimization curve

using a Pareto Front strategy with the active output power and the grid winding voltage fixed at 5kW and 400V, respectively. In this case study, the total active mass is minimized for discrete values of possible required efficiency constraints. The machine 2D views for some iterations are also presented. The stack length and the external diameter have their maximum constraint set to the initial machine value to fit into the same frame.

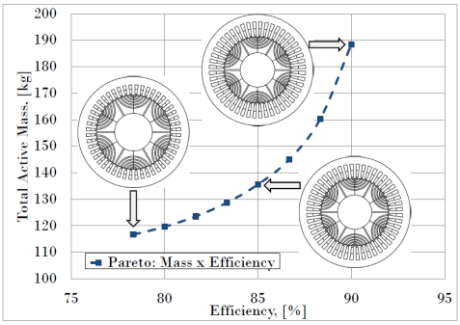

Figure 1. Pareto Front: Mass *versus* Efficiency.

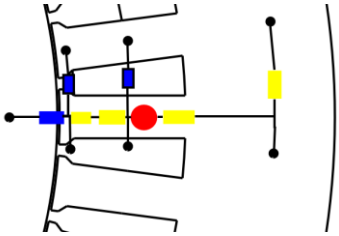

Figure 2. Reluctance Network Model for one stator tooth.

The RNM is an intermediary model between SAM and FEA. It is an improvement over SAM because it allows taking into account magnetic non-linearities providing a good trade-off among global accuracy and calculation time. Most importantly, it permits to couple the model with deterministic optimization algorithms (e.g. SQP), whereas still considering several constrained input/output parameters. To build it, a first FEA is performed to identify the most significant flux paths and the machine is discretized in many reluctances representing flux tubes. Fig. 2 shows the reluctance network for a stator tooth. The proposed RNM is a dynamic model, adapted for multi-static calculations. For that, a model, implemented in java, is created to manage rotor movement from the RNM given by Reluctool. Fig. 3 and 4 compare FEA and the RNM by using a multi-static calculation for a 1kW test machine. The Dynamic RNM (optimization oriented) is faster than FEA and the models have clearly a good agreement. Additionally, it allows considering parameters like torque ripple and voltage harmonics as output constraints in the OM, which would be hard to implement by using the SAM. Model comparisons and details on the RNM implementation as well as on the calculation of the Jacobian matrix in order to allow fast gradient optimizations will be detailed in the full paper.

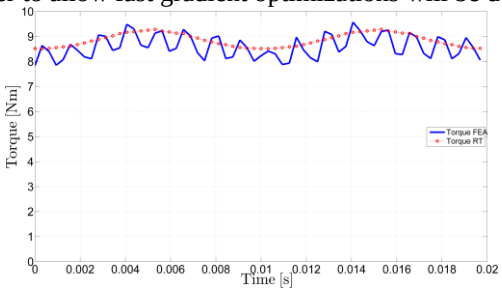

Figure 3. Torque versus time.

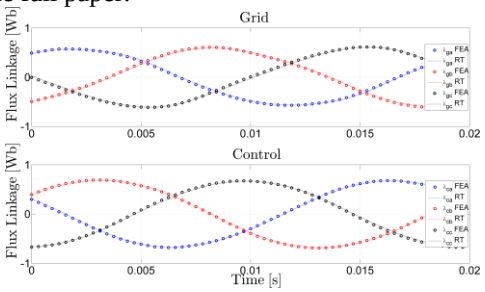

Figure 4. Flux Linkage in Grid and Control windings.

CONCLUSIONS

The results show that the proposed methodology and models coupled to deterministic optimization algorithms are very interesting for the design of electrical machines, especially in new designs and topologies such as the BDFRM. They provide fast and accurate results to define an initial machine with many unknown parameters. A FEA strategy can be used in further design stages to refine only a reduced number of parameters, saving considerably time and costs in the design process.

REFERENCES

[1] A. M. Knight, R. E. Betz, and D. G. Dorrell, "Design and Analysis of Brushless Doubly Fed Reluctance Machines," *IEEE Trans. Ind. Appl.*, vol. 49, no. 1, pp. 50–58, Jan. 2013.

[2] D. G. Dorrell, A. M. Knight, W. K. Song, and R. E. Betz, "Saturation and Ducting Effects in a Brushless Doubly-Fed Reluctance Machine," *IEEE Trans. Magn.*, vol. 49, no. 7, pp. 3933–3936, Jul. 2013.

[3] R. E. Betz and M. G. Jovanovic, "Introduction to the Space Vector Modeling of the Brushless Doubly Fed Reluctance Machine," *Electr. Power Components Syst.*, vol. 31, no. 8, pp. 729–755, Aug. 2003.

[4] Cades, "Cades Solutions - http://vesta-system.cades-solutions.com/. Version 2.9.2." Vesta-Systems, Grenoble, 2012.

[5] T. Staudt, F. Wurtz, N. J. Batistela, P. Kuo-Peng, and M. Granza, "Semi-Analytical Model for Design and Optimization of Brushless Doubly-Fed Reluctance Machines," in *IEEE Conference on Electromagnetic Field Computation, CEFC*, 2014.

13th International Workshop on Optimization and Inverse Problems in Electromagnetism
September 10 – 12, 2014, Delft, The Netherlands

OPTIMIZATION AND COMPARISON OF SUPERCONDUCTING GENERATOR TOPOLOGIES FOR A 10 MW WIND TURBINE APPLICATION

Dong Liu*, Henk Polinder*, Asger B. Abrahamsen**, Ewoud Stehouwer***, Ben Hendriks*** and Niklas Magnusson****

*TU Delft, Faculty of Electrical Engineering, Mekelweg 4, 2628 CD Delft, Netherlands
E-mail: d.liu-1@tudelft.nl, h.polinder@tudelft.nl

** Technical University of Denmark, DTU Wind Energy, Frederiksborgvej 399, 4000 Roskilde, Denmark
E-mail: asab@dtu.dk

***DNV-GL, Leiden, Netherlands. E-mail: ewoud.stehouwer@dnvgl.com, ben.hendriks@dnvgl.com

****SINTEF Energy Research, Trondheim, Norway. E-mail: niklas.magnusson@sintef.no

Abstract. A direct-drive superconducting generator (DDSG) is proposed for 10 MW wind turbines in the INNWIND.EU project. To fit the generator into the "king-pin" conceptual nacelle design, the generator structure with inner stationary superconducting field winding and outer rotating copper armature winding is investigated in the first research phase. This paper presents a method using finite element (FE) analysis to minimize the active material cost of the "king-pin" fitted DDSG by optimizing the geometrical variables. By implementing this method, three superconducting generator topologies are compared in terms of the active material cost and mass, the synchronous reactance and the phase resistance. The optimization method and the comparison results will provide a reference to DDSG designers.

Keywords: Comparison, finite element, optimization, superconducting generator, wind turbine

INTRODUCTION

A novel wind turbine nacelle is proposed in the INNWIND.EU project and it applies a stationary shaft "king-pin" architecture with the superconducting generator mounted in front of the hub [1]. A suitable option of the generator structure is inner stationary superconducting field winding with outer rotating copper armature winding [2]. Three typical superconducting machine topologies are considered under this structure: non-magnetic core with iron armature yoke (T1), non-magnetic armature teeth with iron yokes (T2) and iron core (T3) [3].

A key performance indicator that is essential to distinguish these superconducting machine topologies is the cost. For a long time the high cost has been one of the main challenges for superconducting machines to be commercialized. This paper will compare the overall active material cost of superconductor, copper and core materials (iron and/or composites). Each topology is optimized to achieve its minimal active material cost. The calculation of this cost involves a few steps of numerical computation. The first part of this paper will present a method implementing FE analysis to calculate the active material cost and the synchronous reactance. The second part will present the comparisons within the three superconducting generator topologies.

METHODS

The generator is designed for 10 MW, 9.65 rpm and 3.3 kV. It is operated at its maximum torque point when the electromotive force is in phase with the corresponding phase current, or in other words the d-axis is 90 electrical degrees with respect to the axis of phase A just when phase A is carrying its maximum current. The superconductor is operated with its maximum current density determined by its critical characteristics with a 25% safety margin. The generator axial length is varied according to the actual electromagnetic (EM) torque production per unit length in each topology with the armature bore diameter being fixed to 5 m.

The superconductor used is MgB2 at the temperature of 20 K and its price is 4 €/m. The composite material for non-magnetic core structures is glass fiber G10 (~15 €/kg) which has a similar mechanical strength as steel but the mass density is only 1/4. Copper and iron cost 15 €/kg and 3 €/kg, respectively.

With the genetic algorithm (GA) for optimization processing, the procedure of calculating the active material cost follows the flow diagram as illustrated in Fig. 1. When determining the operating current density and the EM torque per unit length, FE methods are used, because the B-J load curve of the field coil and the B-H magnetization curve of the magnetic iron are both non-linear.

With the optimization results, FE methods are also applied to determine the number of turns per phase to fulfill the nominal no-load terminal voltage and to calculate the synchronous reactance, taking into account the saturation of magnetic iron due to the strong field excitation.

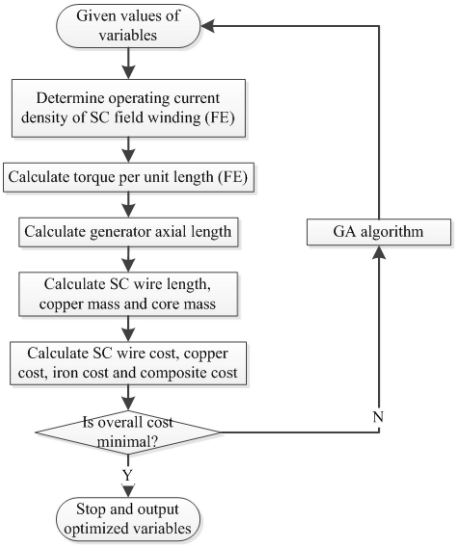

Figure 1. Flow diagram of calculating the overall active material cost and implementing GA for optimization

COMPARISONS

After the optimization has been finished, the minimized active material cost of each topology is compared in Fig. 2 in which the corresponding mass is also shown. The axial lengths of T1, T2 and T3 are 3.11 m, 2.41 m and 2.12 m respectively. Compared with the non-magnetic core, using iron core effectively reduces the active material cost with a limited influence on the mass. The synchronous reactance and the phase resistance shown in Fig. 3 implies that, by using more iron, the saturation gets more severe and the copper loss decreases.

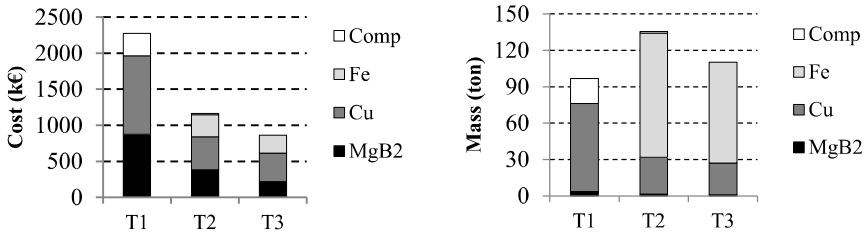

Figure 2. Active material cost (left) and mass (right) of compared topologies

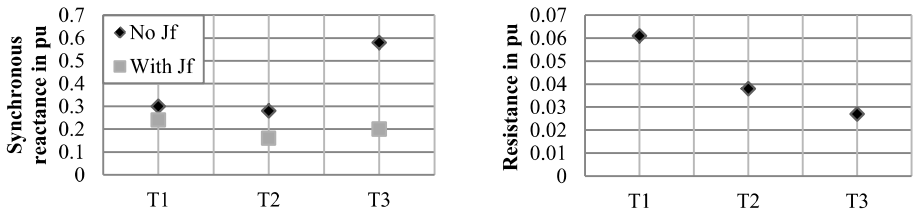

Figure 3. Synchronous reactance (left) and phase resistance (right)

CONCLUSIONS

Three superconducting generator topologies has been optimized for the minimal active material cost, implementing finite element analyses in determining the operating field current density and the EM torque. Comparisons are made within the three topologies in terms of cost, mass, synchronous reactance and phase resistance. Using more iron core results in a less active material cost and a smaller copper loss with a limited increase of mass and heavier saturation.

REFERENCES

[1] INNWIND.EU, "www.innwind.eu," [Online]. [Accessed May 2014].

[2] Fair R 2012. “Superconductivity for Large Scale Wind Turbines”, DOE report DE-EE0005143.

[3] Ronghai, Q., Yingzhen, L., & Jin, W.. “Review of Superconducting Generator Topologies for Direct-Drive Wind Turbines”, *IEEE Transactions on Applied Superconductivity*, 2013. 23(3), p. 5201108-5201108.

FITTING MEASURED PHOTOVOLTAIC CURRENT-VOLTAGE CURVES: AN EFFECTIVE BENCHMARK FOR THE OPTIMIZATION TECHNIQUES

Antonino LAUDANI*, Francesco RIGANTI FULGINEI*, Gabriele M. LOZITO*, Alessandro SALVINI* and Salvatore COCO**

*Dipartimento di Ingegneria, Università di Roma Tre, Via V. Volterra 62, 00146 Roma, Italy
{alaudani, riganti, gabrielemaria.lozito, asalvini}@uniroma3.it

**DIEEI, Università di Catania, V.le A. Doria, 6, 95125 Catania, Italy
coco@dieei.unict.it

Abstract. The one-diode equivalent circuit of photovoltaic (PV) panels is widely utilized both on scientific research and on industrial applications. In particular, the inverse problem regarding the identification of the related model by fitting the experimental data represents a very strong task to face. The high complexity in searching the best parameters to be adopted for the one-diode model, makes this optimization problem a new real benchmark which can be used for testing performances and robustness of the optimization algorithms. In this work, thanks to the existence of different cases of study available in literature, we compare several kinds of optimization procedure by using this new benchmark.

Keywords: benchmarks, inverse Problem, one-diode model, optimization, photovoltaic modeling

INTRODUCTION

In the last years, the identification of the one-diode model of photovoltaic (PV) panels from experimental data has been widely addressed. Indeed, many kinds of optimization techniques have been proposed to solve the inverse problem related to the extraction of the five parameters by fitting the experimental data. In this direction, soft-computing techniques have been also recently tested in the resolution of this kind of problems: differential evolution and penalty differential evolution method; Artificial Bee Colony optimization algorithm and Harmonic Search-based algorithm; Simulated Annealing, Bacterial Foraging, Swarm Intelligence, etc (see [1] and the references within). In any case, the matter related to the identification of the five-parameter model of PV panels has represented an open problem involving both the fields of PV modeling and of optimization algorithms. Recently, the reduced forms of the five parameter model, proposed in [1], have given a suitable response to the aspect of the PV modeling, achieving an accuracy never reached before in the identification by any optimization methods. Indeed, the reduced forms have provided important benefits: the reduction of the dimension of the search space; making convex the original non-convex optimization problem, giving the opportunity to use deterministic methods instead of heuristic/stochastic ones with a remarkable reduction of computational costs and execution times. At this point, thanks to the availability of several cases of study, coming from experimental data, and of their optimal identification results, this problem can be viewed as a new real benchmark, for the comparison of the performance of optimization algorithms in the solution of this real inverse problem.

THE IDENTIFICATION OF THE ONE-DIODE MODEL FROM I-V EXPERIMENTAL DATA

The well-know one-diode equivalent circuit for a single PV solar cell consists of a current generator I_{irr} (irradiance current), in parallel with one diode and one shunt resistance R_{SH}; the circuit is completed by a series connected resistance R_S [2]. The correspondent I-V relation is the following:

$$I = I_{irr} - I_0\left[e^{\left(\frac{V+IR_S}{N_S n V_T}\right)} - 1\right] - \frac{V+IR_S}{R_{SH}} \tag{1}$$

where $V_T = kT/q$ (q is the electron charge, k is the Boltzmann constant and T is the cell temperature); n is the cell ideality factor; I_0 is the cell reverse saturation current. The knowledge of the five unknowns/parameters I_{irr}, I_0, n, R_S and R_{SH}, which give the name "five-parameter" to the model, allows tracing the I-V curve for fixed temperature and irradiance values. In order to do this it is useful to employ the explicit expression, which provides the current I in function of the voltage V and of five parameters $X = [I_{irr}, I_0, n, R_S, R_{SH}]$, by using the Lambert W function [1]:

$$I = f_I(V,X) = \frac{R_{SH}\left(I_{irr}+I_0\right)-V}{R_S+R_{SH}} - \frac{N_S n V_T}{R_S} W\left(\frac{I_0}{N_S n V_T}\frac{R_S R_{SH}}{R_S+R_{SH}} e^{\frac{R_{SH}}{R_S+R_{SH}}\frac{V+R_S\left(I_{irr}+I_0\right)}{N_S n V_T}}\right) \quad (2)$$

The matter of the five-parameter model identification from I-V experimental curves basically consists on a nonlinear least squares optimization problem. Indeed, given a set of N couples (I_n, V_n), with n=1...N, of measured current and voltage values respectively, we want to find the vector *X* which minimize the squared error (SE) between the values of current $I(V_n) = f_I(V_n,X)$ calculated in correspondence to the voltages V_n and the values of measured current I_n:

$$SE = \sum_{n=1}^{N}\left[I_n - f_I(V_n,X)\right]^2 \quad (3)$$

Clearly, from a more general point of view, the choice of the functional expressions may also be different, leading to different results. The extraction of the five parameters from experimental I-V curves is a very hard multimodal problem to such an extent that it could be also considered as a real benchmark for any kind of optimization technique. Indeed, the presence of several local minima (multimodal problem) prevents utilizing directly deterministic algorithms since they are strongly sensitive to the initial guesses (i.e. the starting values of the five parameters): by changing them, the algorithm could remain trapped in a different local minimum and then, return a different solution.

CASES OF STUDY AND RESULTS

Two cases of study are widely addressed in literature. They have been proposed in [3] and are commonly used to test the effectiveness of the extraction procedure. In particular, the data from [3] refer to a solar module (Photowatt-PWP 201, at 45 °C) in which 36 polycrystalline silicon cells are connected in series (Case Study \#1) and to a 57 mm diameter commercial (R.T.C France) silicon solar cell (at 33 °C) (Case Study 2). In the last years, the most famous soft-computing techniques has been used to solve these two cases of study, but unfortunately, the aim of these works was to achieve accurate results in term of parameters without take into account the computational performance of the adopted technique. Now, thanks to the results found in [1], we know that these two cases of study are as inverse problems: 1) hard to solve, since highly dependent from initial guesses; 2) multimodal, indeed, although optimal values of the parameters have been found, a large set of quasi-optimal solutions exists. These two characteristic make the two real cases ideal to be used as benchmark. In the following tables some of the best results in terms of RMSE proposed in literature by using different techniques are reported. In the full paper, all the issues regarding these benchmarks will be addressed, together with a comparison of the performance of some effective heuristic, and with the code suitable to define all the characteristics of these benchmarks.

Table 1. Results for test case #1

Authors	Methods	RMSE
Laudani et al (2014)	Red. forms + deterministic	2.0465E-3
El-Naggar et al. (2012)	Simulated annealing	2.7e-3
Gong & Cai (2013)	Adaptive differential evol.	2.4251E-3
Jiang et al. (2013)	Improved differential evol.	2.4e-3

Table 2. Results for test case #2

Authors	Methods	RMSE
Laudani et al (2014)	Red. forms / deterministic	7.7301E-4
El-Naggar et al. (2012)	Simulated annealing	1.7E-3
Gong et al. (2013)	Adaptive differential evol.	9.8602E-4
Jiang et al. (2013)	Improved differential evol.	9.8900E-4
Askarzadeh et al. (2012)	Harmony search algorithms	9.9097E-4
Askarzadeh et al. (2013)	Artificial bee swarm opt.	9.9124E-4

REFERENCES

[1] A. Laudani, F. Riganti Fulginei, A. Salvini, High performing extraction procedure for the one-diode model of a photovoltaic panel from experimental I-V curves by using reduced forms. Solar Energy, vol. 103, 2014, pp. 316 – 326.

[2] A. Luque and S. Hegedus. *Handbook of photovoltaic science and engineering*. John Wiley & Sons, 2011.

[3] T. Easwarkhanthan, J. Bottin, I. Bouhouch, and C. Boutri. Nonlinear minimization algorithm for determining the solar cell parameters with microcomputers. International Journal of Solar Energy, vol. 4, 1986, pp. 1–12

OPTIMAL SIZING INTEGRATING POWER MANAGEMENT FOR A MICROGRID WITH STORAGE

Rémy RIGO-MARIANI*, Bruno SARENI* and Xavier ROBOAM*

* Université de Toulouse, LAPLACE, UMR CNRS-INPT-UPS,
ENSEEIHT, 2 rue Camichel, 31 071 Toulouse, France – e-mail: {rrigo-ma, sareni, roboam}@laplace.univ-tlse.fr

Abstract. The paper presents an optimal design process for a microgrid with an industrial load associated to a photovoltaic power plant and a storage unit based on high speed flywheel. The power management is simplified with a fast linear programming algorithm which allows simulating the whole system over a long period of time integrating both operating and sizing loops. The overall design procedure is led by the Efficient Global Optimization that interpolates the objective function with a kriging technique. Then, the optimal sizes for both storage and PV production are found in a reduced number of objective function evaluations.

Keywords: efficient global optimization, kriging, linear programming, microgrid, optimal sizing

INTRODUCTION

With the development of decentralized power stations based on renewable energy sources, distribution networks have progressively included meshed structures [1]. It can be considered as an association of various "microgrids" both consumer and producer that have to be run independently while granting the global balance between load and generation. Adding a storage device allows more flexible operations. The management as well as the sizing of such systems have to be optimized considering environmental (solar, wind conditions) and economic data [2]. The study focuses on a microgrid with an industrial load associated to a photovoltaic power plant (PV) and a storage unit composed of high speed flywheels (FW). In section 1 the problem is introduced and a particular attention is attached to the management procedure that is coupled with the sizing problem. Section 2 gives details about the algorithm that performs the optimal sizing and some results are presented.

1. INTEGRATED SIZING/MANAGEMENT OPTIMIZATION

The optimal sizing aims at finding the best values of the PV panels (P_{PV} in kW) and the flywheel (E_{FW} in kWh). Given a system configuration with its sizing, an optimal planning tries to find the best operating costs. Thus a compromise has to be found between the operating and the investment cost [2]. A fast Linear Programming (LP) approach estimates the operating cost on a large time scale (i.e. one year) [3]. It minimizes the day by day cost with corresponding prices for the purchased energy (C_p) and the sold production (C_s) as well as the forecasts for consumption P_{load} and production P_{prod} (that depends on environmental features). On a 24 h of time horizon (with a time step of one hour) the goal is to find the best values for the microgrid degrees of freedom $\mathbf{P_{ref}} = [\mathbf{P_{st}}\ \mathbf{P_{st\text{-}l}}\ \mathbf{\Delta P_{PV}}]$ that determine the flows through the meters P_p and P_s and finally allow the computation of the cost C_i for the i^{th} day as in (1). Given a microgrid size, the investment cost C_{inv} is computed with prices of the PV panels (2000 €/kW) and of the flywheels (1500 €/kWh) over 20 years of life. Then, bounds for $\mathbf{P_{ref}}$ are generated depending on the component sizes. The management loop computes the operating cost C_{op} by summing all daily optimized costs C_i as shown in Fig 1*b*. Finally, the Total Cost of Ownership (TCO) related to the microgrid is obtained by summing operational and investment costs.

$$C_i(\mathbf{P_{ref}}) = \sum_{t=0}^{t=24h} C_p(t) \times P_p(t) - C_s(t) \times P_s(t) \quad (1)$$

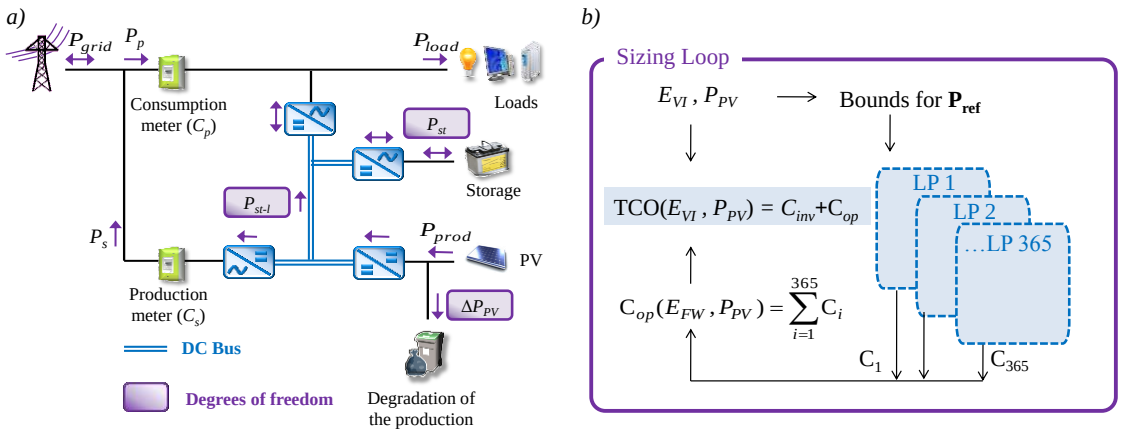

Figure 1: Studied problem - *a)*microgrid topology - *b)*integrated sizing/management optimization

2. MICROGRID SIZING WITH THE EFFICIENT GLOBAL OPTIMIZATION

A whole year simulation lasts less than one minute with the LP. To avoid a long CPU time and a high number of objective function evaluations the sizing loop is performed using the Efficient Global Optimization (EGO) [4]. This method is based on the interpolation of the objective function with the kriging technique that estimates the function in the unexplored points with probabilistically laws [5]. Starting from randomly chosen test points (E_{FW}, P_{PV}) the EGO investigates the search space and maximizes the Expected Improvement (EI) criterion (Fig. 2*a*). This coefficient evaluates the balance between unknown areas and spaces where the objective function appears to be the most interesting (i.e. with the lowest TCO costs). The algorithm stops when the maximum number of objective function evaluations is reached or when there is no improvement of the objective function during a given number of iterations.

Optimizations are performed according to two prices policies. Results are given in Table 1 and compared in each case with a situation "INIT" without flywheel storage and PV production where all the consumed energy is purchased from the main grid. In Scenario1, the electricity is sold at a high price (C_s = 10 c€/kWh) and C_p is moderate equals to 10 c€/kWh from 10 p.m. to 6 a.m. and 18 c€/kWh otherwise. At the optimal point, there is no storage and P_{PV} is set to its upper bound (i.e. 500 kW here) to generate a maximum profit. If the purchased cost increases like in Scenario 2 (C_p = 16 c€/kWh from 10 p.m. to 6 a.m. and 26 c€/kWh otherwise) and selling the production is not subsidized (C_s = 0c€/kWh) adding a storage device becomes interesting with an optimum value at 44 kWh. In the same time the PV capacity is moderate at 282 kW and the self-consumption as well as the storage management allow decreasing the annual electric bill by 13 %. Fig. 2*b* illustrates the EGO convergence in the case of 10 starting points randomly initialized with a Latin Hypercube Sampling and 30 iterations.

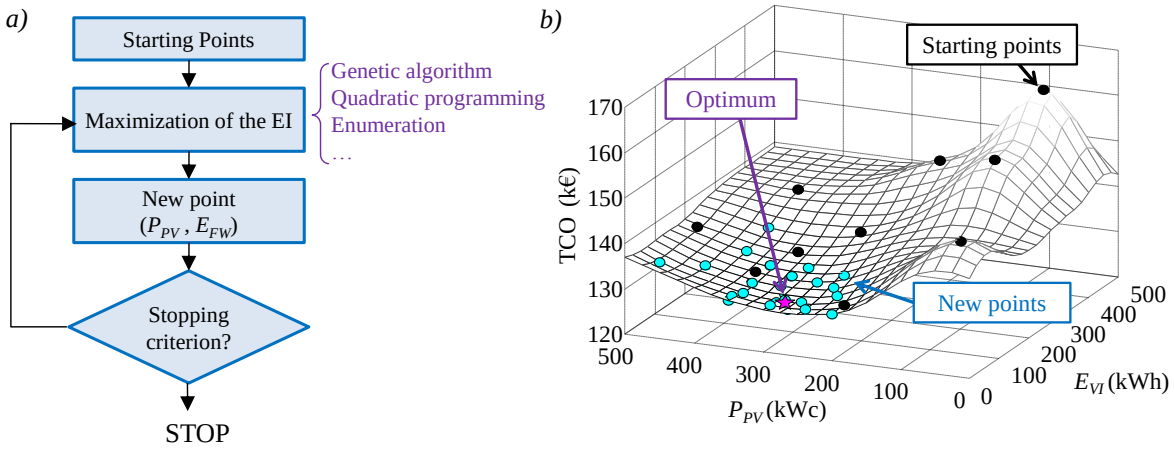

Figure 2: EGO - *a)* algorithm architecture - *b)* results obtained under the scenario 2

Table 1. Optimization results: microgrid configuration and annual costs in k€

	Optimal configuration (E_{FW}, P_{PV})	FW cost	PV cost	Purchase energy	Sold energy	TOTAL	INIT
Scenario 1	[0 , 500 kW]	0.0	50.0	64.1	24.2	**90.0**	97.0
Scenario 2	[44 kWh , 282 kW]	3.3	28.1	98.6	0.0	**130.0**	149.3

CONCLUSIONS

Based on a simplified power management method sped up by the linear programming, this study has investigated a 2-level optimization process integrating the power flow scheduling and the microgrid sizing. The sizing algorithm based on the EGO allows finding solutions in a reduce number of evaluations (less than 50). The return results strongly depends on the considered prices policies and it appears that costs of the purchased energy should drastically increase to justify the investment in a storage unit.

REFERENCES

[1] G. Celli, F. Pilo, G. Pisano, V. Allegranza, R. Cicoria and A. Iaria, "Meshed vs. radial MV distribution network in presence of large amount of DG", *Power Systems Conference and Exposition*, IEEE PES, 2004.

[2] J.W. Whitefoot, A.R. Mechtenberg, D.L. Peters et P.Y. Papalambros, "Optimal Component Sizing and Forward-Looking Dispatch of an Electrical Microgrid for Energy Storage Planning", *ASME 2011 International Design Engineering Technical Conferences and Computers and Information in Engineering Conference*, Washington, 2011.

[3] R. Rigo-Mariani, B. Sareni, X. Roboam, "A fast optimization strategy for power dispatching in a microgrid with storage", *39th annual conference of the IEEE Indusrial Electronics Society* (IECON'2013), Vienna, 2013.

[4] D.R. Jones, M Schonlau,W.J. Welch, Efficient Global Optimization of Expensive Black-Box Functions, *Journal of Global Optimization*, Vol. 13, pp. 455–492, 1998.

[5] J.P.C. Kleijnen, *Kriging metamodeling in simulation: a review*, Discussion paper, Tilburg University, 2007.

MILP FORMULATION FOR LARGE SCALE PEAK SHAVING PROBLEMS IN LOW VOLTAGE SMART GRIDS

Clémentine BENOIT*, Aurélien MERCIER*, Frédéric WURTZ* and Yvon BESANGER*

* Univ. Grenoble Alpes, G2Elab, France

Abstract. In this paper, we present a MILP formulation of a peak load reduction through load shifting problem. A low voltage network having 53 loads is considered over 29 days, with a 5 minutes step time. Each load can be shifted at most once a day, and a payback effect has been considered.

Keywords: CPLEX, Demand Side Management, MILP, Peak Shaving, Large Scale Systems.

INTRODUCTION

Reducing the peak power is a well-known challenge for the electrical network, that is becoming more and more relevant [1,2]. With the Smart Grid paradigm that has highlighted the need of flexibility coming from the consumer's side, peak shaving through Demand Side Management is becoming a major concern for electrical networks. Load shifting has been studied a lot [3,4], but this paper aims at modeling it in a very precise way, in order to see how much the peak load can really be decreased. In this context, a French pilot project named GreenLys [5] has been initiated.

THE PEAK SHAVING PROBLEM

Non linearity

The objective function is the minimization of the peak current at the substation over the studied period. In order to be exact, this current has to be calculated using the usual Load Flow equations that are shown below:

(1) $I \in \{nodes\} \quad S_I = V_I * \overline{I_I} = V_I * \sum_{J \in \{NODES\}} \overline{Y_{IJ}} * \overline{V_J}$

With S_I , V_J and I_I being the complex power, voltage and current at node I, and Y the network admittance matrix. These equations are nonlinear, which make the optimization problem difficult to solve (and even more difficult when binary variables are needed). The problem becomes linear when loads are considered as having a constant impedance instead of having a constant power (the equations are then simply the Ohm's law). Unfortunately, because of the nature of the problem, this is not applicable here: the decision variables are the loads themselves, thus the loads impedances are variables.

Binary variables

The load shifting model had to meet several requirements, which are listed below. This DSM (Demand Side Management) strategy has very little impact on consumers. Because the objective is to find out how much a realistic load shifting can help reducing the peak power, meeting these requirements is very important here. They have induced the use of binary variables.

- the payback effect recovers 100% of the shifted energy
- the highest power of the payback is 140% higher than the average shifted power
- the shifting lasts one hour, and the payback effect twice
- during a shifting, the heating system is completely turned off
- each load cannot be shifted more than once a day

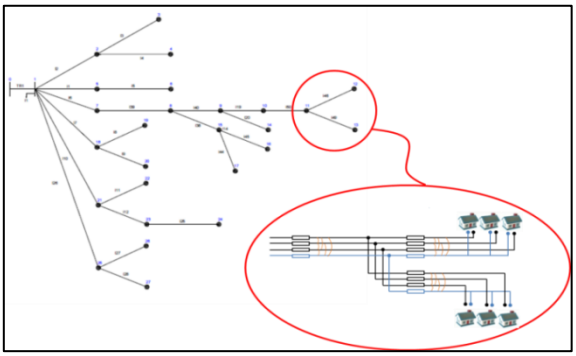

Figure 1. Low voltage network simplified representation

Problem's size

- LV networks are three-phase four-wire networks, which multiply by four every single variable used
- 5 minutes step time is needed to avoid smoothing the data (and most importantly the peak, which is under study here)
- The aim is to reduce the peak over a long period (29 winter days here), which increases even more the problem's size.

Finally, we have 4*4 variables for each node, so considering 28 nodes and 29*288 step time, we end up with 3,741,696 variables only to solve the Load Flow equations. Adding the constraints coming from the load shifting, that includes binary variables, the problem becomes really big.

FORMULATION AND RESOLUTION

Formulation as MILP

Power Flow simplification :

However, it is not obvious that such a high level of modeling is needed for this problem. A comparison has thus been done, between:

- The exact current at the substation obtained using the usual Load Flow equations on the LV network shown Figure 1. Load curves are real data, taken over two days, with a 5 minutes step time.
- The simple sum of the power consumed by the same loads, without taking into account any losses, voltage drop, nor unbalance.

As a result, the error has never exceeds 0.8% for a large range of power. The simplification is thus validated.

DSM model :

The DSM has been modeled using binary variables. Concerning the payback effect, although the natural formulation is nonlinear, it has been written in a linear way in order to solve the problem as a MILP.

Modeling system and solver

Using the formulation previously described, the problem still have lots of variables, but it has been modeled as a MILP, for which large scale problems can be solved. This has led to the use of GAMS and CPLEX. GAMS is a modeling tool particularly adapted for large scale systems. It includes a presolver feature able to reduce the size of the problem. CPLEX is a state of the art solver for MILP problems, able to solve large and numerically difficult problem through an evolved branch-and-bound search.

Results

The next figure shows that the peak power has been decreased by more than 25%, while having almost no impact on the inhabitants' comfort. Indeed, it has been measured that cutting the heating system for one hour induce a negligible drop in temperatures.

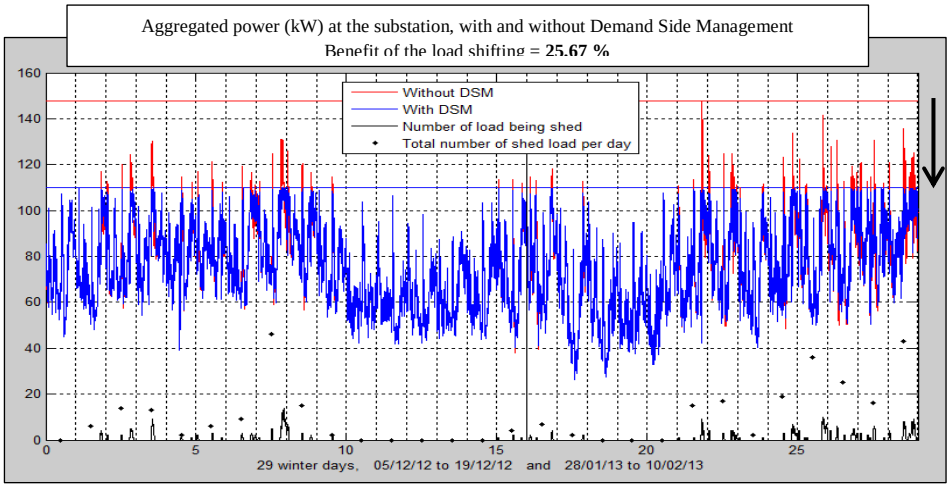

Figure 2. Result of the optimization

CONCLUSIONS

The proposed formulation has allowed finding how much the peak power can theoretically be decreased using a load shifting model as realistic as possible. This was a large scale problem, with binary variables, initially nonlinear. It has been modeled as a MILP in order to be solved.

REFERENCES

[1] Thèse de Cyril Vuillecard, 2013, "Méthode de construction d'une offre d'effacement électrique par technologies gaz naturel"

[2] Rapport Poignant-Sido: http://www.developpement-urable.gouv.fr/IMG/pdf/Rapport_Poignant-Sido.pdf

[3] W.C. Chu, B.K. Chen, and C.K. Fu, "Scheduling of direct load control to minimize load reduction for a utility suffering from generation shortage," IEEE Trans. Power Syst., vol. 8, Nov. 1993, pp. 1525-1529.

[4] Carolina M. Affonso, Luiz C.P. da Silva, Potential benefits of implementing load management to improve power system security, International Journal of Electrical Power & Energy Systems, Volume 32, Issue 6, July 2010, Pages 704-710, ISSN 0142-0615

[5] GREENLYS project, supported by the French agency ADEME through the program "Programme Réseaux Electriques Intelligents des Investissements d'Avenir": http://www.greenlys.fr

PSO ALGORITHMS AND GPGPU TECHNIQUE FOR ELECTROMAGNETIC PROBLEMS

Anton DUCA*, Laurentiu DUCA**, Gabriela CIUPRINA*,
Egemen YILMAZ*** and Tolga ALTINOZ****

*Politehnica University of Bucharest, Faculty of Electrical Engineering, Bucharest, Romania
E-mail: anton.duca@upb.ro, gabriela.ciuprina@upb.ro

**Politehnica University of Bucharest, Faculty of Computer Science, Bucharest, Romania
E-mail: laurentiu.duca@cs.pub.ro

***Ankara University, Department of Electrical and Electronics Engineering, Golbasi, Ankara, Turkey
E-mail: aeyilmaz@eng.ankara.edu.tr

**** TED University, Department of Electrical and Electronics Engineering, Kolej, Ankara, Turkey
E-mail: tolga.altinoz@tedu.edu.tr

Abstract. This paper studies the efficiency of the GPGPU (General Purpose Computation on Graphics Processing Units) technique for the implementation of a parallel PSO (Particle Swarm Optimization) algorithm applied for the optimization of electromagnetic field devices. Several sequential PSO algorithms are compared in order to find the most suitable one for the electromagnetic device to be optimized. The best PSO algorithm is parallelized using GPGPU technique, and the sequential and parallel implementations are compared using as criteria the speed up and the solution quality. For testing, the TEAM22 benchmark electromagnetic problem was chosen.

Keywords: PSO, GPGPU, electromagnetic field, optimization, TEAM22.

PARTICLE SWARM OPTIMIZATION (PSO)

PSO is an iterative optimization algorithm initially proposed by Kennedy and Eberhart [1]. The classic PSO algorithm has the roots in biology and is inspired from the social behavior inside a bird flock or a fish school. Each particle in the swarm is described by the current position and velocity. The position encapsulates the potential solution of the optimization problem while the velocity describes the way the position is modified .

During time, in order to improve the performance of the classic PSO different methods were proposed. Some of the most efficient PSO based algorithms available today are SPSO (Standard PSO), QPSO (Quantum-behaved PSO) and DPSO (Discrete PSO).

Currently at the third version (SPSO 2011), the SPSO brings changes to the original algorithm in terms of neighborhood, initialization, velocity and position update equations, and confinement [2]. The SPSO 2011 uses an adaptive random topology (a particular case of stochastic star) which changes the graph of the information links after each unsuccessful iteration. The initialization for velocity and position is made in order to avoid leaving the search space, especially when the number of optimization variables is high. The velocity formula introduces the center of gravity term for rigorously obtain easy “exploitation” and “exploration”. The gravity term depends of three points: the current position, a point relative to the previous best position, and a point relative to the previous best neighborhood position.

In PSO the trajectories of the moving particles are according to Newton mechanics. QPSO is a quantum system, each particle having a quantum based behavior [3]. The quantum behavior of a particle is described by a wave function Ψ (Schroedinger equation), with $|\Psi|^2$ being the probability density function for a position of a particle. On the other hand, while for the PSO algorithm the particles converge to the solution through the global best, in QPSO the particles exert greater influence on each other through a mean best, thus the probability to be trapped in local minimum is smaller.

The PSO, SPSO and QPSO algorithms generate solutions containing real numbers. For discrete optimization problems in order to obtain discrete (binary) results the values at each step have to be rounded. Another approach proposed for discrete optimization problems is DPSO [4]. In DPSO one potential solution can contain only discrete values from the search space. Because of this, many DPSO algorithms are a combination of PSO and GA (Genetic Algorithms), and perform operations as mutation and crossover over the swarm particles. Although they were designed for discrete problems, the DPSO algorithms can also be used for continuous problems were a finite precision for the optimisation variables is acceptable.

In this paper SPSO, QPSO, and DPSO algorithms are used for the optimization of an electromagnetic device in order to decide which one is the most effective method. PSO algorithms are known as global search zero-order optimization methods. Their main drawback is the large number of objective function evaluations

needed. In the case of real world problems this leads to a significant computation time for the sequential implementations. Thus optimization algorithms are very well suited for parallel implementations.

GENERAL PURPOSE COMPUTATION ON GRAPHICS PROCESSING UNITS (GPGPU)

Driven by the market demand for realtime, high-definition 3D graphics, the GPU (Graphic Processor Unit) has evolved into a highly parallel, multithreaded, manycore processor with tremendous computational horsepower and very high memory bandwidth [5]. While a CPU focuses on the data caching and flow control, the GPU is specialized for compute-intensive, highly parallel computation (exactly what graphics rendering is about) and therefore designed such that more transistors are devoted to data processing. More specifically, the GPU is especially well suited to address problems that can be expressed as data-parallel computations (the same program is executed on many data elements in parallel) with high arithmetic intensity (the ratio of arithmetic operations to memory operations).

In order to use the GPU for general purpose computation and to solve complex computational problems from different and various domains (not only graphics rendering) several programming models such as CUDA and OpenCL have been created. Introduced in 2006 by Nvidia, CUDA (Compute Unified Device Architecture) is a programming model which comes with a software environment that allows developers to use high level programming languages like C for writing general purpose parallel applications.

In the current paper CUDA language is used to implement a parallel version of the best PSO algorithm for solving the electromagnetic optimization problem. The parallel and the sequential implementations will be compared in terms of speed up and solution fitness for different swarm sizes. The main theoretical advantages of the parallel versus sequential implementation are the speed up and the possibility to increase the swarm size without a significant increase of the global processing time (due to the parallel evaluation of the particles).

THE TEAM22 BENCHMARK PROBLEM

For testing and comparing the PSO based algorithms the TEAM22 benchmark electromagnetic problem was chosen as optimization problem [6].

Two concentric coils carrying current with opposite direction (Fig. 1) and running under superconducting conditions offer the opportunity to store a significant amount of energy in their magnetic fields while keeping the stray field within certain limits. An optimal design of the system should therefore couple the desired value of energy to be stored with a minimal stray field. The objective function has eight parameters, radius, height, thickness and current density of both coils.

The full paper will study the efficiency of GPGPU technique applied to the best PSO algorithm for solving the TEAM 22 problem. The comparison between the parallel and sequential implementations is measured in terms of speed up and solution fitness. The influence of the population is discussed as well.

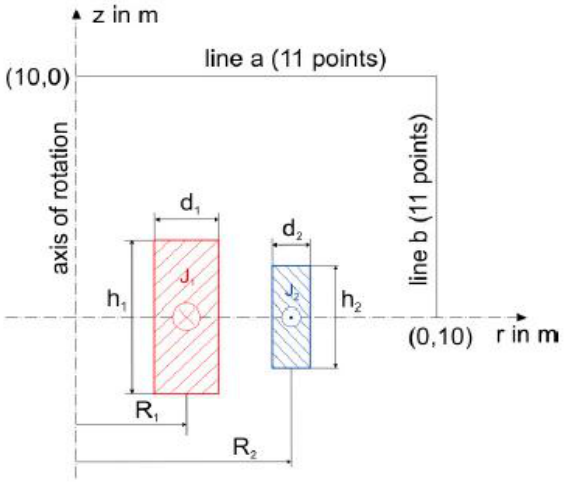

Figure 1. Problem configuration.

Acknowledgments

This work was supported by the Romanian Government program PN-II-PT-PCCA-2011-3, managed by ANCS, CNDI– UEFISCDI, grant no. 5/2012. This study was also supported by the joint grant from ANCS-UEFISCDI (Nr. 605/01.01.2013) and TUBITAK (Nr. 112E168).

REFERENCES

[1] J. Kennedy, and R Eberhart, Particle swarm optimization, Proceedings of IEEE International Conference on Neural Networks, 1995, pp. 1942-1948.

[2] M. Clerc, Standard Particle Swarm Optimisation, Open access archive HAL (http://clerc.maurice.free.fr/pso/SPSO_descriptions.pdf), 2012.

[3] J. Sun, W. Fang, V. Palade, X. Wua, W. Xu, Quantum-behaved particle swarm optimization with gaussian distributed local attractor point, Applied Mathematics and Computation, vol. 218, 2011, pp. 3763–3775.

[4] Q.-K. Pan, M. F. Tasgetiren, Y.-C. Liang, A discrete particle swarm optimization algorithm for the no-wait flowshop scheduling problem with makespan and total flowtime criteria, Journal Computers & Operations Research, vol. 35, 2008, pp. 2807–2839.

[5] Nvidia CUDA C programming guide, http://docs.nvidia.com/cuda/cuda-c-programming-guide.

[6] TEAM22 benchmark problem, http://www.compumag.org/jsite/team.html.

AUTOMATIC THERMAL MODEL GENERATOR FOR MULTIPHYSICS SIZING OPTIMIZATION

Arnaud BARASTON, Laurent GERBAUD, Vincent REINBOLD, Thomas BOUSSEY, Frederic WURTZ

Grenoble Electrical Engineering Lab (G2ELab), UMR 5529, BP46 – 38402 Saint-Martin-d'Hères Cedex, FRANCE, Tel: +330 476 826 360 / Fax: +330 476 826 300
E-mail: arnaud.baraston@g2elab.grenoble-inp.fr, laurent.gerbaud@g2elab.grenoble-inp.fr

Abstract. This paper deals with the multiphysics modeling of mechatronic systems (building energy management, electrical drive). It focuses on the automatic modeling of thermal phenomena using equivalent circuit description. From such a description, the paper proposes an approach able to automatically generate files with the corresponding model equations and their Jacobian (useful for optimization algorithm like SQP). For multiphysics problems, the thermal model is coupled to other models thanks to CADES environment. A main specificity of the approach is the ability to deal with the selectivity of the inputs and outputs of the generated model according to the problem specifications, which reduces drastically the size of the model and the computational complexity. The approach is applied on the sizing of an electrical machine.

Keywords: Automatic, Modeling, Multiphysics, Optimization, Thermal.

INTRODUCTION

In a modeling context to size a system, a multi physical approach is often required for more realistic and global results. The paper proposes to add static thermal phenomena to a system model by using an equivalent thermal circuit approach. When numerous constraints appear in the system specifications, an optimization algorithm like SQP is well adapted for the sizing. However, this requires the calculation of the model gradients.

One of the main features proposed in the paper is the concept of selectivity, described in Fig. 1. There, only the selected parameters that vary during the optimization appear in the model and its Jacobian, in order to reduce the calculation time and memory (RAM). The main purpose is the automatic generation of the model solving and its Jacobian for any optimization algorithms.

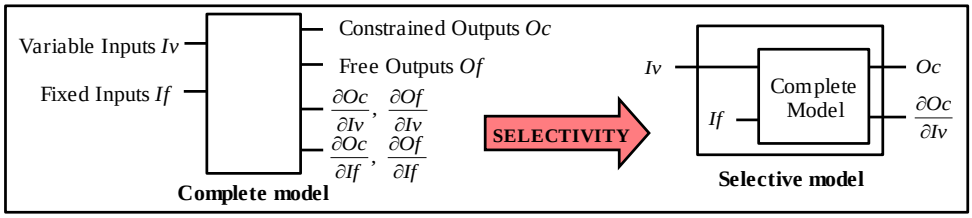

Figure 1. Concept of selectivity, selective model with required inputs and outputs only.

THERMAL MODELING AND SELECTIVITY

The thermal modeling of an electrical device aims to give temperatures at different points in order to calculate the thermal evolution of material characteristics and size coolers [1]. The thermal equivalent circuit of the system is a way to deal with such a modeling in a system or in an optimization context. Here, it is essential to describe the thermal resistors with numerous parameters rather than a simple value in order to optimize the system according to its numerous physical and geometrical parameters. To aid the modeling and to deal with the Jacobian of the model, the paper proposes a database that contains predefined resistors, where each component is described by the equations to calculate its thermal resistance and gradients according to the corresponding geometrical and physical parameters.

A thermal equivalent circuit is similar to a reluctance network used for electromagnetism modeling, both are localized constants models. However, for thermal problems, nodal approach is more suited because temperatures (equivalent to voltages) have to be calculated, whereas magnetic fluxes (equivalent to currents) are calculated with a mesh approach in electromagnetism [2]. From such a description, using Kirchhoff's laws, the paper proposes to automate the building of the linear system of equations and their Jacobians. For their solving and to compute the matrix invert of this equation system (needed for the Jacobian), the paper proposes to use a LU method. According to the selected parameters and criteria to optimize, the generated model only deals with the variables and the partial Jacobian required by the specifications (like previously defined in Fig. 1). By this way, the sizing model defined according to the specifications, is smaller and faster. The complete formulation of the thermal model and its Jacobian will be detailed in the full paper.

IMPLEMENTATION OF THE AUTOMATIC MODELING

The described approach is implemented as a model generator named ThermoTool (see Fig. 2). The designer describes the thermal equivalent circuit of its application, using the components available in the component database. If some components do not exist, like the one studied in [3] for example, he can create them by writing their equations and their gradients in XML representation. The generated thermal models are translated in Java code. They are coupled to other models thanks to the modeling language of CADES framework (SML) [4]. Then, a global optimization model is obtained and generated as an ICAr component software [4], available for several optimization environments (CADES Optimizer, Matlab, GotIt…).

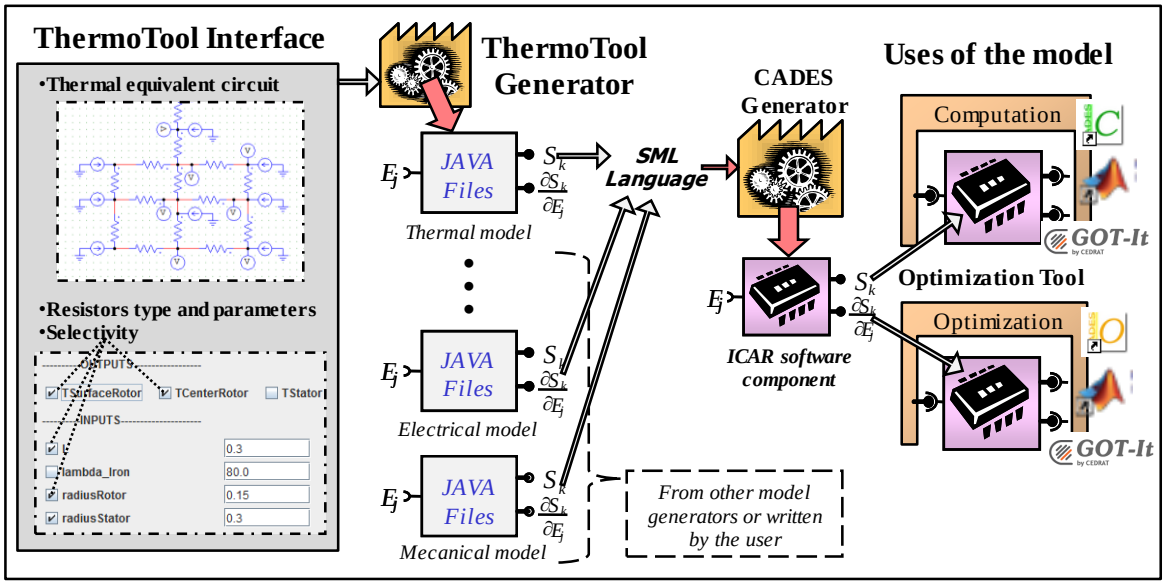

Figure 2. Different steps of the multiphysics optimization approach with ThermoTool

APPLICATION

A thermal optimization has been carried out on the sizing of an electrical machine to reduce a specific temperature point according some geometrical parameters. The whole thermal model has 19 inputs and 14 outputs. The equivalent circuit of the system was defined with line and cylindrical conduction resistors and convection resistors. Then, a SQP (VF13) algorithm was used for the optimization process within CADES.

CONCLUSIONS

The first version of ThermoTool is a basic prototype that is already convenient for thermal equivalent circuit modeling and automatic generation of the files required for the sizing of mechatronic systems by optimization. However, at the present time, the user creates a new component by hand-writing, giving its equations and corresponding gradients in a XML database. In future work, the components will be described only by symbolic expressions, and automatic derivation will be used to build the corresponding Jacobian. The approach has already been used in a thermal optimization of an electrical machine. A CADES multiphysics optimization of an electrical motor (Toyota PRIUS) is currently undergoing and will be described in the full paper. The thermal model without selectivity has 29 inputs and inputs. The complete multiphysical model has at least 24 inputs and more than 100 outputs after selectivity. The sizing is carried out using SQP optimization.

ACKNOWLEDGEMENT

Funding for this project was provided by the French ANR project FIABILITE.

REFERENCES

[1] J. Legranger, G. Friedrich, S. Vivier and J.-C. Mipo. Combination of finite-element and analytical models in the optimal multidomain design of machines: application to an interior permanent-magnet starter generator. IEEE Trans. Ind. Appl., Vol. 46, no 1, pp. 232-239.

[2] B. Du Peloux, L. Gerbaud, F. Wurtz, V. Leconte & F. Dorschner. Automatic generation of sizing static models based on reluctance networks for the optimization of electromagnetic devices, IEEE Transactions on Magnetics, 2006, 42, pp. 715-718.

[3] R.S. Li. Optimization of thermal via design parameters based on an analytical thermal resistance model. Proceedings of the sixth intersociety conference on thermal and thermomechanical phenomena in electronic systems, 1998, pp. 475-480.

[4] B. Delinchant, D. Duret, L Estrabaut, L. Gerbaud, H. Nguyen Huu, B. du Peloux, H.L. Rakotoarison, F. Verdiere, F. Wurtz, "An Optimizer using the Software Component Paradigm for the Optimization of Engineering Systems", COMPEL, the international journal for computation and mathematics in electrical and electronic engineering, Vol. 26, no 2, 2007, pp.368-379

TIME REDUCTION OF THE DYNAMIC PROGRAMMING COMPUTATION IN THE CASE OF HYBRID VEHICLE

Emmanuel VINOT*

*IFSTTAR, 25 Avenue François Mitterrand, 69500 Bron, France
E-mail: emmanuel.vinot@ifsttar.fr

Abstract. Deterministic Dynamic Programming is frequently used to solve the management problem of hybrid vehicles (choice of mode and power sharing between thermal and electric sources). However, it is time consuming and thus difficult to use in global sizing optimization or in parametric studies. This paper presents a comparison between three methods to compute the DDP problems. These methods are applied on the well known case of the Toyota PRIUS. It proves that a dense matrix method can reduce the computation time by up to 10 compared to classical solving methods.

Keywords: Deterministic Dynamic Programming, Solving Algorithms, Hybrid Vehicle

INTRODUCTION

Hybrid Electric Vehicles (HEVs) are an effective solution to reduce CO_2 and pollutant emissions [1]. The electrical driveline provides additional functionality to the drive train. Among them, regenerative braking and electrical propulsion mode are the most efficient to improve systems efficiency. Combined electrical and thermal propulsion and battery recharge by engine also allow substantial gain. Finally, engine and wheel speed decoupling, as in series parallel hybrid such as Toyota PRIUS, is another possibility to reduce the fuel consumption.

These different capabilities have to be used in the best manner to reduce the fuel consumption as much as possible. The choice of this operating mode (i.e. the power energy management) is thus a key point of the efficiency of hybrid architectures [2].

The fuel consumption of a hybrid vehicle can only be announced taking into account the battery discharge over a driving cycle long enough to be representative of real use conditions. In fact, the power management law cannot be simply developed to minimize the fuel consumption in each step of time but has to globally respect a global amount of discharge of the battery.

Optimal energy management methods are then very useful to determine the best management law along a known in advance representative driving cycle. These methods are obviously applied offline as they need to know in advance the drive cycle. Optimal off-line management remains nevertheless of great importance to develop efficient online management laws, to perform objective comparisons between hybrid solutions [3], to size component, and in optimal global design process to avoid the unknown and non-monotonic impact of the management on the fuel economy.

Two off-line methods are currently used in order to calculate optimal management; the Pontryagin's minimum principle and the Deterministic Dynamic Programming. These two methods can take a long time to achieve the optimal management over a drive cycle of several hundreds of seconds. This can be a critical point especially in comparative or parametric studies and even more critical in design process when the fuel consumption of thousands of solutions needs be calculated. It is then of high importance to reduce the computer effort as much as possible during such calculation.

In this paper, the authors choose to focus on DDP [4] and investigate the different possibilities to reduce the calculation time. The DDP principle is to find the optimal battery state of charge trajectory to minimize fuel consumption along a known in advance drive cycle. This is performed in a restrictive SOC versus time meshed area (graph) limited by battery maximum charge and discharge possibility fixed by the systems. Another specification when applying DDP to hybrid vehicles is the consideration of all electric modes. If the battery state of charge is sampled (for numerical consideration) you have to make sure that one of the sampled state corresponds to electric mode with no fuel consumption associate.

Several manners to improve time calculation can then be investigated:

- Reduce the size of the graph as much as possible.
- Build the graph to ensure that the electrical modes correspond to existing edges.
- Use vectorial calculus in edges cost calculation. For that all edges costs of the graph are calculated in one time before solving the graph.
- Improve the manner to solve the DP problem avoiding loops and big matrix.

In this paper, the authors present the method they used to reduce the DDP calculation time to a handful of second (3 to 30). The four precedent points are treated in the final paper. Then, an example on the THS [5] architecture is presented.

METHOD TO SOLVE THE DDP

In HEVs DDP problem leads to find the optimal SOC trajectory to minimize the fuel consumption along a known in advance driving cycle. This is performed in a meshed area (Fig. 1). Points of consecutive columns are linked by edges associated to fuel consumption. The sum of the fuel consumptions on a trajectory is the objective to minimize.

This part deals with three different manners to solve the DDP problem (Fig.1):

(i) A first intuitive method which uses a loop on each point of a column inside the loop at each time k.

(ii) A matrix method which treats each point of a column in a vectorial manner but uses great sparse matrix with lot of non defined elements.

(iii) A third method based on dense matrix referencing to index in a global matrix of cost and weight.

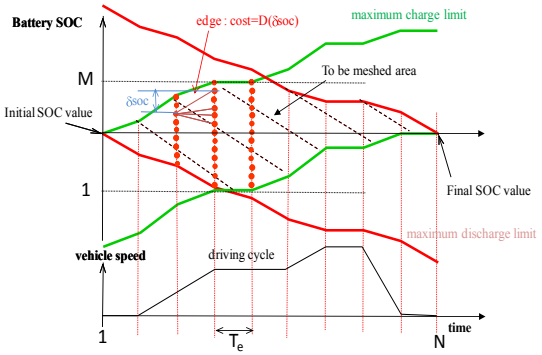

Figure 1. This is the figure caption for centred figure.

APPLICATION ON THE TOYOTA PRIUS-II

The previously presented methods of optimal management have been applied to different type of hybrid architectures including different HEV architectures. In this paper, to provide data on computer effort during the process of optimisation, the well known Toyota PRIUS [5], (Fig.2) is chosen as an example. Table 1 shows the time to compute the DDP problem using a CPU running at 2660 MHz and 24 GB of memory. A matrix method (ii) easy to program does not seem to be really efficient. However, reduction by a factor 4 to 7 can be obtained with the third method (iii) based on dense matrix compared to the easiest methods.

Table 1. Simulation time on the example of Toyota Hybrid System.

	drive cycle			
	URBAN	ROAD	HIGHWAY	NEDC
graph precision	-0.05			
time of cycle in s	560	843	1805	1181
million of edge	3.5	6.3	18	7.9
time of edge cost calculation in s	1	1.9	5.1	2.5
fuel consumption in l/100 km	3.772	4.124	5.309	3.720
	time to solve DP in s			
A: point to point method	3.8	7.2	18.7	10.4
B: Matrix method	3.0	4.9	13.5	6.9
C: Index matrix method	0.6	1.2	4.6	1.9

Figure 2. Toyota PRIUS system.

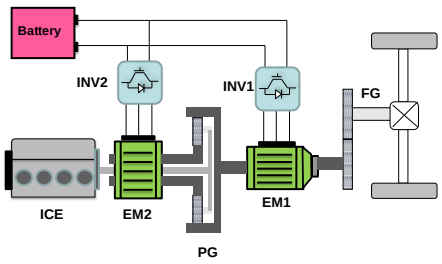

CONCLUSIONS

This paper presents a method to compute in an efficient manner the dynamic programming problem in the case of hybrid vehicles. The example of the Toyota PRIUS is presented but the method remains valid for all hybrid architectures. Reduction of a factor up to 10 can easily be achieved. Final paper will also present the manners to reduce the size of the graph. It will explain why and how to the electrical mode is taken into account. The calculus of the cost for THS will be described and more results with different precision of the graph will be shown.

REFERENCES

[1] C. Chan, «The state of the art of electric and hybrid vehicles,» *Proceedings of the IEEE*, vol. 90, n°12, pp. 247-275, 2002.

[2] M. Koot, J. Kessels, B. de Jager, W. Heemels, P. Van den Bosch et M. Steinbuch, «Energy management strategies for vehicular electric power systems,» *Vehicular Technology, IEEE Transactions on*, vol. 54, pp. 771-782, 2005.

[3] E. Vinot, R. Trigui, B. Jeanneret, J. Scordia et F. Badin, «HEVs comparison and components sizing using dynamic programming,» *Vehicle Power and Propulsion Conference, 2007. VPPC 2007. IEEE*, 2007.

[4] D. E. Kirk, Optimal control theory: an introduction, Courier Dover Publications, 2012.

[5] E. Vinot, J. Scordia, R. Trigui, B. Jeanneret et F. Badin, «Model simulation, validation and case study of the 2004 THS of Toyota Prius,» *International Journal of Vehicle Systems Modelling and Testing*, vol. 3, n°13, pp. 139-167, 2008.

13th International Workshop on Optimization and Inverse Problems in Electromagnetism
September 10 – 12, 2014, Delft, The Netherlands

OPTIMAL DESIGN OF CORRECTION COILS IN TOKAMAK FUSION DEVICES

Giuseppe CALABRO'*, Andrea G. CHIARIELLO**, Alessandro FORMISANO**, Francesco LEDDA**, Raffaele MARTONE**, Francesco PIZZO** and Giuseppe RAMOGIDA*

*Unità Tecnica Fusione, C.R. ENEA Frascati, Via E. Fermi 45, CP 65 - 00044 Frascati, Roma, Italy
**Dipartimento di Ingegneria Industriale e dell'Informazione, Seconda Università degli Studi di Napoli, Via Roma 29,Aversa (CE), ITALY; e-mail: Alessandro.Formisano@unina2.it

Abstract. Magnetic field map in magnetically confined thermonuclear fusion devices must be carefully controlled, in order to achieve desired performance. Residual error fields, which are in any case present, must be reduced using suitably designed "additional" coils. Since the feeding currents in coils for shape and position control are time-varying, also correction currents waveform must be optimized to achieve best performance. In this paper, the optimization of shape and power supply waveforms of such additional coils is tackled, with reference to FAST Tokamak.

Keywords: Thermouclear Fusion, Superconducting Magnets, Correction Coils, Optimal Design.

INTRODUCTION

One of the most relevant performance indexes in the magnets system of the thermonuclear fusion reactors is the discrepancy between the design and the actual field maps. As an example, an excessively distorted map may induce magnetic islands, leading to a stopping of the plasma rotation. Discrepancies in the magnetic field from the design one are mainly generated from lack of axial symmetry in the magnetic systems and in the structures (e.g. the presence of neutral beam injection systems or the finite number of toroidal field coils), but also small errors induced by tolerances in manufacturing and assembly of active coils in the machine can lead to severe loss of performance, especially in larger Tokamaks.
Since a part of field sources are time-varying (e.g. currents in plasma shape and position control coils), and the containing vessel is not completely symmetric (e.g. due to the segmentation to reduce induced currents or the ports and apertures for diagnostics), also the contribution of eddy currents in the conducting structures must be considered in the field error.

To reduce these errors in the magnetic field, in modern Tokamak projects additional sets of coils are included, each set being specialized to correct a specific field error component. Such coils are powered by independent power supplies, whose characteristics must be carefully chosen to guarantee best performance to the correction system. The typical approach in the choice of currents in these coils is mainly aimed at producing a static map able to counteract error fields in the most critical moments of the plasma discharge. This is achieved by minimizing the "residual" difference of the field from the design map. Anyway, the performance index measuring the impact of errors in the magnetic field is typically defined, rather than as a norm of the difference field evaluated in a set of control points, as a summation of the amplitudes of the most relevant spatial harmonics of the field error. This implies precise design constraints in the shape and position of additional correction coils (e.g., they must be suitably distributed in toroidal direction, and also suitably connected to reject toroidally constant fields), while still leaving a number of degrees of freedom to the designer, which can be exploited to improve performance of the system.

In addition, since the fundamental mode along toroidal direction and the first few modes along the poloidal direction are only considered in the field error description, and usually the independent correction currents are larger in number than the degrees of freedom, the choice of currents can be faced also by solving a set of under-determined equations in order to make coefficient vanish, or alternatively, considering also other aspects than just error field compensation.

In the paper, some possible approaches to the optimal design of the coils for the reduction of field errors and the definition of their currents waveform are described; their performance are illustrated and assessed with reference to the FAST Tokamak.

FAST EXPERIMENT

The Fusion Advanced Study Torus (FAST) proposal for a high magnetic field, compact size Tokamak machine has been designed as a very flexible tool able to investigate plasma interaction, to analyze power exhaust options and to study in an integrated way fast particles physics and steady state operation features in ITER and DEMO relevant conditions. Table 1 presents its main physical characteristics, while Fig. 1, left, presents an artist's view of FAST; more details can be found in [3].

To further increase the flexibility, two additional systems for field error reduction have been added to the FAST design: an Active Ripple Compensating System (ARCS), dedicated to decrease, at any toroidal field level, the ripple induced by the finite number of toroidal field coils, and a Feedback Active Control System (FACS), designed to control the potentially dangerous MagnetoHydroDynamic (MHD) modes, allowing then low safety factor operation and possibly Edge Localized Modes (ELM) activity mitigation.

In the paper, the optimization of the shape and waveform of ARCS will be discussed. See Fig. 1, right, for a schematic view of the ARCS system.

Table 1. FAST Reference Scenario Parameters

Plasma Current (MA)	6.5
Toroidal Field (T)	7.5
Major Radius (m)	1.82
Minor Radius	0.64
Elongation	1.7
Triangularity	0.4
Safety Factor	3
Flat-top duration (s)	13
Heating and Current Drive Power (MW)	40

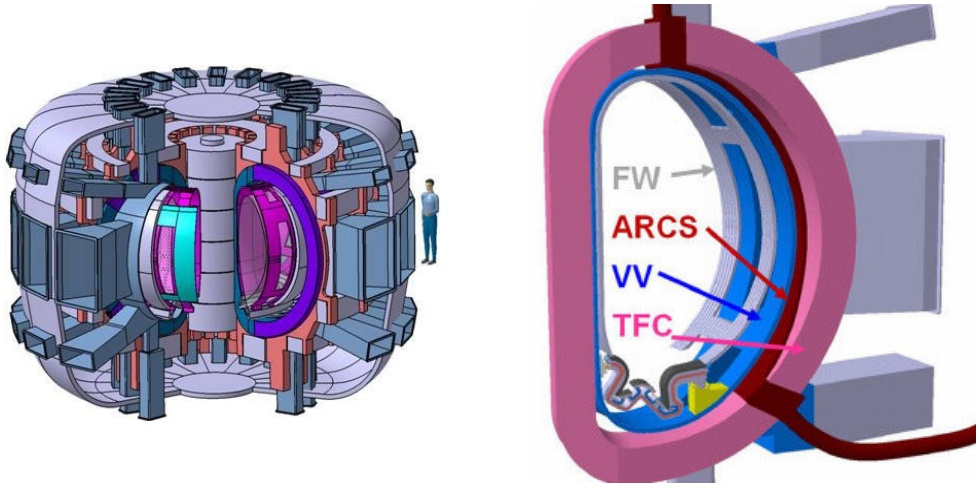

Figure 1. An artist's view of FAST (left) and its out-vessel ARCS coil placed between the Vacuum Vessel and Toroidal Field Coil (right).

CONCLUSIONS

In this work first results for the optimal design of Active Ripple Compensating System in the FAST Tokamak are presented. In the full paper, a detailed description of the coils shape and position optimization process is presented, and some preliminary results about the choice of correction currents are reported.

ACKNOWLDGEMENTS

This work was partially supported by the EU under the Contract of Association between EURATOM and ENEA/CREATE, and by the Italian MIUR under PRIN grant 2010SPS9B3.

REFERENCES

[1] J. Knaster et al., "ITER non-axisymmetric error fields induced by its magnet system", *Fusion Engineering and Design*, Vol. 86, 2011, pp. 1053-1056

[2] A. Bonito Oliva et al., "Optimization of current waveforms in ITER correction coils", *IEEE Trans. on Appl. Superconductivity*, Vol. 22, 2012, pp.

[3] G. Ramogida et al., "Active toroidal field ripple compensation and MHD feedback control coils in FAST", *Fusion Engineering and Design*, Vol. 88, 2013, pp. 1156 – 1160.

A MODIFIED MIGRATION MODEL BIOGEOGRAPHY EVOLUTIONARY APPROACH FOR ELECTROMAGNETIC DEVICE MULTIOBJECTIVE OPTIMIZATION

Mahmoud SAYED*, Ahmed ABDALLH** and Luc DUPRÉ**

* Electrical Power and Machines Department, Cairo University,

EG-12613 Giza, Egypt

** Department of Electrical Energy, Systems and Automation, Ghent University,

Sint-Pietersnieuwstraat 41, BE-9000, Ghent, Belgium

E-mails: fecu.msayed@gmail.com, ahmed.abdallh@ieee.org, luc.dupre@ugent.be

Abstract. In this paper, we present an efficient and robust algorithm for multiobjective optimization of electromagnetic devices. The recently developed biogeography-based optimization (BBO) is modified by adapting its migration model function so as to improve its convergence. The proposed Modified Migration Model biogeography-based optimization (MMMBBO) algorithm is applied into the optimal geometrical design of an electromagnetic actuator. This multiobjective optimization problem is solved by maximizing the output force as well as minimizing the total weight of the actuator. The comparison between the optimization results using BBO and MMMBBO shows the superiority of the proposed approach.

Keywords: Actuator, biogeography-based optimization, electromagnetic device, evolutionary computation.

INTRODUCTION

In last decades, several evolutionary algorithms (EAs) have been utilized for the optimization of electromagnetic devices, such as genetic algorithm, etc. Recently, a biogeography-based optimization (BBO) technique has been presented as an alternative global heuristic algorithm [1], which emulates the geographical distribution of biological organisms. In fact, BBO is based on the migration of species across habitats [2]. In the BBO model, problem solutions are represented as islands, and the sharing of features between solutions is represented as immigration and emigration between the islands. In BBO algorithm, habitats and habitat suitability index (HSI) are respectively the analogous to the problem solution and fitness in other EAs. Migration in BBO is reciprocal which means there is both immigration and emigration between habitats. Their respective rates, λ and μ, are determined using the HSI of a habitat; a habitat with a high HSI has a low immigration rate and consequently a high emigration rate, and vice-versa. The migration rates are directly related to the number of species (S) in a habitat. This migration process increases the diversity of the habitat and contributes for species information sharing and the mutation probability. These concepts are used in the BBO algorithm to find the optimal solution. The immigration and emigration rates are calculated respectively using $\mu_s = \left(ES/S_{\max}\right)$, and $\lambda_s = I\left(1-\left(S/S_{\max}\right)\right)$, where E and I are the maximum rate of emigration and immigration. $S_{\max}$ is the largest possible number of species.

MODIFIED MIGRATION MODEL BIOGEOGRAPHY-BASED OPTIMIZATION

In the BBO algorithm, there are two main operators: migration and mutation. The selection of the optimal solution is fundamentally based on immigration and emigration rates [3]. Consequently, in this paper, we propose a new formulation for the migration model that describes immigration and emigration rates in order to improve the convergence performance for the optimization problems, for example $\mu_s = \left(ES^n/S_{\max}\right)$, where (n) controls the convergence of the optimal solution. The BBO and MMMBBO are used to for the optimal geometrical design of an electromagnetic actuator, see [4, 5]. The multiobjective optimization problem is formulated to maximize the output force and to minimize the total weight.

PRELIMINARY RESULTS

First we applied the proposed methodology into the 3-parameter TEAM benchmark problem 22 [6]. The results obtained in this benchmark problem validate the importance of the modification in the conventional BBO optimization technique.

Moreover, the BBO and MMMBBO have been successfully applied into our electromagnetic application, which is modeled using 2D finite element method. Figure 1 shows the geometry of the considered electromagnetic device. It is an electromagnetic actuator with 6 design parameters. Figure 2 shows a comparison between the convergence history of the BBO and MMMBBO. The fitness values for both approaches are given in the caption. In the full paper, we present the complete algorithm with the mathematical impact of the proposed modification. Comparison with other EAs will be provided.

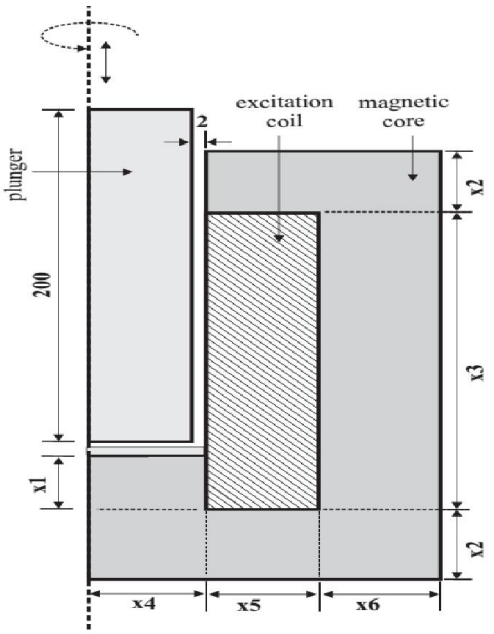

Figure 1: Geometry of the considered electromagnetic actuator.

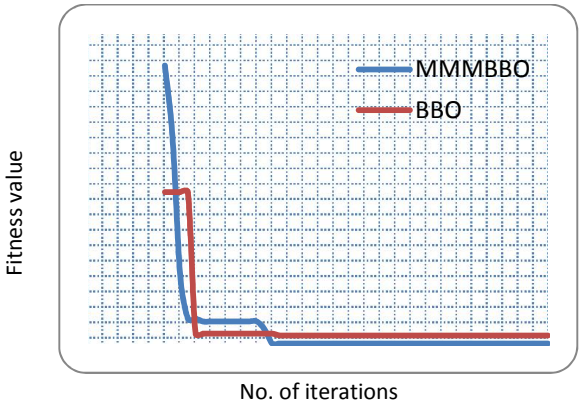

Figure 2: The comparison between the convergence history of the BBO and MMMBBO (n = 6). The fitness values of the BBO and MMMBBO are 2.06e-4 and 1.417e-8, respectively.

CONCLUSIONS

An efficient modification on the tradition biogeography-based optimization was presented. The proposed Modified Migration Model biogeography-based optimization (MMMBBO) algorithm was applied into the optimal geometrical design of an electromagnetic actuator. The obtained results reveal the effectiveness of the proposed MMMBBO.

ACKNOWLEDGEMENTS

The second author gratefully acknowledges the financial support of the Special Research Fund (BOF) of Ghent University.

REFERENCES

[1] D. Simon, “Biogeography-based optimization,” IEEE Trans. on Evolutionary Computation, vol. 12, pp. 702-713, 2008.
[2] A. Wallace, The Geographical Distribution of Animals (Two Volumes). Boston, MA: Adamant Media Corporation, 2005.
[3] H. Ma, “An analysis of the equilibrium of migration models for biogeography-based optimization”, Information Sciences, vol. 180, pp. 3444–3464, 2010.
[4] J. Biedinger and D. Lemoine, “Shape Sensitivity Analysis of Magnetic Forces”, IEEE Trans. on Mag., vol. 30, pp. 2309-2516 ,1997.
[5] M. C. Silva, L. S. Coelho, and L. Lebensztajn, “Multiobjective biogeography-based optimization based on predator–prey approach,” IEEE Trans. Magn., vol. 48, no. 2, pp. 951–954, Feb. 2012
[6] P. G. Alotto P. G. Alotto et al., SMES Optimization Benchmark: TEAM Workshop Problem 22 [Online]. Available: http://www.igte.tugraz.at/team22.

13th International Workshop on Optimization and Inverse Problems in Electromagnetism
September 10 – 12, 2014, Delft, The Netherlands

MAXIMIZATION OF TEMPERATURE BUILD-UP IN BIPOLAR RFA USING PULSED VOLTAGE PROFILES

Frederik SOETAERT*, Guillaume CREVECOEUR* and Luc DUPRE*

*Ghent University, Department of Electrical Energy, Systems and Automation, B-9000, Ghent, Belgium
E-mail: frederik.soetaert@ugent.be

Abstract. Radiofrequency ablation (RFA) is an auspicious alternative cancer treatment that creates heat by means of electrodes that are subject to radiofrequency voltage differences. We propose the use of a bipolar RFA device, with two electrodes, that applies a pulsed voltage profile. To understand the physical phenomena to a better extent, we have implemented a 3D finite element model of pulsed bipolar RFA. We furthermore propose a numerical optimization of the pulsed voltage profile in order to obtain a temperature build-up in tumor regions that normally survive RFA. Numerical results confirm that this optimization results in a larger temperature build-up and thus increases the efficacy of the treatment.

Keywords: cancer therapy, cost functional formulation, numerical algorithms, optimization, radiofrequency ablation.

INTRODUCTION

Unfortunately, traditional cancer therapies are not always an adequate or effective treatment and usually cause serious adverse effects. This occurs especially when treating liver cancer. Primary liver tumors, so-called hepatocellular carcinoma (HCC), occur in approximately 782000 cases per year [1]. The five-year survival rate for HCC is however only 12%. Therefore, alternative strategies that apply heat to cancerous tissue are being developed to increase this five-year survival rate. Radiofrequency ablation (RFA) is such an auspicious alternative cancer therapy where the tissue is heated by means of one or more electrodes, injecting radiofrequency currents.

In order to treat large tumors, the ablation zone's size needs to increase. This requires multiple sequential ablations to create overlapping ablation zones. Despite all efforts, there is not much freedom regarding the size and shape of the ablation zone. Therefore, we numerically explore the possibility of a bipolar RFA device where two electrodes are driven by a current source. The numerical model consists of two coupled subproblems. Firstly, the Poisson differential equation needs to be solved to calculate the electric fields. The thermal subproblem on the other hand is characterized by the Pennes' bioheat equation, in which an additional electric heat source is included. By means of this forward numerical model, we can optimize the voltage profile in order to maximize the temperature build-up in regions that normally survive RFA.

METHODS

Forward model

The electromagnetic phenomena in RFA are described by the Poisson equation:

$$\nabla \cdot \left[\sigma \nabla \phi(\vec{r},t)\right] = 0 \tag{1}$$

with the electric potential φ and electrical conductivity σ, as a function of space and time. The resulting electric field $\vec{E}$ generates heat $q_E = \sigma\left|\vec{E}(\vec{r},t)\right|^2$. The termal subproblem is based on the biological heat transfer model of Pennes' with the additional electric heat source q_E:

$$\rho\, c \frac{\partial T(\vec{r},t)}{\partial t} = \nabla \cdot \left[k \nabla T(\vec{r},t)\right] - \omega \rho_b c_b \left(T(\vec{r},t) - T_c\right) + q_E \tag{2}$$

with temperature T, mass density of the tissue ρ (blood: ρ_b), specific heat capacity of the tissue c (blood: c_b), thermal conductivity k, capillary blood perfusion rate ω and body temperature T_c. To gain insight in the physical phenomena, we have implemented a 3D finite element model. The liver is approximated as a sphere with a diameter of 8 cm and there are two stainless steel electrode tips with a diameter of 1mm and the distance between both electrodes is 2 cm.

Optimization of pulsed voltage profile

In commercial RFA devices, the applied power is usually switched off during an arbitrary time once a certain temperature threshold is exceeded. We on the other hand propose the use of pulsed electromagnetic heat sources [2]. Here, the voltage is switched on until the maximum temperature in the tissue reaches 80°C. Subsequently, the voltage is switched off during a fixed switch-off time τ_f. Varying this τ_f alters the governing

diffusion processes. Figure 1(left) shows the impact of the fixed switch-off time on the temperature build-up at a distance of 5 mm from one electrode (along the line between both electrodes) in function of the activation time. This activation time is the cumulative time of the active phases. It is immediately clear that in the beginning the longer switch-off time of 10 s results in the highest temperature. However, the temperature build-up at longer activation times is higher when using the shorter switch-off times of 2 and 5 s.

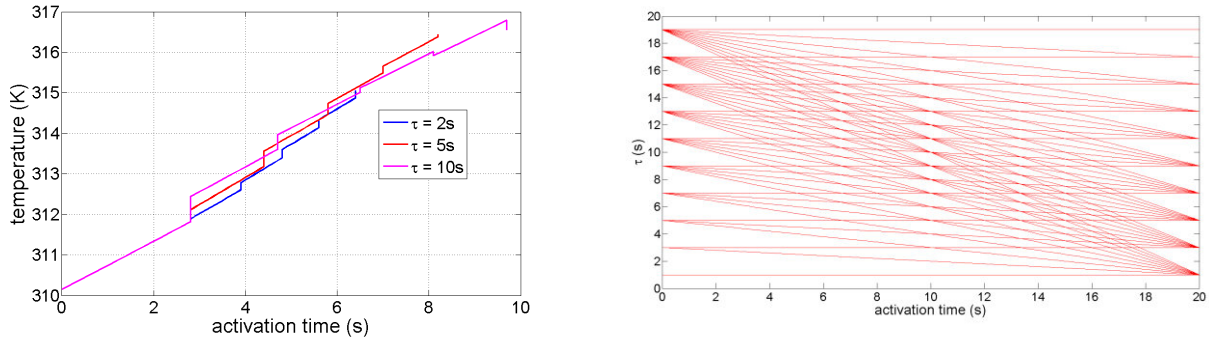

Figure 1. Temperature build-up at a distance of 5 mm from one electrode for different fixed switch-off times (left). Possible switch-off time relations depending on the activation time (right).

This observation motivates our proposal of a linearly decreasing switch-off time in function of the activation time:

(3) $$\tau = a + \frac{b}{10} t$$

where the parameters that need to be optimized are $\alpha = \begin{bmatrix} a & b \end{bmatrix}^T$. We define the cost function F(α) as the temperature in the center of the liver at the last time step. The optimization problem can thus be formulated as:

(4) $$\alpha^* = \arg\max_{\alpha} F(\alpha)$$

subjected to constraints such that $b < 0$ and $\tau > 1$. See the possible switch-off time relations in figure 1 (right).

RESULTS AND DISCUSSION

We performed several numerical analyses by varying the α parameters a and b. The maximum allowed a was 20, whereas the minimal b was -9.5. The optimal α* corresponded with $[5\ -2]^T$. An overview of the simulations is given in figure 2.

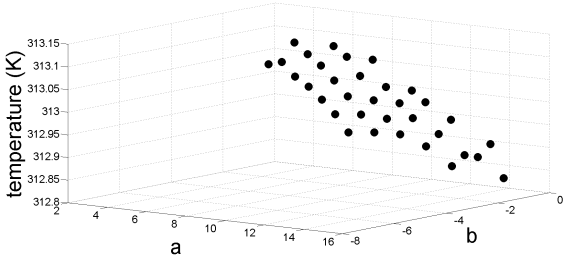

Figure 2. Temperature build-up in center of liver in function of the α parameters.

The optimal parameters result in a larger temperature build-up in the center of the liver, which normally survives a bipolar RFA procedure, and thus increase the efficacy of the treatment. Furthermore, this computer-supported treatment planning makes outcome less dependent on the experience of the treating physician.

REFERENCES

[1] J. Ferlay, I. Soerjomataram, M. Ervik, R. Dikshit, S. Eser, C. Mathers, M. Rebelo, D. Parkin, D. Forman and F. Bray. GLOBOCAN 2012 v1.0, Cancer Incidence and Mortality Worldwide: IARC CancerBase No. 11, 2012.

[2] F. Soetaert, G. Crevecoeur and L. Dupré, Pulsed bipolar radiofrequency ablation for the treatment of liver cancer. XII-th International Workshop on Optimization and Inverse Problems in Electromagnetism, 2012, pp. 96-97.

OPTIMAL PROBE DESIGN FOR LORENTZ FORCE EDDY CURRENT TESTING

Konstantin PORZIG*, Reinhard SCHMIDT*, Marek ZIOLKOWSKI*†, Matthias CARLSTEDT*, Hartmut BRAUER* and Hannes TOEPFER*

*TU Ilmenau, Dept. of Advanced Electromagnetics, Helmholtzplatz 2, 98693 Ilmenau, Germany
†West Pomeranian University of Technology, Dept. of Applied Informatics, Sikorski Str. 37, 70313 Szczecin, Poland

E-mail: konstantin.porzig@tu-ilmenau.de

Abstract. Lorentz force eddy current testing is a contactless method to investigate conductive materials regarding the presence of inclusions and defects. The performance of such a system strongly depends on the applied probe which acts as an electromagnetic field source and sensor at the same time. We propose an optimization strategy to maximize the absolute defect response signal while ensuring technical feasibility. The present study shows that cylindrical magnets should be preferably used for deep lying subsurface defects while Halbach cylinders outperform the latter in case of surface flaws due to a more focal magnetic field.

Keywords: Eddy current testing, Non-destructive testing, Nonlinear programming, Finite element method.

INTRODUCTION

In Lorentz force eddy current testing (LET), a conductive specimen is tested by applying relative motion between a permanent magnet and the object under test [1]. In consequence, eddy currents are induced inside the conductor which are disturbed in presence of a defect. This effect can be measured by a force sensor attached to the permanent magnet due to the presence of Lorentz forces. The principle of LET together with a characteristic perturbation of the drag-force F_x is shown in Fig. 1 together with the geometry and magnetization direction of the Halbach cylinder configuration containing a small iron plate to concentrate the magnetic field on the surface of the moving conductor. The absolute defect response signal (ADS) is defined by the difference between the forces in a conductor free of defects F_{x0} and the point of maximum perturbation F_{xd}. This quantity strongly depends on the geometry and location of the magnet and the defect.

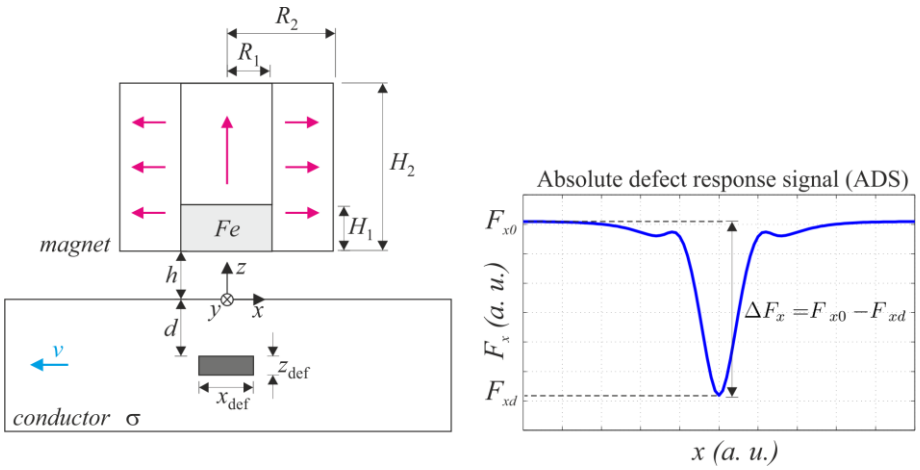

Figure 1. Principle of Lorentz force eddy current testing and cross section of the Halbach cylinder configuration used in the optimization framework to maximize the absolute defect response signal of a defect located in conductive material.

PROBLEM DEFINITION

The goal of the optimization is to maximize the ADS of the LET system (objective function, $f(\mathbf{x})$) by varying the geometric parameters of the magnet (design variables, $\mathbf{x}$) while satisfying the given range of the force sensor (constraints, F_{x0}^{max}) at a given lift-off distance h, velocity v, conductivity σ, defect size (x_{def}, y_{def}, z_{def}) and defect depth d (parameters, $\mathbf{p}$). Table 1 shows the goal function $f(\mathbf{x})$ as well as the inequality constraint $c(\mathbf{x})$ for the drag-force F_x, the design variables $\mathbf{x}$ and the applied limits for the magnet volume V_{mag}.

Table 1. Definition of the optimization problem to maximize the absolute defect response signal (ADS) in LET.

Goal function	Inequality constraint	Design variables	Limits
$f(\mathbf{x},\mathbf{p}) = F_{xd}(\mathbf{x},\mathbf{p}) - F_{x0}(\mathbf{x},\mathbf{p})$ $\min_{\mathbf{x}} f(\mathbf{x},\mathbf{p})$	$c(\mathbf{x},\mathbf{p}) = -\left(\int_{\Omega} \mathbf{j}\times\mathbf{B}\,\mathrm{d}\Omega\right)\mathbf{e}_x - F_{x0}^{max}$ $c(\mathbf{x},\mathbf{p}) \le 0$	$\mathbf{x} = \left\{V_{mag}, \frac{R_1}{R_2}, \frac{H_2}{R_2}, \frac{H_1}{H_2}\right\}$	$0 < V_{\mathrm{mag}} \le V_{\mathrm{mag}}^{\max}$ $0 < R_1/R_2 \le 1$ $0 < H_2/R_2 \le 4$ $0 < H_1/H_2 \le 1$

METHODS

In order to solve the forward problem, a time efficient forward FEM model is developed by using COMSOL Multiphysics [2]. This includes the assumption of low magnetic Reynolds numbers i.e. symmetric field and force profiles. Therefore, the *Weak Reaction Approach* is applied in a three step algorithm [3]. In the first step, the primary magnetic field of the permanent magnet is calculated with a scalar magnetic potential formulation (ψ) in 2D making use of the axisymmetry of the problem which significantly reduces computational cost. In this step, the nonlinearity of the iron plate (*BH* curve) is taken into account. Secondly, the primary magnetic field is transformed to 3D space and the induced eddy currents inside the conductor in motion which is free of defects are calculated by means of a scalar electric potential formulation (φ). In order to determine the ADS, a third simulation is performed, where the conductor contains an equivalent cuboidal defect with volume V_{def} = 50 mm³ of size (5x5x2) mm³ located at a depth of d. This forward solution is used in combination to a sequential quadratic programming (SQP) algorithm using a multi-start approach to avoid convergence to local minima or plateaus.

RESULTS AND CONCLUSION

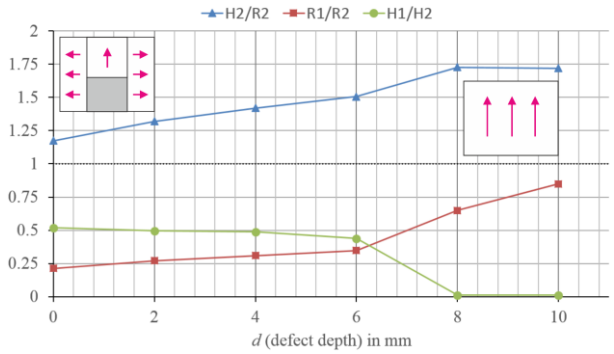

Figure 2. Optimized geometrical parameters of the Halbach magnet as a function of defect depth d.

The optimization is performed for different defect depths, ranging from surface defects at d = 0 mm to deep lying defects at d = 10 mm. The optimized geometrical parameters of the magnet are shown in Fig. 2 as a function of defect depth. All results converged to the defined maximum magnet volume (V_{mag} = 8000 mm³). The constraint of maximum force ($F_{x0}^{\max}$ = 3 N at v = 0.5 m/s and h = 1 mm, σ = 30.61 MS/m) is reached as well, which indicates, that optimal magnet geometries are located at the constraint boundaries. The results in Fig. 2 show, that the geometry of an optimized magnet system depends on the depth of the defect. In case of surface defects, a clear Halbach structure with an iron plate emerged ($R_1/R_2 < 1$, $H_1/H_2 > 0$). However, with increasing defect depth, the optimized structure tends towards a standard cylinder without any ferromagnetic material ($R_1/R_2 \to 1$, $H_1/H_2 \to 0$).

CONCLUSION

The present work provides a first approach to increase the ADS in a LET system to detect defects in electrical conductive materials. The study showed, that the underlying conditions and the detection goal clearly defines the geometry of an optimized magnet system. A Halbach magnet supported by passive ferromagnetic material outperforms standard cylinders in case of defects located close to the surface of the conductor. However, for the detection of deep lying defects, standard cylindrical magnets are proposed. Future work will be related to experimental validation of the results.

REFERENCES

[1] R. P. Uhlig, M. Zec, H. Brauer and A. Thess. Lorentz force eddy current testing, a prototype model. Journal of Nondestructive Evaluation, vol. 31, 2012, pp. 357-372.

[2] COMSOL Multiphysics®. 2014. Version 4.4. COMSOL, Inc., Burlington, MA, USA.

[3] M. Zec, R. P. Uhlig, M. Ziolkowski and H. Brauer. Finite element analysis of nondestructive testing eddy current problems with moving parts. IEEE Transactions on Magnetics, vol. 49, 2013, pp. 4785-4794.

OPTIMIZATION OF ENERGY STORAGE SCHEDULING IN ENERGY HUBS

Arianna GHEZZI*, Giambattista GRUOSSO**, and Maurizio REPETTO***

*MONET Srl, Via Vittorio Amedeo II 22, 10121 Torino, Italy, E-mail: a.ghezzi@monet-tech.it

**Dip. di Elettronica Informazione e Bioingegneria, Politecnico di Milano, Piazza L.Da Vinci 32, 20133 Milano Italy, E-mail: gruosso@elet.polimi.it

*** Dip. Energia, Politecnico di Torino, C.so Duca degli Abruzzi 24, 10129 Torino, Italy, E-mail: Maurizio.repetto@polito.it

Abstract. A energy hub is a local energy system where generation, loads and storage are interacting among them and with external infrastructure. The power production scheduling of the various modules can be handled by an optimization procedure that tries to minimize the overall energy cost on a given time period, for instance one day. In this paper a new kind of shape functions is used to model the power going in and out of the storage system. These functions satisfy some basic properties of the storage and reduce the number of degrees of freedom of the optimization. The new shape functions are described and some examples, showing their advantages, are presented.

Keywords: Energy Management, Energy hub, Energy storage, Pattern Search.

INTRODUCTION

The management of energy systems with storage must rely on some strategy for its usage. If a renewable power source is present, for instance a Photo-Voltaic (PV) plant, energy produced by the source, in excess to user request, can be stored for later use. Due to the variability of energy output by renewables and to the limited size of the storage, this strategy must be adapted on the basis of weather and load forecasts to be sure that all surplus energy can be stored and used when it is most convenient, for instance when the price of energy purchased from the grid is more expensive. In addition technical constraints of the energy storage module, as for instance maximum and minimum value for stored energy, maximum power etc. must be satisfied.

This problem is often approached by means of the definition of a scheduling time interval, for instance one day, and discretizing it in a number N_i of sub-intervals, within which the quantities defining the power flow within the system, for instance a produced power, are considered as constant. In this way, the operating quantities become the variables of the optimization problem. If the number N_i of time intervals becomes large particularly efficient optimization procedures, able to deal with large scale problems, must be employed, as for instance Mixed Integer Linear Programming [1, 2]. This approach is quite efficient for the off-line optimization of energy hubs when powerful computational resources can be employed. Otherwise, when an on-line optimization has to be performed, the computational tools available are constrained by the hardware dedicated to the management usually limited in computational resources like memory and speed. A drastic reduction of the number of optimization variables can be achieved by formulating the problem not in terms of instant quantities but as sum of particular shape functions approximating the time behavior of the power quantities with a lower number of degrees of freedom.

APPROXIMATION OF STORAGE POWER

The storage module inserted inside a PV based energy hub is generally used on a one day cycle: it is charged during the day, when PV is supplying power, and is discharged in the other hours. The first hypothesis that can be made is about periodicity of the storage management: at the end of the one day process storage must be left in the same state that at in the beginning. In this way the storage power must have a null net balance. The simplest shape that satisfies this assumption is reported in Figure 1 and is made up by two pulses of equal width τ, that can be delayed by means of the two values δ_1 and δ_2 to fit with the PV production and with the load demand. Energy storage is represented by the load convention so that a positive value of power means a charging power. The shape function is defined as periodic in the 24 hours period so that if part of the pulses overflows the midnight, it is applied in the first hours of the day, as shown in figure 1 (b). In Figure 2 the application of the storage shape function to a case of one day scheduling on a quarter of hour base is shown. The system is made up of on PV plant and by a load whose profiles are defined. For each of the 96 time instants, the power balance equation is given by:

$$P_{grid} + P_{PV} - P_{st} - P_{load} = 0 \tag{1}$$

so that, once the optimizer has defined the power going in/out of the storage P_{st} for all 96 time intervals, the power purchased by the grid is obtained as difference. The use of the proposed approach has allowed the reduction of the degrees of freedom from 96 to 6. The objective function is defined as:

$$o = \sum_{i=1}^{N_i} c_p(t_i) P_{grid}(t_i) \Delta t \tag{2}$$

where c_p is the unit power purchasing price and Δt is the time discretization step. In this case a Pattern Search algorithm is used to reduce the energy cost which depends on the electrical power purchased from the electrical grid. In the present example, the procedure has reached a cost reduction factor of 44 during the search in 92 iterations. Figure 2 (a) shows the time behaviors of the power quantities and it highlights how the process has reduced the consumption of grid power.

The use of an efficient scheme for representing the power flows in and out of the storage is a key issue for reducing the number of degrees of freedom enabling the optimization even under scarce computational resources.

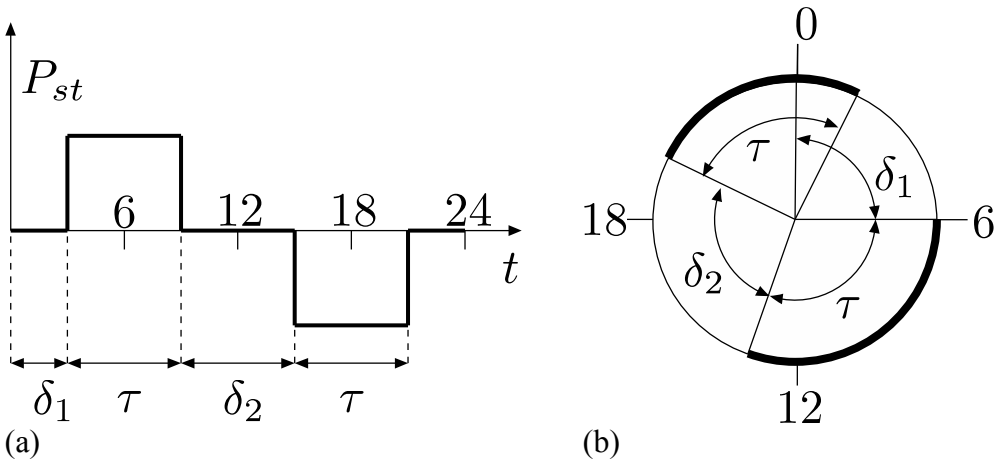

Figure 1. Shape function for storage power description. (a) on a 24 hour basis basis; (b) as a periodic 24 hours time basis.

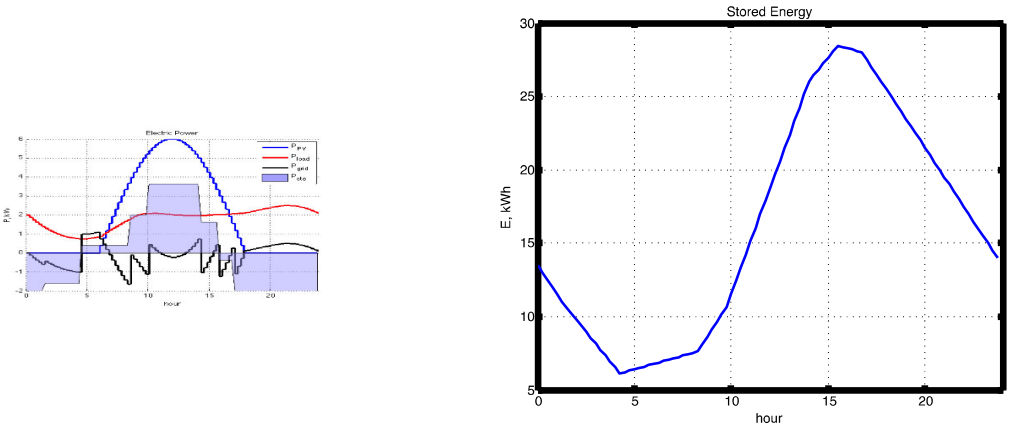

Figure 2. Diagram of power flows inside the energy hub (a) and of the stored energy (b).

REFERENCES

[1] M. Geidl, G. Andersson, Optimal power flow of multiple energy carriers, IEEE Transactions on Power Systems 22 (1) (2007) 145–155.

[2] A. Canova, C. Cavallero, F. Freschi, L. Giaccone, M. Repetto, M. Tartaglia, Comparative economical analysis of a small scale trigenerative plant: A case study, 2007, pp. 1456–1459. M. Young. *The Technical Writer's Handbook.* Mill Valley. CA, University Science, 1989.

A GENERIC INVERSE PROBLEM ALGORITHM FOR THE IDENTIFICATION OF THE MAGNETIC MATERIAL PROPERTIES OF ELECTROMAGNETIC DEVICES COUPLED WITH STOCHASTIC UNCERTAINTY ANALYSIS

Ahmed ABDALLH and Luc DUPRÉ

Department of Electrical Energy, Systems and Automation, Ghent University,

Sint-Pietersnieuwstraat 41, BE-9000, Ghent, Belgium

E-mails: ahmed.abdallh@ieee.org, luc.dupre@ugent.be

Abstract. Magnetic characteristics of the core materials of electromagnetic devices are retrieved by solving a combined experimental-numerical electromagnetic inverse problem. However, both measurement noise and uncertainties of the forward model may deteriorate the accuracy of the recovered solution. In this perspective, we review the use of the electromagnetic inverse problem for the identification of the magnetic material properties. The inverse algorithm is combined with a stochastic uncertainty analysis for *a priori* qualitative error estimation and a quantitative error reduction. The complete inverse methodology is applied onto the identification of several macroscopic properties of the magnetic material of a wide range of rotating electrical machines. Numerical and experimental validations of the proposed approach are presented. This complete inverse algorithm can be applied into a wide range of applications in electromagnetic community.

Keywords: Inverse problem, magnetic material characterization, stochastic uncertainty analysis.

INTRODUCTION

Soft magnetic materials are present in many electromagnetic devices and are widely used in industrial applications. In order to analyze magnetically such applications, e.g. by numerical techniques, the magnetic characteristics of the material inside the device have to be known. There are several standard measurement techniques for characterizing magnetic materials, e.g. an Epstein frame is commonly used for identifying the magnetic properties of a material. However, this requires extra samples of the magnetic material used in the electromagnetic device. These extra samples are often not available. Moreover, the characteristics of the magnetic material may be altered during the device manufacturing. Therefore, it is convenient to characterize the material on the specific geometry of the device itself. In practice, the direct identification of the magnetic material exclusively based on magnetic measurements is quite difficult and sometimes impossible, due to the complexity of the electromagnetic device geometry. Therefore, an alternative method is needed.

Recently, the authors have reconstructed some important macroscopic magnetic features, such as a single-valued *B-H* curve, hysteresis loop, and iron loss parameters, of the core material of several rotating electric machines by a combined experimental-numerical electromagnetic inverse problem [1] - [3]. These inverse problems are coupled with a stochastic uncertainty analysis in order to estimate and/or reduce the error originates from different kinds of uncertainties. The goal of this paper is to present the complete algorithm of this unified electromagnetic inverse approach.

METHODOLOGY

Basically, in order to estimate the unknown parameters $\mathbf{x}$, an inverse problem has to be solved by iteratively minimizing the residuals between the experimental observations of the magnetic system $\mathbf{W}$ and the modeled ones $\mathbf{\Phi}$. In other words, the functional $\mathrm{T} = \|\mathbf{W} - \mathbf{\Phi}(\mathbf{x})\|^2$ needs to be minimized $\tilde{\boldsymbol{x}} = \operatorname{argmin} \mathrm{T}$, with $\tilde{\boldsymbol{x}}$ being the recovered unknown parameters using the inverse approach. The resolution of the inverse procedure highly depends on both measurements and modeling accuracy. In other words, T can depend on the definition of the inverse problem, i.e. the place where the measurements are conducted, the objective function to be minimized, etc. This resolution is due to measurement noise, available uncertainties in the forward mathematical model parameter values, or the simplifications in the used model.

In practice, the actual measurements $\mathbf{W}$, can be expressed as $\mathbf{W} = \mathbf{\Phi}(\mathbf{x}) + \boldsymbol{e}_n + \boldsymbol{e}_m$, with $\boldsymbol{e}_n$ and $\boldsymbol{e}_m$ being the measurement noise and the modeling uncertainties, respectively. In fact, the modeling error $\boldsymbol{e}_m$ can be divided into two main parts: the modeling error due to the uncertainty of some model parameters $\mathbf{b}$, and the modeling error due to the simplification of the used mathematical model. Due to such errors, when minimizing the cost function T, the values of the recovered parameters $\tilde{\boldsymbol{x}}$ and the actual parameter values $\boldsymbol{x}^*$ are not necessary equal, i.e. $\tilde{\boldsymbol{x}} \neq \boldsymbol{x}^*$.

Error estimation in the inverse problem solutions

In order to *a priori* estimate, in a qualitative way, the level of inaccuracy in the inverse problem solution due to noisy measurements and/or uncertainties in the model parameters, we propose to use the stochastic Cramér-Rao lower bound (sCRB) technique. The sCRB is based on the calculation of the Fisher Information matrix, which is based on the sensitivity analysis of the forward model to the uncertain parameter.

Error reduction in the inverse problem solutions

However, estimating 'qualitatively' the error in the inverse problem is not enough, the developed algorithm should decrease that error as well. Therefore, two efficient numerical techniques, namely the minimum path of the uncertainty (MPU) technique and the stochastic Bayesian approach, have been used for minimizing 'quantitatively' the modeling error.

The mathematical proof of the aforementioned techniques, as well as the numerical and experimental validation, will be given in the full paper. Fig. 1 shows the general flow chart of the combined experimental-numerical inverse algorithm for the identification of magnetic material properties of an electromagnetic device

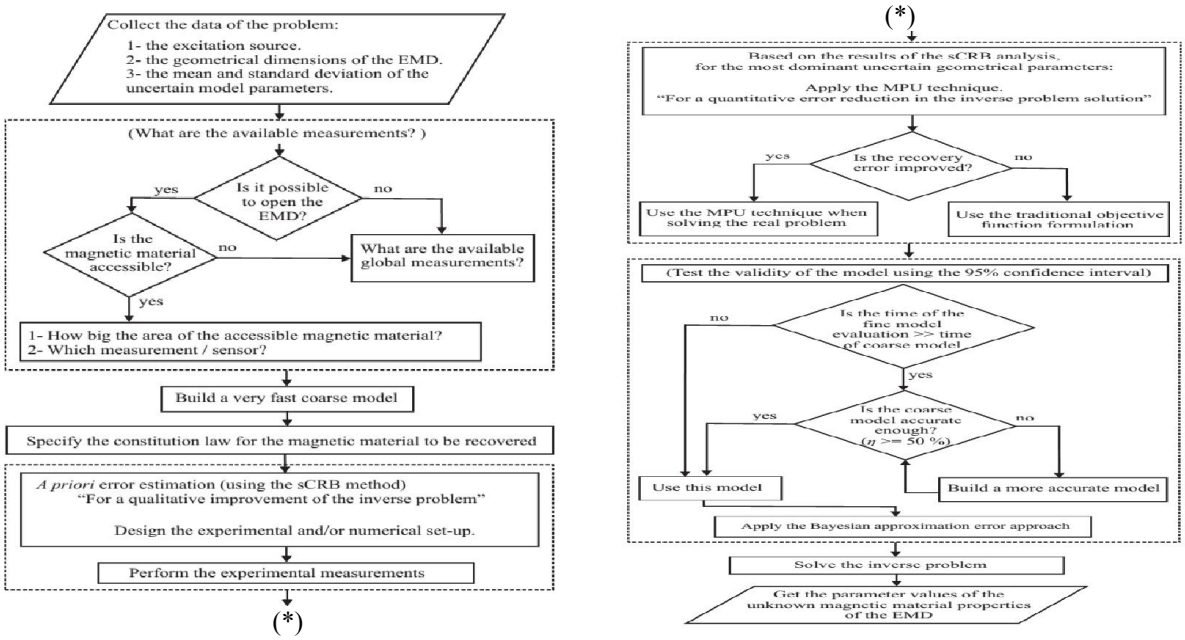

Figure 1: The general flow chart of the combined experimental-numerical inverse algorithm for the identification of magnetic material properties of an electromagnetic device, [3].

CONCLUSIONS

An efficient coupled experimental-numerical inverse problem is proposed for characterizing the properties of a magnetic material. The proposed methodology is not only capable of estimating *a priori* the error in the inverse problem solution, but also to reduce quantitatively such errors.

ACKNOWLEDGEMENTS

The authors gratefully acknowledge the financial support of the Special Research Fund (BOF) of Ghent University.

REFERENCES

[1] A. Abdallh, An inverse problem based methodology with uncertainty analysis for the identification of magnetic material characteristics of electromagnetic devices. Ph.D. Thesis, Ghent University, Belgium, 2012. Available online: https://biblio.ugent.be/publication/2125626.

[2] A. Abdallh and L. Dupré, "Magnetic material characterization using an inverse problem approach," book chapter in Advanced Magnetic Materials, ISBN 978-953-51-0637-1, InTech, 2012.

[3] A. Abdallh and L. Dupré, A unified electromagnetic inverse problem algorithm for the identification of the magnetic material characteristics of electromagnetic devices including uncertainty analysis: A review and application, IEEE Trans. on Magn., in-review.

HIGHER-ORDER MULTIOBJECTIVE DESIGN OF MEMS

Paolo DI BARBA*, Antonio SAVINI* and Sławomir WIAK**

* University of Pavia, Dept of Electrical, Computer and Biomedical Engineering, Via Ferrata 5, I-27100 Pavia
E-mail: paolo.dibarba@unipv.it, savini@unipv.it

**Łódź University of Technology, Inst. of Mechatronics and Information Systems, ul. Stefanowskiego 18/22, 90-924 Łódź, slawomir.wiak@p.lodz.pl

Abstract. An evolution strategy approximating a single Pareto-optimal solution in an objective space exhibiting more than two objectives, and a modification of a standard NSGA-II code controlling the spread-out of unfeasible solutions are proposed. The optimal design of a magnetic micro-switch is considered as the case study.

Keywords: evolutionary computing, finite-element analysis, MEMS, multiobjective optimal design.

INTRODUCTION

The automated optimal design of MEMS might be approached in a systematic way in terms of non-linear multi-objective optimization of objective functions subject to a set of constraints [1]. In particular, higher-order optimization problems exhibit three objective functions or more. In this respect, finite-element method and evolutionary computing are a standard approach to field analysis and synthesis, respectively.

Mutation is the main operator in an evolution strategy algorithm: the best between parent and offspring survives in the next generation. Should an offspring violate constraints, it is overlooked; so, if a set of parents generates a set of offsprings within a parallel-processing scheme, the failure of a single offspring to fulfil constraints has no influence on the other parallel-processed offsprings. However, the diversity of population might be modest.

In turn, cross-over is the main operator in non-dominated sorting genetic algorithms (NSGA): the recombination of a pair of genes within the current chromosome substantially enhances the diversity of solutions; however, the probability of constraint violation might be high. In fact, diversity and feasibility are somehow in conflict, and the failure of a gene pair tends to spread out of the feasible region in an uncontrolled way.

Moving from these remarks, two methodological issues are here proposed: an evolution strategy approximating a Pareto-optimal solution in an objective space exhibiting more than two objectives, and a straightforward modification of a standard NSGA-II code [2] controlling the spread-out of unfeasible solutions.

OPTIMIZATION METHODS

Individual-based: Paretian evolution strategy (P-EStra)

An offspring is accepted if, and only if, it strongly dominates all the objectives, provided problem constraints are fulfilled. As a consequence, the algorithm finds a trajectory leading the start solution substantially closer to a single non-dominated solution. The algorithm stops if the search radius is small enough.

Population-based: modified NSGA-II

It is assumed that the initial population composed of n_p individuals fulfils constraints. Should the i-th individual of the j-th generation be unfeasible, it is replaced by the k-th out of n_p randomly selected in the initial population ($i=1,n_p$, $j=1,n_g$, $k=1,n_p$). The algorithm stops after n_g generations.

CASE STUDY: MAGNETIC MICROSWITCH

Field analysis problem

A micromagnetic device used as an optical switch [3] is considered (Fig. 1) as the case study: it consists of a NdFeB magnet, two conductors carrying like currents, and a ferromagnetic plate (mirror) free to rotate around its axis. The torque holding the plate at the prescribed angle is due to the field of the permanent magnet in the absence of current, while the actuation torque necessary to switch the plate angle is due to the field variation caused by a current pulse in the conductors. The 2D field analysis problem consists of finding the magnetic field distribution given device geometry, plate angle and current value; a typical finite-element mesh is composed of 2,300 triangles; second-order polynomial Lagrangian elements are considered, originating approximately 75,000 nodal unknowns. The corresponding torque-angle curve has been computed based on the virtual work principle.

Optimal design problem and results

While in [4] the conflict of sensitivity and design criterion was investigated, here a 3D objective space is considered. The optimal design problem reads: having prescribed lower thresholds for holding torque (10^{-8} Nm) and actuation torque (10^{-9} Nm), given mirror position $\phi = 10°$, find the geometry of magnet and conductors, as well as the current pulse amplitude, such that: power loss in conductors (f_1), weigthed material cost (f_2), and excitation system volume *i.e.* conductors and magnet, (f_3) are simultaneously minimized in the Pareto sense. P-EStra results are shown in Fig. 2: it can be remarked that objective functions and design variables change substantially. In turn, modified NSGA-II results are shown in Fig. 3. Constraints are violated at each generations (Fig. 4): the number of swapped individuals per generation varies between 5 and 14 out of 20, but final solutions are all feasible and improve the initial ones.

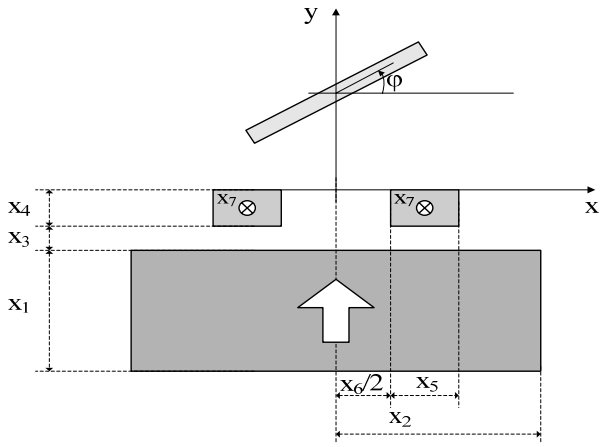

Figure 1. Geometry of the magnetic MEMS and design variables: x_1 magnet height, x_2 magnet length, x_3 magnet air-gap, x_4 conductor height, x_5 conductor length, x_6 conductor air-gap, x_7 current pulse amplitude. The plate gravity-centre is located 500 μm above the x axis (plate size: 1 mm times 25 μm times 500 μm).

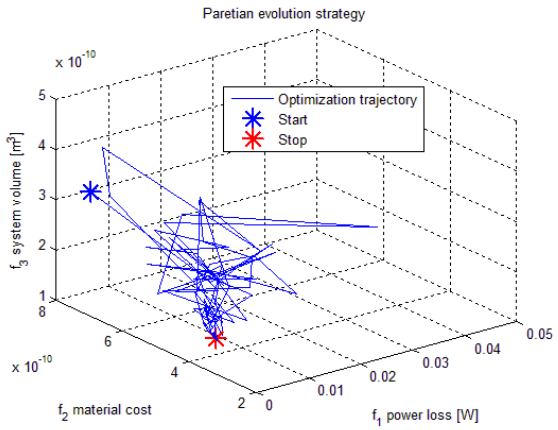

Figure 2. Paretian evolution strategy: optimization trajectory in the objective space.
Objective function movement $f_k(stop)/f_k(start)$, k=1,3 : 0.218, 0.444, 0.507.
Design variable movement $x_k(stop)/x_k(start)$, k=1,7 : 1.098, 0.841, 0.159, 1.066, 0.902, 0.388, 0.298.

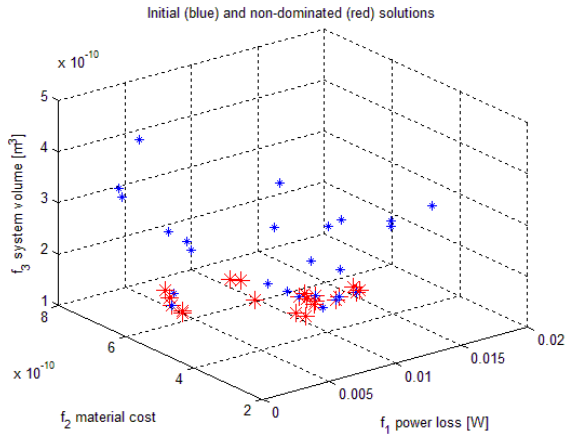

Figure 3. Modified NSGA-II: 20 individuals, 50 generations (genetic operators: simulated binary crossover with probability 0.9, polynomial mutation with probability 0.1).

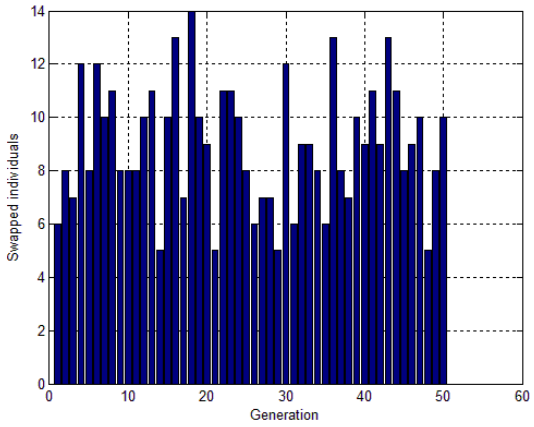

Figure 4. Modified NSGA-II: failure of offsprings against generation.

CONCLUSIONS

Two methods of higher-order multiobjective optimization based on evolutionary computing have been proposed and compared. An application in MEMS design has been presented.

REFERENCES

[1] R. Chereches, P. Di Barba, V. Topa, M. Purcar, S. Wiak, "Optimal shape design of electrostatic microactuators. A multiobjecitve formulatiom", *IJAEM*, 30 (2009), 65-76.

[2] NSGA-II: www.iitk.ac.in/kangal/codes [last visited July 2013]

[3] B. Delinchant, H.L. Rakotoarison, V. Ardon, O. Chabedec and O. Cugat, "Gradient based optimization of semi-numerical models with symbolic sensitivity: Application to simple ferromagnetic MEMS switch device", *IJAEM*, 30 (2009), 189-200.

[4] P. Di Barba, A. Savini, and S. Wiak, "Minimizing design criterion and sensitivity: a cost-effective evolutionary approach with applications in Mechatronics", Proc. ISEF-2013. In press on *IJAEM*.

A ROBUST MULTI-OBJECTIVE DESIGN OF ELECTROMAGNETIC DEVICES

Min LI*, Rodrigo SILVA*, Armin SALIMI*, Frederico GUIMARÃES** and David LOWTHER*

* McGill University, Department of Electrical and Computer Engineering, 3480 University, H3A 0E9, Montreal, Canada
E-mail: david.lowther@mail.mcgill.ca

** Universidade Federal de Minas Gerais, Department of Electrical Engineering, 6627 Avenida Presidente Antônio Carlos, Belo Horizonte, MG 31270-010, Brazil

Abstract. This paper presents a robust formulation for multi-objective design problems. The robustness of solutions, expressed as maximum deviation from the nominal performance, is controlled by a constraint specified by the designer while the mean performance is being optimized. This robust design formulation does not increase the number of objectives in the problem and is easy to incorporate into some of the existing multi-objective genetic algorithms (MOGA), such as the non-dominated sorting genetic algorithm (NSGA).

Keywords: Electrical machine design, Multi-Objective optimization, Robust design.

INTRODUCTION

Robust design seeks solutions that are less sensitive to variations in the design variables and environmental conditions. A multi-objective approach for robust design is employed for a single objective design optimization problem, where the mean and variance of the solutions are treated as conflicting objectives [1]. Another multi-objective robust design approach is proposed in [2] using alternative objectives which are easier to compute. This paper proposes a method which extends the robust design formation in [2] for multi-objective design problems without doubling the number of objectives.

METHODOLOGY

Multi-objective approach to robust design

A robust design problem may be defined in a multi-objective way with respect to statistical quantities as:

$$\min\begin{bmatrix} E[f(x)] \\ V[f(x)] \end{bmatrix}, \tag{1}$$

where f(x) is a scalar objective function, $E[f(x)]$ is the mean value and $V[f(x)]$ is the variance of f.

Another approach considered equivalent to (1), is given in [2] as:

$$\min\begin{bmatrix} f(x) \\ f_w(x) - f(x) \end{bmatrix}, \tag{2}$$

where f_w(x), the worst case value of f on an uncertainty set U(x), is defined as:

$$f_w(x) = \max_{\xi \in U(x)} f(\xi) \cdot \tag{3}$$

The nominal value, $f(x)$, is a good approximation of the mean value under the assumption of a normal distribution of x, and $f_w(x) - f(x)$ can be viewed as the maximum deviation from the mean. This robust design formulation may be extended to multi-objective design problems. However, a drawback is that it doubles the number of objectives in the original design problem.

Robust design for multi-objective optimization problems

In order to avoid adding more objectives to the original problem, (1) can be transformed to:

$$\begin{aligned} &\min E[f_i(x)] \quad i = 1,2,...,n \\ &s.t. V[f_i(x)] \le \sigma_i \end{aligned}, \tag{4}$$

where the variances of f_i can be treated as constraints to guarantee robustness. In practice, we may use $f_w(x) - f(x)$ instead of $V[f(x)]$, since this information is easier to compute.

Figure 1 shows a model of an interior permanent magnet (IPM) motor in a design problem. The two objectives are the torque ripple (%) and the average torque (Nm). For a given solution, we plot the variation of the function values (using a Monte-Carlo simulation) in the objective space over an uncertainty set. The nominal value of the two objectives, (f_1, f_2), is shown in the center of the figure; and the worst cases in each objective (f_{1w} and f_{2w}) are indicated with black triangles. As can be observed, the distances between the worst case values and the nominal values provide a good measure for the maximum deviation of the perturbed objective function values from the nominal value.

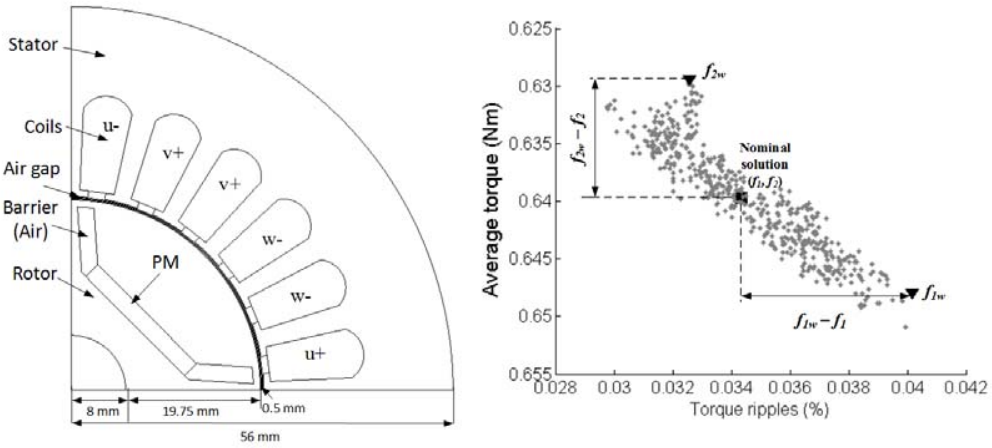

Figure 1: IPM design set up and objective function values

Thus a robust design scheme for multi-objective optimization can be formulated as:

$$\begin{aligned} &\min\ f_i(x) \quad i = 1,2,...,n \\ &s.t.\ |\ f_{iw}(x) - f_i(x)\ | \le \tau_i \end{aligned} \tag{5}$$

where τ_i can be defined by the designer for controlling the deviation of the performance.

Combining the robustness measure with MOGA

NSGA-II is a popular algorithm for solving multi-objective optimization problems [3]. We can incorporate the robust design formulation defined in (5), into the algorithm by defining a new dominance relation in a similar fashion to the work done in [4], [5]. For two solutions A and B, solution A is said to 'robust-dominate' a solution B, if any of the following conditions are true:

1. If A is feasible (robust) and B is not.

2. Solutions A and B are both infeasible, but the worst-cases of A dominates the worst cases of B (based on the usual Pareto dominance).

3. If A and B are both feasible (robust), the nominal value of A dominates that of B.

CONCLUSIONS

This paper presented a novel robust design formulation for multi-objective optimal design problems. The robustness (variance) of the solution is guaranteed with a constraint defined by the designer. And the number of objectives in the robust design problem stays the same as that of the original design problem. In the extended paper, the feasibility robustness (to avoid constraint violation) will also be studied and the Pareto front of robust solutions of an IPM motor design will be presented.

REFERENCES

[1] S.-B. Yoon, I.-S. Jung, D.-S. Hyun, J.-P. Hong, and Y.-J. Kim, "Robust shape optimization of electromechanical devices," *Magnetics, IEEE Transactions on*, vol. 35, pp. 1710-1713, 1999.

[2] F. G. Guimaraes, D. A. Lowther, and J. A. Ramirez, "Multiobjective approaches for robust electromagnetic design," *Magnetics, IEEE Transactions on*, vol. 42, pp. 1207-1210, 2006.

[3] K. Deb, A. Pratap, S. Agarwal, and T. Meyarivan, "A fast and elitist multiobjective genetic algorithm: NSGA-II," *Evolutionary Computation*, IEEE Transactions on, vol. 6, no. 2, p. 182.97, 2002.

[4] K. Deb, A. Pratap, and T. Meyarivan, "Constrained test problems for multi-objective evolutionary optimization," in *Evolutionary Multi-Criterion Optimization*, 2001, pp. 284-298.

[5] M. Miyakawa, K. Takadama, and H. Sato, "Two-stage non-dominated sorting and directed mating for solving problems with multi-objectives and constraints," presented at the Proceedings of the 15th annual conference on Genetic and evolutionary computation, Amsterdam, The Netherlands, 2013.

13th International Workshop on Optimization and Inverse Problems in Electromagnetism
September 10 – 12, 2014, Delft, The Netherlands

DESIGN OF OPTIMAL MAGNETIC CIRCUITS BASED ON EFFICIENT PENALIZATION FUNCTIONS VIA DENSITY METHODS

Satafa SANOGO* and Frédéric MESSINE*

*Université de Toulouse, Laplace (CNRS UMR5213, Toulouse INP), F- 31071 Toulouse

{sanogo, messine}@laplace.univ-tlse.fr

Abstract. The design of magnetic circuit structures for electric space thrusters is difficult inverse problems. Indeed, they are often formulated as discrete nonlinear and nonconvex large-scale optimization ones. To solve them the variables has to be relaxed from discrete to continuous and then by using an adjoint variable method to compute the gradient, a local search optimization algorithm can be performed. Nevertheless, a penalization method has to be added to render the optimal solutions the closest possible as discrete ones. In this paper, we focus on this last point by proposing some generalized interpolation schemes and by showing their great efficiency on numerical examples.

Keywords: Adjoint Variable Method, Intermediate values, Inverse problem, Thrusters, Topology Optimization.

INTRODUCTION

For designing a device, the engineers generally solve direct problem with the aid of simplified models by defining the device structure and its parameters and then they deal with the technical specifications and modifications. The obtained solutions are based on intuitions and empirically studies with previous experiences. In this paper, we bring methods and approaches to formulate mathematically the inverse problem like an optimization one. For instance, with a given magnetic cartography in a part Ω_T of the design domain Ω which is represented numerically by its magnetic field value denoted B_0, we want to design a device, which will be able to produce this flux distribution. In this case, a suitable objective functional is to minimize the error between a computed value B in the target area Ω_T and B_0. For such a problem the variables are material properties and sources. In addition, we have also some geometric constraints and the values of the different used materials and sources are bounded. **Figure 1.** (a) shows the principle of the inverse problem. In this works, we focus on the topology of magnetic circuit depending on a ferromagnetic material distribution and we consider as material properties and sources, the permeability (μ), the current density (J) and the permanent magnet (M). The design system parameter μ, J and M are variable in $\Omega_v(\mu)$, $\Omega_v(J)$ and $\Omega_v(M)$ respectively (and fixed otherwise), see **Figure 1.** (b). Then, these parameters are represented by the vector **p**.

Solution methods are based on the SIMP method (Solid Isotropic Material with Penalization) [1, 2, 3], which is a material density method and is also a variant of the homogenization method. The SIMP approach is among the most widely used in TO algorithm, owing to its efficiency. Moreover, most TO software own an implementation of SIMP technique. In this approach, two functions are introduced. A first one denoted by ρ to define amount of material in each point of the design domain, $\rho(x)$ belongs to [0,1] for all point x in Ω and $\rho = 1$ for material points with strong property ($\mathbf{p}_{max}$) and $\rho = 0$ in weak property ($\mathbf{p}_{min}$) material points. This continuous functional ρ is then considered as a design variable, see **Figure 1.** (c). A second one, denoted by g to parameterize the material properties in function of ρ in each point and verify $g(\rho(x)) = \mathbf{p}(x)$ such that $g(0) = \mathbf{p}_{min}$ and $g(1) = \mathbf{p}_{max}$ where $\mathbf{p}(x)$ is the material property at the point x of the design space.
The functions ρ and g are called material density function and Material Interpolation Scheme (MIS) or penalization function respectively.

We get an analytical expression of the design sensitivity by using adjoint variable method. Then, we can apply a descent-based algorithm such as quasi-newton algorithm. Indeed in general, these optimization algorithms are the most efficient, more details can be found in [1].

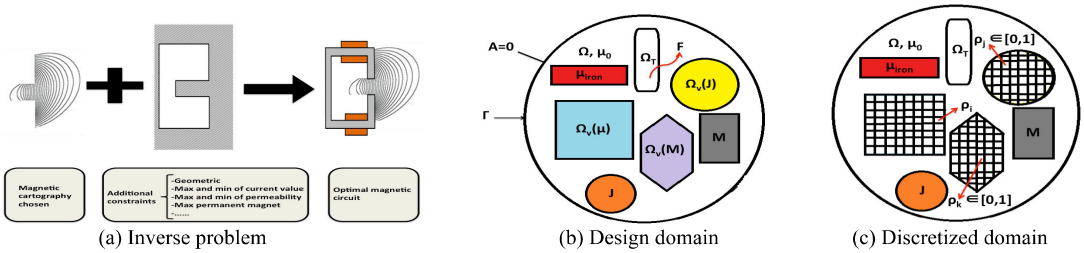

(a) Inverse problem (b) Design domain (c) Discretized domain

Figure 1. (a) Principle of an inverse problem for designing an electromagnetic circuit. (b) The considered design domain of our topology optimization problem with different variable areas and the objective function defined in the target area. (c) The material density ρ (ρ_1, …, ρ_i,…, ρ_N) is defined over design mesh.

PROPOSED PENALIZATION FUNCTIONS

With the SIMP method, the challenges are both convergence problems and how to interpret the intermediate densities (ID) (for $0 < \rho < 1$) in term of physical materials of our disposal for designing the devices. Then, a common technique consists to use the function g for reducing the emergence of these intermediate values in the final optimal design. In the literature, we find a classical MIS function given by [1, 2, 3]:

(1) $g_{c,n}(\rho) = \mathrm{p_{min}} + (\mathrm{p_{max}} - \mathrm{p_{min}})\rho^n$, with $\rho \in [0,1]$ and $n > 1$.

Formula (1) is the most used due to its simplicity (encoded facilities). The exponent n is the penalty factor indeed the number of ID decreases when n increases, thus that give us a control on the appearance of ID in the optimal solution. The difficulties here are that $g_{c,n}$ induces some numerical instabilities and bad convergence at the neighbourhood of 0 and especially with high values of the penalty factor.

In this paper, we propose some alternative MIS, which are most efficient to avoid numerical difficulties and present a weak rate of ID in the optimal solution comparing to the classical MIS. These new penalization functions are polynomial and more general than (1) since we consider all the monomials $(\rho^i, i = 1, \dots n)$, they are given by:

(2) $g_n(\rho) = a_0 + a_1\rho + \cdots + a_n\rho^n$, with $\rho \in [0,1]$, $n > 1$ and $a_i \in \mathbb{R}$.

Like in (1) n is the penalty factor. The formula (2) has the efficient of the classical MIS to prevent the appearance of ID and the qualities of filtering technique to introduce numerical stability [3]. In (2), we impose to the weight a_1 to be nonzero in that case this new penalization function has always a linear part. And that permits to deal with any neighbourhood of 0 without numerical difficulties. In addition, the choice of the set $(a_i)_i$ can be done with properties of the function g_n described in the introduction. This choice depends also on the considered design problem. For numerical simulations, we propose the following polynomial MIS:

1. Uniform sequence MIS function: (3) $g_{u,n}(\rho) = a_0 + a_1 \sum_{i=1}^{n} \rho^i$, $a_0 = \mathrm{p_{min}}$, $a_1 = \frac{\mathrm{p_{max}} - \mathrm{p_{min}}}{n}$.
2. Geometric sequence MIS function: (4) $g_{g,n} = a_0 + \sum_{i=1}^{n} a_1 \alpha_1^{i-1}\rho^i$, $a_0 = \mathrm{p_{min}}$, $\alpha_1 = 10$.
3. Arithmetic-Geometric sequence MIS function: (5) $g_{ag,n} = a_0 + \sum_{i=1}^{n} \left[\alpha_1^{i-1}\left(a_1 - \frac{\alpha_0}{1-\alpha_1}\right) + \frac{\alpha_0}{1-\alpha_1}\right]\rho^i$, $\alpha_0 = 1.5$, $\alpha_1 = 0.01$.

CONCLUSIONS

In previous works, we have proposed a TO code for designing a Hall effect Thruster magnetic circuit. We have performed with this Solver 198 testing problems in order to evaluate the performance of our proposed penalization functions (3), (4) and (5) and the classical (1). This performance was based on the technique introduced in [4]. And two criteria was analyzed: the number of ID in the optimal design (τ), the minimum value of the cost function (fopt). In conclusion, the performance profile of the different scheme depicted on **Figure 2**., it is clear that our proposed polynomial penalization functions are more benefit. Moreover for the Uniform sequence MIS function the performance is the best with respect to both criteria.

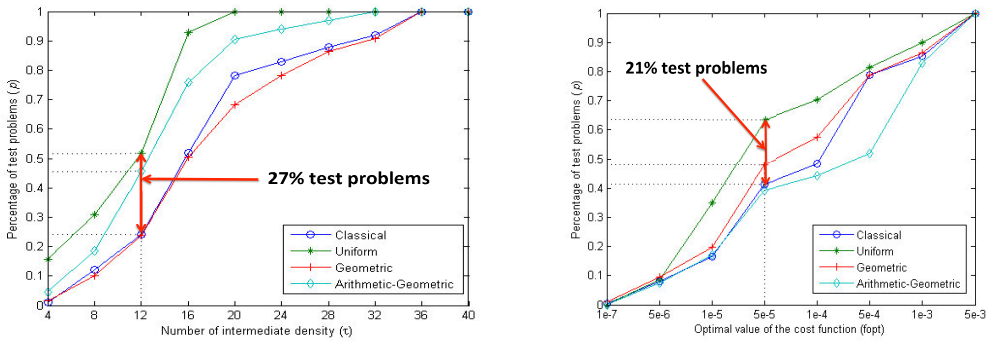

(a) Performance Profiles for intermediate densities (b) Performance Profiles for the objective function value

Figure 2. Performance profile analysis by implementing in our TO code the selected schemes. Straight segments in dotted show the different ratio for τ = 12 and fopt = 5e-5.

REFERENCES

[1] S. Sanogo, F. Messine, C. Hénaux and R. Vilamot, Topology Optimization for Magnetic Circuits dedicated to Electric Propulsion , submitted in IEEE Trans Mag (2014).

[2] G. I. N. Rozvany, Aims, scope, methods, history and unified terminology of computer-aided topology optimization in structural mechanics, Struct. Multidisc. Optim., vol. 21, 2001, pp. 90-108, Springer-Verlag.

[3] M. P. Bendsøe, and O. Sigmund, Topology Optimization Theory, Methods and Applications, Springer-Verlag Berlin Heidelberg 2003.

[4] E. Dolan, and J. More., Benchmarking optimization software with performance profiles, Math. Prog. Series A, Vol. 91 (2), pp. 201-213, 2002.

AN ITERATIVE METHOD FOR SELECTING DECISION VARIABLES IN ANALYTICAL OPTIMIZATION PROBLEMS

Houdhayfa Ounis, Xavier Roboam, Bruno Sareni

Université de Toulouse, LAPLACE, UMR CNRS-INPT-UPS, 2 rue Camichel, 31071 Toulouse, France
{ounis, roboam, sareni}@laplace.univ-tlse.fr

Abstract. In this paper, we present an iterative method to assist the designer in the setting of decision variables in an optimization problem with analytical models. This method is based on a Direct Structure Matrix (DSM) which allows a clear representation of interactions between variables. This approach is applied to the geometrical model of a High Speed Permanent Magnet Synchronous Machine (HSPMSM).

Keywords: DSM (Direct Structure Matrix), Decision variables, Optimization, Model structuring

INTRODUCTION

Till now, the choice of the decision variable vector in an optimization problem is done by experts and no method has been proposed to automatically perform this process. However, a poor choice of decision variables can easily penalize the search for an optimal solution (losing degrees of freedom), or increase the complexity of the optimization problem. In this paper, we propose an iterative method based on a Direct Structure Matrix (DSM) [1], [2] of the model for the choice of the decision variables. This method can take several criteria into account for selecting decision variables according to the need and interest of the designer.

DECISION VARIABLE SELECTION

To better understand the method, it is applied to the following simple model defined by equations (1)-(4):

$$x_4 = 2x_3x_6 \quad (1)$$

$$x_5 = 2x_2 \quad (2)$$

$$x_6 = x_1 + 2x_4 \quad (3)$$

$$x_7 = x_3x_6 \quad (4)$$

Fig.1 shows the matrix representation of the model (non-oriented DSM), each variable being represented by a row and a column identically labeled and each cell representing the interaction between two variables and containing the equation numbers if couplings occur.

	x_1	x_2	x_3	x_4	x_5	x_6	x_7
x_1				3		3	
x_2					2		
x_3				1		1,4	4
x_4	3		1			1,3	
x_5		2					
x_6	3		1,4	1,3			4
x_7			4			4	

Figure 1 : Non-oriented DSM

	x_1	x_2	x_3	x_4	x_5	x_6	x_7
x_1						3	
x_2					2		
x_3				1			4
x_4						3	
x_5							
x_6				1			4
x_7							

Figure 2 : Oriented DSM

This model includes four equations and seven variables which imply a minimum number of decision variables equal to "3". Choosing arbitrarily "[x_1, x_2, x_3]" as decision variables leads to a non-triangular oriented DSM (it can be seen from Fig. 2 that equations (1) and (3) are coupled). In our example, all equations are reversible and the model should be rewritten in order to remove this coupling. In the case of non-reversible equations, the choice of this decision variable vector is not relevant. The process of the proposed selection method of the decision variables is illustrated in Fig.3. The starting point of this method is the non-oriented DSM for which all interactions between all variables in the model are shown. Selection criteria are imposed by the designer depending on the problem specificities (e.g. variable sensitivity with respect to the model outputs). In our case, we use the simplest version of the method by choosing the frequency occurrence of the variables (called index 1) in the model (see Table.1) and the number of coupled variables (called index 2) per equation (see Table 2). The following steps are followed:

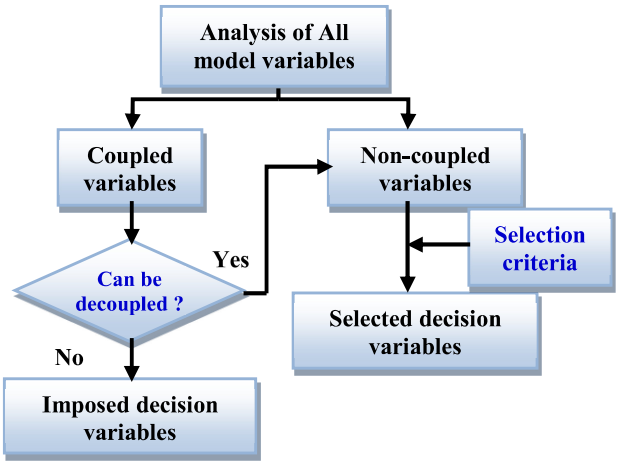

Figure 3: Selection method of the decision variables

Table 1 : Variable frequency

Parameter	x_1	x_2	x_3	x_4	x_5	x_6	x_7
Index 1	1	1	3	2	1	3	1

Table 2 : Number of coupled variables per equation

Equation number	1	2	3	4
Index 2 (Number of coupled variables)	3	2	3	2

- Step 1: select as decision variable the variable with the highest frequency (index 1).
- Step 2: decrease the number of variables (index 2) in the equations containing the selected variable.
- Step 3: Remove from the set of selectable variables all variables that can be computed from a given equation characterized by an index 2 of 1 and go to step 2, otherwise go to step 1.
- Repeat until index 2 equals 1 in all equations.

In the considered example, the method selects [x_3, x_6, x_2] as decision variables and removes the coupling problem illustrated in Fig. 2. Fig. 4 shows the "oriented and sequenced DSM" of the problem (variables are ranked according to their order of calculation); variables identically colored can be computed in parallel in a calculation process.

	x_3	x_6	x_2	x_5	x_4	x_7	x_1
x_3						3	
x_6					2		
x_2				1			4
x_5						3	
x_4							
x_7							4
x_1							

Figure 4 : Oriented and sequenced DSM

"HSPMSM" EXAMPLE

The geometrical model of a High Speed Permanent Magnet Synchronous Machine is given in details in [3]. It includes "81" variables and "70" equations. "11" decision variables (current density "J_s", number of pole pairs "p", number of slots per pole per phase "N_{epp}", equivalent gap "g", yoke induction "B_y", radius length ratio "R_{lr}", slot depth radius ratio "R_{dr}", magnet filling coefficient "K_p", slot filling coefficient "K_r", rated speed "N_{bp}" and rated torque "T_{bp}") have been initially imposed by expertise. Table 3 shows the comparison these variables and those given by our method (only differences are underlined here). In the original problem, the calculation of the bore radius "r_s" is done through simplifying assumptions because of coupling in the equations of the model (without these assumptions, an additional decision variable must be added for solving the problem). The application of our selection method has overcome this problem by selecting the radius "r_s" and "l_r" instead of "R_{dr}" and "R_{lr}" and confirms the choice of the expert for the remaining decision variables.

Table3 : Comparison between original and new decision variables

Original decision variables	New decision variables
R_{dr} : slot depth/radius	r_s : bore radius
R_{lr} : radius/length	l_r : length

REFERENCES

[1] Tyson R. Browning. Applying the Design Structure Matrix to System Decomposition and Integration Problems: A Review and New Directions. IEEE Trans. On Engineering Management, Vol. 48, N° 3, 2001, pp.292-306.

[2] Steward.D.V. The design Sturture System: A Method for Managing the Design of Complex Systems, IEEE Trans. On Engineering Management. T, Vol. 28,1981, pp.71-74.

[3] De Andrade A., Lesage A., Sareni B., Meynard T., Roboam X., Ruelland R., Couderc M. Integrated optimal design for power systems of more electrical aircraft", MEA conference, 2012.

TOWARDS 2D AND 3D IMAGING OF MAGNETIC NANOPARTICLES USING EPR MEASUREMENTS

Annelies COENE*, Guillaume CREVECOEUR* and Luc DUPRE*

*Ghent University, Department of Electrical Energy, Systems and Automation, B-9000, Ghent, Belgium
E-mail: annelies.coene@ugent.be

Abstract. Electron Paramagnetic Resonance (EPR) is a promising technique for visualizing the distribution of magnetic nanoparticles (MNP) non-invasively. Currently EPR is only able to recover 1-dimensional (1D) MNP distributions. In this paper we extend 1D EPR towards 2D and 3D. We solve the associated inverse problem by Truncated Singular Value Decomposition (TSVD), Non-Negative Least Squares and a combination of both algorithms. Furthermore, we investigate the impact of noise on the reconstruction results.

Keywords: Electron Paramagnetic Resonance (EPR), image reconstruction, inverse problem, magnetic nanoparticle (MNP).

INTRODUCTION

Magnetic nanoparticles (MNP) provide interesting possibilities for biomedical applications [1]. Their small diameters in the range of 10-100 nm, enable them to access regions in the body for e.g. hyperthermia treatment or targeted drug delivery. Furthermore, their high saturation magnetization makes them detectable from a distance so they can also be used for non-invasive disease detection. On the other hand, problems arise in obtaining their spatial distribution throughout the body. An accurate knowledge is required of the spatial MNP distribution to ensure a safe and powerful working of previously mentioned applications.

A promising technique for visualizing this distribution is Electron Paramagnetic Resonance (EPR). EPR is similar to MRI but regards the magnetic moments of electrons instead of nuclei. It is only recently that EPR can be employed with smaller frequencies (250 MHz) so to penetrate the human body and to allow biomedical use [2,3]. In a first stage only the total MNP concentration in a volume could be obtained, however by moving the sample along a line (translation) it was possible to recover the 1D MNP distribution referred to as 1D EPR [4].

In this paper we extend 1D EPR to 2D by performing a translation and to 3D by using translation/rotation of the sample. Furthermore, we compare the advantages and disadvantages of three solvers for the associated inverse problem: Truncated Singular Value Decomposition (TSVD), Non-Negative Linear Squares (NNLS) and a combination of both algorithms (TSVD + NNLS). Additionally, we investigate the noise robustness of the proposed 3D EPR technique.

METHODS

EPR measurements

The unknown spatial MNP distribution is represented by **c**, a 1D vector composed of N elements. In a typical 1D EPR measurement, the sample is moved for X adjacent positions along a line (translation) resulting in X measurements:

$$\mathbf{S} = [S_1,\ldots,S_x,\ldots,S_X] \quad (1)$$

This EPR measurement can be modeled as:

$$\mathbf{S}(\mathbf{c}) = \mathbf{F}.\mathbf{c} \quad (2)$$

F is a XxN dimensional matrix which connects the MNP distribution to the EPR measurement. **F** consists of scaled measurement values from an accurately known single voxel (N = 1) MNP sample that was measured on these positions ($x = 1,\ldots,X$), referred to as the response function $R(x)$. $R(x)$ is scaled so it corresponds to the measurement values of 1 unit concentration. For every position of $\mathbf{c}_n$ ($n = 1,..,N$) in each measurement, the corresponding response value is employed. $R(x)$ (and thus **F**) depends on hardware properties of the EPR setup.

To enable 2D and 3D EPR, R depends on the spatial variables: $R(x,y)$ and $R(r,\theta,z)$. In 2D EPR only translations in the 2 dimensions of the volume are performed, whereas for 3D reconstruction the volume is additionally rotated, so to allow faster measurements. In the latter case, for every translation of 1 position a full rotation is performed of the sample.

Obtaining the spatial MNP distribution

The MNP distribution is found by minimizing the model solution with respect to the EPR measurement, $\mathbf{S}_{EPR}$:

$$\mathbf{c}^* = \arg\min_{\mathbf{c}} \left\| \mathbf{S}(\mathbf{c}) - \mathbf{S}_{EPR} \right\| \quad (3)$$

In this paper we employ a combination of TSVD and NNLS. TSVD has the disadvantages that it allows non-plausible solutions with negative MNP amounts and that it smoothens the solution, NNLS on the other hand removes negative solutions, but has a larger mean error on the reconstruction when compared to TSVD. Therefore, we suggest to first solve the inverse problem by TSVD and then by NNLS. Finally, the positive NNLS amounts are substituted by the solutions of TSVD.

RESULTS AND DISCUSSION

We simulated an EPR measurement for a cylindrical volume with a radius of 4 mm (limited due to the current size of the EPR setup) and a length of 4 cm and made a reconstruction with TSVD, NNLS and TSVD + NNLS. A correlation coefficient (CC) is associated to the reconstruction, with a score of 100% meaning a perfect reconstruction. We obtain following scores : TSDV: 92%, NNLS: 90%, TSVD + NNLS: 94%. Because of smaller differences in the theta-direction for *R*, difficulties arise in the reconstruction. In the full paper necessary requirements are investigated for *R* to obtain accurate reconstructions.

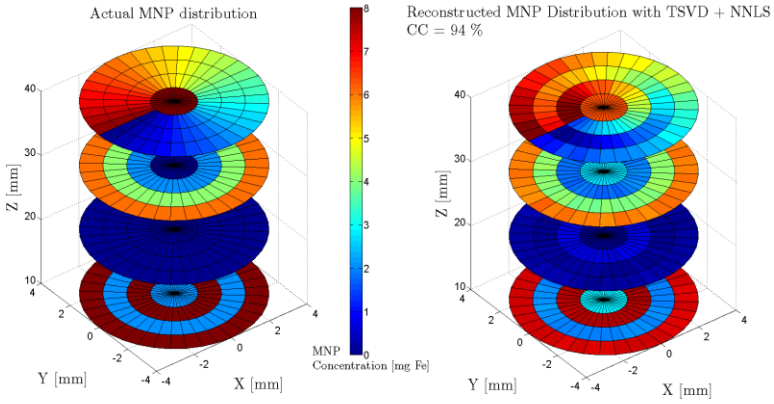

Figure 1. Left side shows the actual MNP distribution while the right side shows a reconstruction with TSVD + NNLS.

Furthermore, we investigated the impact of noise on the different algorithms. White Gaussian noise is generated in steps of 1% and for every noise level 200 simulations (noise measurements) are performed which are then averaged. Fig. 2 shows the averaged CC for 200 noise experiments. TSVD is more noise robust than NNLS. Due to the bad results of NNLS, the combination of both algorithms has no added value anymore.

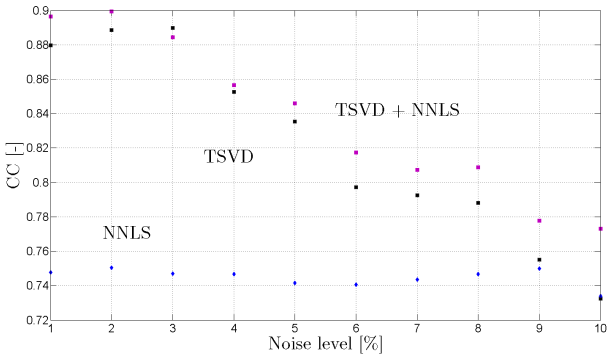

Figure 2. Noise robustness of the different solvers in case of 3D reconstruction using EPR data.

REFERENCES

[1] QA Pankhurst, et al. J Phys D: Appl Phys, vol 42, 2009.
[2] P. Vaes and S. Teughels, "Isolating active electron spin signals in EPR," Patent WO/2012/126 968, Sep. 28, 2012.
[3] X. Li, et al. Electronics Letters, vol. 49, no. 25, pp. 1600–1601, 2013.
[4] A. Coene, et al. J Phys D: Appl Phys, vol. 46, no. 24, 2013.

A RECONSTRUCTION OF DIELECTRIC OBJECTS BURIED UNDER A ROUGH SURFACE

Özgür ÖZDEMİR*, Yasemin ALTUNCU**

* Istanbul Technical University, Electronics and Telecommunication Engineering, 34469, Istanbul, *TURKEY*

E-mail: ozdemiroz3@itu.edu.tr

**Niğde University, Electrical-Electronics Engineering, 51240, Niğde, *TURKEY*

E-mail: yaltuncu@nigde.edu.tr

Abstract. We propose a computationally efficient method to reconstruct dielectric objects buried in a half-space with rough surface. Cauchy Data is exploited to formulate the total field inside the homogeneous neighborhood of the scatterers using homogeneous Green's function instead of background Green's function. Then Born-type linearization is employed to reconstruct the object from measured scattered field. The feasibility and efficiency of the method are demonstrated through numerical experiments.

Keywords: Buried object reconstruction, Rough surface, Born Approximation, Layered media

INTRODUCTION

A reconstruction of object properties such as location, shape and electromagnetic parameters from the knowledge of scattered electromagnetic field is called as an inverse scattering problem and it has very important application areas such as mine detection and non-destructive testing. Most of the reconstruction methods exploits integral equation formulation of the scattered field in terms of Greens function of the background and induced sources. Computational cost of these method is mostly governed by the Green's function calculation. As in the case of inhomogeneous or layered media with rough interface, an analytic form of Green's function might not be available and it has to be calculated numerically which may increase the computational burden of the method dramatically [1].

Here we propose a novel formulation of the total field which is defined as the sum of incident and scattered field for two-dimensional object embedded in a two-layered planar medium for TM polarized illumination. To this aim, we exploit the Cauchy Data, i.e. boundary data, which allow us to formulate the field inside the homogeneous neighborhood of the target in terms of homogeneous Green's function instead of background medium. As a result, the proposed formulation significantly improves the efficiency of the reconstruction algorithms. Within the novel formulation, we introduce pseudo incident field and pseudo scattered field which are in general different than classical incident and scattered field definition. Having formulated scattering problem, we consider Born-type approximation to linearize the highly nonlinear inverse scattering problem. According to Born approximation, the total field in the object can be replaced by incident field provided that the object is weakly scatterer. Herein, we use pseudo incident field to replace the total field. We shall note that this work is the extension of our previous work to the planar medium [2] which is developed for cylindrical medium.

We will present numerical experiments to verify the efficiency of the proposed approach for rough interfaced two-layered medium by comparing it with classical Born approximation method. Green's function of background medium which is required in classical method is calculated numerically with Buried Object Approach (BOA) as given in [1].

MATHEMATICAL FORMULATION

We consider a dielectric object D embedded in a lower half space Ω with rough surface $\partial\Omega$ as given in Figure 1. Upper half-space is assumed to be free-space and nonmagnetic lower half space is characterized with relative permittivity ε_1 which is complex in general. Both transmitters and receivers are placed into upper medium, hence only limited data is available. The total electric field which is defined as $\vec{E}(\boldsymbol{r}) = u(\boldsymbol{r})\vec{e}_z$ can be written as the summation of incident field u_i and scattered field u_s, i.e. $u(\boldsymbol{r}) = u_i(\boldsymbol{r}) + u_s(\boldsymbol{r})$. For the sake of simplicity, the vector notation is omitted through the paper. Let's consider the total field in the lower half space that satisfies the Helmholtz equation,

$$\Delta u(r) + k_1^2 u(r) = \begin{cases} 0, & r \in \Omega \backslash D \\ (k_1^2 - k_d^2)u(r) & r \in D \end{cases} \quad (1)$$

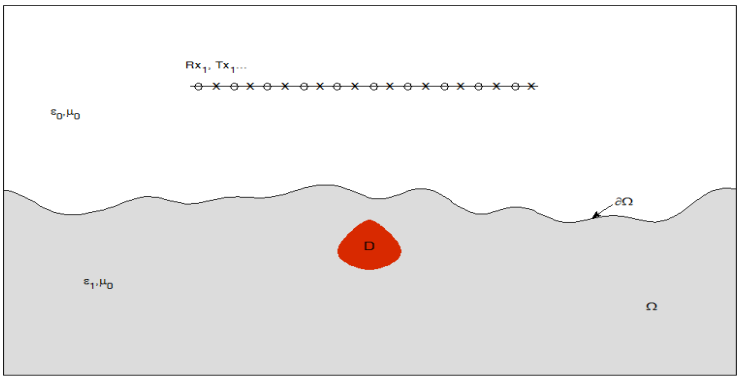

Figure 1. Problem geometry.

where k_1 and k_d are wavenumber of lower half-space and the object, respectively. The fundamental solution of the Helmholtz equation in lower medium is denoted as $\Phi(\boldsymbol{r};\boldsymbol{r}') = \frac{i}{4}H_0^1(k_1|\boldsymbol{r}-\boldsymbol{r}'|)$ and satisfy the following equation

(2) $\Phi(\boldsymbol{r};\boldsymbol{r}') + k_1^2\Phi(\boldsymbol{r};\boldsymbol{r}')) = -\delta(\boldsymbol{r}-\boldsymbol{r}') \qquad \boldsymbol{r},\boldsymbol{r}' \in \boldsymbol{\Omega}$

Then we apply the Green's theorem to equation (1) and (2) and obtain the following

(3) $u(\boldsymbol{r}) = \int_{\partial\Omega}\left\{\frac{\partial u}{\partial n}(\boldsymbol{r}')\Phi(\boldsymbol{r};\boldsymbol{r}') - u(\boldsymbol{r}')\frac{\partial \Phi}{\partial n}(\boldsymbol{r};\boldsymbol{r}')\right\}ds(\boldsymbol{r}') + k_1^2\int_D \Phi(\boldsymbol{r};\boldsymbol{r}')\chi(\boldsymbol{r}')u(\boldsymbol{r}')d\boldsymbol{r}'$

The first integral at the right hand side is called as a *pseudo incident field* $\tilde{u}_i$ and the second integral as a *pseudo scattered field* $\tilde{u}_s$ which are different than the classical definition of which in general. $\chi(\boldsymbol{r}')$ is called as an object function and is the unknown to be determined in the inverse problem. Herein we apply Born type approximation in order to solve this problem and replace the total field in the reconstruction domain B with pseudo incident field as

(4) $\tilde{u}_s(\boldsymbol{r}') = k_1^2\int_B \Phi(\boldsymbol{r};\boldsymbol{r}')\chi(\boldsymbol{r}')\tilde{u}_i(\boldsymbol{r}')d\boldsymbol{r}'$

Note that the determination of pseudo incident field requires the knowledge of total field and its normal derivative on the boundary that is to say Cauchy Data, however we only know the scattered field on the measurement line placed into upper half-space. Here we use Single Layer potential approach to determine the required Cauchy Data from the measurement field [3].

CONCLUSIONS

We've introduced an efficient reconstruction method for buried dielectric object. The efficiency arises from the use of homogenous Green's function instead of two-layered rough interfaced background Green's function. However we need Cauchy Data which might be difficult to obtain in real experiments. Therefore we use a preprocessing step to recover required data from measurement field. We show that the proposed method is more efficient than the classical one. We are currently working on to use Cauchy Data formulation to reconstruct highly scatterers which cannot be accomplished by Born approximation using optimization type inversion algorithm.

REFERENCES

[1] Y. Altuncu, I. Akduman, and A. Yapar. Detecting and locating dielectric objects buried under a rough interface. IEEE Geosci. Remote Sens. Lett., vol. 4, no. 2, 2007, pp. 251–255.

[2] O. Ozdemir and H. Haddar. Linearized Cauchy data inversion method for two-dimensional buried target imaging. IEEE Trans. Antennas Propagat., vol. 61, no. 6, 2013, pp. 3244–3251.

[3] D. Colton and R. Kress, *Inverse Acoustic and Electromagnetic Scattering Theory*. Berlin, Germany: Springer-Verlag, 1998.

UNDERDETERMINED MAGNETOSTATIC INVERSE PROBLEM: BAYES THEOREM APPLICATION

O. Pinaud[1,2], JL. Coulomb[1,2], O. Chadebec[1,2], LL. Rouve[1,2], JM. Guichon[1,2]

[1] Univ. Grenoble Alpes, G2ELab, F-38000 Grenoble, France
[2] CNRS, G2Elab, F-38000 Grenoble, France
Olivier.pinaud@g2elab.grenoble-inp.fr

Abstract. This paper deals with the use of the Bayesian approach to inverse an underdetermined problem. The modeled *a priori* information is statistically studied using either Unscented Transform (UT) method or Monte Carlo (MC) method to estimate the mean value and standard deviation. The whole approach is applied to an experimental setup illustrating an electric vehicle power circuitry. This demonstrates the strength of coupling modeling and measurements for complex systems identification.

Keywords: Bayes theorem, Inverse problem, Magnetostatic, Monte Carlo, Unscented Transform.

INTRODUCTION

This work takes part on a project aiming to evaluate the magnetic field inside electric vehicles [1]. In this paper, we focus on the magnetostatic field created by an electric power circuitry. This field is described by a truncated spherical harmonic expansion [2] written inside the studied area. Harmonic coefficients must be identified by using only a very few sensors set around the studied zone (fig.1). To overcome the inversion failure due to a drastic lack of sensors, a Bayesian approach [3] is applied. A *priori* information is introduced: it comes from a direct model describing the assumed average state of sources. This information helps the inverse problem to succeed but requires a statistical study for the *a priori* model.

THE BAYESIAN INVERSE PROBLEM

For a given radius $r \leq r_0$, spherical harmonic expansion of the magnetic induction B inside an area (blue sphere on fig.1) can be truncated at the order $n = N_{max}$. When the number of tri-axes sensors is K, the spherical harmonic coefficients (SHC) are linked to magnetic induction by the following linear problem

$$A.X = B_{mes} \quad (1)$$

A is a $(3K, N_{max}^2+2N_{max})$ matrix depending on the sensor position, X is a $(N_{max}^2+2N_{max})$ vector of $a_{n,m}$ SHC and B_{mes} is a (3K) vector of the magnetic induction components.

A statistical view of this problem leads to the probability of having B_{mes} given a deterministic coefficient vector X: it is the likelihood density probability $p(B_{mes}|X)$. Using a Gaussian repartition, the solution maximizing this probability is:

$$X_{ML} = (A^t.S_m^{-1}.A)^{-1}.A^t.S_m^{-1}.B_{mes} \quad (2)$$

S_m is the (3K, 3K) covariance matrix linked to measurements and the chosen mathematical model. Bayes theorem permits the use of probabilistic *a priori* information p(X) to write the *a posteriori* probability of having a coefficient vector X given the observed induction B_{mes}: $p(X|B_{mes}) \sim p(B_{mes}|X).p(X)$. Using a Gaussian repartition, the solution maximizing this probability is:

$$X_{MAP} = X_0 + (A^t S_m^{-1} A + S_0^{-1})^{-1} A^t S_m^{-1} (B_{mes} - AX_0) \quad (3)$$

X_0 is the $(N_{max}^2+2N_{max})$ *a priori* vector and S_0 is the $(N_{max}^2+2N_{max,}\ N_{max}^2+2N_{max})$ covariance matrix of X_0, both obtained by a statistical study of the *a priori* model.

STATISTICAL STUDY OF THE A PRIORI INFORMATION

The whole studied electric power circuitry is described by straight conductors. Each coordinate of the 49 points describing the inductor geometry will be treated as a random variable. Each point is defined by 3 independent parameters : positions towards x-axis, y-axis and z-axis. Then the mean values (μ_x, μ_y, μ_z) define the "average state model" and standard deviations (σ_x, σ_y, σ_z) define the assumed uncertain interval.

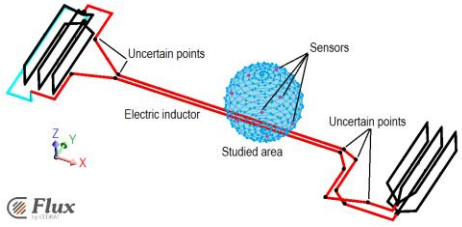

Figure 1 Illustration of the *a priori* electric current repartition

We are interested in the spherical harmonic coefficient repartition describing the magnetic induction inside a specific zone (the blue sphere). Previous work has shown that the magnetostatic field inside the studied area must be written till the 6th order (N_{max}). Then 48 coefficients are needed and must be statistically studied to define the 48 by 48 covariance matrix. The 147 independent parameters are

defined by a Gaussian probabilistic density function with the corresponding mean value and standard deviation. The first idea is to use Monte Carlo (MC) method to estimate the output mean value and standard deviation but the main drawback concerns the computation cost. It is why we propose to use Unscented Transform (UT) method [4,5,6] to estimate the statistic moments of the output random variable. Assuming the output probabilistic density repartition, this method deterministically selects sigma points (depending on input variable probability distribution) to compute output values and estimate the main statistic moments.

EXPERIMENTAL RESULTS

A first statistical study is done by defining all the 147 geometric parameters as random variable. Unscented Transform only makes 295 deterministic computations (algorithm principle) while Monte Carlo asks for several thousands of them. A more dedicated study shows that for the specific zone that we focus on, not all the points have a major effect. So the number of stochastic geometric parameters could be reduced to only 36 (see full black points on red inductors on fig.1). Unscented Transform then approximates the output covariance matrix with only 73 computations while Monte Carlo still needs several thousands of computations. Both obtained covariance matrices are quite similar and will be used in the following inverse problem.

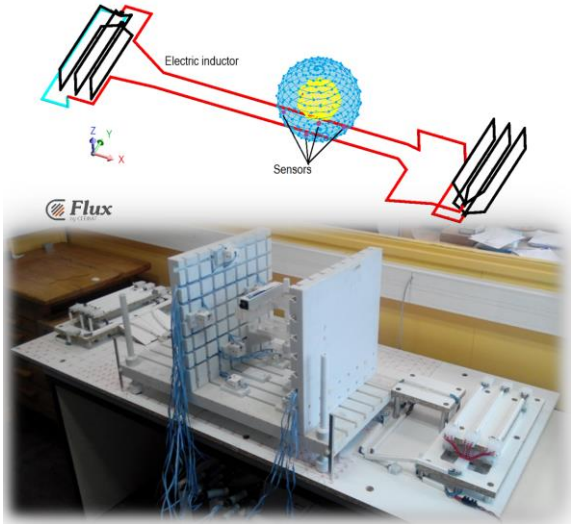

Figure 2 Experimental setup illustration

The experimental electric current repartition (fig.2) is different from the *a priori* information but modeling shows the same maximum spherical harmonic expansion order (N_{max}). Only 6 tri-axes sensors can be placed close to the (blue) identification sphere so the problem is drastically underdetermined. Other 6 tri-axes sensors are placed inside the studied zone for a posteriori checking purpose.

The maximum of likelihood solution (2) fails to identify all the coefficients because there are not enough sensors.

The maximum *a posteriori* solution (3) gives far better results thanks to the use of *a priori* information.

Table 1 gives some results to compare both identification solutions and illustrates the Bayesian approach strength.

Table 1. Experimental results sample

Verification sensor number	Measured module (T)	Identification		A priori error
		ML error	MAP error	
1	8,137E-06	48.1%	16.5%	-71.4%
3	10,748E-06	59.1%	2.8%	-73.2%
5	7,753E-06	4.9%	1.1%	-73.7%
Mean error		**37.4%**	**6.8%**	**-72.8%**

CONCLUSIONS

Unscented Transform clearly demonstrates its strength against Monte Carlo in term of computational time cost. This will be useful when the a priori model will require much computation time (when integrating some ferromagnetic parts for example).

A priori information used into a Bayesian approach of an underdetermined inverse problem clearly helps for complex sources identification. Merging modeling and measurements seems to be an optimized configuration in the context of magnetic induction evaluation inside electric vehicles.

REFERENCES

[1] Pinaud O., Chadebec O., Rouve L.-L., and al., "Forward Model Computation of Magnetostatic Fields Inside Electric Vehicles", IEEE Transactions on Magnetics, vol.50, no.2, 2014.

[2] Rouve L.-L., "Application of the spherical harmonic model to identify the magnetic state of a system and to extrapolate its signature," in Applied Electromagnetics and Mechanics 15, Amsterdam, The Netherlands :IOS Press, 1999, pp.136-144

[3] Tarantola A., *Inverse Problem Theory*. Amsterdam, The Netherlands: Elsevier, 1987.

[4] Simon J. Julier, "The Scaled Unscented Transformation", Proceeding in American Control Conference, 2002.

[5] Simon J. Juiller, "A New Method for Filtering Nonlinear Systems", Proceeding in American Control Conference, 1995.

[6] Ferber De Vieira Lessa M, and al., "Conducted EMI of DC-DC Converters With Parametric Uncertainties", IEEE Transactions on Electromagnetic Compatibility, Vol. 55, n° 4, pp. 699 – 706, 2013

CURRENT DENSITY RECONSTRUCTION FOR INVERSE CALCULATIONS OF DEFECTS IN LORENTZ FORCE EVALUATION

J. Mengelkamp*, K. Porzig†, M. Carlstedt†, M. Ziolkowski†, H. Brauer† and J. Haueisen*

* Dept. of Biomedical Engineering and Informatics; † Dept. of Advanced Electromagnetics
Technische Universität Ilmenau, Germany; contact: judith.mengelkamp@tu-ilmenau.de

Abstract. We apply the method of current density reconstruction to perform inverse calculations of defects in Lorentz Force Evaluation (LFE). Superior to previously introduced conductivity estimation, this approach is not limited to laminated materials. We apply the method to solid bodies performing the inversion in a fully three-dimensional source space. The results of defect reconstructions in solid and laminated specimen show comparable and acceptable errors. Thus, current density reconstruction is a promising method for LFE.

Keywords: forward solution, inverse problem, minimum norm estimation, nondestructive testing, permanent magnet

INTRODUCTION

In this contribution we present a new inversion method for Lorentz Force Evaluation (LFE) based on current density estimation. LFE is a new nondestructive testing technique to detect and estimate defects in electrically conductive materials [1]. A conductive specimen moves relative to a permanent magnet and due to the relative movement eddy currents are induced in the specimen. The interaction between the eddy currents and the primary magnetic field yields Lorentz forces, which are measured. If a defect is present in the material, characteristic perturbations in the eddy currents and, thus, in the force signals occur. The authors in [1] reconstructed a defect by estimating the conductivity. However, this approach is restricted to laminated materials such as composites, because only on the condition of assumed anisotropy an analytic forward and inverse solution can be calculated. Contrary to the conductivity estimation, current density reconstructions (CDR) have been applied in the framework of nondestructive testing, e.g. in magnetic flux leakage data [2].

We introduce the CDR approach to LFE and solve the inverse problem using a minimum-L2-norm estimation. Since this method requires no additional constraints, we can extend it to solid specimens. To demonstrate the efficiency of the method we compare results of LFE problem setups using a laminated and a solid specimen by evaluating force signals obtained from numerical simulations.

METHODS

Problem Description

The principle setup for LFE using a laminated and a solid specimen is shown in Fig. 1. The permanent magnet has the magnetization $\mathbf{M}=M\mathbf{e}_z$ and is located at the lift-off distance δz above the conductive bar. The laminated specimen, consisting of a set of stacked sheets, as well as the solid specimen have the dimensions $l_x \times l_y \times l_z$, the conductivity σ_0 and are moving with the velocity $\mathbf{v}$. In the laminated specimen a defect of cylindrical shape with the diameter D=6 mm, the height h=2 mm and the depth d=2 mm is present. The solid specimen has a spherical defect with D=6 mm and d=4 mm. We evaluate simulation data in a two-dimensional plane located at δz.

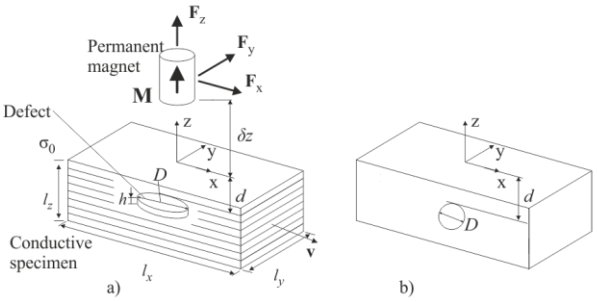

Figure 1. Principle setup of LFE. a) laminated specimen with cylindrical defect, b) solid specimen with spherical defect.

Forward Solution

Under the assumption that the velocity of the moving object $\mathbf{v}$ is small enough, the influence of the secondary magnetic field produced by the induced eddy currents can be neglected (weak reaction approach). Then, the eddy currents in the conductive region can be calculated using Ohm's law for moving conductors $\mathbf{j} = \sigma_0(-\nabla\varphi + \mathbf{v}\times\mathbf{B})$, where φ is the electric scalar potential and $\mathbf{B}$ the primary magnetic field. For given $\mathbf{j}$ the resulting three-component Lorentz forces are calculated as

(1) $$\mathbf{F} = \int_V \mathbf{j} \times \mathbf{B} dV,$$

with V being the volume of the specimen. In case of the laminated specimen anisotropy is assumed since the currents are only flowing in the single sheets (xy-plane) and it holds j_z=0. Contrary, in a solid isotropic bar all three current density components have to be considered. For forward and inverse calculations, the continuous current density distribution is discretized into a uniformly distributed set of electric current dipoles [1].

Inverse Solution

We solve the linear inverse problem $\mathbf{F}=\mathbf{L}\cdot\mathbf{j}$ with respect to the unknown current density distribution by applying the truncated singular value decomposition

(2) $$\mathbf{j} = \mathbf{L}_r^+ \cdot \mathbf{F} = \left(\mathbf{U} \cdot \Sigma_r \cdot \mathbf{V}^{\mathrm{T}}\right)^+ \cdot \mathbf{F}.$$

The gain matrix $\mathbf{L}$ contains information on the forward model including observation points and dipole positions. The rank r of the pseudo-inverse $\mathbf{L}_r^+$ is defined as the number of considered singular values, which is determined by the relative regularization parameter σ_r.

For the laminated specimen, we perform the reconstruction in two steps [1]. Firstly, we reconstruct the depth of the defect by estimation of the CDR in the xz-plane. Secondly, the CDR in the xy-plane at the obtained depth is computed. For the solid bar we solve the inverse problem in a three-dimensional source space. To compensate the tendency to reconstruct superficial sources we apply a depth weighting of the gain matrix $\mathbf{L'}=\mathbf{L}\cdot\mathbf{W}$. The weighting matrix $\mathbf{W}$ depends on a parameter p=0.2 and is defined as

(3) $$\mathbf{W} = \mathrm{diag}\left(\left\|\mathbf{L}_i\right\|_2^{-1/p}\right),$$

with $\mathbf{L}_i$ denoting the i-th column of $\mathbf{L}$. We vary σ_r in order to assess its influence. For evaluation of the results we subtract from the obtained CDR the current density of a specimen without a defect. Thus, high magnitudes in the reconstructed CDR indicate the presence of a defect. We extract the most important region by applying a threshold $th=(Q_{\max}+Q_{\mathrm{mean}})/2$ to the solution with Q denoting the dipole magnitude. The depth of the defect in the laminated specimen is estimated by the weighted average of the dipole positions. The location and extension of the defect in the xy-plane in the laminated as well as in the 3D space in the solid specimen are estimated by fitting an equivalent ellipsoid to the thresholded solution and evaluating its center of gravity (COG) and length of semi-axis [3].

RESULTS AND CONCLUSIONS

The results are depicted in Fig. 2. The depth of the defect in the laminated specimen is reconstructed correctly, if σ_r is in the range of 0.5 to 0.8 (Fig. 1a). In the xy-plane, the COG of the equivalent ellipsoid equals the COG of the real defect for all evaluated σ_r. Thus, the position of the defect is estimated accurately. The reconstructed xy-extensions differ from the real diameter by up to twice the real value (Fig. 2b). The best approximation is obtained for σ_r=0.03, where the errors for the x- and y-extension equal 0.2 mm and 2.2 mm, respectively. The results of the 3D reconstruction of the spherical defect in the solid specimen show apart from two exceptions errors less than 2 mm. However, the spherical defect shape is not well reconstructed (see the errors in Fig. 1c and the ellipsoid in Fig. 1d). Considering that we performed a 3D reconstruction using 2D observation data, the errors are in an acceptable range.

For the first time an approach for solving the inverse problem in LFE in a three-dimensional space is presented. Based on the successful results obtained from simulation data we will apply the method to measurement data in the next step.

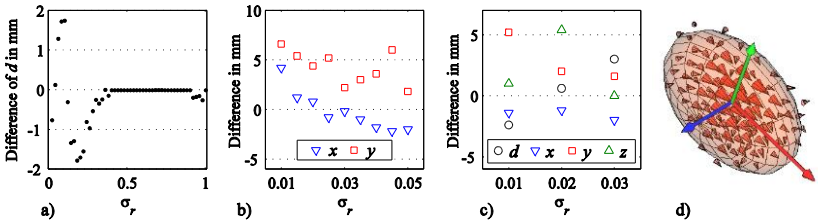

Figure 2. Reconstruction results. Differences between estimated and real defect parameters: a) depth and b) xy-extension of defect in anisotropic bar, c) depth and xyz-extensions of defect in isotropic bar. d) Equivalent ellipsoid fitted to a thresholded CDR of the defect in the isotropic specimen with σ_r = 0.03.

REFERENCES

[1] B. Petković, J. Haueisen, M. Zec, R. Uhlig, H. Brauer, and M. Ziolkowski. Lorentz force evaluation: A new approximation method for defect reconstruction. NDT & E International, vol. 59, 2013, pp. 57–67.

[2] J. Haueisen, R. Unger, T. Beuker, and M. Bellemann. Evaluation of inverse algorithms in the analysis of magnetic flux leakage data. IEEE Trans. Magn., vol. 38, no. 3, 2002, pp. 1481–1488.

[3] M. Ziolkowski, J. Haueisen, and U. Leder. Visualization procedures for volume and surface current density distributions in cardiac regions. vol. 2, no. 2, 2000, pp. 1–10.

EXPERIMENTAL SENSITIVITY ANALYSIS OF MAGNETORELAXOMETRIC IMAGING

Maik Liebl*, **, Uwe Steinhoff*, Frank Wiekhorst*, Daniel Baumgarten**, Jens Haueisen** and Lutz Trahms*

*Physikalisch-Technische Bundesanstalt, Abbestrasse 2-12, 14059 Berlin, Germany
E-mail: maik.liebl@ptb.de

**Institute of Biomedical Engineering and Informatics, Technische Universität Ilmenau, 98693 Ilmenau, Germany

Abstract. In magnetorelaxometry (MRX) the amount of magnetic nanoparticles (MNP) in a sample can be quantified by measuring the amplitude of its time-delayed response to a sudden change of an external magnetizing field. For the quantitative imaging of MNP distributions the MRX method is expanded by a sequential application of multiple spatially distinct magnetizing fields to the sample. However, each magnetizing step prolongs the measurement duration. Here, we experimentally investigate the potential of reducing the number of magnetization steps. In a fixed measurement setup using a 304 channel magnetometer we varied crucial imaging parameters (distance of the sample to coils and sensors, number of coils and sensors and the excitation current). We found even a slight improvement of reconstruction quality by omitting selected magnetization steps. Amplitude variation of a constant magnetizing current had no influence, while combining different magnetizing amplitudes improved the reconstruction.

Keywords: Magnetic Nanoparticle Reconstruction, Magnetorelaxometry, Minimum-Norm-Estimation

INTRODUCTION

Magnetic nanoparticles (MNP) are used for novel cancer treatment approaches [1], where the quantitative knowledge of the MNP distribution inside a body is essential. In magnetorelaxometry (MRX) a MNP sample can be non-invasively quantified by measuring the relaxation of the MNP magnetic net moment after a sudden change of an external magnetizing field. For quantitative imaging of an extended MNP distribution the MRX method is sequentially repeated with spatially varying inhomogeneous magnetizing fields [2,3,4]. Then the MNP responses originate subsequently from different areas and magnetization orientations inside the sample and the MNP distribution can be reconstructed by solving an inverse problem. Due to relaxation times of the MNP in the millisecond-second range, MRX is a time consuming imaging technique, where every magnetization step prolongs the measurement duration. A sensitivity analysis on experimental data can help to find a compromise between the number of magnetization steps and reconstruction quality for a given measurement setup.

METHODS

Measurement setup

A two-dimensional phantom comprising a P-shaped MNP distribution of 15 individual gypsum cubes of 1 cm^3 volume containing MNP at an iron concentration of 6±0.07 mg iron/cube was measured in a fixed setup under the 304 channel magnetometer system. The phantom was positioned between two parallel layers of excitation coils below the sensor plane with 15 magnetization coils above the phantom and 15 excitation coils below the phantom (each coil with d=4 cm and I=800 mA) that are activated consecutively. The phantom was measured in three different distances between the magnetization coil array and the magnetometers (further experimental details are described in [5]): **a)** close to the magnetometer system (6 cm) and the (upper) excitation coils (1 cm); **b)** far from the magnetometer system (12 cm), but close to the (lower) excitation coils (1 cm); **c)** far from the magnetometer system (9 cm) and excitation coils (3.5 cm). The total measurement duration for each phantom position ranged to 10 min (including 10 averages for improving the signal-to-noise ratio).

Forward and Inverse Problem

The sample volume is divided into K voxels with the aim to quantify the MNP amount $X_{\mathrm{MNP,k}}$ in each voxel. Separating geometry and source parameters for the magnetization in the K voxels detected by N sensors and a sequential application of P different magnetizing fields $\mathbf{H}_{\mathrm{k,p}}$ a general forward problem for the detected relaxation amplitudes $\Delta\mathbf{B}$ can be stated:

$$\Delta\mathbf{B} = \mathbf{L}\mathbf{X}_{\mathrm{MNP}} \quad \text{with } \mathbf{L} \text{ of dimensions } K \text{ x } NP \tag{1}$$

A detailed mathematical model can be found in [4]. The reconstruction of $\mathbf{X}_{\mathrm{MNP,est}}$ can be achieved using inverse algorithm. Here we use a minimum-norm estimation (MNE) calculated by a truncated singular value

decomposition (TSVD) employing the Moore-Penrose pseudoinverse $\mathbf{L}^{+}=(\mathbf{L}^{T}\mathbf{L})^{-1}\mathbf{L}^{T}$. The linear system of equation is solved by:

(2) $$\mathbf{X}_{MNP,est}=\mathbf{L}^{+}\Delta\mathbf{B}$$

A two-dimensional reconstruction grid k=(10×10) of 1 cm^2 spatial resolution was defined using the a-priori information of the vertical z-distance of the MNP distribution from the magnetometer system. As a measure for the goodness of reconstruction we calculate the correlation coefficient (maximum correlation is 1) between estimated $\mathbf{X}_{MNP,est}$ and nominal $\mathbf{X}_{MNP,nom}$ MNP distribution. To monitor the influence of the truncated SVD cutoff parameter λ relaxation amplitudes $\Delta\mathbf{B}$ are calculated from $\mathbf{X}_{MNP,nom}$ by equation 1 and $\mathbf{X}_{MNP,sim}$ is reconstructed by equation 2 using the same λ as in the reconstructions for $\mathbf{X}_{MNP,est}$. The number of $N_{coils} \times N_{sensors}$ is subsequently decreased by switching off coil-sensor combinations with relaxation amplitudes below a threshold $\kappa=0.01\text{-}0.6\cdot\Delta B_{max}$ (λ is chosen so to have the highest correlation coefficient for the maximum of $N_{coils} \times N_{sensors}$).

RESULTS AND DISCUSSION

The correlation coefficients for measurements and simulations of the three different configurations are shown in figure 1. The correlation coefficients for cases a) and b) are higher than for case c) where the coils are far from the sample. Hence, in this type of MRX setup the distance of the magnetization coils to the MNP distribution determines the quality of the reconstruction. For all cases the maximum correlation coefficient is achieved below the maximum number of $N_{coils} \times N_{sensors}$ (a) 23, b) 15 and c) 17 coil excitations). In figure 2 the influence of the excitation current for case c) is shown. We find that increasing the excitation current does not significantly improve the quality of the reconstruction. Confirming the theoretical predictions in [4] an improvement of the correlation coefficient was achieved by a first implementation of a sensitivity based approach where the coils close to the sensor system were driven with I=600 mA while coils far from the sensor system used I=1.2 A.

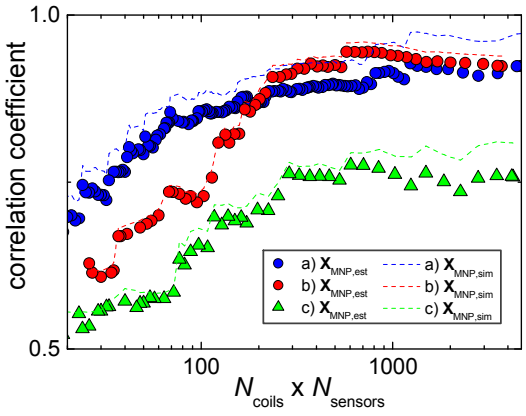

Figure 1. Correlation coefficient for cases a), b) and c)

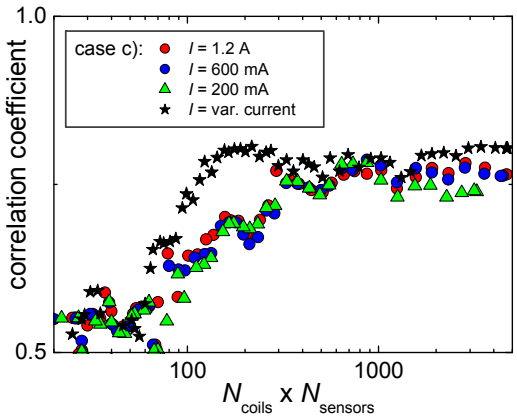

Figure 2. Correlation coefficient for case c) and different currents

CONCLUSION

We studied the influence of crucial imaging parameters in MRX using multiple excitation coils and demonstrate the potential to increase the reconstruction quality while the measurement duration can be reduced by omitting selected magnetization steps. A sensitivity based approach [4] is able to further reduce the measurement duration as experimentally demonstrated. Allowing a 10% decrease of the initial correlation coefficient the measurement duration could be reduced to 2, 2.5 and 4 min for cases a), b) and c), respectively.

ACKNOWLEGDEMENT

This work was financially supported by the DFG research programs “Magnetische Nanopartikel für die Krebstherapie” TR408/4-3 and “Magnetische Nanopartikel für die Zelluläre und Molekulare MR-Bildgebung” TR408/5-2.

REFERENCES

[1] Q.A. Pankhurst et al. Applications of magnetic nanoparticles in biomedicine. J. Phys. D: Appl. Phys., vol. 36, 2003, pp. 167-181.

[2] J.P. Wikswo et al. Magnetic Susceptibility Imaging for Nondestructive Evaluation. IEEE Trans. Appl. Supercond., vol. 3, 1993, pp. 1995-2002.

[3] U. Steinhoff et al. Bildgebung magnetischer Nanopartikel basierend auf Magnetrelaxometrie mit sequentieller Aktivierung inhomogener Anregungsfelder, Biomed. Tech., vol. 55, 2010, pp. 22-25

[4] G. Crevecoeur et al. Advancements in Magnetic Nanoparticle Reconstruction Using Sequential Activation of Excitation Coil Arrays Using Magnetorelaxometry. IEEE Trans. Magn., vol. 48, 2012, pp. 1313-1316.

[5] M. Liebl et al. Quantitative reconstruction of a magnetic nanoparticle distribution using a non-negativity constraint. Biomed. Tech., vol. 58, 2013, doi: 10.1515/bmt-2013-4261

TOPOLOGY OPTIMIZATION – RECENT APPLICATIONS AND GENERALIZATIONS

Matias Stolpe

Invited Lecture

University of Denmark

ABSTRACT

Topology optimization is a collection of theory, mathematical models, and numerical methods within optimal design. Topology optimization is often used in the conceptual design phase to propose innovative structures and materials. The presentation begins with an overview of topology optimization and some of the theoretical and numerical challenges in this field. Examples of some recently proposed applications for topology optimization are also presented.

Since the introduction of topology optimization several generalizations have been introduced. We focus on the powerful approach of Free Material Optimization (FMO) in which the design parameterization describes both the material distribution and the local material properties in the structure. The optimization problems in FMO are generally non convex Semi Definite Programs (SDPs). These nonstandard problems have many small matrix inequalities and special optimization methods utilizing this property have to be developed and implemented. By modifying existing interior-point methods it is possible to obtain high quality solutions to large-scale FMO problems for 3D structures using only a modest number of iterations. The main bottleneck is the computation of the search directions. This requires the solution of a very large-scale saddle point system which becomes increasingly ill-conditioned as the optimum is approached. We propose special purpose preconditioners combined with Krylov subspace methods for the saddle-point system and numerically show that they are capable of dealing with the increasing ill-conditioning. The numerical results confirm that the combination of techniques generates an efficient and robust method which is capable of routinely solving large-scale FMO problems on 3D design domains. The presentation concludes with an overview of the outstanding theoretical and numerical challenges in FMO.

NUMERICAL ANALYSIS ON THE FORCE IN AN LINEAR RELUCTANCE VARIABLE MOTOR

Nolvi Francisco BAGGIO FILHO*, Roniele BELUSSO*, Tamara Francisca BAGGIO**

*Federal Institute of Rio Grande do Sul. Av. São Vicente, nº 785, 95180-00, Farroupilha, RS, Brazil
**Federal University of Rio Grande do Sul. Av. Osvaldo Aranha, 99, 90035-190, Porto Alegre, RS, Brazil
E-mail: nolvi.filho@farroupilha.ifrs.edu.br

Abstract. Currently, many industrial processes require a precise linear motion. Usually this movement is achieved with the use of rotary motors combined with an electrical control systems and mechanical systems such as gears, pulleys and bearings. Other types of devices are based on linear motors, where the linear motion is obtained directly. The Linear Stepper Motor (MLP) is an excellent solution for industrial applications that require precise positioning and high speed. This study presents an MLP formed of a linear structure and static ferromagnetic material, and a mover structure which are mounted three coils. Mechanical suspension systems allow a linear movement between static and mover part, maintaining a constant air gap. The operating principle is based on the tendency of alignment of magnetic flux through the path of least reluctance; the force proportional to the intensity of the electric current and the speed proportional to the frequency of the excitation coils. The study of this device is still based on the use of a numerical analysis to verify the relationship between electric current applied and planar and normal force developed. In addition, the magnetic field in the air gap region is also monitored.

Keywords: Linear stepper motor, longitudinal force, magnetic flux, magnetic reluctance variable .

INTRODUCTION

Currently, industrial manufacturing processes require linear motion. Usually, it can be achieved with stepper rotary motor responsible for handling in the *x*-axis, in a Cartesian coordinate system. Other types of devices are based on linear motors, consisting of a static and a moving part. The control is carried out through digital control methods combined with electronics.

Linear reluctance variable motors (LRVM) are an excellent solution for positioning applications that require rapid acceleration and high-speed moves with low mass payloads. Mechanical simplicity and precise open-loop operation are additional features of this kind of linear motor. The LRVM is not subject to the same linear velocity and acceleration limitations inherent in systems converting rotary to linear motion [1, 2, 3].

With the linear motor as proposed in this work, the movement along of the *x*-axis, in the both sides, can be obtained from a single traction driver, without the need of mechanical system converters like belts, pulleys and gears. The mover part has a ferromagnetic core formed by a massive steel 1020 where are fixed three coils, electrically independents, responsible by the magnetic excitation field, from a electrical excitation. The secondary comprehends the static ferromagnetic massive steel 1020 core. Figure 1 shows the proposed structure while the table 1 shows the main characteristics. The primary and the secondary are separated from each other by a uniform air-gap [4, 5,6].

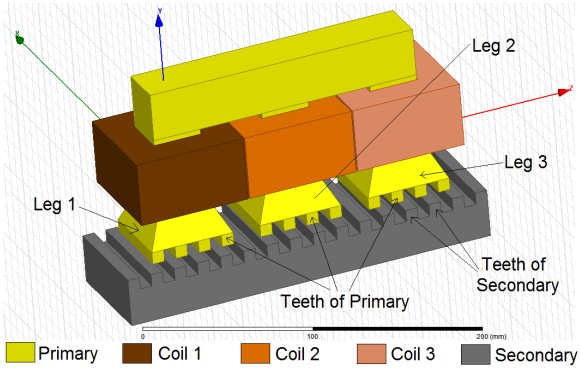

Figure 1. Proposed linear reluctance variable motor and its parts

Table 1. Metric characteristics of linear motor

Item	Value/Material
Number of phases	3
Number of coils	3
Number of turn per coil	250
Number of legs	3
Number of teeth per leg	4
Air gap	1mm
Material of core	Massive steel 1020
Operation range	0 – 4 Àmpères
Height of primary	112,5mm
Height of secondary	30mm
Maximum length of primary	192,5mm
Maximum legth of secondary	367,5mm
Maximum width of primary	52,5mm
Maximum width of secondary	70mm

NUMERICAL ANALYSIS

Numerical analyses of LRVM are carried out by means of FEM using a commercial package. A three-dimensional model or virtual prototype was developed, since the distribution of magnetic flux density flux

occurs in space, and the topology of the linear motor does not present symmetries to allow an analysis in two dimensions. The total number of finite elements in the virtual model is 125.365 and 145.546 differential equation for the solution.

Planar traction force

The planar traction force, essential for the operation of the device is monitored from the virtual model. For force measurements were chosen three different values of electric current to excite the three coils individually in three different positions. The situations provided for the test are divided into:

- Situation #1: teeth of leg 1 are aligned with four teeth of secondary core. In the first moment only the coil 2 is energized; in the second moment only the coil 3 is energized;
- Situation #2: teeth of leg 2 are aligned with four teeth of secondary core. In the first moment only the coil 1 is energized; in the second moment only the coil 3 is energized;
- Situation #3: teeth of leg 3 are aligned with four teeth of secondary core. In the first moment only the coil 1 is energized; in the second moment only the coil 2 is energized;

Results on the planar force in different situations are presented in table 2, 3 and 4.

Table 2. Situation #1

Current	Air gap mm	Planar force (N)	
		Coil 2 on	Coil 2 off
		Coil 3 off	Coil 3 on
1.5A	0.5	2.65	1.84
	1.0	1.20	0.81
	2.0	0.37	0.26
2.5A	0.5	11.01	7.96
	1.0	5.08	3.48
	2.0	1.55	1.12
4.0A	0.5	27.73	22.18
	1.0	17.06	12.33
	2.0	6.08	4.46

Table 3. Situation #2

Current	Air gap mm	Planar force (N)	
		Coil 1 on	Coil 1 off
		Coil 3 off	Coil 3 on
1.5A	0.5	2.36	2.17
	1.0	1.01	0.91
	2.0	0.32	0.29
2.5A	0.5	10.03	9.17
	1.0	4.35	3.92
	2.0	1.37	1.23
4.0A	0.5	27.16	24.34
	1.0	15.16	13.51
	2.0	5.41	4.86

Table 4. Situation #3

Current	Air gap mm	Planar force (N)	
		Coil 1 on	Coil 1 off
		Coil 2 off	Coil 2 on
1.5A	0.5	1.93	2.72
	1.0	0.90	1.09
	2.0	0.30	0.34
2.5A	0.5	8.39	11.32
	1.0	3.90	4.63
	2.0	1.26	1.44
4.0A	0.5	23.66	28.31
	1.0	13.90	15.44
	2.0	5.05	5.61

It is possible to see, from the tables, that planar force in directly proportional to the current applied in the coils and inversely proportional length of the air gap. The produced forces are enough to move the structure in the required direction. This direction is determined by the sequence of excitation coils. Average, when the air gap is 0,5mm, the force, as function of the electrical current, present a sensibility of 1,51N/A from 1,5A applied in the coil; 3,86N/A from 2,5A applied in the coil and; 6,41N/A from 4.0A applied in the coil.

CONCLUSIONS

The electromagnetic motor proposed in this paper present an alternative solution for industrial application that requires high speed motion having a simple and very flexible control. The flexibility of the prototype to adapt in specific situation is also an important advantage of this structure.

The normal force of attraction between the primary and the secondary-is inherent in the process, can also be used to support the primary if the system is placed inverted.

ACKNOWLEDGEMENT

The work presented in this paper is a research project which is being developed at Federal Institute of Rio Grande do Sul, Campus Farroupilha, supported by internal foment.

REFERENCES

[1] S. Nasar and I. Boldea, Linear electric actuators: theory, design, and applications. Englewood Cliffs: Prentice-Hall, 1987.

[2] N. F. Baggio Filho, Study on the Planar Induction Actuator. Porto Alegre, 2012. Ph.D. Degree Thesis, Post-Graduate Program in Electrical Engineering by Federal University of Rio Grande do Sul.

[3] J. Perssons, Soft Magnetic Composite Material – Use for Electrical Machines. The University, Newcastle Upon Tyne, UK.

[4] J. R. Melcher, Continuum Electromechanics. Cambridge: MIT Press, 1981.

[5] N. Ida and J. P. A. Bastos, Electromagnetics and Calculation of Fields. 2ed. New York: Springer – Verlag, 1986.

[6] K. Binns, P. Lawrenso and C. Trombridge, The Analytical and Numerical Solution of Electric and Magnetic Field. Chichester: John Wiley, 1999.

COMPARISON BETWEEN SYSTEM DESIGN OPTIMIZATION STRATEGIES FOR MORE ELECTRIC AIRCRAFT NETWORKS

Djamel Hadbi[*], [**], Nicolas Retière[*], Frederic Wurtz[*], Xavier Roboam[**], Bruno Sareni[**]

[*]Univ. Grenoble Alpes, G2Elab, F-38000 Grenoble, France, CNRS, G2Elab, F-38000 Grenoble, France
firstname.lastname@g2elab.grenoble-inp.fr

[**]Université de Toulouse, LAPLACE, UMR CNRS-INPT-UPS, 2 rue Camichel, 31071 Toulouse, France
firstname.lastname@laplace.univ-tlse.fr

Abstract. Nowadays, embedded aircraft system contains electrical devices which must cooperate in safe and light weight network. For designing such systems, different local strategies have been developed but no global optimization has been performed so far. In this paper, we present and compare three strategies applied to the sizing of a whole network of more electric aircraft: a simplified case study with only two components is considered to illustrate methodological issues. The quality of the solution found from each method is compared, with regards to the "cost of the collaborative approach" and the volume of data generation. This comparison should provide system designers an evaluation of the applicability of these methods according to the nature of the design problem.

Keywords: system design, integrated design, multilevel optimization, embedded electrical system.

INTRODUCTION

Modern engineering products are becoming increasingly complex, particularly in industries such as railway, aerospace and automotive [1], [2]. Conventionally, expertise and classical analysis methods, especially those based on simulations are used, aided by optimization methods in some part of the process. Each sub-system is designed separately by his manufacturer using his own model and process: this method is called "mechanistic approach". Another approach called "simultaneous design" may be developed to integrate all the components of a system into a single optimization. This extreme approach requires full cooperation for best results [2]. Another diametrically opposite approach enables to design a system with a minimal collaboration. This method called Extended Pareto Fronts was developed for the design of a railway application [3]. Industrial design imposes other constraints, integration of a large scale multidisciplinary system, privacy issues and decision level are fundamental criteria to elaborate feasible and efficient system design method [2].

I. DESIGN MODEL OF A SIMPLIFIED STUDIED CASE

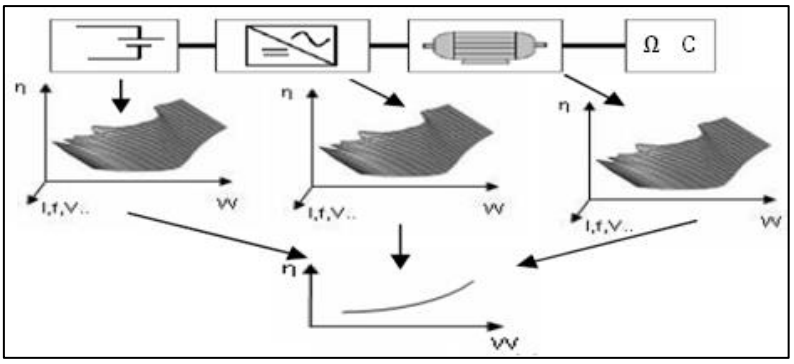

Figure 1. Design of an actuator by Extended Pareto Front Method

Extended Pareto Front Method (EPFM) is based on the decomposition of a system in several devices, each of them being previously optimized separately, only coupled by global variables (i. e. I, f, V in the figure 1). It intends to limit the communication of data between the suppliers. Only Extended Pareto Optimal Fronts (space solution) are provided by suppliers to the system designer. First, a necessary condition has to be checked: in a suitable decomposition, the system objective function has to be calculated by means of the objective functions of sub-problems. If so, a classification of all problem variables allows identifying global variables that describe couplings on the system. In the above example, there are N=3 couplings variables, i.e. current (I), frequency (f) and voltage (V) of the bus, completed by O=2 objective functions for weight (W) and device efficiency (η). So a N+O-dimension solution space is built for each component of the system. Gathering the Extended Pareto Fronts of all amenities, the system manufacturer shall be able to make tradeoffs within the sets of solutions in order to obtain the best solution at the system level. Of course, not any combination of equipment is possible; the manufacturer must be careful of the consistency of coupling variables that ensure the compatibility of the chosen amenities.

II. DESIGN OF A SIMPLIFIED EMBEDDED ELECTRIC NETWORK

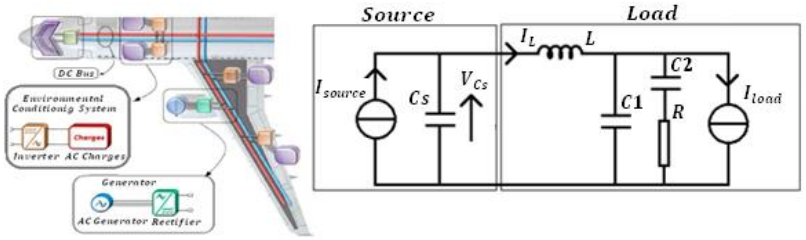

Figure 2. An example of a simplified embedded electric network

Embedded electric networks contain a high number of sources and loads connected to several buses: the issue is then to analyze applicability of optimization methods to this class of complex system. In our study, related to the development of strategies for system design, we initially relied on a "simplified" network, which is voluntary limited to a single load in order to establish and compare optimization methods. It consists of a single generating channel, connected with a unique non-linear load. This channel includes a generator, a rectifier and an output filter. The load comprises an actuator, an inverter and an input filter. We investigate the design of this channel (especially the filtering device sizing) using the three approaches previously presented: the optimization goal is to minimize the whole network weight in compliance with quality standards; (current and voltage harmonics are limited to a maximum threshold in a frequency band). Let us note that this case study consists of a single objective optimization for which the previous method (EPFM) of course remains applicable.

III. QUALITATIVE COMPARISON OF RESULTS

As shown in the figure 2 (left part), the values of the objective function obtained by two collaborative methods, the simultaneous design approach and Extended Pareto Front Method are better than the value of the objective function obtained with a conventional method ("mechanistic approach") based on expertise and classical analysis methods.

Collaboration level and calculation cost are conflicting characteristics as illustrated of the right part of figure 2: higher is the collaboration level, lower the necessary computational cost to reach the perfect solution. The mapping of the space solution of a sub-problem grows exponentially with the number of coupling variables (if there are P values of M input global variable, P^M optimizations are done). High level of collaboration means that subsystem manufacturers need to share and communicate their models for the design process. So it's easy for the system integrator to improve the whole system generating a small amount of data. On the other side, a low level of collaboration means that each subsystem designer keeps its design secret, so that he must provide more data to aircraft manufacturer to enable him finding the optimal combination of subsystems.

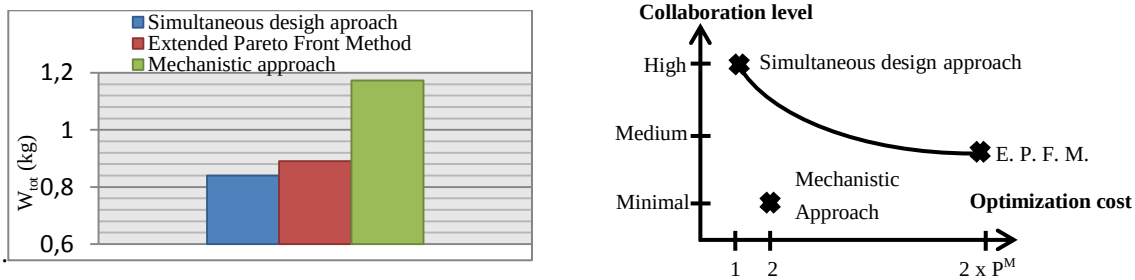

Figure 3. Comparison of optimization approaches in terms of objective function and costs (collaboration vs computation cost)

CONCLUSION

Through our work, we managed to check out conditions are necessary to elaborate a design strategy for complex system: collaboration and data generation. Thanks to this, we have proposed a multilevel collaborative design strategy while limiting the data exchanged by the designer of system components which is a requirement for industrial systems such as embedded networks.

REFERENCES

[1] F. Moussouni-Messad, "Multi-level and multi-objective design optimization tools for handling complex systems", these (PHD) de l'Ecole Centrale de Lille 2009.

[2] X. Roboam & al, "Integrated design by optimization of electrical energy systems'', edited by ISTE Wiley, 2012, ISBN 978-1-84821-389-0.

[3] H. Nguyen-Huu , N. Retière, F. Wutz, "A new approach for building the global Pareto border of an electromagnetic system by using the Pareto borders of each sub-component of the system", IEEE-CEFC 2008 (International Conference on Electromagnetic Field Computation), ID: OC1-4 in proceeding of the conference.

A MULTILEVEL DOUBLE LOOP APPROACH FOR THE DESIGN OF ONBOARD FLIGHT NETWORKS

Djamel Hadbi[*, **], Nicolas Retière[*], Frederic Wurtz[*], Xavier Roboam[**], Bruno Sareni[**]

[*]Univ. Grenoble Alpes, G2Elab, F-38000 Grenoble, France, CNRS, G2Elab, F-38000 Grenoble, France
firstname.lastname@g2elab.grenoble-inp.fr

[**]Université de Toulouse, LAPLACE, UMR CNRS-INPT-UPS, 2 rue Camichel, 31071 Toulouse, France
firstname.lastname@laplace.univ-tlse.fr

Abstract. After testing different existing design methods for complex problems, we have concluded that a good approach based on system decomposition must coordinate the design process of components to reach the system optimum. In this paper, we present a multilevel collaborative approach for designing complex systems based on several loops (here 2). A system level optimization loop added to lead optimizations of components at their optimal solutions. This method was applied to the sizing of a simplified embedded electric network with single source–load configuration.

Keywords: integrated design, collaborative multilevel optimization, embedded electrical system.

INTRODUCTION

Thanks to capabilities of optimization in solving nonlinear and multimodal design problems, and to face increasing system complexity, practitioners attempted to propose multilevel schemes [1], [2]. J.-F. M. Barthelemy proposed a classification of the multilevel optimization problems and identified several methods for solving certain classes of multilevel design problems [3]. He focused on two phases which are decomposition and coordination. Our works in GENOME project (optimized management of energy) allowed us to verify these conclusions and to add another key element: the "system level optimality". Decomposing a system and coordinating sub-system designs is not enough to reach the optimum of the original non-decomposed system. Sub-system optimizations have to be guided to reach the best system solution [1], [2]. In this paper, we present a new multilevel method inspired by the design of embedded electrical system. An additional level of optimization is used to choose the best solutions among all feasible coordinated solutions.

I. PROBLEM CLASSIFICATION

The matrix of dependencies is a powerful analysis method that describes the couplings between functions and variables [3]. In some cases, the decomposition is imposed by confidentiality constraints that condition the work of each team in the global design process of the system. So, methods based on decoupling variables are not suitable to deal with such problems. In such cases, other formulations have to be proposed to manage coupling variables.

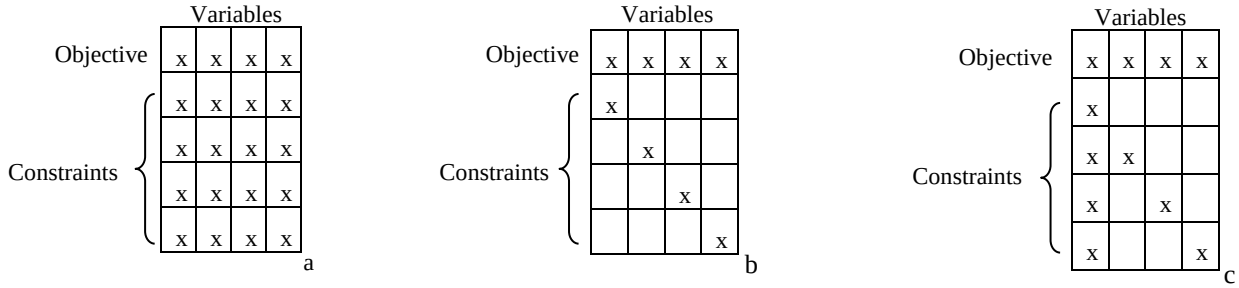

Figure 1. Dependency matrix with coupling variables: (a) block full, (b) block-angular, (c) quasi-block-angular

The second characteristic of the design problems often encountered in the design of embedded systems is that the objective functions at the system level can be expressed in terms of objective functions associated with each subsystem, e.g., the mass of an energy channel is the sum of all its components.

Figure 2. Objective function decomposition

II. MULTILEVEL DOUBLE LOOP METHOD

The original non decomposed problem depends of all design variables, each sub-objective function (W_{source}, W_{load}) depends on its own design variables, but constraints depend on all design variables.

$$(1)\quad \begin{cases} \min\limits_{Cs,C1,C2,L} W_{tot}(Cs,C1,C2,L) = \min\limits_{Cs,C1,C2,L}\left(W_{source}(Cs) + W_{load}(C1,C2,L)\right) \\ G_1(Cs,C1,C2,L) = V_{Cs_f} - V_{Cs_f}^{STANDARD} \le 0 \\ G_2(Cs,C1,C2,L) = I_{L_f} \le I_{L_f}^{STANDARD} \le 0 \end{cases} \qquad Cs, C1, C2, L \text{ are design variables}$$

Coupling variables (V_{CS}, I_L) have to ensure coherence between subsystems: there are coupled between themselves and depend on design variables. Due to frequency model of subsystems, voltage and current harmonic at a given frequency are related by the transfer function which depends on filter parameters.

$$(2)\quad \begin{cases} V_{Cs_f} = l_1\left(Cs, I_{L_f}\right) \\ I_{L_f} = l_2\left(C1, C2, L, V_{Cs_f}\right) \end{cases} \qquad V_{Cs_f} \text{ and } I_{L_f} \text{ are coupling variables of the system}$$

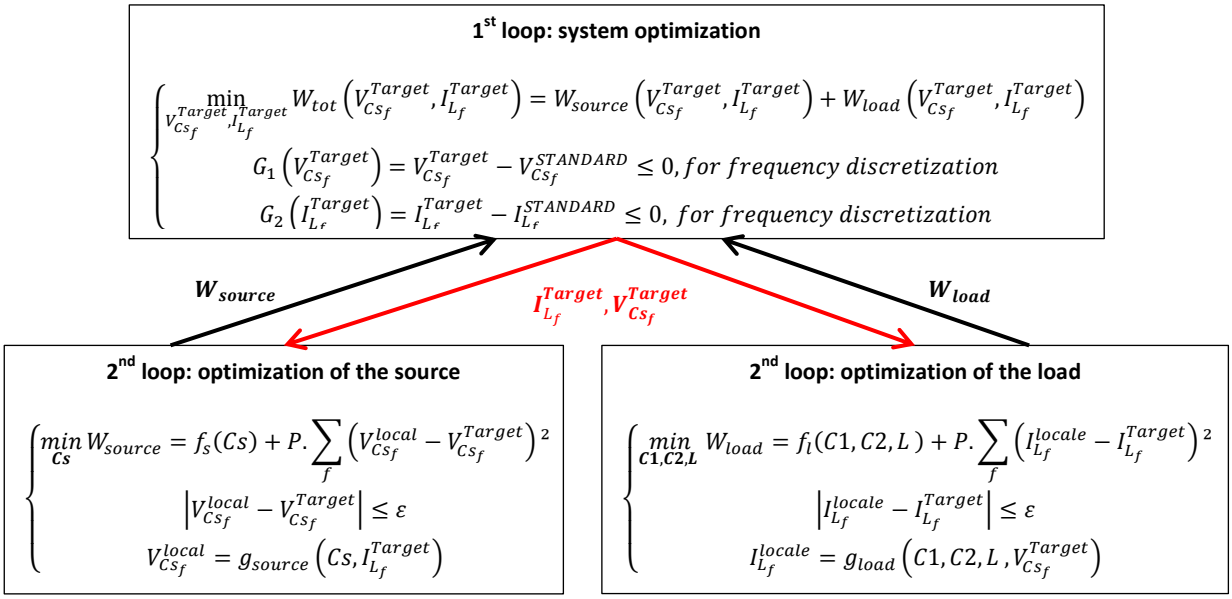

Figure 3. Architecture of the multilevel double loop optimization method

The proposed approach uses two levels of optimization. In the system level, the goal is to find values of coupling variables minimizing system level objective function. Each component optimization search the best solution in terms of design variables, but targeting coupling variables proposed at system level.

In the sub-system optimization, each optimization try to find the local optimum which respect to the values of coupling variables. The sub-objective function is penalized if targets on coupling variables are not fulfilled: in such a case, a penalty function is sent to the system level. The penalty term (P) must be very high in order to avoid the non-feasibility of the solution. With this configuration, the system level has to find feasible (P=0) and optimal design.

Table 1. Objective function value

Simultaneous design approach		Multilevel double loop approach	
Number of evaluations	50 000	Number of evaluations	1 500 000
Total weight (kg)	0.840	Total weight (kg)	0.839

Using a genetic optimization algorithm we were able to converge at the same optimal solution found by using a simultaneous optimization on a whole system. The number of evaluation of subsystems was:

$$(3)\quad N.ev. = N.ev.\,at\ system\ level\ \times 2\ \times\ N.ev.\,at\ subsystem\ level$$

Without knowing the internal models of subsystems, we managed to find the optimal system solution by exchanging only on data networks that are common to subsystems.

REFERENCES

[1] H Nguyen Huu, "Méthodes et outils pour la conception de composants intégrés dans un réseau électrique embarqué ", thèse (PHD) de l'université Joseph Fourier, Grenoble, France, 2008.

[2] Roboam, X. ; Sareni, B. ; Andrade, A.D, "More Electricity in the Air: Toward Optimized Electrical Networks Embedded in More-Electrical Aircraft ", Industrial Electronics Magazine, IEEE Volume: 6 ,Dec. 2012, pp. 6-17.

[3] J.-F. M. Barthelemy, "Engineering design application of multilevel optimization methods", in Computer Aided Optimum Design of Structures, Brebbia, CA, S. Hernandez, Ed. Berlin, Germany: Springer-Verlag, 1989, pp. 113–122.

MULTI-OBJECTIVE ROBUST OPTIMIZATION OF LOW FREQUENCY ELECTROMAGNETIC DESIGN PROBLEMS USING NEW MULTI-OBJECTIVE ROBUSTNESS MEASURE

Armin SALIMI* and David LOWTHER*

*McGill University, Department of Electrical and Computer Engineering, McConnell Engineering Building, 3480 University Street, Montreal, QC H3A 0E9, Canada, E-mail: armin.salimi@mail.mcgill.ca

Abstract. Optimizing for multiple objectives and obtaining a robust design are two challenging and important areas in electromagnetic design optimization and design optimization in general, yet the combination of these two which means achieving a robust multi-objectively optimized design is a subject rarely visited. In this paper a new metric for measuring robustness in a multi-objective space is introduced. The metric is then used as a constraint while performing multi-objective optimization on test problems and the results are presented.

Keywords: multi-objective robustness, robust optimization, weighted hyper-volume.

INTRODUCTION

The problem of obtaining robust solutions and measuring robustness has been well discussed in the context of single-objective optimization [1]; but little work has been done to tackle the issue of robustness in multi-objective spaces. Considering that using most of the existing single-objective robustness measures would lead to at least doubling the number of objectives when dealing with multi-objective problems, it seems necessary to pay more attention to the concept of robustness from a multi-objective point of view. To address this issue, a multi-objective measure for robustness based on the concept of weighted hyper-volume [2] with emphasis on the Pareto relations of dominance is proposed in this paper.

MULTI-OBJECTIVE ROBUSTNESS MEASURE

Due to the involvement of uncertainties and uncontrollability in the variables (design or otherwise), there exists a region associated with each solution point (both in the design space and in the objective space) which corresponds to the possible end results of the design while aiming for a specific solution point. In other words, the final outcome is not certainly the targeted solution, but rather a solution located somewhere in the vicinity of the targeted solution. In this context the region associated with all the possible solution points while aiming for a certain solution point is called the *perturbation region* of that point. The assumption is that the perturbation region of each solution point is a connected space (in both design and objective spaces) including the solution point itself.

Looking at the perturbation region of a solution from a Pareto optimality point of view, one can divide it into three sub-regions; i.e. the sub-region dominated by the original solution, the sub-region that is dominant with respect to the original solution, and the sub-region indifferent to the original solution. Here it is suggested that these three sub-regions should be treated differently as each of these regions may be of a different level of interest to the decision maker. In this context the magnitude of the *perturbation region hyper-volume* is denoted as *PRHV*. Also, the magnitudes of the three aforementioned sub-regions are denoted as $PRHV_{dominated}$, $PRHV_{dominant}$, *and* $PRHV_{indifferent}$, respectively.

In this paper it is proposed that the magnitude of the hyper-volume of the perturbation region (or parts of it) in the objective space be used as a measure for robustness. The choice of the sub-regions taken into account and how they are combined to form a robustness measure should reflect the decision maker's preferences and their understanding of robustness. For instance, in some cases all kinds of perturbations in the values of objective functions may be considered undesirable, whereas in other cases only the perturbations that result in a worse (dominated) solution may be deemed unpleasant. In the former case the hyper-volume of the whole perturbation region (*PRHV*) should be used as the measure of robustness while in the latter case only the hyper-volume of the dominated sub-region ($PRHV_{dominated}$) should be taken into account. This way of expressing preferences is similar to assigning different weights to different areas when using the weighted hyper-volume.

Due to space limitations, only $PRHV_{dominated}$ is used as the multi-objective measure of robustness in the test problems in this paper. The reason for choosing $PRHV_{dominated}$ is that in a considerable number of real-world design optimization problems only solutions which appear to be worse than the original solution in terms of objective values are considered undesirable.

TEST RESULTS

The test problem chosen to be presented in this digest is a modification of the simple test problem in [3] which is presented as a guideline to building test problems using the "bottom-up approach". Heavy bias has been introduced into the mapping from the design space to the objective space of this test problem in order to build a simple 2x2 test problem with variations in sensitivity across the objective space.

Figure (2) shows the design space and the objective space of this problem. The design space is uniformly sampled and the points have been mapped to the objective space in order to illustrate the existing bias in the mapping. Denser areas in the objective space are less sensitive to parameter changes in the design space hence they can be considered more robust. The $PRHV_{dominated}$ value for all the sample points has been evaluated and compared to a constraint value. In figure (2), red dots show the non-robust points while blue dots show the points that do not violate the robustness constraint. As can be seen in the figure, less dense (more sensitive) areas have relatively higher $PRHV_{dominated}$ values and do not satisfy the robustness constraint. The results of running NSGAII [4] with the constraint handling method introduced in [5] are also shown in figure (2). As can be seen, the algorithm finds the Pareto front (solution points marked as black stars) on the edge of the robust region of the objective space.

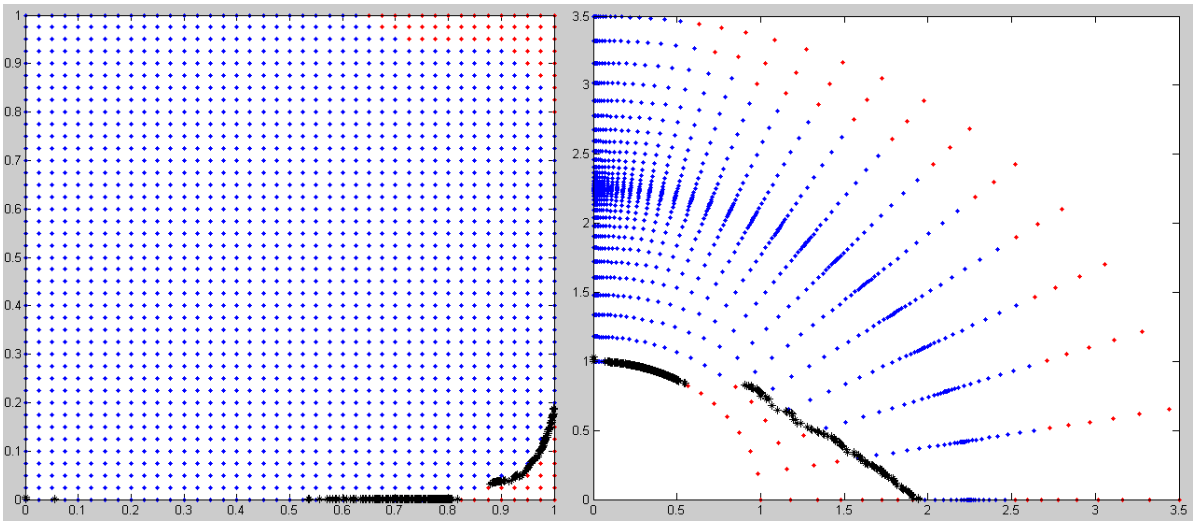

Figure 2. Design space (left) and objective space (right) of the test problem

CONCLUSIONS

In this paper a new multi-objective measure for robustness to be used in multi-objective robust design optimization problems has been introduced. The proposed measure which can work in the absence of probability distribution information has been integrated into NSGAII and the resultant algorithm has been used to optimize test problems. The results obtained from one test problem which show the alignment of the measure with the sensitivity interpretation of the concept of robustness have been presented here. Further explanation of the measure, the results obtained from other test problems, and more detailed analysis of the obtained results will follow in the extended paper.

REFERENCES

[1] H. Beyer, B. Sendhoff. Robust optimization – a comprehensive survey. Computer Methods in Applied Mechanics and Engineering, vol. 196, no. 33-34, 2007, pp. 3190-3218.

[2] E. Zitzler, D. Brockhoff and L. Thiele. The hypervolume indicator revisited: on the design of pareto-compliant indicators via weighted integration. Conference on Evolutionary Multi-Criterion Optimization, vol. 4403 of LNCS, 2007, pp. 862–876.

[3] K. Deb, L. Thiele, M. Laumanns and E. Zitzler. Scalable test problems for evolutionary multi-objective optimization. In *Evolutionary Multiobjective Optimization: Theoretical Advances and Application*. 2005, pp. 105-145, Springer.

[4] K. Deb, A. Pratap, S. Agarwal and T. Meyarivan. A fast and elitist multiobjective genetic algorithm: NSGA-II. IEEE Transactions on Evolutionary Computation, vol. 6, no. 2, 2002, pp. 182–197.

[5] G. Yen. An adaptive penalty function for handling constraint in multi-objective evolutionary optimization. In *Constraint-Handling in Evolutionary Optimization*. 2009, pp. 121-143, Springer.

CONTINUOUS FLOCK-OF-STARLINGS OPTIMIZATION FOR A GENERAL MAGNETIC HYSTERESIS MODEL

Ermanno CARDELLI * , Antonio FABA*, Antonino LAUDANI **, Francesco RIGANTI FULGINEI ** and Alessandro SALVINI **

*University of Perugia, Department of Engineering, Via G. Duranti 93, 06125 Perugia, Italy
E-mail: {ermanno.cardelli, antonio.faba}@unipg.it

**Roma Tre University, Department of Engineering, Via V. Volterra 62, 00146, Roma, Italy
E-mail: {alaudani, riganti, asalvini}@uniroma3.it

Abstract. A new general typology of optimization algorithm inspired to classical swarm intelligence, the Continuous Flock-Of-Starlings Optimization (CFSO), is used to face the inverse problem of modeling magnetic materials. It is obtained by translating the numerical swarm/flock-based algorithms into differential equations in the time domain and employing analytical closed-forms written in the continuum. The modeling of magnetic hysteresis is very important for the development of magnetic materials and the accurate design of electrical machines. Recently several hysteresis vector models have been proposed and discussed; one of them is the Vector Hysteron Model (VHM) which is a natural extension of the Preisach theory to the vector case. In this work we present a CFSO based approach for the identification of VHM in order to reproduce scalar and rotational hysteresis loops. Experimental validations are made for both NOG (Not oriented grain) and OG (Oriented grain) steels.

Keywords: Swarm Intelligence, Inverse problems, Magnetic materials, Optimization problem, Vector Hysteresis.

INTRODUCTION

The Swarm Intelligence applied to optimization was first introduced by James Kennedy and Russell Eberhart in 1995. Since this algorithm originally simulated the behavior of a swarm of insects, it was called Particle Swarm Intelligence (PSO). Obviously, a large series of changes from the original PSO have been proposed in order to improve its performances. By linking the particle behaviors via a neighbor-velocity matching, the PSO algorithm becomes the so called Flock of Starlings Optimization (FSO) [1] inspired to a naturalistic work presented in [2]. In particular, FSO uses topology for exchanging the information about the current velocity of each connected particles. The correspondent continuous model, named Continuous FSO (CFSO), was firstly introduced in [3] and its closed forms [4] allows updating of position and velocity of each particle without requiring numerical integration, drastically reducing the computational costs. The CFSO shows several features that make it very interesting and promising such as, among other, the possibility of a supervised approach of tuning parameters [5]. In this paper the CFSO is used to face the inverse problem of modelling magnetic materials. The Vector Hysteron Model (VHM) [6][7], which is a natural extension of the Preisach theory to the vector case, has been adopted for the simulation of behavior of soft magnetic materials. Validations have been made for both NOG (Not oriented grain) and OG (Oriented grain) steels and will be presented in the paper.

CONTINUOUS FLOCK-OF-STARLINGS OPTIMIZATION

In [3] and [4] it has been proved that it is possible to convert the numerical swarm optimization algorithm, PSO or FSO, into continuous time-domain dynamical systems described by a set of state-equations. The state equations equivalent to the rules used by the swarm-algorithms for updating velocity u_k and position x_k of generic *k*-th particle are:

$$\dot{u}_k(t) = \tilde{\omega} u_k(t) + \tilde{\lambda}(p_{best\,k}(t) - x_k(t)) + \tilde{\gamma}(g_{best}(t) - x_k(t)) + \sum_{m=1}^{N} \tilde{h}_{km} u_m(t) \tag{1}$$

$$\dot{x}_k(t) = u_k(t) \tag{2}$$

where the parameters $(\tilde{\omega}, \tilde{\lambda}, \tilde{\gamma}, \tilde{h}_{km})$ are, respectively, the so-called inertial, cognitive and social coefficients. Clearly, $\tilde{h}_{km} = \tilde{h}$ (for the sake of simplicity we assume one only value, $\tilde{h}$, for all controlled birds) if the *k-th* bird controls the *m-th* one, $\tilde{h}_{km} = 0$ otherwise. The equations (1) and (2) constitute the analytic model of CFSO and their closed forms allow to manage the whole optimization process [5].

THE VECTOR HYSTERON MODEL

The Vector Hysteron Model (VHM) is able to describe the magnetic hysteresis in three dimensions [7]. Nevertheless, in this work we will consider only the two dimensional case where a distribution of circular hysteron is defined on the magnetic field plane. Since a single hysteron generates an unitary magnetic induction [6], the value of the magnetic induction is obtained as a superposition of the contribution of each hysteron. The magnetic behavior of a material can be reconstructed using this model when an accurate identification of the hysteron distribution is performed. We used the Lorentian functions for defining the position and the radius of the hysterons. The used standard deviation are σ_x and σ_y for the position and σ_r for the radius. In addition a fourth parameter H_c is used in order to approximate with accuracy the coercitive field of the magnetic material. In this work the identification of those parameters for NOG and OG steel samples is described.

EXPERIMENTAL VALIDATIONS

The good agreement between computed and measured data for different magnetization processes, shown in Fig. 1, proved the effectiveness of the presented approach. In the extended paper more details and results will be presented and discussed.

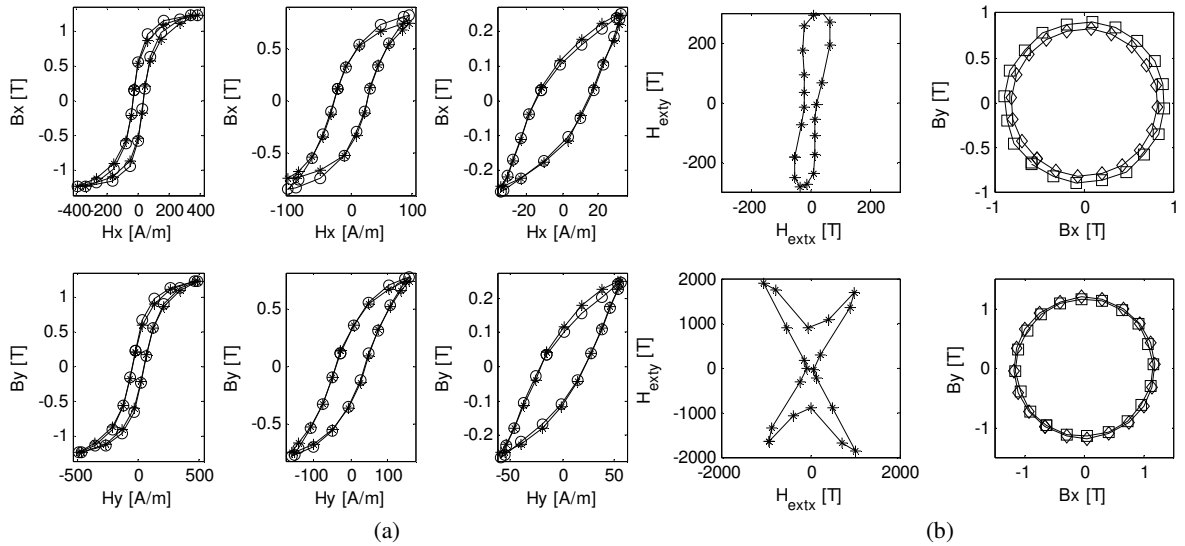

Figure 1. (a) NOG steel, on the first row three scalar hysteresis loops measured (stars), and computed (circles), along the rolling direction; on the second row three scalar hysteresis loops along the opposite direction. (b) OG steel, magnetic field loci measured (star), magnetic induction loci measured (diamond), and computed (square).

REFERENCES

[1] F. Riganti Fulginei and A. Salvini "Hysteresis model identification by the Flock-of-Starlings Optimization", International Journal of Applied Electromagnetics And Mechanics, vol. 30, no. 3-4; p. 321-331, 2009.

[2] M. Ballerini et al. "Interaction ruling animal collective behavior depends on topological rather than metric distance: Evidence from a field study", Proceedings of the National Academy of Science, pp.1232-1237, 2008.

[3] S. Coco, A. Laudani, F. Riganti Fulginei and A. Salvini, "Accurate design of Helmholtz coils for ELF Bioelectromagnetic interaction by means of continuous FSO", International Journal of Applied Electromagnetics and Mechanics, vol. 39, no. 1-4, pp. 651-656, 2012.

[4] A. Laudani, F. Riganti Fulginei and A. Salvini, "Closed Forms for the Fully-Connected Continuous Flock of Starlings Optimization Algorithm", 15th International Conference on Computer Modeling and Simulation (UKSim2013), Cambridge, United Kingdom, April, 2013

[5] A. Laudani, F. Riganti Fulginei, A. Salvini, M. Schmid, and S. Conforto, "CFSO3: A New Supervised Swarm-Based Optimization Algorithm," Mathematical Problems in Engineering, vol. 2013, Article ID 560614, 13 pages, 2013

[6] E. Cardelli, "A general hysteresis operator for the modeling of vector fields," IEEE Trans. Magn., vol. 47, no. 8, pp. 2056–2067, Aug. 2011.

[7] E. Cardelli, E. Della Torre, and A. Faba, "A general vector hysteresis operator: Extension to the 3-D case," IEEE Trans. Magn., vol. 46, no. 12, pp. 3990–4000, Dec. 2010

INVERSE-PROBLEM BASED PARAMETER ESTIMATION FOR PERMANENT-MAGNET SYNCHRONOUS MACHINES IN DIFFERENT LOADING CONDITIONS

Paavo RASILO*,**, Ahmed ABDALLH*, Ahmed HEMEIDA*,
Peter SERGEANT*,***, Marko HINKKANEN** and Luc DUPRÉ*

*Department of Electrical Energy, Systems and Automation, Ghent University,
Sint-Pietersnieuwstraat 41, BE-9000 Ghent, Belgium

**Department of Electrical Engineering and Automation, Aalto University,
P.O. Box 13000, FI-00076 Aalto, Finland

***Department of Industrial Technology and Construction, Ghent University,
V. Vaerwyckweg 1, BE-9000 Ghent, Belgium

E-mail: paavo.rasilo@aalto.fi

Abstract. The parameter identification for the direct-quadrature (d-q) axis model of a permanent-magnet (PM) synchronous motor is formulated as an electromagnetic inverse problem. The d-q model parameters are solved by comparison of the d-q model to a state-space model utilizing lookup tables of finite-element simulation results. The d-q inductances and the PM flux linkage are estimated for different operating points. The results compare reasonably to measurements.

Keywords: Finite-element methods, inverse problems, parameter identification, permanent magnet synchronous machines, state-space models.

INTRODUCTION

The control algorithms for permanent-magnet (PM) synchronous machine drives are typically based on the direct-quadrature (d-q) axis equivalent circuit. In the simplest form, the d-q model assumes constant values for the inductances L_d and L_q and PM flux linkage ψ_pm, as well as perfect decoupling of the flux-current relations of the d- and q-axes. In a real machine, however, higher-order permeance harmonics, magnetic saturation, hysteresis, anisotropy and eddy currents make the flux-current relationships dependent on loading, frequency and rotor angle, and can also cause cross-coupling between the d- and q-axes fluxes and currents.

A large amount of research has been dedicated to parameter estimation of PM machine parameters. Typically, the d-q model inductances are automatically identified during the commissioning of the drive using frequency-response or signal-injection methods in standstill [1], [2]. In addition, the parameters can be adapted during the actual operation [3], [4]. However, due to the large amount of control, estimation and adaptation algorithms utilizing the d-q model, the fundamental concept of parameter identification is easily obscured. Since the simple d-q model is not necessarily able to completely describe the behavior of the real machine, the parameter estimation should not be seen as the problem of finding "correct" parameter values for different operating points. Instead, it should be considered as an *inverse* or *optimization* problem [5], so that the best parameter values are the ones that make the d-q model predict a machine behavior that is as closely as possible to the real machine behavior. From this point-of-view, the parameter values do not need to be limited to a certain operating point but can also be optimized over a whole loading cycle.

In this paper, we adopt an electromagnetic inverse-problem approach for identifying the d-q model parameters for a 2.2-kW, 75-Hz, 6-pole interior-PM synchronous motor. The motor is first modeled in several operating points with a finite-element (FE)-based state-space (FE/SS) model [6], which allows taking into account the spatial permeance harmonics and magnetic saturation, but is hundreds of times faster than a time-stepping FE model. We then formulate the estimation of the d-q model parameters L_d, L_q and ψ_pm as an inverse problem in order to iteratively minimize the difference between the results from the FE/SS and d-q models. In order to validate the inverse approach, the obtained parameter values are compared to measurement results.

METHODS AND RESULTS

The FE/SS model has been implemented in the MATLAB/Simulink environment and is comprehensively described in [6]. The stator currents $\boldsymbol{i}_{\alpha\beta}$ (in the stator α-β reference frame) and the electromagnetic torque T are expressed as functions of the stator flux-linkages $\boldsymbol{\psi}_{\alpha\beta}$ and rotor angle θ_r using static FE results stored in lookup tables. The voltage equation and torque are thus given by

$$\boldsymbol{u}_{\alpha\beta} = R\boldsymbol{i}_{\alpha\beta,\mathrm{FE}}\left(\boldsymbol{\psi}_{\alpha\beta},\theta_\mathrm{r}\right)+\frac{d\boldsymbol{\psi}_{\alpha\beta}}{dt} \tag{1}$$

$$T = T_\mathrm{FE}\left(\boldsymbol{\psi}_{\alpha\beta},\theta_\mathrm{r}\right). \tag{2}$$

The d-q model is described by

$$\begin{bmatrix} u_\mathrm{d} \\ u_\mathrm{q} \end{bmatrix} = \begin{bmatrix} L_\mathrm{d} & 0 \\ 0 & L_\mathrm{q} \end{bmatrix} \frac{d}{dt}\begin{bmatrix} i_\mathrm{d} \\ i_\mathrm{q} \end{bmatrix} + \begin{bmatrix} R & -\omega_\mathrm{r} L_\mathrm{q} \\ \omega_\mathrm{r} L_\mathrm{d} & R \end{bmatrix}\begin{bmatrix} i_\mathrm{d} \\ i_\mathrm{q} \end{bmatrix} + \begin{bmatrix} 0 \\ \omega_\mathrm{r}\psi_\mathrm{pm} \end{bmatrix} \tag{3}$$

$$T = \frac{3}{2}p\left[\psi_\mathrm{pm} i_\mathrm{q} + \left(L_\mathrm{d} - L_\mathrm{q}\right) i_\mathrm{d} i_\mathrm{q}\right], \tag{4}$$

in which ω_r is the (electrical) rotor speed and p is the number of pole pairs. The parameters to be identified for the d-q model are $\boldsymbol{x} = (L_\mathrm{d}, L_\mathrm{q}, \psi_\mathrm{pm})$. The identification problem is formulated to find the parameter set $\tilde{\boldsymbol{x}}$ which minimizes the difference between the stator current waveforms $\boldsymbol{i}$ (vector including the samples) solved from the FE/SS and d-q models:

$$\tilde{\boldsymbol{x}} = \arg\min_{\boldsymbol{x}} \left\| \boldsymbol{i}_\mathrm{dq}\left(\boldsymbol{x}\right) - \boldsymbol{i}_\mathrm{FE}\left(\boldsymbol{x}\right) \right\|^2 \tag{5}$$

For comparison, the inductances of the machine were experimentally determined by open-circuiting the b- and c-phase windings, supplying a 28-V, 50-Hz voltage to a-phase, and measuring the a-phase current and c-phase voltage as a function of the rotor angle. The PM flux linkage was also measured from the back-emf [3].

Figure 1 shows preliminary inverse-problem results for different operating conditions, in which the voltage has been scaled linearly with the speed. It is clear that especially L_q depends significantly on the loading. The measured parameter values L_d = 0.108 H, L_d = 0.153 H and ψ_pm = 0.944 Wb correspond well to the variation ranges of Figure 1.

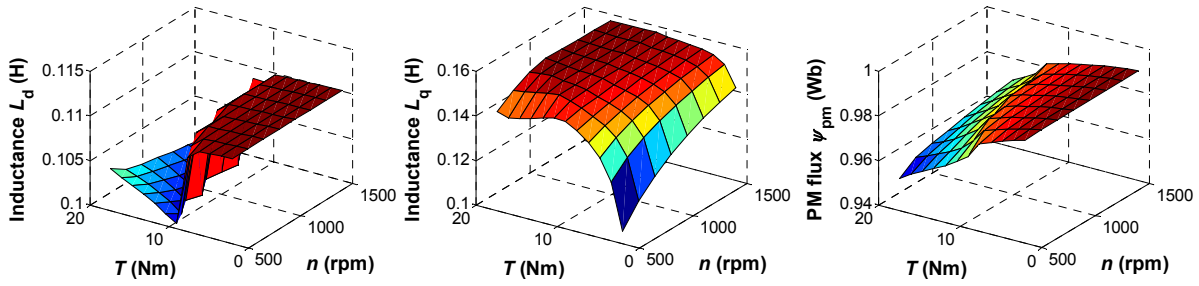

Figure 1. Dependency of solved L_d, L_q, ψ_pm on the average torque T and rotation speed n.

CONCLUSIONS

The results show that reasonable parameter values can be estimated with the electromagnetic inverse-problem formulation by comparison of the d-q model to an FE-based state-space model. In the full paper, we will focus on the uncertainties related to the inverse problem. In addition, we will also search for parameter values which optimize the d-q model performance over several loading points. A standard signal-injection method will also be performed numerically in order to validate the proposed inverse approach.

REFERENCES

[1] T. L. Vandoorn, F. M. De Belie, T. J. Vyncke, J. A. Melkebeek, P. Lataire, "Generation of multisinusoidal test signals for the identification of synchronous-machine parameters by using voltage-source inverter," *IEEE Trans. Ind. Electr.*, vol. 57, no. 1, pp. 430-439, 2010.

[2] G. Wang, L. Qu, H. Zhan, J. Xu,L. Ding, H. Zhang, D. Xu, "Self-commissioning of permanent magnet synchronous machine drives at standstill considering inverter nonlinearities," *IEEE Trans. Power Electr.* (in press), 2014.

[3] A. Piippo, M. Hinkkanen, J. Luomi, "Adaptation of motor parameters in sensorless PMSM drives," *IEEE Trans. Ind. Appl.*, vol. 45, no. 1, pp. 203-212, 2009.

[4] J. S. V. S. Kumar, P. S. Kumar, M. Rambabu, "Model reference adaptive controller-based speed and q-axis inductance estimation for permanent magnet synchronous motor drive by utilizing reactive power," in *Proc. ICEAS*, Khandagiri, India, 2011.

[5] M. Hadef, M. R. Mekideche, A. Djerdir, A Miraoui, "An inverse problem approach for parameter estimation of interior permanent magnet synchronous motors," *Progr. in Electromagn. Res. B*, vol. 31, pp. 15-28, 2011.

[6] P. Rasilo, M.-A. Lemesle, A. Belahcen, A. Arkkio, M. Hinkkanen, "Comparison of finite-element based state-space models for PM synchronous machines," *IEEE Trans. Energy Convers.*, vol. 29, no. 2, pp. 535-543, 2014.

DEMAGNETIZATION CURRENT EVALUATIONS USING FINITE ELEMENT METHOD AND MAGNETIC EQUIVALENT CIRCUIT MODELING AND OPTIMUM DESIGN IN A POLE CHANGING MEMORY MOTOR

Jung Ho Lee*, Su Yong Kim* and Young Hyun Kim*

* Department of Electrical Engineering Hanbat National University, Daejeon, 305-719, KOREA

E-mail: kimyh@hanbat.ac.kr

Abstract. This paper deals with the demagnetization current evaluations using Finite Element Method (FEM) and magnetic equivalent circuit modeling in a Pole Changing Memory Motor (PCMM). The focus of this paper is the characteristics evaluation relative to the current density and the magnet numbers of machine for pole changing condition in PCMMs. Magnetic equivalent circuit modeling method and demagnetizing currents characteristics of PCMM according to the magnet thickness variation are introduced. Finally, this paper deals with optimum design criteria to minimize the torque ripple, to maximize torque density of a PCMM using Response Surface Methodology (RSM).

Keywords: Demagnetizing current, FEM, PCMM, RSM

INTRODUCTION

Memory motors combine the flux controllability of a PM (permanent magnet) machine with the high power density of conventional electric machines [1]-[2]. They utilize the flux concentration principle which allows the generation of air-gap flux densities that are typical for high-efficiency machines. Memory motors can be built either as variable-flux or pole-changing machines. In both machine types, the magnetization of PMs can be simply varied by using a short current pulse, with no need for permanent demagnetizing current as in a conventional internal PM machine operating in at flux weakening mode. The operation of a memory motor is based on its ability to use a small stator current to change the magnetization of its magnets. This study illustrates how the magnetization of rotor magnets can be continually varied by applying a short pulse of stator current. In this paper, we introduce the magnetic equivalent circuit modeling and parameter calculation method for the selection of fundamental design variables for a pole changing memory motor (PCMM). A demagnetizing current evaluation method for a PCMM are presented and a characteristic analysis are performed in the situation of pole changing due to the demagnetizing short pulse current. And this paper presents, finally, the optimum design relative to the torque density and ripple on the basis of the design variables of magnet thickness and current in order to improve performance of a PCMM.

PRINCIPLE OF OPERATION OF THE PCMM

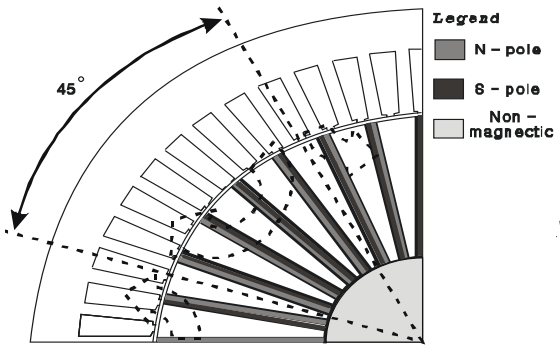

Figure 1. 8-pole magnetized PCMM.

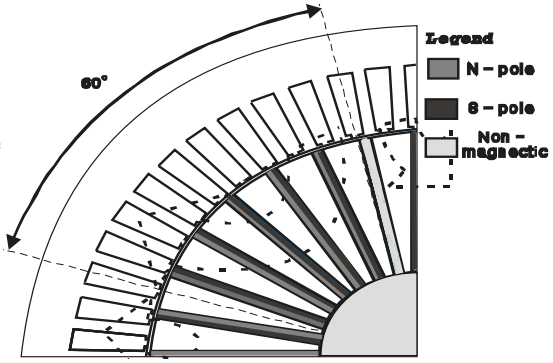

Figure 2. 6-pole magnetized PCMM.

Fig. 1 shows the cross-sectional view of a pole-changing memory motor with 32 tangentially magnetized magnets. On the rotor side there are four magnets per pole, all of which are magnetized in the same direction. The rotor wreath is built of PMs along with iron segments and is mechanically fixed to a nonmagnetic shaft. After the stator winding is reconnected into a six-pole configuration, a short pulse of stator current changes the rotor eight-pole to a six-pole magnetization, as shown in Fig. 2. Since the number of magnets per pole is no longer an integer (32/6=5.333...), some magnets can remain demagnetized.

MAGNETIC EQUIVALENT CIRCUIT AND DETERMINATION OF AIR GAP FLUX DENSITY

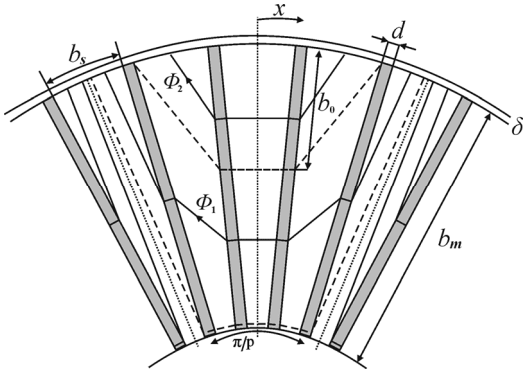

Figure 3. Cross-sectional view of the PCMM with four magnets per pole.

Assume that the rotor is built with 4 magnets per pole, and that all magnets are magnetized. The approximate flux density distribution in that case is shown in Fig. 3. The flux Φ_1 in Fig. 3 goes through the whole area of the left and right magnets, but only through a portion of the center magnet with radial height b_m-b_0. The flux Φ_2 in Fig. 3 goes only through a portion of the center magnet with radial height b_0. Since the magnets are tangentially magnetized, and there is no current in the rotor slots, one may write the tangential component of rotor slot flux density.

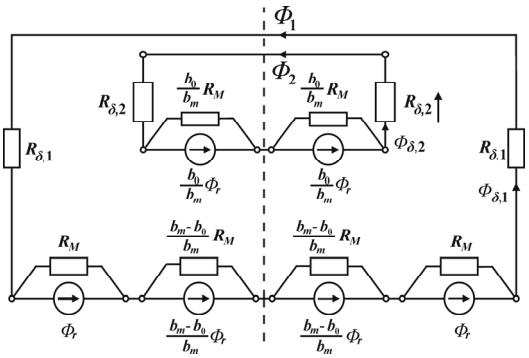

Figure 4. Magnetic equivalent circuit of proposed model.

Denoting by B_r the residual magnetism of the rotor magnets, and their coercive force H_c, one can define the quantities of the magnetic equivalent circuit in Fig. 4.

Where, G_m ; magnetic reluctance
$R_{\delta,1}$, $R_{\delta,2}$; air gap reluctance
$\Phi_{\delta,1}$, $\Phi_{\delta,2}$; air gap flux
$B_{\delta,1}$, $B_{\delta,2}$; air gap flux density

CONCLUSIONS

In this paper, we introduce the magnetic equivalent circuit modeling and parameter calculation method for the selection fundamental design variables in a Pole Changing Memory Motor (PCMM). In addition, the input demagnetizing currents for the 8/6 pole switching are selected in each PM thickness using the derived magnetic equivalent circuit and FEM. The demagnetizing characteristic of a PM of PCMMs according to the selected stator current are investigated. With this procedure, it is possible to investigate the influence of short pulse current components on the overall magnetization from an 8-pole to 6-pole configuration. And this paper presents a RSM optimization technique in order to reduce the torque ripple of a PCMM. Starting from an existing design, the best design solution is selected.

REFERENCES

[1] V.Ostovic, "Memory motor-A new class of controllable flux PM machines for a true wide speed operation," *in Conf. Rec. IEEE-IAS Annu*, Meeting, 2001, pp. 2577-2584.

[2] V. Ostovic, "Pole changing permanent magnet machines," *IEEE Trans. on Industry Applycations*, Vol. 38, No.6, pp.1493-1499 Dec. 2002

OPTIMUM DESIGN CRITERIA OF VARIABLE FLUX MEMORY MOTOR USING MAGNETIC EQUIVALENT CIRCUIT MODELING AND RESPONSE SURFACE METHODOLOGY

Jung Ho Lee*, Jung Woo Kim* and Young Hyun Kim*

* Electrical Engineering Department, Hanbat National University, Daejeon, 305-719 Korea
E-mail: kimyh@hanbat.ac.kr

Abstract. This paper deals with the optimum design criteria of a Variable Flux Memory Motor (VFMM) using magnetic equivalent circuit modeling and Response Surface Methodology (RSM). The focus of this paper is found firstly a design solution through the comparison of torque and efficiency according to magnetizing direction and quantity of permanent magnet and dimensions variations and, secondly, a mixed resolution with Central Composite Design (CCD) is introduced and analysis of variance (ANOVA) is conducted to determine the significance of the fitted regression model.

Keywords: FEM, Preisach modeling, VFMM.

INTRODUCTION

Memory motors combine the flux controllability of a PM machine with the high power density of conventional electric machines[1]-[2]. The distinguishing features of a Variable-Flux Memory Motor (VFMM) are the air-gap flux created by rotor magnets can be continuously varied within a fraction of the period of stator current and the re-magnetization current is smaller than rated machine current. The load current cannot demagnetize the magnets.

The effects of re- and demagnetization are important issues in the performance of VFMM. Therefore, whereas in other kind of machines a rough estimation of magnetization of PMs is acceptable, their importance in variable-flux memory motors justifies a greater effort.

In this paper, a coupled finite element analysis and Preisach modeling for a VFMM is presented and the characteristics analysis is performed under continuous re- and demagnetization. And this paper deals with the optimum design criteria of a VFMM using magnetic equivalent circuit modeling and Response Surface Methodology (RSM). The proposed procedure allows to define the rotor magnet shape, dimensions starting from an existing motor or a preliminary design.

PRINCIPLE AND ANALYTICAL MODELING OF VFMM

Operation principles of VFMM

A cross-sectional view of a four-pole VFMM is shown in Fig. 1. Tangentially magnetized PMs with N-poles and S-poles drive flux through the air gap into the stator. The rotor is built as a sandwich of PMs, soft iron, and nonmagnetic material, all of them being mechanically fixed to a nonmagnetic shaft. After applying a pulse of stator current in the opposite direction, the rotor magnets are partially demagnetized. A barrier in the magnets is created on a distance from the shaft surface that separates zones with old and new magnetization direction within each rotor magnet. The trapezoidal form of rotor magnets is a guarantee that the effects of re-magnetization current can be spatially controlled. The distance at which the flux density in the gap is equal to zero is called the zero flux radius..

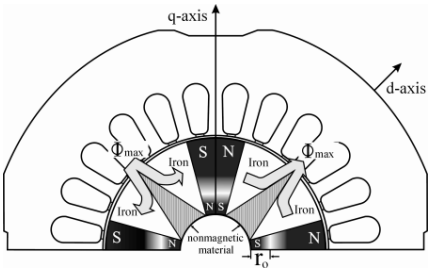

Figure 1. Cross-sectional view of a partially magnetized VFMM.

Analytical modeling of VFMM

The half-pole model of a VFMM rotor is shown in Fig. 2, in which the following notation was used:

d_1, d_2 : PM width on the shaft and air-gap side, respectively.

b_M : magnet radial length.

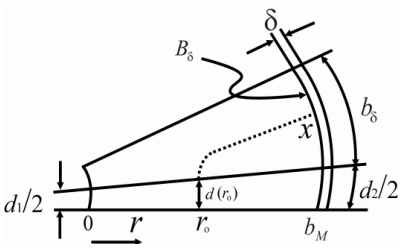

Figure 2. Cross-sectional view of a half pole of a VFMM.

Denoting the remanent flux density of the magnet B_r , its coercive force H_c, the air-gap flux density B_δ, and the machine length l, one can express the differential of magnet permeance dG_M and differential of gap permeance dG_δ as

(1) $$dG_M = \frac{B_r l d_r}{H_c d(r)} = \frac{B_r l}{H_c\left[d_1 + \frac{d_2 - d_1}{b_M} r\right]} dr \ , \ dG_\delta = \frac{\mu_0 l}{\delta} dx$$

$$d\Phi_r = d\Phi_M = d\Phi_\delta \ , \ \ d\Phi_\delta = B_\delta l dx \ , \ d\Phi_r = B_r l dr$$

One can further write

(2) $$d\Phi_\delta = \frac{d\Phi_r}{1 + \frac{dG_M}{dG_\delta}}$$

which leads to the differential equation

(3) $$\frac{dx}{dr} = \frac{B_r}{B_\delta} - \frac{\delta}{d_1 + \frac{d_2 - d_1}{b_M} r} \cdot \frac{B_r}{\mu_0 H_c}$$

The solution of which gives the circumferential coordinate x with the same potential as radial coordinate r

(4) $$x = \frac{B_r}{B_\delta} r - \frac{\delta B_r}{\mu_0 H_c} \cdot \frac{b_M}{d_2 - d_1} \ln\left(\frac{d_2 - d_1}{d_1 b_M} r + 1\right)$$

Points x and r in this equation define coordinates of a flux line going through the air gap (x) and the magnet (r). Therefore, this equation describes equipotential contours in the rotor pole and is called the flux contour equation. The flux contour equation is used to quantify the two most important parameters of a variable-flux memory-motor.

The maximum air-gap flux density B_δ is evaluated by substituting $x = b_\delta$ for $r = b_M$ in the flux contour equation. Since the circumferential dimension b_δ is equal to one-half pole pitch τ_p minus magnet width d_2 , one can express the air-gap flux density B_δ as

(5) $$B_\delta = \frac{B_r}{\frac{B_r}{\mu_0 H_c} \cdot \frac{\delta / \tau_p}{d_2' - d_1 / \tau_p} \ln \frac{d_2'}{d_1 / \tau_p} + \frac{\pi}{pc}\left(\frac{1}{2} - d_2'\right)}$$

with c standing for the ratio between magnet radial dimension and rotor radius, and $d_2' = \frac{d_2}{\tau_p}$.

CONCLUSIONS

A magnetizing characteristic analysis method has been proposed, which is suited for evaluation of machines with magnetic non-linearity, hysteresis phenomena and magnetizations.The magnetizing direction and quantity of a variable-flux memory motor (VFMM) according to stator MMF are investigated on the basis of the proposed analysis method. With this procedure, it is possible to investigate the influence of short pulse d-axis stator current components on overall magnetization.

Computer modeling and simulation results for operation characteristics of PMs shows the superiority of the proposed coupled finite element analysis and Preisach modeling.

REFERENCES

[1] V. Ostovic, “Pole changing permanent magnet machines,” IEEE Trans. on Industry Applications, Vol. 38, No.6, pp.1493-1499 Dec. 2002 C. Maxwell, A Treatise on Electricity and Magnetism, Clarendon Press, London, 1892.

[2] V.Ostovic, “Memory motor-A new class of controllable flux PM machines for a true wide speed operation,” in Conf. Rec. IEEE-IAS Annu, Meeting, 2001, pp. 2577-2584.

COMPARISON OF OPTIMIZATION FORMULATIONS TO DESIGN AN HYBRID RAILWAY POWER SUBSTATION

Maxime PLOYARD*, Stéphane BRISSET*, Florent DELHAYE* and Julien POUGET**

*L2EP – Ecole Centrale de Lille, Villeneuve d'Ascq, France, e-mail: maxime.ployard@ec-lille.fr, stephane.brisset@ec-lille.fr, florent.delhaye@ec-lille.fr

**SNCF Innovation & Research Department, Paris, France, e-mail: julien.pouget@sncf.fr

Abstract. This paper presents the design of a Hybrid Railway Power Substation. Two optimization formulations are investigated to obtain the optimal design and the energy management strategy that minimize the total cost of HRPS during an operating period of one year.

Keywords: Hybrid railway power substation, multi-sources system, energy storage, design, optimization, linear programming.

INTRODUCTION

Because of the rail network development, power demand of Hybrid Railway Power Substation (HRPS) becomes increasingly important [1]. The integration of renewables energies could compensate this need. Nevertheless the known intermittency factor of these energies makes difficult to estimate the amount of produced power [2]. By introducing a storage device, the HRPS may operate without the grid and could ensure a good power quality [1]. The storage device should be accurately used according to the consumed power, the produced power and the evolution of prices fixed by power supplier [3]. To enhance the design of HRPS, the energy management strategy should be suitable in the long term. However, a high number of unknowns is induced by these temporal variables and thereby two different formulations are investigated within the linear programing. By taking into account economical aspects, the optimal design of each source and the energy management strategy are known for a time step of ten minutes during one year.

1-MODEL AND OPTIMIZATION PROBLEM DESCRIPTION OF HRPS

The studied HRPS is presented in Fig. 1, it is composed of photovoltaic panels, wind turbines and a storage system connected to the substation through an AC bus. Renewable energy production illustrated by one-way power flows on Fig. 1, depends of the photovoltaic panels surface S_{pv} and the swept surface of wind turbines S_w. For the storage device, the quantity of maximal energy E_{max} defines the capability of storage, then power $P_{sto}(t)$ or energy $E_{sto}(t)$ can both express the temporal fluctuation of storage device for the optimization process.

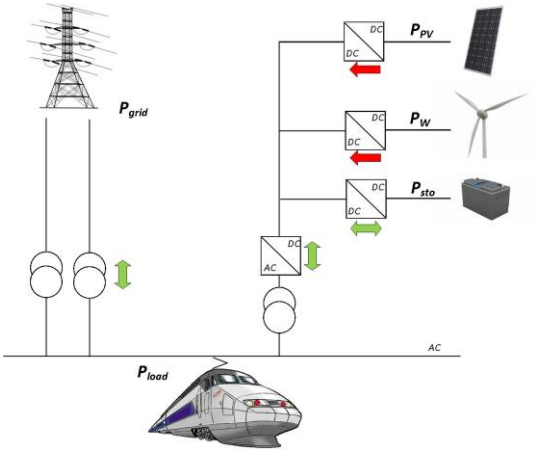

Figure 1. Overview of Hybrid Railway Power Substation.

According to measurements of wind speed and solar irradiation and for a given consumption during one year, all power flows of this multi-source system have to satisfy the power balance given in (1) [4]. The power from the grid P_{grid} is decomposed in two parts, the power received P^+_{grid} and the power sent P^-_{grid}.

(1) $$P_{grid}(t) = P^+_{grid}(t) + P^-_{grid}(t) = P_{load}(t) - P_{sto}(t) - P_{PV}(t) - P_W(t)$$

The objective function is expressed in (2) for an annual operating mode by considering investments cost of each device and also the purchasing C^{+}_{grid} and selling C^{-}_{grid} of electricity [3].

$$C = \sum_1^T C^{+}_{grid}(t) \cdot P^{+}_{grid}(t) \cdot \Delta t + \sum_1^T C^{-}_{grid}(t) \cdot P^{-}_{grid}(t) \cdot \Delta t + C_{sto}.E_{max} + C_{PV}.S_{PV} + C_W.S_W \quad (2)$$

In Table 1, two optimization problems are proposed through energy and power formulations of storage device. In power formulation, the stored energy is computed from the initial state of charge and also from the power stored at previous time steps. On the contrary, energy formulation considers only the maximal power of the storage. Dimensional variables of HRPS and grid power flow are the same on both optimizations.

Table 1. Description of each optimization problem formulation

Formulation		**power**	**energy**
Variables	common	$S_{PV}, S_W, E_{max}, E_{init}, P^{+}_{grid}(t), P^{-}_{grid}(t)$	
	specific	$P_{sto}(t)$	$E_{sto}(t)$
Constraints	energy bounds	$0 \leq E_{init} - \Delta t.\sum_1^T P_{sto}(t) \leq E_{max}$	$0 \leq E_{sto}(t) \leq E_{max}$
	power bounds	$-P_{max} \leq P_{sto}(t) \leq P_{max}$	$-P_{max} \leq \frac{E_{sto}(t) - E_{sto}(t-1)}{\Delta t} \leq P_{max}$
	periodicity	$\sum_1^T P_{sto}(t) = 0$	$E_{sto}(T) = E_{init}$

2-COMPARAISON OF FORMULATIONS

For both optimization problems, linear programming is used. However it requires specific matrices to express equality and inequality constraints. Due to a time step of ten minutes, each temporal variable induces 52560 unknowns for one year cycle, therefore sparse matrices are employed. On Table 2, both formulations are compared according to the size of equality and inequality matrices and the memory required to store them.

Table 2. Comparison of memory requirements for both formulations

Formulation	**power**		**energy**	
	Expression	Memory	Expression	Memory
Size of matrices	$(3.T+1)$ x $(3.T+4)$	185 GB (full)	$(3.T+1)$ x $(3.T+4)$	185 GB (full)
Number of nonzero	$10.T + T^2$	62 GB (sparse)	$10.T + 2$	12 MB (sparse)

Fig. 2.a. and Fig. 2.b. present respectively the nonzero elements of equality and inequality matrices for power and energy formulations during one day. On Fig. 2.a., the power formulation induces a higher number of nonzero elements which makes difficult the storage of matrices for a high number of unknowns. By employing energy formulation, the memory required is greatly reduced and the optimization of HRPS is achievable in a short time.

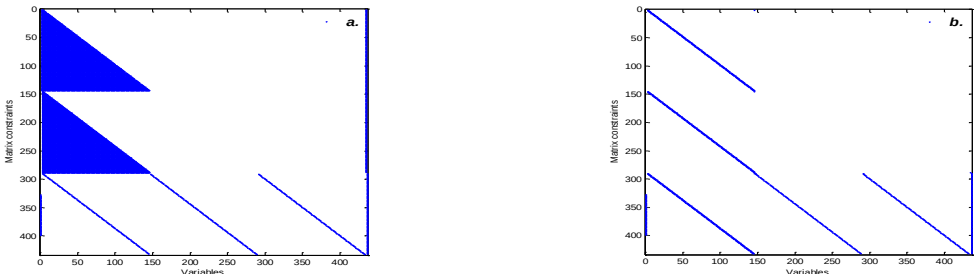

Figure 2. Comparison of matrices for one day

REFERENCES

[1] M. Aeberhard, C. Courtois, and P. Ladoux, "Railway traction power supply from the state of the art to future trends," in *Power Electronics Electrical Drives Automation and Motion (SPEEDAM), 2010 International Symposium on*, 2010, pp. 1350–1355.

[2] C. Clastres, T. Ha Pham, F. Wurtz, and S. Bacha, "Ancillary services and optimal household energy management with photovoltaic production," *Energy*, vol. 35, no. 1, pp. 55–64, 2010.

[3] R. Rigo-Mariani, B. Sareni, and X. Roboam, "A fast optimization strategy for power dispatching in a microgrid with storage," in *Industrial Electronics Society, IECON 2013-39th Annual Conference of the IEEE*, 2013, pp. 7902–7907.

[4] P. Pankovits, M. Ployard, J. Pouget, S. Brisset, D. Abbes, and B. Robyns, "Design and operation optimization of a hybrid railway power substation," in *Power Electronics and Applications (EPE), 2013 15th European Conference on*, 2013, pp. 1–8.

INCREASED ENERGY EFFICIENCY THROUGH SUPERVISORY CONTROL OF STORAGE COMPONENTS MODELLED USING HYBRID PETRI NETS

Guillaume CREVECOEUR*, Annelies COENE* and Luc DUPRE*

*Ghent University, Department of Electrical Energy, Systems and Automation, Sint-Pietersnieuwstraat 41, B-9000 Ghent, Belgium E-mail: guillaume.crevecoeur@ugent.be

Abstract. To accommodate the fluctuating demand with variable energy sources, means of energy storage need to be added into the energy grid. The complexity of the interactions between the various components in an energy grid need to be efficiently modeled for simulation purposes and for increasing the energy efficacy of power grids. In order to take into account the hybrid nature of the system, i.e. discrete and continuous time-varying processes, the modeling is performed using Petri nets adapted for energy grids. Supervisory control is implemented to attain optimal energy dynamics. This is implemented by finding the optimal control places and transitions in Petri net formulations that alter the connectivity between the various components and thus the topology of the system. We were able to reduce the use of conventional energy production by 5.5% using the supervisory controller.

Keywords: energy dynamics, energy efficiency, hybrid systems, supervisory control

INTRODUCTION

The increased production of renewable energy on a large scale, brings about a set of problems. The production rate of renewable energy directly depends on the amount of solar irradiation and wind speeds. The penetration of solar energy is restricted to only 7% of the total energy production (in Belgium) when no energy storage is used. To accommodate the demand at any time, energy storage is therefore needed. Significant renewable energy sources are restricted to solar and wind energy while the conventional energy production consists of nuclear power plants and traditional coal and gas (COGAS) power plans. The latter are adaptable in time to the aggregated energy demand.

So to understand to a better extent the operation of energy systems, and to increase its efficiency by implementing control mechanisms that plan loading and unloading of the energy, modelling techniques are required. Petri nets - originating from graph theory - form excellent tools [1]. Petri nets enable the mathematical modelling of concurrency and conflicts between components. The components, i.e. solar panels, windmills, energy consumers, power storage, energy transportation and net connection with combined gas and steam (COGAS) and nuclear energy production; have distinct specifications and dynamics that need to be accounted for in the modelling. So to minimize the excess of produced energy and the optimal penetration of renewable energy, supervisory control [2] is implemented that changes the incidence or connectivity between the various components in the complex network. The simulation thereof yields the energy changes in and between the various components.

METHODS

Hybrid Petri nets for energy systems

Systems consisting of discrete and continuously varying processes are hybrid systems and in order to accommodate the complexity, graph modeling can be applied. Petri net is a modeling formalism that consists of four main components: places (P_i), transitions (T_i) and arcs connecting the first two. The fourth component are the tokens having transitions from one place to another within the Petri net. The state of the system is given by the tokens in the places at any given moment. In order to satisfy given specifications, conditions, etc.., Petri nets can be adapted for use in different situations. The adaptations can be divided in extensions and abbreviations [3]. Extensions extend the capabilities of the PN whereas abbreviations simplify the working and the representation of PN. An extensive detailed model was implemented, see figure 1, based on Petri nets of the components: variable energy production (photovoltaic and wind energy), variable energy consumption, energy storage, transportation of energy, and connection to the main grid. The different adaptations mentioned above are implemented in a software platform. An example of a component, i.e. the storage component, as implemented in the system, is visualized in figure 1. The changes in states of the Petri net are defined as

$$\vec{x}(k+1) = \vec{x}(k) + \vec{v}(k)A \tag{1}$$

with $\vec{x}(k)$ being the state vector at time instant k, $\vec{v}(k)$ the firing vector and A the connectivity matrix.

The equation in figure 1 illustrates the elements within the connectivity matrix of a storage component. The overall Petri net consists of a total connectivity matrix that incorporates the connectivity submatrices of the different components. This matrix holds information on the links between these components and on the conditions for having transitions from one component to another.

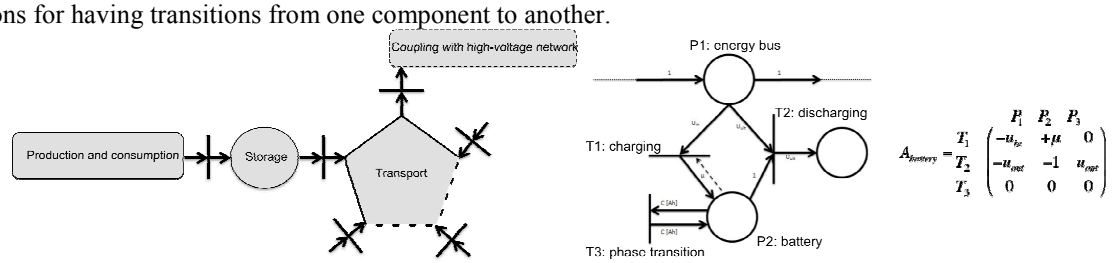

Figure 1. Connection of components modeled through Petri nets (left) with example of the storage component (right).

Supervisory control for increased energy efficiency

In a timed Petri net, i.e. graph model incorporating a clock structure, the triggering event and thus the next state is chosen on the basis of

(3) $$\dot{v}(k) = \arg \min_{i \in \Gamma(x(k))} y_i$$

with Γ being the feasibility function depending on the state at time instant k and y_i being the clock value of the event. This minimization is necessary so to determine the next state of the system and depends on various constraints within the model. Supervisory control is implemented for reducing the amount of unused energy. Therefore, the storage component in the energy grid needs to be adapted and controlled. So to alter the dynamics, the connectivity matrix needs to be extended with additional supervisory control places and transitions.

RESULTS AND DISCUSSION

Results of the implemented supervisory control method are shown in Figure 2. The simulation is performed here for 2 blocks and the total simulation time is 7 days with a time step of 10 minutes. The simulation results show that the operation of all components and their interactions can be modelled in a modular and universal way, in which the total computational time varies between 5 and 75 minutes for 2 to 8 blocks. Results show a 5.5% reduction of usage of traditional (COGAS) energy plants compared to the same system (topology and components) without supervision.

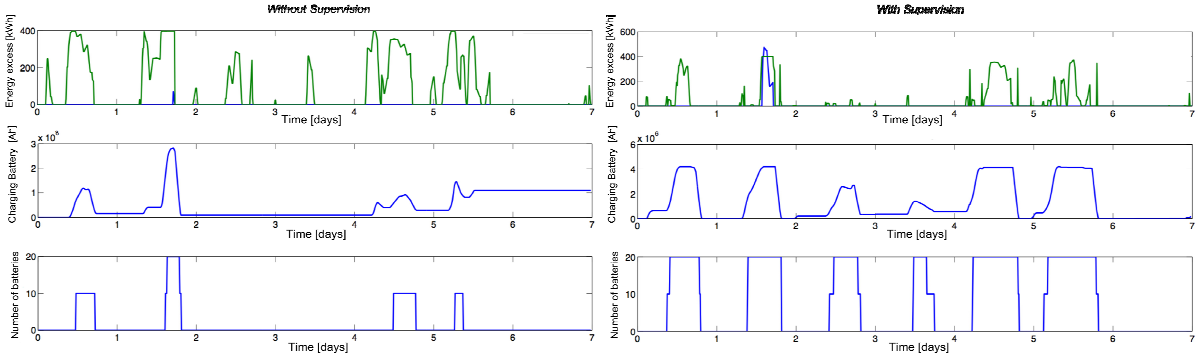

Figure 2. Energy efficiency of 2 blocks without supervision (left) and with supervision (right).

CONCLUSION

Based on Petri net graph formalisms, an energy grid is simulated. In order to increase the efficacy of the dynamics so to satisfy certain conditions of transition, supervisory control was implemented that alters the dynamics within the system. Results show that through supervisory control of the storage components, the usage of traditional energy plants can be reduced.

REFERENCES

[1] R. David and H. Alla, "Petri nets for modeling of dynamic systems: A survey," Automatica, vol. 30, no. 2, pp. 175-202, 1994.

[2] F. Guerin, D. Lefebvre, and V. Loisel, "Supervisory control design for systems of multiple sources of energy," Control Engineering Practice, vol. 20, pp. 1310–1324, 2012.

[3] Y. Katsigiannis, P. Georgilakis, and G. Tsinarakis, "A Novel Colored Fluid Stochastic Petri Net Simulation Model for Reliability Evaluation of Wind/PV/Diesel Small Isolated Power Systems," IEEE Transactions on Systems, Man and Cybernetics – Part A: Systems and Humans, vol. 40, no. 6, pp. 1296-1309, 2010.

NUMERICAL PERFORMANCE OF HOLE SENSITIVITY-BASED LEVEL SET METHOD FOR TOPOLOGY OPTIMIZATION IN ELECTROMAGNETIC SYSTEM

Seung Geon Hong, Kang Hyouk Lee, and Il Han Park

Sungkyunkwan University, School of Electronic Electrical Engineering, Suwon, Korea
E-mail: ssgun14@skku.edu

Abstract. To show usefulness of hole sensitivity of electromagnetic systems, the level set method with the hole sensitivity is applied to shape and topology optimization of synchronous reluctance motor. The numerical results of design model are compared with the ones without the hole sensitivity. The results show that the performance of optimization with hole sensitivity is 12% better than the performance without it.

Keywords: hole sensitivity, continuum shape sensitivity, level set method, shape and topology optimization, electromagnetic system.

INTRODUCTION

Recently the level set method was introduced for topology design optimization of electromagnetic systems. The authors succeeded in combine the level set method with the continuum shape sensitivity of closed analytical form [1]. This design approach enables not only representation of precise and clear shapes, but also it shows numerical advantages of good convergence and reduced computational time. In addition, its numerical implementation becomes very easy since optimization searching algorithm is transformed into a transient analysis algorithm with respect to a parameter of pseudo-time. However, the level set method has a drawback that the degree of freedom in topology gradually decreases along with iterative design process. Even though initial design is taken to have high degree of freedom in topology, only merging and disappearing of given material regions are shown, but generating of new region does not appear. This change of getting simpler in topology can not assure its convergence to optimal design. Therefore, this method needs to be imporved so that it is suitable for design problem with more complexity in topology. To settle this problem, topological sensitivity formula of analytic hole sensitivity was derived and its feasibility was shown in the recent paper [2]. The hole sensitivity is expected to contribute to generating the global optimal design for the topology optimization problems.

In this paper, the level set method with the exact hole sensitivity is applied to a more practical design problem to show its usefulness and analyze its numerical characteristics in topology variation, converged value of objective function, program implementation, computational time, etc. The numerical results from design model of a 6-pole synchronous reluctance motor are compared with the ones by the level set method without the hole sensitivity.

HOLE SENSITIVITY IN MAGNETOSTATIC SYSTEM

The continuum shape sensitivity is derived using the material derivative concept of continuum mechanics and adjoint variable technique. In 2D magnetostatic system, the continuum shape sensitivity is derived as [2]

$$G_s(A_z, \lambda) = (1/\mu_1 - 1/\mu_2)\vec{B}(A_z^*) \cdot \vec{B}(\lambda^{**}), \tag{1}$$

where A_z is vector potential and λ denotes the adjoint variable.

Fig. 1 shows a virtual hole at $\vec{x} \in \Omega^*$ with radius $r \to 0$. Using the virtual-hole concept and the continuum shape sensitivity, the hole sensitivity in magneto static system is derived in a closed analytical form as [3]

$$G_h(\vec{x}) = \frac{2}{\mu_1}\frac{\mu_2 - \mu_1}{\mu_2 + \mu_1}\vec{B}(A_z^*) \cdot \vec{B}(\lambda^*). \tag{2}$$

The hole sensitivity is used in combination with the level set method for the topology optimization to get better topology design.

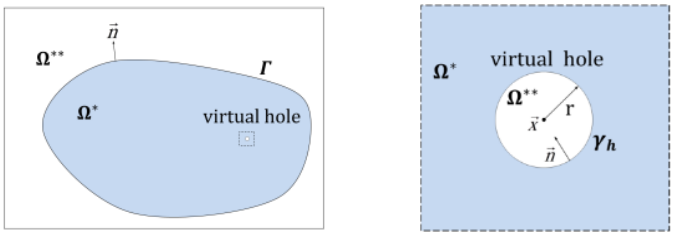

(a) Design domain with a virtual hole (b) Enlarged virtual hole

Figure 1. Magnetostatic system with a virtual hole.

DESIGN PROBLEM OF 6-POLE SYNCHRONOUS RELUCTANCE MOTOR

The design objective of this problem of 6-pole synchronous reluctance motor is to generate a maximum torque. To maximize torque generation, the objective function is taken as to maximize difference in the magnetic system energy between d-axis and q-axis. In this magnetic system, the ferromagnetic material and air each occupy 50% area of the design domain. Fig. 1 shows the final design of rotor shape. The results show that the performance of optimization with hole sensitivity is 12% better than the performance without it.

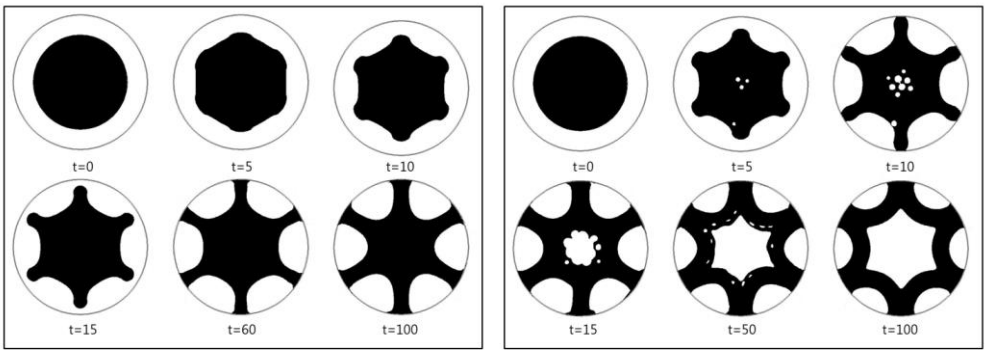

(a) Topology variation using shape sensitivity (b) Topology variation using shape and hole sensitivity

Figure 2. Comparison of the rotor shapes between shape sensitivity model and shape and hole sensitivity model.

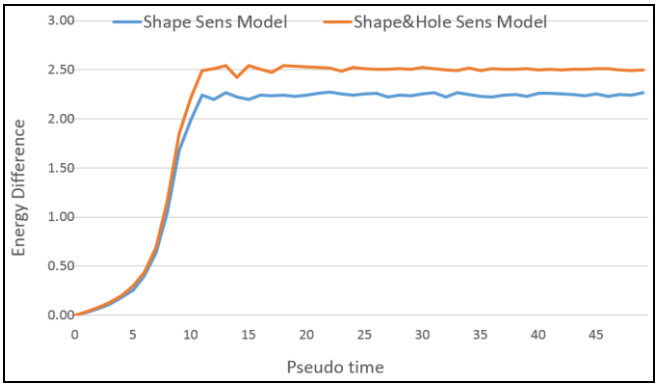

Figure 3. Change of objective-function value in pseudo time domain..

REFERENCES

[1] I. Park, J. L. Coulomb, and S. Hahn, "Design sensitivity analysis for nonlinear magnetostatic problems by continuum approach," *J. de Phys. III*, vol. 2, no. 11, pp. 2045-2053, Nov. 1992.

[2] Young Sun Kim, Se-Hee Lee, Hong Soon Choi and Il Han Park, "Shape formation of ferrofluid under external magnetic fields using level set method," *Journal of Applied Physics*, 105, 07D539, April, 2009.

[3] S. G. Hong, K. H. Lee and I. H. Park, "Derivation of Hole Sensitivity Formula for Topology Optimization in Magnetostatic System Using Virtual Hole Concept and Shape Sensitivity," presented at the 16th biennial IEEE Conference on Electromagnetic Field Computation, Annecy, FR, 2014.

RECONSTRUCTION OF 3D DIELECTRIC OBJECTS BURIED UNDER 2D ROUGH SURFACES BY USING CONTRAST SOURCE INVERSION METHOD

Yasemin ALTUNCU*

*Nigde University, Department of Electrical and Electronics Engineering, Nigde, TURKEY

E-mail: yaltuncu@nigde.edu.tr

Abstract. A numerical method based on contrast source inversion (CSI) algorithm is proposed to reconstruct complex dielectric permittivity variation of an inaccessible 3D dielectric object buried under 2D rough surface. The initial step of the method is to introduce the data and object equations involving the dyadic Green's function of the background medium which consist of a rough interfaced half-space. The Green's function is calculated numerically by buried object approach (BOA). Then data and object equations are solved iteratively as updating unknown contrast source and contrast function at each step for minimization of a defined cost functional. Some numerical implementations are given to exhibit the performance of the presented method.

Keywords: Buried object approach, Contrast source, 2D rough interface.

INTRODUCTION

The reconstruction of the geometrical and material properties of an inaccessible object is rather important in terms of practical application since it can be directly implemented to the real life problem. Therefore, it is possible to find a large amount of studies using different inversion algorithm about this issue [1-3]. The contrast source inversion method (CSI) [4] is one of the most popular one. It is not required to solve the forward scattering problem at each iteration step and the unknown contrast function and the contrast source that is the multiplication of the contrast function and the total electric field are updated iteratively to minimize the cost functional.

In this work, conjugate gradient (CG) based CSI algorithm is applied to inverse scattering problem of 3D dielectric objects buried under 2D rough surface. In this context, the object equation and data equation involving the dyadic Green's function of the rough interfaced half-space are introduced first. The Green's function is computed numerically by using BOA method [5]. Afterwards, the object and data equations are solved iteratively to determine the complex dielectric constant variation through the defined object domain in which 3D dielectric object is assumed to be located.

FORMULATION

The geometry is shown in Fig.1. Here the unknown 3D dielectric object denoted B is buried in to the lower half of the two half-space media separated by 2D locally rough interface. The constitutive parameters of upper and lower half mediums are $\epsilon_1, \mu_0, \sigma_1$ and $\epsilon_2, \mu_0, \sigma_2$, respectively, while those of buried dielectric are $\epsilon(\boldsymbol{r}), \mu_0, \sigma(\boldsymbol{r})$. Here μ_0 is the permeability of free space and $\boldsymbol{r}(x, y, z)$ is the position vector in 3D space. In this configuration, the domain D where the dielectric object is assumed to be located is called object domain. Here the considered inverse problem is to determine the complex permittivity of the buried dielectric from scattered fields measured at various points in a data domain denoted S which is above the rough surface.

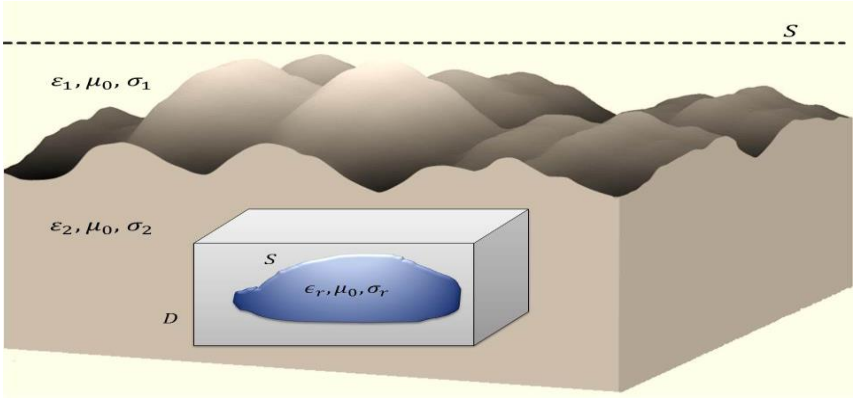

Figure 1. Geometry of the problem

The illuminations of the object domain by transmitters are carried out sequentially through N_j incident waves denoted $\boldsymbol{E}_j^i(\boldsymbol{r}) = \boldsymbol{E}^i(\boldsymbol{r}, \boldsymbol{r}_j)$ where $\boldsymbol{r}_j, j = 1,2,..,N_j$ is the position of the j'th source. The total electric field related to j'th illumination represented by $\boldsymbol{E}_j\ (\boldsymbol{r})$ is sum of two electric fields as,

(1) $$\boldsymbol{E}_j\ (\boldsymbol{r}) = \boldsymbol{E}_j^o(\boldsymbol{r}) + \boldsymbol{E}_j^s(\boldsymbol{r})$$

where $\boldsymbol{E}_j^o$ is the background electric field which is the total field in the absence of the buried scatterer and $\boldsymbol{E}_j^s$ is scattered electric field resulting from the presence of this scatterer. The background field $\boldsymbol{E}_j^o(\boldsymbol{r})$ is calculated numerically by BOA method in which 2D roughness of the interface is modelled as 3D dielectric objects located into the half-spaces remain on the both sides of a fictional planar interface. The contrast function to be determined is obtained by solving the following object equation,

(2) $$\boldsymbol{E}_j\ (\boldsymbol{r}) = \boldsymbol{E}_j^o(\boldsymbol{r}) + k_2^2 \int_D \overline{\mathbf{G}}\,(\boldsymbol{r}, \boldsymbol{r}')\chi(\boldsymbol{r}')\boldsymbol{E}_j(\boldsymbol{r}')d\boldsymbol{v}' \qquad \boldsymbol{r} \in D$$

and data equation,

(3) $$\boldsymbol{E}_j^s(\boldsymbol{r}) = k_2^2 \int_D \overline{\mathbf{G}}\,(\boldsymbol{r}, \boldsymbol{r}')\chi(\boldsymbol{r}')\boldsymbol{E}_j(\boldsymbol{r}')d\boldsymbol{v}' \qquad \boldsymbol{r} \in S$$

iteratively. In the above two equations $\overline{\mathbf{G}}$ is the dyadic Green's function of the background medium consist of two half-space with rough interface. Due to the fact that, it is not possible an analytical expression for $\overline{\mathbf{G}}$ it is calculated numerically using the BOA method. $\chi(\boldsymbol{r})$ is the contrast function defined as following,

(4) $$\chi(\boldsymbol{r}) = \frac{k^2(\boldsymbol{r})}{k_2^2} - 1$$

where k_2 and $k(\boldsymbol{r})$ denote wavenumbers in lower half-space and at point $\boldsymbol{r}$. The CSI algorithm is followed to figure out the unknown contrast function given in (4). To this end, the contrast source which is the product of total field and contrast function is defined first as,

(5) $$\boldsymbol{W}_j(\boldsymbol{r}) = \chi(\boldsymbol{r})\boldsymbol{E}_j(\boldsymbol{r})$$

and then the object and data equations are rewritten in terms of this function in compact forms

(6) $$\boldsymbol{W}_j = \chi\boldsymbol{E}_j^o + k_2^2\,\overline{\mathbf{G}}_D\boldsymbol{W}_j$$

and

(7) $$\boldsymbol{E}_j^s = k_2^2\overline{\mathbf{G}}_s\boldsymbol{W}_j.$$

where

(8) $$\overline{\mathbf{G}}_{S,D}\boldsymbol{W}_j = \int_D \overline{\mathbf{G}}\,(\boldsymbol{r}, \boldsymbol{r}')\chi(\boldsymbol{r}')\boldsymbol{E}_j(\boldsymbol{r}')d\boldsymbol{v}' \quad \boldsymbol{r} \in S, D.$$

The unknown contrast source and contrast are updated in (6) and (7) to minimize the cost functional defined by,

(9) $$F = \frac{\sum_j \left\|\boldsymbol{E}_j^s - \overline{\mathbf{G}}_s\boldsymbol{W}_j\right\|_S^2}{\sum_j \left\|\boldsymbol{E}_j^s\right\|_S^2} + \frac{\sum_j \left\|\chi\boldsymbol{E}_j^o - \boldsymbol{W}_j + \overline{\mathbf{G}}_D\boldsymbol{W}_j\right\|_D^2}{\sum_j \left\|\chi\boldsymbol{E}_j^o\right\|_D^2}$$

in which $\|\cdot\|_{S,D}^2$ is the norm on S or D.

CONCLUSIONS

CSI method is implemented to the solution of inverse scattering problem corresponding to 3D dielectric object buried under 2D local rough surface. The dyadic Green's function of the background medium involved in the object and data equations are obtained by BOA method, numerically. The complex dielectric permittivity of the buried dielectric is reconstructed by updating the contrast source and contrast function for minimization of a defined cost functional. The method can be applied to reconstruct an inhomogeneous dielectric object with arbitrary geometry buried under an arbitrary rough surface.

REFERENCES

[1] A. Galli, D. Comite, I. Catapano, G. Gennarelli, F. Soldovieri, and E. Pettinelli. 3D imaging of buried dielectric targets with a tomographic microwave approach applied to GPR synthetic data. International Journal of Antennas and Propagation, vol. 2013

[2] X. Chen, D. Liang and K. Huang. Microwave imaging 3-d buried objects using parallel genetic algorithm combined with FDTD technique. Journal of Electromagnetic Waves and Applications, vol.17, 2003, pp.1761-1774.

[3] A. Abubakar, P. M. van den Berg and S. Y. Semenov. Two- and three-dimensional algorithms for microwave imaging and inverse scattering. Journal of Electromagnetic Waves and Applications, vol.17, 2003, pp.209-231.

[4] P. M. Van Den Berg and R. E. Kleinman. A contrast source inversion method. Inverse Problems, vol. 13, 1997, pp. 1607–1620.

[5] Y. Altuncu , A. Yapar, I. Akduman. On the scattering of electromagnetic waves by bodies buried in a half-space with locally rough interface. IEEE Trans. Geosci. Remote Sens., vol 44, 2006

POWER FLOW OPTIMIZATION IN A MICRO-GRID WITH TWO KINDS OF ENERGY STORAGE

R. Rigo-Marianni*, V. Roccuzzo**, B. Sareni*, M. Repetto**, X. Roboam*

* Université de Toulouse, UMR CNRS-INPT-UPS

2 rue Ch Camichel, BP 7122, 31071 TOULOUSE cedex 7, France

E-mail : {remy.rigo-mariani, bruno.sareni, xavier.roboam}@laplace.univ-tlse.fr

**Dipartimento Energia, Politecnico di Torino

Corso Duca degli Abruzzi 24, 10129 TORINO, Italy

E-mail: maurizio.repetto@polito.it

Abstract. The paper presents the optimization of the power flows inside a micro-grid with renewable sources and two kinds of storage. The optimization is carried out on a period of one day at one hour discretization and the variables are the degrees of freedom that allow controlling the whole system in order to minimize the electrical bill. Different optimization approaches are used and results compared both in terms of accuracy and of computational efficiency.

Keywords: Clearing, elitist niching, differential evolution, mixed integer linear programming, optimal power flow, smart grids.

INTRODUCTION

A micro-grid is a portion of the electrical distribution system, containing both Distributed Generation (DG) and local electrical loads, which can exchange power with the main electrical network through a point of delivery. The management of the micro-grid requires to choose the most appropriate mix of power production and power purchase from the grid to minimize the overall energy cost fulfilling both user needs and technical constraints at the same time. This optimal scheduling is often performed considering prices policy and forecasts for both consumption and production. If DG is controllable, as in the case of internal combustion engines gen-sets, it can be a variable of the optimization, on the contrary, if it is based on a renewable energy source like Photo-Voltaics (PV) it is taken as an assigned power production profile. If energy storage is present another degree of freedom is available: energy storage can in fact decouple the time instant of power production from that of its consumption or its sell to the grid when the price is economically more convenient. Different optimization techniques can be used for the optimal power flow definition depending on the simulation model of the micro-grid: if all components are described by linear input-output relations, Mixed Integer Linear Programming (MILP) technique can be used [1] but if nonlinear relations are present heuristic optimization techniques should be considered [2].

MICRO-GRID OPTIMIZATION

The micro-grid used for optimization is outlined in Fig. 1*a* and contains:

- Consumption: a building with a commercial load with a daily peak value of 50 kW;
- Production: PV arrays with a total capacity of 175 kW;
- Storage: a 50 kW/50 kWh high speed flywheel and a 50 kW/50 kWh Li-Ion battery;
- Grid: connection to the electrical infrastructure takes into account a Time-Of-Use fare scheme for the purchasing of electrical power with on and off peak unit costs, while a flat selling cost of energy to the grid is considered. In addition a limit on the maximum level of power sold to the grid can be inserted.

The model of the flywheel is extracted from data provided by the manufacturer and the ageing effects are considered. The Li-ion battery is represented thanks to the Schepherd model [3] and the state of health (*SOH*) of the elements is computed by integrating the energy exchanged with the system as in (1) where $\underline{E_{BATexch}}$ represents the total amount of energy that the battery can exchanged before its end of life.

$$SOH(t) = 100 - \frac{100}{E_{BATexch}} \int_o^t |P_{BAT}| dt \quad (1)$$

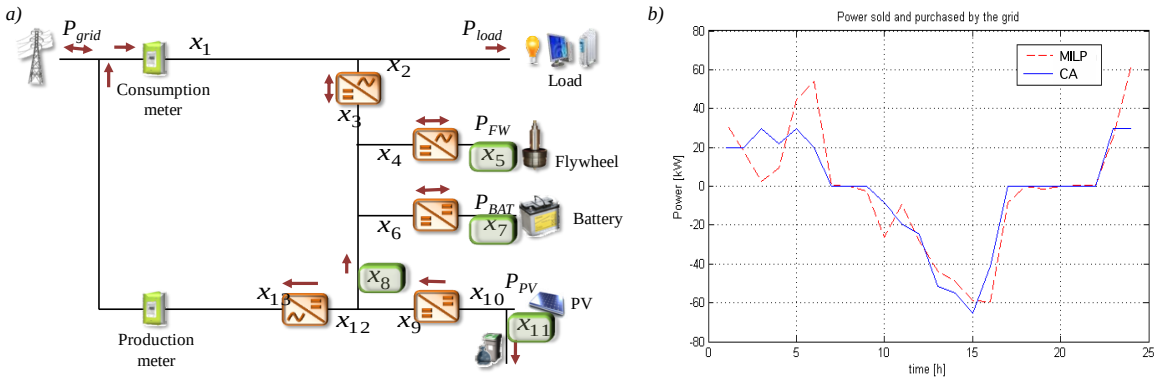

Figure 1: Power flow optimization - a) studied microgrid - b) example of obtained results for the grid power Pgrid

The time scheduling period is one day discretized on a one hour basis within which the variables are considered to be constant. The optimization variables are the four degrees of freedom that allow controlling the whole system knowing the values of the consumption (P_{load}) and the production (P_{PV}):

- the power flowing from/to the flywheel unit;
- the power flowing from/to the battery unit;
- the share of the power flowing from the PV arrays to the common DC bus which is not sold to the grid;
- a derating factor of PV production which denotes the capacity to decrease the PV production (MPPT degradation) in order to fulfill grid constraints, in particular when the electrical grid does not allow (or limits) the injection of the PV production.

The power flow optimization aims at minimizing the total cost on a given day computed from the cost of the purchased energy (C_p) and the prices of the sold production (C_s). It finds the appropriate values of the degrees of freedom that control the power thought the meters (i.e x_1 and x_{11}) and allows the computation of the final cost C as in (2):

$$C = \sum_{t=0}^{t=24h} x_1(t) \times C_p(t) - x_{11}(t) \times C_s(t) \quad (2)$$

Different constraints related to the the power flows direction are also introduced and limitations of the power exchanged with the main grid (P_{grid}) are taken into account. Three different optimization procedures have been used: the first based on a MILP optimization considering a linearized model of the system [1] and two evolutionary algorithms, in particular on Clearing Algorithm (CA) [4] and Niching Differential Evolution [5]. For both metaheuristics the constraints are computed in a vector $\mathbf{C_{nl}}$ and are included into the objective function f_{obj} with a penalty coefficient λ (typically $\lambda = 10^6$) as in (3):

$$f_{obj} = C + \lambda \times \sum \mathbf{C_{nl}} \quad (3)$$

We have displayed in Fig. 1*b* the grid power obtained from MLP and CA on a particular day. Those results show a convergence to the same attraction region. An extensive discussion and comparisons will be shown at the Workshop. The different approaches will be analyzed according to the optimal cost and computational time. A particular attention will also be paid to the power profiles of both storage devices with regard to their ageing effects.

REFERENCES

[1] Canova, A., Cavallero, C., Freschi, F., Giaccone, L., Repetto, M., Tartaglia, M., Optimal energy management, 2009, IEEE Industry Applications Magazine, 15, pp. 62-65.

[2] Sareni, B. and Roboam, X., Simultaneous Design by Means of Evolutionary Computation, Integrated Design by Optimization of Electrical Energy Systems, John Wiley & Sons, Inc., 2013.

[3] Shepherd, C.M. "Design of Primary and Secondary Cells - Part 2. An equation describing battery discharge," Journal of Electrochemical Society, Volume 112, Jul. Page(s): 657-664, 1965.

[4] Pétrowski, A., A clearing procedure as a niching method for genetic algorithms in Proc. 1996 IEEE Int. Conf. Evolutionary Computation, Nagoya, Japan, pp. 798–803, 1996.

[5] Epitropakis, M.G., Li, X., Burke, E.K., A dynamic Archive Niching Differential Evolution Algorithm for Multimodal Optimization 2013 IEEE Congress on Evolutionary Computation, Cancun, Mexico, 2013.

SELECTIVITY AND IMPROVEMENT OF THE MODELLING OF POWER ELECTRONICQ FREQUENCY MODELS FOR OPTIMISATION

Laurent GERBAUD, Jean-Luc Schanen

Grenoble Electrical Engineering Lab (G2ELab), UMR 5529, BP46 – 38402 Saint-Martin-d'Hères Cedex, FRANCE, Tel: +330 476 826 360 / Fax: +330 476 826 300
E-mail: Laurent.gerbaud@g2elab.grenoble-inp.fr, Jean-Luc.Schanen@g2elab.grenoble-inp.fr

Abstract. The paper deals with frequency modelling of power electronics for the sizing by optimization. Generally, a model is not dedicated to particular specifications and optimization algorithms. If the specifications for the optimization are not considered at the modelling step, this may induce great useless modelling and computation. This may also limit the sizing great applications, due to large memory consumption and large CPU time. The paper proposes to formulate the sizing model, not in a general way, but by considering the optimization algorithm used and the specifications of the sizing at the modelling steps. So, there are the inputs and outputs for the generated model. The paper focuses on the automatic building of EMC frequency models and applied it to the design of electrical systems of aircraft.

Keywords: Automatic modelling, optimization-oriented modelling, selectivity, specification-oriented modelling, SQP

I. INTRODUCTION

Frequency model is a part of the EMC sizing model of a more complex system, such aircraft air-condition, electrical drives, etc [1]. The digest focus only on this frequency modelling. The coupling of the model with specific criteria expressions (gain, current, impedances) and with other sizing equations (losses, mass, volume, performances…) thanks to CADES framework, will be detailed in the full paper.

The power electronics frequency modelling is based on Kirchoff's law. Using an algorithm based on Welsh [2], a set of equations representing the Kirchoff's laws and the behaviour of the components is automatically built in the frequency domain. Its general expression is given by Eqn. 1.

(1) $$A(P)\cdot X = B(Y(freq))\,.$$

X contains the unknown currents and voltages of the circuits; its size is n_X.

B represents the contribution of the voltage and current sources Y at a frequency *freq*; its size is n_Y

P represents the parameters of the passive components; its size is n_P

Eqn. 1 is a complex linear expression solved by a complex LU decomposition based on Jampack library (available at: ftp://math.nist.gov/pub/Jampack/Jampack/). The obtained values of X are named X_0.

For some optimisation using gradient-based algorithm (e.g. SQP, interior point method, etc.), the model jacobian can be directly deduced using the theorem of implicit functions [1]:

(2) $$\left[\frac{\partial X_0}{\partial P_i}\right] = -[A]^{-1}\cdot\left[\frac{\partial (A\cdot X_0 - B)}{\partial P_i}\right], i = 1..n_P\,.$$

Here, the invert of A is used, so it can be used also to solve Eqn. 1.

II. PERFORMING THE SOLVING

In the following of the digest:

- *Xs* is the selected outputs that are constrained in an interval or fixed
- *Ps* is the selected inputs that are constrained in an interval
- *Pf* is the non-selected inputs that are fixed
- *Xf* is the non-selected outputs that are free.

For optimization algorithms that do not use the gradients of the sizing model, Eqn. 1 has to be solved using directly LU decomposition, than by using the invert of A.

However, the specifications for the optimisation fixe some inputs and ignore some outputs of the sizing model. In the frequency model used for the optimisation of EMC filter, the frequency model input set contains at less the frequency (*freq*) and the corresponding complex values of the perturbation sources (*Y*), so, at less some tens to some hundreds of variables that are fixed. So, it is very important in such an application, to avoid the

computation of the derivative of the constrained outputs according to the fixed inputs, as to not derivate the free outputs.

In this way, two solving cases appear. If all the model inputs and outputs are constrained in the optimisation, i.e. *Xs*=*X*, the use of Eqn. 2 is a good fashion. If only some of the inputs and outputs are constrained, a LU solving is simple and it can be used for the computation of the jacobian of the selected outputs *Xs* according the selected inputs *Ys*, which are changed by the optimisation process (see fig. 1).

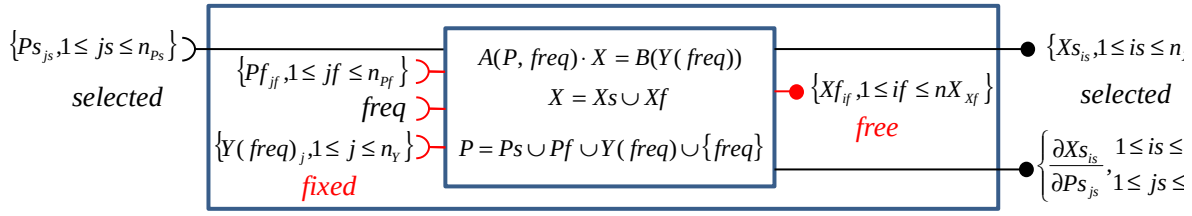

Figure 1. Frequency model with selectivity

In this second case, the derivatives are calculated thanks to the solving of Eqn. 3 by the same LU decomposition of the solving of Eqn. 1:

$$A.\left[\frac{\partial Xs_0}{\partial P_{is}}\right] = -\left[\frac{\partial A}{\partial P_{is}} \cdot X_0\right]. \quad (3)$$

As B does not depend on P, it does not appear in the equations. Complementary, as there are few mutual inductors in the EMC modelling context, the matrix representing an electrical circuit are very sparse and their derivative according the selected parameters represented often one component of A or some if there are mutual inductances. A part of the derivatives according P also depends on the frequency (for capacitances and inductances). As the model is computed at each optimisation iteration, for several frequencies (at less some tens) [1], [3], it is also useful to share some calculations. In this way, the paper proposes to store the derivative of *A* according *Ps* in very small sparse matrixes and to separate the calculations that depend on the frequency from the calculation free of the frequency. These aspects will be detailed in the full paper.

III. CONCLUSIONS

The modelling approach has been implemented in java code, as an evolution of the model generator presented in [1]. The model generator creates the model for one frequency and its calls for several frequencies. Then, CADES is used to include the frequency model in a larger sizing model (as presented in [1]). Without selectivity, the simple use of LU solving compare to the use of the invert of A saves some day of computation on the application of [3] with an optimisation with evolutionary algorithm (10 constraints). The selectivity drastically improves the solving (CPU time and memory) as it will be detailed in the full paper.

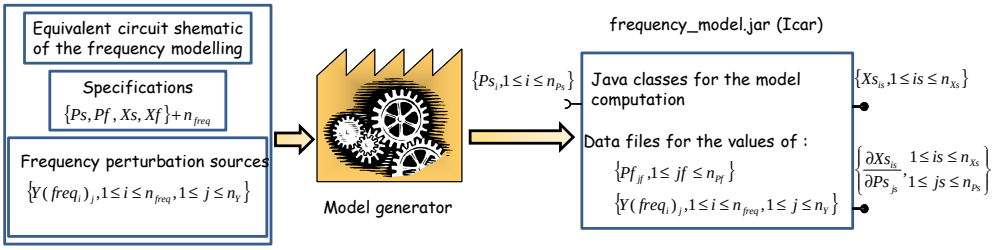

Figure 2. Implementation of the frequency model generator

AKNOWLEDGEMENT

The authors thank Liebherr aerospace Toulouse to allow them to use their applications.

REFERENCES

[1] L. Gerbaud, B. Touré, J.-L. Schanen, J-P Carayon, “Modelling Process and Optimisation of EMC Filters for Power electronics Applications”, The international journal for computation and mathematics in electrical and electronic engineering (COMPEL), COMPEL, Issue 3 of COMPEL in 2012 - issue 31/3, pp 747-763

[2] V. Rajagopalan, (1987), "Computer-aided analysis of power electronic systems", New York, Marcel Dekker Inc.

[3] B. Touré, J.-L. Schanen, L. Gerbaud, T. Meynard, R. Ruelland, “EMC Modeling of Drives for Aircraft Applications: Modeling Process, EMI Filter Optimization and Technological choice”, IEEE Transactions on Power Electronics, Volume 28, issue 3, March 2013, p1145-1156

AID FOR THE MODELING OF AC SINGLE-PHASE POWER GRID FOR STUDIES USING OPTIMISATION

Hoa XUAN NGUYEN, Abir REZGUI, Laurent GERBAUD, Nicolas RETIERE, Frederic WURTZ

Grenoble Electrical Engineering Lab (G2ELab), UMR 5529, BP46 – 38402 Saint-Martin-d'Hères Cedex, FRANCE, Tel: +330 476 826 360 / Fax: +330 476 826 300
E-mail: Laurent.gerbaud@g2elab.grenoble-inp.fr

Abstract. This paper deals with an automatic modelling of power grid for studies using optimization algorithms: optimal power flow, design, or both. The optimization of such an application is often carried out using Interior Point method, due to the non-linearity of the modelling and the large number of constraints (some hundreds of thousands). In the paper, two implementations of such a method are used: Knitro [1] (from GAMS[2]) and IPOpt [3]. The modelling is based on a nodal approach. The gradient of the model is also automatically built. The models are generated in two formats: the modelling language of GAMS and under java native code for the optimization with IPOpt. The model Hessian is approximated by IPOpt. The approach has been applied on the reference power grids defined in the literature. At the present time, for the first modelling prototype, only alternative single-phase power grids are considered.

Keywords: Power Grid, Modelling, OPF, Interior point optimization

INTRODUCTION

The optimization of power flow in power grids is a well-known problem, and studied for several decades. The paper aims to give an aid to the modelling, not only for optimization used to compute the power flow in a power grid, but also for optimization allowing to size part of the power grid. In such an approach, the optimal control used for the power flow management is a part of the complete sizing modelling. The paper focuses on the modelling of the power grid for optimization. It proposes to use GAMS or CADES framework to link the power grid model to other aspects, e.g. sizing criteria. The paper does not discuss this last aspect, it illustrates the modelling on the restricted problem of optimal power Flow (OPF), using interior point optimization from Knitro (from GAMS) or IPOpt (from java language).

I. MODELLING PROCESS

In this case, the optimization process is defined as shown in Fig. 1. From the schematic of the power grid, some additional sizing equations and a description of the optimization specifications (the nature and some default values), the paper proposes to generate automatically the optimization model in two fashions.

- A gams script (i.e. a file in GAMS modelling language) of the optimization model and the optimization specifications. The designer has only to choose the objective function and to define the connection of the model to an optimization algorithm. The user can change the specification values.
- A java code of the optimization model with its Jacobian computation. The specifications are also generated in an XML file available for CADES-Optimizer. At the present time, the connection of the model to IPOpt is carried out thanks to a dedicated java program.

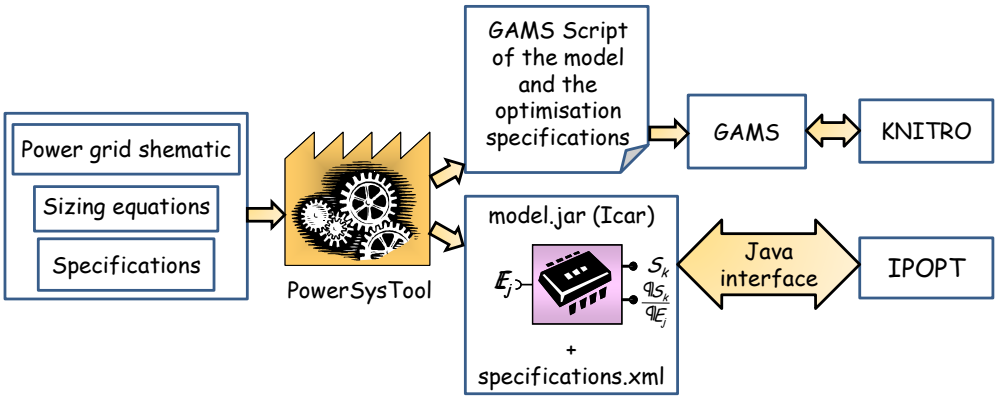

Figure 1. Modelling and optimization process.

MODEL GENERATOR

The modelling of the power grid is based on a nodal approach. Each component of the power grid (generator, load, etc.) is defined by four variables: its voltage amplitude, its voltage phase, its active and its reactive power. Among these variables, two must be fixed. Thus, according to the fixed variables, several causal models are defined and available for designers. It is also possible to add new components. Note that the non linearity of the modelling is due to the power expressions.

From the schematic of the power grid, a nodal modeling is carried out using Kirchoff's laws. Then, the behaviors of the components are added. For IPOpt, the Jacobian is automatically built and stored as a sparse matrix. The Hessian should be built, but at the present time, the approach uses the numerical approximation provided by IPopt. These modelling aspects will be detailed in the full paper.

AUTOMATIC FILE GENERATION FOR MULTIPHYSIC OPTIMIZATION WITH CADES

The architecture of this modelling process is based on the Reluctool architecture [4]. However, some differences exist:

- The model are generated in two formats, as presented before : Gams script and java code
- The ICAr software components are not generated yet.
- The Jacobian is stored as a sparse matrix

APPLICATION EXAMPLE

A 4-node network which theoretical solution is available [5] carried out, as a 14-node network from IEEE data base of reference cases. Both IPopt and Knitro implementations of interior point optimization give good results. More results will be presented in the full paper.

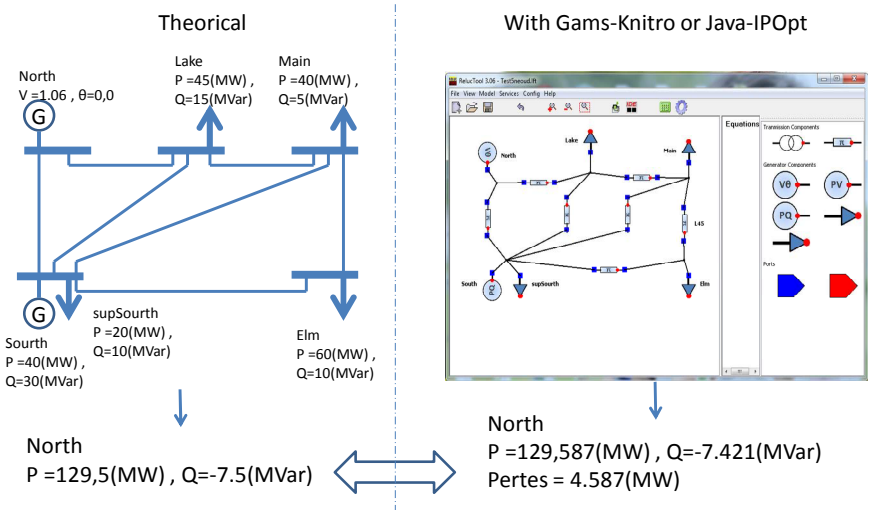

Figure 2. Simple application test

CONCLUSIONS

The implementation of the approach has been made from the architecture of Reluctool. The resulting prototype, named PowerSysTool, is available for alternative single-phase power grid representation or application. Some extensions have to be carried to deal with power flow optimization or sizing by optimization of power grid.

AKNOWLEDGEMENT

Funding for this project was provided by a grant from ANR project CONIFER.

REFERENCES

[1] [1] Nocedal, Jorge; Wright, Stephen J. (2006). Numerical Optimization, 2nd Edition. Springer. ISBN 0-387-30303-0.

[2] [2] http://www.gams.com

[3] [3] A. Wächter and L. T. Biegler, On the Implementation of a Primal-Dual Interior Point Filter Line Search Algorithm for Large-Scale Nonlinear Programming, Mathematical Programming 106(1), pp. 25-57, 2006

[4] [4] H. Nguyen Xuan; L. Gerbaud, L. Garbuio, F. Wurtz, "Computation Code of Software Component for the Design by Optimization of Electromagnetical Devices », IEEE-Transaction on magnetics vol.50, no.2, Feb. 2014

[5] M. Crow *Computational Methods for Electric Power Systems.* Boca Raton, Florida, CRC Press, 2003

OPTIMAL POWER FLOW WITH STORAGE: APPLICATION TO DC RAILWAY ELECTRIFICATION SYSTEMS

Olivier BOSSI* **, Julien POUGET*, Nicolas RETIERE** and Laurent GERBAUD**

*SNCF – Innovation and Research, 40 avenue des Terroirs de France – 75611 Paris Cedex 12, FRANCE,
Tel: +33 (0)1 57 23 62 48
E-mail: olivier.bossi@sncf.fr, julien.pouget@sncf.fr

**Grenoble Electrical Engineering Lab (G2ELab), UMR 5529, BP 46 – 38402 Saint-Martin-d'Hères Cedex, FRANCE, Tel: +33 (0)4 76 82 63 60/Fax: +33 (0)4 76 82 63 00
E-mail : nicolas.retiere@g2elab.grenoble-inp.fr, laurent.gerbaud@g2elab.grenoble-inp.fr

Abstract. This paper describes methodology to design a new electrical railway system using optimization. An Optimal Power Flow (OPF) model of the railway, including energy storage system, is presented. Then, an application case is described. Finally, the problem has been implemented in the GAMS optimization environment. This non linear problem is solved with the Interior Point optimization method (KNITRO). The performances of the optimization process and results are discussed.

Keywords: GAMS, Energy storage systems, Interior Point Optimization Method, Optimal Power Flow, Railways.

INTRODUCTION

Increasing traffic is a challenge for railway networks. In order to meet the demand of the railway operators, more trains with a greater capacity have to be planned.. Thus, the electrical railway infrastructures need improvements in order to sustain more demanding exploitation and energy consumption. One of the challenging aspects is to provide a good power quality to every electric train. This is a condition to use the rolling stock at their standard performances.

In order to achieve these goals, new electrification infrastructures have to be designed, introducing power electronics, energy storage and direct integration of renewable energies.

Due to the increasing complexity of these new infrastructures, traditional engineering methods based on designers expertise and simulation tools reach their limits. The paper presents a railway network model. This one deals with the loads moving according to the train schedules. It also takes into account energy storage elements. Then, an application to an existing railway is presented. The optimization models have been implemented and solved using commercial available optimization tools (GAMS [1] with KNITRO [2] solver).

OPTIMAL POWER FLOW MODEL OF THE DC NETWORK

One of the main features of railway feeding networks is the motion of the loads, inducing frequent topologies changes. A suitable modeling method of the system has been previously developed [3]. This method provides an equivalent fixed topology model, where length of the transmission lines and loads on each node are defined as parameters. Their values are computed in order to describe the behavior of the network according to the practical train timetables from operator's dedicated electro-kinematical simulation tools.

Due to the problem characteristics, the transient dynamics of the network are neglected, therefore electrical system dynamics are represented as successive static states. The steady state linear network equations are built using the modified nodal analysis [4]. Additional non linear equations are used for the trains operating as power loads (1), where current I_c is computed according to the voltage V_c, and train consumed power P_c, which both varies according to time t. Storage unit dynamics are represented using energy W_s as a state variable (2), where Δt is the chosen discretization time step.

(1) $$P_c(t) = V_c(t) \times I_c(t) \qquad \forall t$$

(2) $$W_s(t + \Delta t) = W_s(t) + \Delta t \times P_s(t)$$

Each equation is included as equality constraint in a standard non linear optimization problem. Additional inequality constraints are applied on physical characteristics such as stored energy values (3) or voltage values (4).

(3) $$W_s^{\min} \le W_s(t) \le W_s^{\max} \qquad \forall t$$

(4) $$V_k^{\min} \le V_k(t) \le V_k^{\max} \qquad \forall t$$

The complete optimization model will be detailed in the full paper.

APPLICATION CASE

The application case is based on a section of Paris suburban mass transit system (*Réseau Express Regional*), between the stations of Brétigny and Dourdan. This section is electrified using a DC 1500V overhead system. Train circulations are regularly spaced with a 120km/h top speed and close stops. Its total length is 24.2km. Electrification consists of three feeding and four paralleling substations.

Each feeding substation is assumed to have a short-term storage unit attached. In the paper, optimization tools are used for optimal control in order to provide storage set points.

The objective is to minimize the total energy consumption for a typical traffic peak.

The study time is 4 hours long, and the fast load variations occurring in railway applications impose the choice of a one second time step, which is significantly less than the ten-minute time step of traditional electrical transmission network studies. On the study, 14400 time steps are considered. For each time step, three storage set points and states of charge have to be computed, jointly with 31 nodal voltages, 34 sources currents, leading to a problem with more than one million variables and constraints.

IMPLEMENTATION AND RESOLUTION

The model for optimization has been written using GAMS modeling language and solved using KNITRO Interior Point method implementation.

Optimization results

The storage set points computed by the optimization process are presented in Figure 1.

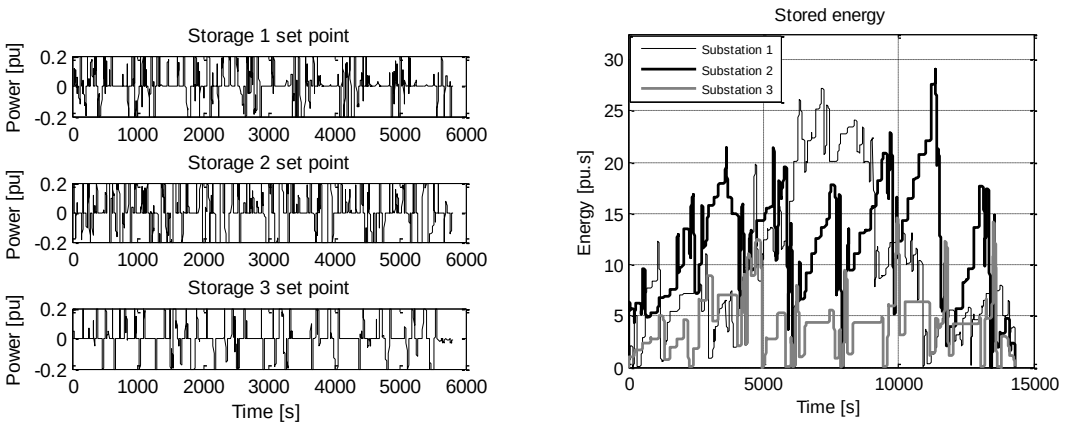

Figure 1. Optimal set points of storage units

A gain of 5% in energy consumption on the optimized cycle is achieved while using storage compared to the initial infrastructures.

Optimization process performances

The global optimization process shows good performances. Running on a server with two Xeon E5506 CPUs, the optimizer takes about 7 hours to converge on a local optimum. The memory overhead is around 10Gb. Due to the relatively low computing resource consumption the optimization process could be run on modern workstations provided enough RAM is available.

CONCLUSIONS

In the paper, an optimization model of a railway network is presented. The model is then applied on a typical engineering case, using commercially available optimization tools. The optimization process finds a more energy efficient solution and shows good performances on large scale problems. The first results prove that the authors are now able to optimize a real railway electrical system despite of its increasing complexity. In the future, a more accurate optimization model will be defined, and to the optimization process will be extended to AC feeding systems.

REFERENCES

[1] http://www.gams.com

[2] Nocedal, Jorge; Wright, Stephen J. (2006). Numerical Optimization, 2nd Edition. Springer. ISBN 0-387-30303-0.

[3] O. Bossi, N. Retière, L. Gerbaud and J. Pouget. Optimal design of a railway electrical supply using various cost criteria. OIPE, 2012.

[4] C.-W. Ho, A. Ruehli and P. Brennan. The modified nodal approach to network analysis. Circuits and Systems, IEEE Transactions on, 1975, 22, 504 – 509

MULTI-OBJECTIVE OPTIMIZATION IN THE LORENTZ FORCE VELOCIMETRY FRAMEWORK

Dzulia Terzijska*, Margherita Porcelli** and Gabriele Eichfelder***

*TU Ilmenau, Department of Electrothermal Energy Conversion, Ehrenbergstraße 29, 98693 Ilmenau, Germany, E-mail: dzulia.terzijska@tu-ilmenau.de

**University of Bologna, Department of Mathematics, Piazza Porta San Donato 5, 40127 Bologna, Italy, E-mail: margherita.porcelli@unibo.it

*** TU Ilmenau, Institute of Mathematics, PF 10 05 65, 98684 Ilmenau, Germany, E-mail: Gabriele.Eichfelder@tu-ilmenau.de

Abstract. We consider an academic problem within the framework of the Lorentz force velocimetry measurement technique. The goal is to increase the Lorentz force in relation to the weight of the magnet system and to determine thereby novel magnet designs. To address this issue we define two multi-objective optimization formulations: one is with continuous variables and the other one is with mixed-integer variables. We investigate and compare these two formulations using the derivative-free NOMAD algorithm.

Keywords: Derivative-Free Algorithm, Lorentz Force Velocimetry, Mixed-Integer Optimization, Multi-Objective Nonlinear Optimization

INTRODUCTION

As computer power increases so does the complexity of the numerical models one wishes to optimize. This often results in expensive objective functions, i.e. whose numerical evaluation is rather CPU time consuming. This is especially the case when objective functions are generated by numerical simulation as, e.g., by extensive 3D FEM models. Generally, for these "black-box" problems, no derivatives can be provided and therefore suitable optimization algorithms are needed to deliver satisfying results in a reasonable amount of time.

The Lorentz force velocimetry framework places in this context. We will use the well-known "derivative-free" algorithm NOMAD [1] (Nonlinear Optimization by Mesh Adaptive Direct search) to solve continuous and mixed-integer multi-objective formulation of the physical problem.

PROBLEM DESCRIPTION

Experimental setup

The novel contactless flow rate measurement technique Lorentz force velocimetry (LFV) [3] for low conductive fluids requires careful numerical optimization of the experimental setup in order to deliver high quality results. The main focus is on the optimization of the magnetic field, i.e. the magnet system with which the force signal is detected.

The experimental setup consists of a cylindrical channel (the fluid is approximated by a solid body [3]) surrounded by eight spherical magnets (figure 1). This setup is of academic nature, since in practice, magnetic structures are generally made of rings or parallelepiped permanent-magnets. The advantage of spherical permanent magnets is their simple analytical description which allows to validate this model.

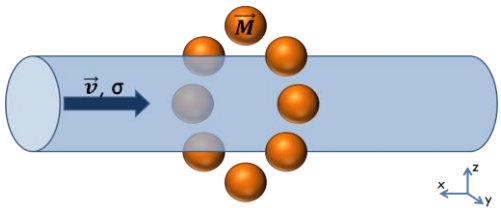

Figure 1. Model setup: cylindrical channel surrounded by 8 spherical magnets (electrical conductivity σ, velocity $\vec{v}$, magnetization $\overrightarrow{M_i}$).

The Lorentz force density F_L [4] is roughly:

$$F_L \sim \sigma \cdot v \cdot B^2 \Leftrightarrow v \sim F_L / \sigma \cdot B^2 \quad (1)$$

where σ is the electrical conductivity of the fluid, v its velocity and B the magnitude of the magnetic flux density produced by a magnet system around the channel. The magnetic flux density induces eddy currents in the fluid. The interaction between eddy currents and magnetic flux density produces a Lorentz force that breaks the fluid flow. By virtue of Newton's law, an opposite force $-F_L$ acts upon and deflects the magnet system. The flow velocity (eq. 1) is determined by measuring the deflection with a balance system.

The sensitivity level of the balance system limits the weight of the magnet system attached to it and thus, the generated Lorentz force. Because of the quadratic dependence of B in (eq. 1), the magnetic field is the most promising parameter to optimize in order to increase the measured force. But for fluids with a higher

electrical conductivity, who produce a stronger force signal (eq. 1), a heavier magnet system can be used to further increase the signal. Thus, the objectives are to increase the Lorentz force in relation to the weight of the magnet system.

Optimization problem

The optimization problem consists in maximizing the Lorentz force in relation to the magnet system weight. Therefore, the objective function has to take into account two conflicting goals: maximize the Lorentz force and minimize the magnetization, summed up over the volume of the magnetic material (surrogate for the weight). To take both objectives into account, we consider a bi-objective optimization setting and attempt to approximate the corresponding Pareto front [2]. A first study considers the weighted sum method as scalarization technique, converting the multi-objective formulation into a single-objective problem by using a convex combination of the objectives for a variety of parameters (denoted w_1, w_2 in (2a|b)). This is done despite the optimization problem being non-convex, because of the simplicity of the scalarized problem (simple differentiable objective function, only box constraints and no additional constraints). It is important that the values of the two objective functions are of the same order of magnitude, the problem data was scaled accordingly. The set of variables are the direction of the magnetization vector $\overrightarrow{M}$, i.e. the azimuth angle $\phi_i \in [-\pi, \pi]$ and the polar angle $\theta_i \in [0, \pi]$, and its value $M_i \geq 0, i = 1, 2, .., 8$. Additionally, we consider a mixed-integer formulation where the magnet dimensions can only assume discrete values $\{0,1\}$ that, in practical applications, means that the magnet exists or not in the system.

We therefore consider the following optimization problems with continuous (2a) and mixed-integer variables (2b):

$$\text{(2a)} \quad \begin{aligned} &\max\ w_1 F_L(\phi,\theta,M) - w_2 \sum_{i=1}^{8} M_i \\ &s.t.\ \phi_i \in [-\pi,\pi], \theta_i \in [0,\pi], M_i \in [0, 10^6] \\ &i = 1, 2, .., 8 \\ &with\ w_1 + w_2 = 1,\ w_1, w_2 \geq 0 \end{aligned}$$

$$\text{(2b)} \quad \begin{aligned} &\max\ w_1 F_L(\phi,\theta,M) - w_2 \sum_{i=1}^{8} 10^6 \cdot M_i \\ &s.t.\ \phi_i \in [-\pi,\pi], \theta_i \in [0,\pi], M_i \in \{0,1\} \\ &i = 1, 2, .., 8 \\ &with\ w_1 + w_2 = 1,\ w_1, w_2 \geq 0 \end{aligned}$$

Numerical setup

We build up a 3D FEM model using COMSOL Multiphysics 4.3b [5] and evaluate the objective functions with an accuracy depending on the quality of the FEM discretization. One function evaluation takes around one minute. Derivatives are not provided.

Taking into account the problem features, we chose to use NOMAD, a derivative free optimization algorithm based on mesh adaptive direct search designed for general nonlinear optimization problems. The main idea of a direct search algorithm is the following. The space of variables is discretized on a "virtual" mesh with a prescribed mesh size parameter. At each iteration, a better value for the objective function is searched for in the neighborhood of the mesh point of the current best solution. If successful, the mesh can be coarsened for the next iteration, otherwise it is refined until the stopping criteria are satisfied.

Numerical results

The numerical results of this preliminary test study will be presented in the poster, including the Pareto front and detailed depiction of the optimized variables.

CONCLUSIONS

The aim of this study was to gain first insight into the optimization procedure in the framework of the Lorentz force velocimetry measurement technique. The non-convex optimization problem is marked by expensive function evaluations. The tested algorithm NOMAD handled successfully the challenge to at least find local optima for this academic problem in a reasonable amount of time and thus, can be used for the optimization of a practical arbitrary magnet configuration.

To obtain preliminary results the weighted sum method was chosen for its simplicity, but the method has some rather unfortunate properties for non-convex optimization. Thus, we first plan to solve the bi-objective optimization problem with BiMADS (the bi-objective formulation of NOMAD) and secondly, to solve a single objective-optimization problem using constraints.

REFERENCES

[1] M.A. Abramson, C. Audet, G. Couture, J.E. Dennis, S. Le Digabel, C. Tribes, The NOMAD project. http://www.gerad.ca/NOMAD/

[2] K. Miettinen. *Nonlinear Multiobjective Optimization*. Springer, 1998.

[3] A. Thess, E. Votyakov and Y. Kolesnikov. Lorentz Force Velocimetry. Phys. Rev. Lett. 96, 2006

[4] P.A. Davidson. *An introduction to magnetohydrodynamics* Cambridge, Cambridge University Press, 2001.

[5] http:/www.comsol.com

IDENTIFICATION OF PARAMETERS OF A STIFF TURBOGENERATOR MODEL FROM THE NUMERICAL FREQUENCY RESPONCE TEST

S. Ionin*, A. Adalev*, N. Korovkin,* M. Roitgarts**, A. Smirnov**

* Saint-Petersburg State Polytechnical University, Electromechanical Department, 29, Polytechnicheskaya str., 195251, Saint-Petersburg, Russia, e-mail: sai1042@mail.ru
** Branch Electrosila of the JSC Power Machines,139, Moskovsky pr., 196105, Saint-Petersburg, Russia, e-mail: Roytgarts_MB@els.power-m.ru

Abstract. The work is related to stiff inverse problems of electrical engineering. A well-known problem of identification of parameters of a turbogenerator lumped-circuit model by means of processing the data of Numerical (FEM) Frequency Response test is considered here. It has been shown that increasing model adequacy (with respect to a better reproducing of the numerical data), leads to rising model stiffness that reveals itself through a ravine-shaped minimized residual functional. The stiff minimization problem is proposed to be solved by means of linear relations between the model parameters allowing to reduce model stiffness and obtain the stable solution with a reliable tolerance.

Keywords: synchronous machine, frequency response, reactances, stiffness, linear relations

INTRODUCTION

Reactances of the synchronous machine such as synchronous reactances (X_d, X_q), transient (X_d', X_q') and subtransient (X_d'', X_q'') reactances are the very important parameters of the machine that determine its cost, reliability, normal and emergency operation characteristics [1]. It is known that a proper reproducing of the frequency response data (measured or calculated by FEM analysis) can be performed by involving higher order parameters into the model (X_d''' and so on). Calculation of these reactances is performed from processing parameters of the equivalent circuit that, in turn, are determined as a solution of the identification problem posed in the frequency domain [2-3]. Numerical experiments are carried out by FEM analysis performed with QuickField software.

IDENTIFICATION ALGORITHM

It is known that synchronous machine could be represented as equivalent circuit given in **Figure 1**. The formula describing the frequency response $Y(js) = 1/X(js)$ of the machine is

(1) $$\sum_{k=1}^{N} A_k \frac{js}{js+\alpha_k},$$ where $A_k = 1/x_k$, $\alpha_k = r_k/x_k$, s - is a relative frequency.

Here the problem of identification of the circuit parameters is posed as minimization of the residual functional of the following form:

(2) $$F(\mathbf{A},\boldsymbol{\alpha}) = \sum_{l=1}^{M} \delta_{1l}^2 + \sum_{l=1}^{M} \delta_{2l}^2,$$ where

(3) $$\delta_{1l}(\mathbf{A},\boldsymbol{\alpha}) = Re\frac{1}{x(js_l)} - \frac{1}{x_c} - s_l^2 \cdot \sum_{k=1}^{N} \frac{A_k}{s_l^2+\alpha_k^2}, \quad \delta_{2l}(\mathbf{A},\boldsymbol{\alpha}) = Im\frac{1}{x(js_l)} - s_l \cdot \sum_{k=1}^{N} \frac{A_k \cdot \alpha_k}{s_l^2+\alpha_k^2}$$

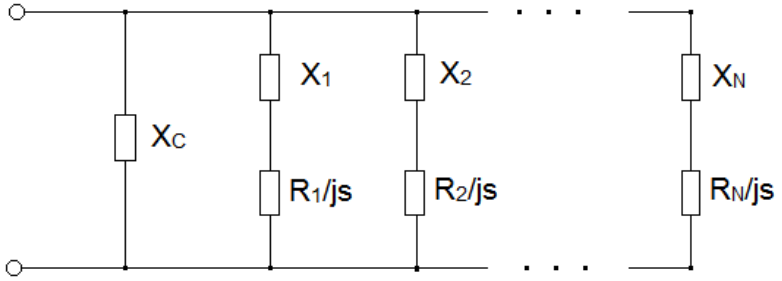

Figure 1.Equivalent circuit of the synchronous machine

PARAMETERS OF THE EQUIVALENT CIRCUIT AND STIFFNESS OF THE PROBLEM

The accuracy of approximation depends on the number of the parallel branches in **Figure 1**. Obviously, accuracy is better for the larger numbers of branches. Meanwhile conditional number of the Hessian matrix of the minimized functional increases along with the number of branches (see **Figure 2)** that indicates stiffness of the turbogenerator model (actually this means that scales of the partial time constants of the branches are extremely different [4]). It provide stochastic dependence between error in the frequency response data and error in the circuit parameters (minimization point). To provide accuracy and stability of the solution it is possible to reduce stiffness of the problem by means of linear relations between the minimization parameters [5]. For the transformed standard formulation of the problem

(4) $$\frac{d\mathbf{P}}{dt} = -\mathbf{F}'(\mathbf{P}), \mathbf{P}(0) = \mathbf{P}_0$$

(5) $$\frac{d\mathbf{P}}{dt} = -\mathbf{F}'' \cdot \mathbf{P} + \mathbf{b}, \mathbf{P}(0) = \mathbf{P}_0$$, where $F(\mathbf{P}) = \frac{1}{2}(\mathbf{F}'' \cdot \mathbf{P}, \mathbf{P}) - (\mathbf{b}, \mathbf{P}), \mathbf{b} = \mathbf{F}'' \cdot \mathbf{P} - \mathbf{F}'$

the following linear relations between the parameters could be obtained by differentiation:

(6) $$(-\mathbf{F}'')^n \cdot \mathbf{P} + (-\mathbf{F}'')^{n-1} \cdot \mathbf{b} = 0$$, n – order of derivation

After that order of the matrix **F''** could be reduced. Finally optimization problem is formulated for the new functional $\mathbf{F_1}$:

(7) $$F_1(x_1,\ldots,x_{k-1},x_{k+1},\ldots x_N) = F(x_1,\ldots,x_{k-1},\{\sum_{\substack{i=1 \\ i\neq k}}^{N} \xi_i \cdot x_i + \xi_0\},x_{k+1},\ldots x_N),$$

$\xi_0, \xi_i, i = \overline{1, N}, i \neq k$ - coefficients of the linear relation

This new functional is less ravined and this simplifies finding of the optimal point with a proper tolerance.

Solution is considered as stable when dependence of both error of the functional and error of solution are monotonous increasing functions. In case of using linear relations such a stability could be obtained.

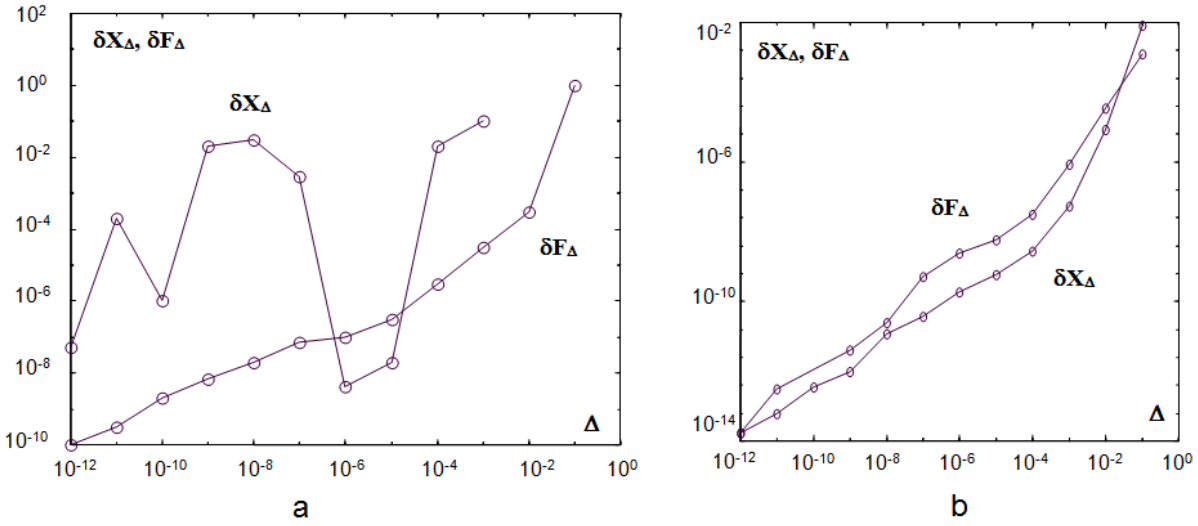

Figure 2. Dependencies of error of solution δX_Δ and error of functional δF_Δ on the error Δ in frequency responce: a) no linear relations are used; b) linear relations are used

REFERENCES

[1] I.Boldea. Synchronous Generators: the Electric Generators Handbook/ I.Boldea. – Taylor & Francis Group, LLC, 2006.

[2] R.Escarela-Perez, T.Niewierowicz, E.Campero-Littlewood.. Synchronous machine parameters from frequency-response finite-element simulations and genetic algorithms.

[3] P.Chmelicek. Synchronous generator reactance prediction using FE analysis. Brno University of Technology, 2010,

[4] V.L.Chechurin, N.V.Korovkin, M.Hayakawa. Inverse Problems in Elecrtic Circuits and Electromagnetics. Springer Science+Business Media LLC, 2007

[5] J.V.Rakitskiy, S.M.Ustinov, I.G.Chernorutskiy. Numerical methods for solving stiff problems , Nauka, 1979 (in Russian)

CONVERGENCE OF APPROXIMATE LINEAR SOLVERS FOR ADAPTIVE RUNGE-KUTTA METHODS APPLIED TO THE SIMULATION OF TRANSIENTS IN POWER SYSTEMS

R. Thomas, D. Lahaye, C. Vuik and L. van der Sluis

TU Delft, Faculty of Electrical Engineering, Mathematics and Computer Science, Mekelweg 4, 2628 CD Delft, The Netherlands
E-mail: r.thomas@tudelft.nl

Abstract. Transients in power systems create high frequency oscillations. Modelling to these high frequency oscillations requires small time steps are needed to be applied. These time steps have in term an effect on the conditioning of the linear system to be solved within an adaptive Runge-Kutta method. This motivates to study the speed of convergence of approximate solvers with re-ordering method(AMD). This study suggests that approximate solvers are adequate to solve the linear equations of adaptive Runge-Kutta methods.

Keywords: AMD, Approximate linear solvers, BIM, iLU(k), integration methods, modelling methods, Re-ordering methods, Runge-Kutta methods, Transients.

INTRODUCTION

When the topology of a linear power system changes, this change generates high frequency oscillations called transient[1]. In order to simulate the power system during transients, the block modelling method[2] is used and an implicit numerical integration method is necessary. In this abstract, an adaptive Runge-Kutta method (diagonally implicit method) is used[3][4].

Implicit methods impose to solve a linear system of equations[5]. In order to solve this system of equations, approximate solvers can be used. A first study has been done on approximate solvers for Runge-Kutta methods[6]. This study shows that it is possible to use approximate solvers to decrease the computation time. In order to understand the effect of approximate solvers on the time solution and the computation time, the speed of convergence and one step of the algorithm are studied with re-ordering method(AMD)[7] for different fill-in of iLU(k)[4]. The study shows that approximate solvers are sufficient and re-ordering method decreases by at least 20% the computation time for large stiff systems.

The abstract is organized as follows, the mathematical description of the problem and the integration method used are shown in the first section. The second section shows the speed of convergence of the approximate solvers for a same structure of power system but with different stiffness with a re-ordering method. The third section shows a step of calculation of the adaptive Runge-Kutta method. Finally, the fourth section draws the conclusions.

BACKGROUND

The modelling method used is the block modelling method [2]. A power system can be described as a differential equation such as:

(1) $\dot{x} = f(x,t) = Ax + Bg(t)$

where $A \in \mathbb{R}^{nbx \times nbx}$, $B \in \mathbb{R}^{nbx \times nbs}$, $g(t) \in \mathbb{R}^{nbs}$, nbx is the number of differential variables and nbs is the numbers of sources. To approximate a solution of Equation (1), one can use an adaptive Runge-Kutta method such as [3][4]:

(2) $(I - a_{ii}\Delta t A)k_i = Au_n + \Delta t \sum_{j=1}^{i-1} a_{ij} A k_i + Bg(t_n + c_{it}\Delta t)$

(3) $u_{n+1} = u_n + \Delta t \sum_{i=1}^{s} b_i k_i$

where $k_i \in \mathbb{R}^{nbx}$, s is the number of stages of the Runge-Kutta method, a_{ij}, b_i and c_i come from the Butcher tableau for $1 < i,j < s$. We can consider $\hat{A} = I - a_{ii}\Delta t A$ and $b = Au_n + \Delta t \sum_{j=1}^{i-1} a_{ij} A k_i + Bg(t_n + c_i \Delta t)$ for next parts of the abstract. The Runge-Kutta method used for the next parts of the paper is the ARK 4 method described in [4] (method of order 4, 6 stages, $a_{11} = 0$ and $a_{ii} = 1/4$ for $2 < i < s = 6$).

CONVERGENCE OF APPROXIMATE SOLVERS

In order to study the speed of convergence of different approximate solvers, we consider two power systems one is non-stiff and the second is stiff. The matrix structure of $A \in \mathbb{R}^{1050 \times 1050}$ and

$B \in \mathbb{R}^{1050\times 39}$ are the same in both test cases to see the effect of the stiffness on the speed of convergence. Let we consider the following equation to be solved according to the Equation (2):

(4) $\hat{A}k_i = b$

In order to compute the speed of convergence of one iteration of ILU(k) as basic iterative method (BIM), we compute the spectral radius ρ of the matrix $I - M^{-1}\hat{A}$ where the matrix $M = LU$ corresponds to the approximation of the matrix $\hat{A}$ due to the ILU(k) decomposition on A. In order to converge to a suitable solution ρ needs to be less than one ($\rho < 1$).

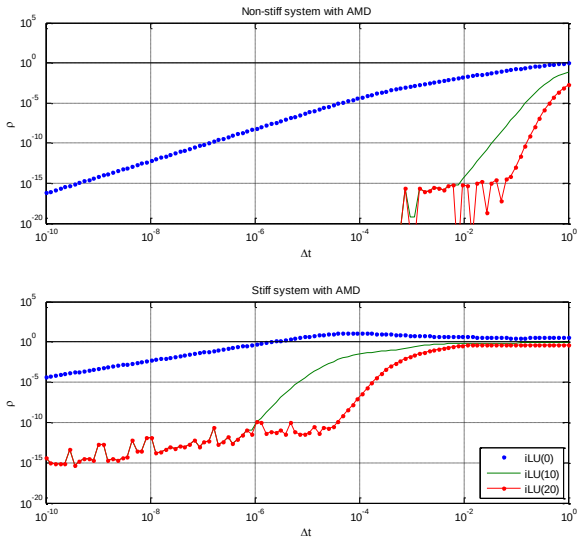

Figure 1. Speed of convergence of different approximate linear solvers for stiff and non-stiff system and with AMD.

Moreover, according to Equation (2), ρ is function of the time step (Δt). Let we consider the following Figure (1) which shows the spectral radius for the non-stiff and stiff system for different Δt with re-ordering method (AMD)[7]. The reordering method is used in order to get a better matrix for the iLU(k) decomposition.

From Figure (1), we can see that, the speed of convergence begins faster when the k begins larger. When theΔt is small, the speed of convergence of the k is the same. Moreover, for the stiff system, k=20 is a good choice because $\rho < 1$ for all Δt.

However, iLU(0) is not the best choice in both cases when the stiffness is important because $\rho > 1$ for $\Delta t > 10^{-5}$ so there is no convergence and smaller time steps need to be applied and consequently, the computation time of all simulation takes more time than with other approximate solvers.

STEPS CALCULATION

Let us consider one step of ARK 4 with one iteration of iLU(0) or iLU(20) BIM with AMD for the stiff system. The initial starting point will be during the transient with an initial Δt of 27,01 us. The first step is rejected all time because is too large ($er > Tol = 10^{-4}$) and so a smaller Δt needs to be used as shown in Table (1).

	iLU(0)	iLU(20)
1st step		
Accepted	0	0
Next Δt	1.36 us	16.71 us
2nd step		
Accepted	1	1
Next Δt	1.36us	14.62 us

Table 1. Time step results.

From Table (1), as seen previously in [6], one iteration of iLU(0) as BIM is not efficient. The initial time step is not suitable. This can be realized on Figure (1) because the $\rho > 1$ for this initial Δt and so according to the time steeping algorithm, because the result is not accurate, a very small time step needs to be applied. Moreover, one iteration of iLU(20) as BIM permits to have a bigger time step and so the computation time is faster with iLU(20).

CONCLUSIONS

In this work, we have studied the convergence of approximate solvers for adaptive Runge-Kutta methods. For non-stiff system, the fill-in of approximate solvers can null (k=0). For larger stiff systems, the fill-in is important because the computation time decreases when the fill-in increases with an appropriate k.

REFERENCES

[1] L. van der Sluis, *Transients in Power Systems*, Wiley, 2001.

[2] R. Thomas, D. Lahaye, C. Vuik and L. van der Sluis, *New Transient Modelling Approach for Adaptive Time-Stepping Algorithm*, in preparation, 2014.

[3] W. Hundsdorfer and J. Verwer, *Numerical Solution Of Time-Dependent Advection-Diffusion-Reaction Equations*, Springer, 2003.

[4] C.A. Kennedy and M.H. Carpenter, *Additive Runge-Kutta Schemes for Convection-Diffusion-Reaction Equations*, Applied Numerical Mathematics, vol 44, p139-181, 2003.

[5] Y. Saad, *Iterative Methods For Sparse Linear Systems*, *PWS Publishing Company*, 1996

[6] R. Thomas, D. Lahaye, C. Vuik and L. van der Sluis, *Approximate Linear Solvers for Adaptive Runge-Kutta Methods Applied to the Simulation of Transients In Power Systems*, SCEE conference 2014.

[7] P.R. Amestoy, T.A. Davis, I.S. Duff, *An approximate minimum degree ordering algorithm*, SIAM. J. Matrix Anal. & Appl., vol. 17, p886–905l, 1996.

SENSITIVITY ANALYSIS AND OPTIMIZATION OF PVDF PIEZOELECTRIC MATERIALS WITH INTERDIGITATED ELECTRODES

Nicolas GALOPIN, Nicolas CHOULET, Benoit DELINCHANT

Univ. Grenoble Alpes, G2Elab, F-38000 Grenoble, France
CNRS, G2Elab, F-38000Grenoble, France

E-mail: benoit.delinchant@G2ELab.grenoble-inp.fr

Abstract. The paper is about efficient sensitivity and optimization procedure applied to piezoelectric device with interdigitated electrodes. Model behavior analysis tools based on Jacobian are more specifically used, and then we are focusing on symbolic Jacobian computation. The electical field modeling is based on conformal mapping which makes appearing semi-analytical expressions based on elliptic integrals and Jacobi special functions.

Keywords: PVDF, Interdigitated Electrodes, Conformal Mapping, Sensitivity Analysis, Optimization, Jacobian, Elliptic integrals

INTRODUCTION

The following figure presents the whole device (on the left part). According to symmetries, only an elementary cell is studied (on the right part).

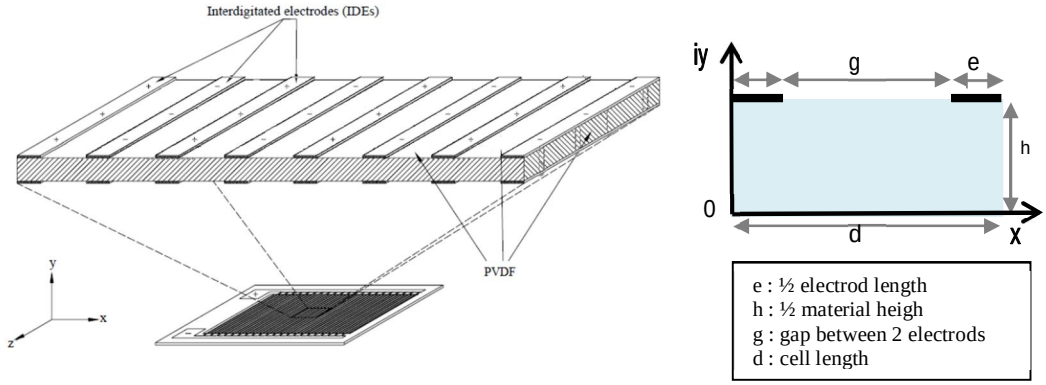

Figure 1. PVDF Piezoelectric Material with Interdigitated Electrodes and an elementary cell

ANALYTICAL MODELING OF THE ELEMENTARY CELL

To determine the distribution of the electric potential in a unit cell, and therefore the electric field, the idea is to start with an area where the distribution is known and to apply transformation rules in order to reach our unit cell area and thus to know the distribution of electric potential therein. We then assume planar capacitor with following for 2D modeling assumptions: (1) the edge effects are neglected; (2) the material is homogeneous isotropic. Conformal mapping used for the transformation is Schwarz and Christoffel one, which retain physical properties such as the electrical potential. For rectangular areas, it involves elliptic integrals of the first kind (1) [1] and also elliptic Jacobi function 'sn' which arise from the inversion of the previous one (2):

$$(1)\quad F(k,x) = \int_0^x \frac{dt}{\sqrt{(1-t^2)(1-k^2t^2)}}$$

$$(2)\quad \sin(x) = sn(F(k,x))$$

Thus, using conformal mapping, the electric potential in the elementary cell is given by the complex formula (3):

$$(3)\quad P(z) = -\frac{V_1-V_2}{2K(k_1)}\,F\left(k,k_\xi\omega\right) + \frac{V_1+V_2}{2}$$

Where V_1, V_2 are electrical potentials, and k, $k_\xi\omega$ and k_1 are expressions based on conformal mapping using 4 sequential geometrical transformations, based on coordinates of each sub domains (v, ξ, ω *and* z), geometrical description, and using elliptic special functions. These expressions will be detailed in the full paper. From the electrical potential, the complex electrical field can be deduced (4):

$$(4)\quad \underline{E}(z) = -\overline{\left(\frac{(V_2-V_1)K(k)}{K(k_\xi)d}\,\frac{\sqrt{1-\omega^2}}{\sqrt{1-\left(k_\xi k\omega\right)^2}}\,k\right)}$$

JACOBIAN OF THE MODEL

The analytical model is using special functions and cannot be simply used in optimization framework like CADES (www.cades-solutions.com). But, if the expert is able to produce the Jacobian of these specific functions, CADES optimization framework is able to compose equations and to produce a Jacobian associated with the global model.

Derivatives of elliptic functions of the first, second and third kinds are given by [2]. Jacobi elliptic functions are required during the conformal mapping process and then the symbolic gradient must be computed using the following forumula (5), in which other Jacobi elliptic functions are appearing (am: Jacobi amplitude, cn: the equivalent of *sn* for cosinus, …) and the incomplete elliptic integral of the second kind *E(k,m)*.

$$(5)\quad \frac{\partial sn(u,m)}{\partial m} = \frac{cn(u,m)*dn(u,m)*[E(am(u,m),m) - m*cd(u,m)*sn(u,m) + (m-1)*u]}{2\,(m-1)\,m}$$

SENSITIVITY ANALYSIS AND OPTIMIZATION BASED ON GRADIENTS

The first optimization study is about electromagnetic field, the coupling with piezoelectric deformation will be studied in a second phase. We want to design the device in order to maximize the electric field but also the homogeneity of it along the horizontal axis in order to maximize the piezoelectric polarization. Our specifications define also constraints such as dielectric breakdown voltage or geometrical constraints. In order to do this, we have defined the objective function as maximization of the electrical field mean:

$$(6)\quad max\left[f(\boldsymbol{x}) = \frac{1}{N}\sum_{i=1}^{N}\vec{E}(z_i)\right]\text{ , where } \mathbf{x} \text{ is the vector of design variables.}$$

But first of all, we want to apply a global sensitivity analysis in order to see which variable is really impacting this objective function. As our model is given the Jacobian, a local sensivity can be done. But in order to take non linearity into account, since parameter variation range is not really short, we have decided to apply a global sensivity measure based on gradients. This sensitivity measure is called DGSM (derivative based sensitivity measure) [3]. It is based on mean and variance of partial derivatives, and it is also majoring the classical Sobol total index which is quite important in order to remove non influent parameter from an optimization process. In our application, there are few parameters and then we are keeping them for the optimization part, but are showing that convergence of DGSM index is 10 time faster than Sobol, for the same parameter hierarchisation.

For the optimization part, we are using both SQP and IPOPT Quasi-Newton algorithms which are using the exact Jacobian that our model is producing, leading to a very fast optimization procedure (less than 20 iterations).

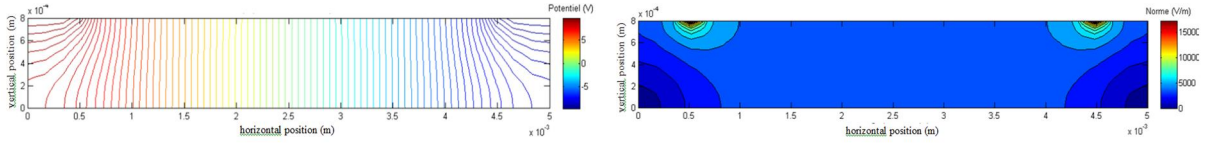

Figure 1. Electric equipotentials and electric field of the elementary cell

CONCLUSIONS

Our paper has presented electrical field modeling for piezoelectric application, based on conformal mapping. This mathematical transformation gives a semi-analytical model based on elliptic and Jacobi elliptic integrals. We have developed a library computing these functions as well as their partial derivatives. It has been implemented as a user function in the CADES framework. Based on this model, we have analyzed its behavior using derivative based global sensitivity measure (DGSM) as well as classical quasi-Newton optimization algorithms. These tools and the methodology of producing gradient for each sub models will be very important for the next step regarding piezoelectric coupling. Indeed, the complexity will reach a point where it will be impossible to analyze simulations without automated tools due to the increasing number of parameters.

REFERENCES

[1] Carlson, B.C. Elliptic integral, in Olver, Frank W. J.; Lozier, Daniel M.; Boisvert, Ronald F.; Clark, Charles W., *NIST Handbook of Mathematical Functions*, Cambridge University Press, 2010

[2] B. Delinchant, F. Wurtz, J.-P. Yonnet, J.-L. Coulomb. Interaction Between Ring-Shaped Permanent Magnets With Symbolic Gradients: Application to Magnetic Bearing System Optimization. IEEE Transactions on Magnetics, Vol. 47, No. 5, May 2011

[3] M. Sobol et al.. “Derivative based global sensitivity measures and their link with global sensitivity indices”. Mathematics and Computers in Simulation, Vol 79, No 10, (June, 2009), pp 3009–3017

ANALYTICAL FREQUENCY MODEL OF A DIODE RECTIFIER: SQP SOLVING VERSUS NEWTON-RAPHSON SOLVING

Le Nhat Hoang TRAN*, Laurent GERBAUD *, Nicolas RETIERE*, H. NGUYEN HUU**

* Grenoble Electrical Engineering Laboratory (G2Elab), UMR 5269 Grenoble INP-UJF-CNRS
E-mail: (le-nhat-hoang.tran; laurent.gerbaud; nicolas.retiere)@g2elab.grenoble-inp.fr

**Danang University of Science and Technology
E-mail: nhhieu@dut.udn.vn

Abstract. Static converters generate current harmonics in grids. Numerous studies on analytical frequency model are preferred to carry out their harmonic modelling in the context of sizing by optimization. Some solving methods are proposed to solve such models. Each solving method has its own advantages and drawbacks. The paper mainly focuses on two approaches: the first with Sequential Quadratic Programming solving (SQP) and the second with Newton-Raphson solving (NR). In this way, the paper presents the performances of each method and compares results of the two methods for the modelling of a single-phase diode rectifier.

Keywords: Analytical modelling, harmonics, Newton-Raphson, single-phase diode rectifier, SQP.

INTRODUCTION

Harmonics generated by power electronic converter can lead to supplementary losses, overheating, and disturbance on their load. To compute their harmonics, an approach commonly used is the time domain simulation combined with FFT analysis. However, this approach is time-consuming and depends on the time step used for the time solving. Some other methods are proposed in [1]-[4] to calculate harmonics. However, they have some limitations:

- only the modeling of controlled converter is considered [1], [2]
- complex mathematical formulations are used [3]- [4]

In this way, alternative approaches are proposed by [5] and [6]. [5] combines an analytical modelling with an optimization algorithm (SQP) to manage uncontrolled switches and to deal with the associated analytical modelling problems. [6] combines an analytical modelling with solving method of non-linear equations (NR). These approaches are available not only for uncontrolled static converter, but also for controlled static converters. However, some convergence problems exist, mainly due to the operating mode modelling.

OPERATING MODE OF A STATIC CONVERTER

The operating mode is defined by the sequence of configurations of the static converter in a steady-state operating period. Every configuration is time limited by two consecutive switching events. However, some static converters have several operating modes according to the value of the load and the passive elements. So, an analytical model may be trapped in an operating mode different than the expected one. For example, the computation of problem of Fig. 1a may give the result of Fig. 1b (square point in Fig. 1b and 1a have the same switching conditions, but do not result from the same operating mode) [5].This problem may happen during the sizing by optimization because the model parameters change at every optimization iteration. In this way, [5] has proposed to add constraints on the switching events to the frequency model. However, this does not seem sufficient to ensure the modelling convergence. Indeed, as there are several possible solutions, there is still a problem left about the initialization of the unknown variables. If it is badly done, the simulation may fail to converge. The authors propose a way to improve that in the following part.

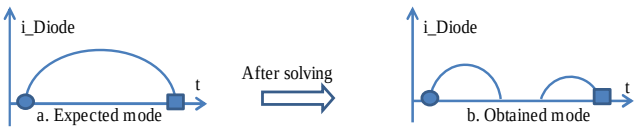

Figure 1. Example for trapped operating mode

MODELING METHODS

The paper assumes that switches are assumed to be ideal [5][6], the static converter operates at steady-state and passive component values are constant at each iteration of the sizing by optimization (e.g. SQP ones).

For a period of the steady-state operating (T), according to Kirchhoff's laws, the state equations are formulated for every configuration. The frequency model is deduced from these equations. This model will be detailed in full paper.

The configuration changes are defined by switching events while respecting the following constraints:

- the state-space vector is time-continuous at configuration changes
- the current or the voltage of non-controlled switches (e.g diodes) are canceled at switching events.

Depending on the complexity of the application cases, these constraints can be translated by the generic equations given by Eqn. 1 or Eqn. 2. The building of these equations will be detailed in the full paper.

(1) $F(x_1, x_2) = 0$

(2) $\min(F(x_3))$ with $g(x_2) = 0$ and $h(x_1) \leq 0$

where :

- x1 contains the durations between the beginning time and the switching events on a steady-state operating period
- x_2 characterizes the continuity of the state-space equations between two operating periods
- x_3 represents the sum of the conducting phase durations
- $h(x_1)$ is the non-controlled switching conditions for the configuration changes, i.e. the switch currents or voltages that change of sign from positive to negative

The paper compares two methods to solve these equations NR and SQP. NR seems very interesting, because there are less unknown variables and no constraints (Eqn. 1). However, the choice of the initial values of x_1 and x_2 is very important for the convergence. It may also be trapped in a bad operating mode. SQP has more unknown variables and constraints (Eqn. 2) than NR and it is less trapped by the choice of the initial values. According to experiments on several applications, the two approaches are compared in table 1.

Table 1. Newton-Raphson solving versus SQP solving

Criterions	Newton-Raphson	SQP
Convergence	+	++
Times of computation	++	+
Impact of initial values	--	-

From the results in table 1, the impact of the initial values of the unknown variables on the convergence is clear. In order to improve that, the authors propose to analyze the eigenvalues of the state system to initialize the duration (x_1) of every configuration. There are two parts in the eigenvalues: the real part representing to time constants and the imaginary part representing the oscillation periods. They may change for each operating mode of the converter and at each optimization iteration of the sizing. In some cases, it is possible to use them to initialize the duration of the configuration in order to improve the convergence of NR and SQP. This has been applied on a single-phase diode rectifier. For the configurations in which the eigenvalues are complex, it is easy to initialize the duration of configurations. So, both NR and SQP have a good convergence. For other modes which have only real eigenvalue, the initialization is partially generic and it is better to use SQP than NR.

Furthermore, thanks to the symmetric operation of static converter, the switching events are considered only on the first half operating period. That allows to reduce the number of calculated variables and also the computation time. This will be detailed in the full paper.

APPLICATION

The approaches and improvements have been applied on several operating modes of a single-phase diode rectifier. The results confirm what has been presented before and that will be detailed in the full paper.

CONCLUSIONS

In the paper, the two methods (NR and SQP) are compared for the computing of the harmonics generated by a static converter. They have improved the convergence of them in some application cases. However, they are still some difficulties to apply both methods to complex applications (e.g. with greater size of the state-space matrix). Further investigations are required to extend their range of application.

REFERENCES

[1] R. Ghandehari, S. Mohamandian, and A. Shoulaie. A new approach to AC/DC converters modelling in time domain for harmonic analysis. Power quality conference, 2010.

[2] J. Arrillaga, B.C. Smith, N.R. Watson, A.R. Wood. *Power system harmonic analysis*. John Wiley & Sons. 1997.

[3] K. L. Lian, Brian K. Perkins, and P. W. Lehn. Harmonic analysis of a three-phase diode bridge rectifier based on sampled-data model. IEEE transaction on power delivery, vol 23, no 2, 2008.

[4] G. Carpinelli, F. Iacovone, A. Russo, P. Varilone, and P.Verde. Analytical modeling for harmonic analysis of line current of vsi-fed drives. IEEE Trans. On power delivery; 2004.

[5] J-F. Lange, L. Gerbaud, H. Nguyen-Huu and J. Roudet. Using constrained optimization algorithm for the modeling of static converter harmonics. The international journal for computation and mathematics in electrical and electronic engineering, vol. 31 No.3, 2012, pp. 764-779.

[6] H. Nguyen-Huu, L.Gerbaud, N.Retière, J. Roudet and F. Wurtz. Analytical modeling of static converters for optimal sizing of on-board electrical systems. IEEE-VPPC, 2010.

MULTI-OBJECTIVE OPTIMIZATION OF THE SIZING OF A HYBRID ELECTRICAL VEHICLE

Vincent REINBOLD*, Laurent GERBAUD* and Emmanuel VINOT**

* Univ. Grenoble Alpes, G2eLab (CNRS UMR5269, INPG, UJF), F-38142 Cedex, Grenoble, France
vincent.reinbold@g2elab.grenoble-inp.fr

** IFSTTAR, LTE, 25 av. François Mitterrand, 69675, Bron, France
emmanel.vinot@ifsttar.fr

Abstract. Hybrid electrical vehicles involve two sources of energy, usually gasoline and electricity. The energy management determines the power sharing between the internal combustion engine (ICE) and the electrical machine (EM). It is highly dependent on the driving cycle (i.e. the use of the vehicle). In this context, the optimal sizing of the EM is determined by: the driving cycle, the power-train characteristics (i.e. ratios and physical limitations e.g. maximum torque available) and the energy management. The key idea of this work is to involve the driving cycle and the environment of the electrical machine in a global multi-objective optimization process taking into account an optimal energy management (OEM).

Keywords: Electrical machine, hybrid electrical vehicle, magnetic circuit, sizing.

INTRODUCTION

Hybrid electrical vehicles (HEV) represent an innovative solution to reduce gas emission and fuel consumption. A possible configuration of the HEV is a parallel two clutches architecture (see Fig. 1). In this architecture, both ICE and EM provide power to the wheels. The energy management determines the propulsion mode (electric, hybrid or thermal) and the power-sharing between the ICE and the EM.

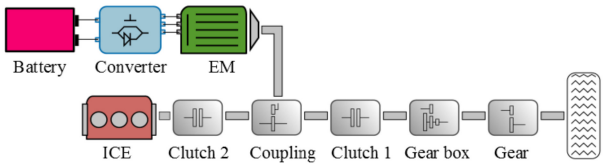

Figure 1. Parallel HEV architecture.

For real time implementation (the sizing of the vehicle is already done), a rule-based strategies are usually used. These are on-line strategy, i.e. the knowledge of the driving cycle is not required. Rule-based strategy highly depends on the sizing of the vehicle and therefore, cannot be used in an optimization process. On the other hand, the optimal energy management (OEM), based on optimization methods, leads to the optimal fuel consumption for a given sizing of the vehicle [1]. However, this strategy requires the knowledge of the driving cycle in advance.

The sizing of the electrical machine is probably the most common optimization problem in electromagnetic research. Usually, the problem is to maximize the efficiency of the EM for given operating points subject to external constraints such as weight, thermal, physical limitations, etc. In a dynamic system, where operating points of the EM are not a priori known, the problem is more complex. In this context, the sizing problem involves a control problem that cannot be neglected. A global optimization has to be performed [2].

Firstly, the paper presents the optimal control problem, which can be seen as a sub-optimization problem. Then, the modelling of the parallel-HEV and the sizing optimization problem is presented. Finally, results are presented for an urban driving cycle.

OPTIMAL CONTROL OF THE HEV

For charge sustaining hybrid vehicles, when the battery only recharges during regenerative braking or when absorbing additional power from the ICE, the global battery discharge is constrained equal to zero over a driving cycle. The energy control of the HEV is only determine by the battery current I_{bat}. The torque of the ICE is determine by the driving mission and the torque provided by the EM. In the paper, dynamic programming algorithm is used to solve the OEM as a sub-problem [1, 3].

OPTIMIZATION OF THE SIZING OF THE HEV

Modelling of the electrical machine

In this study, an internal permanent magnet synchronous motor is studied. The EM is modelled by a magnetic circuit model [4]. It is based on the knowledge of the geometrical parameter set, (e.g. air-gap length, magnet sizes, stator external radius) and winding characteristics. This leads to an efficiency map *rotation speed/torque/efficiency* (in about 10-15s).

Optimization strategy

Fig. 2 shows the optimization strategy of the sizing of the parallel-HEV. OEM is considered as a sub-optimization problem embedded in the global optimization of the sizing of the vehicle. OEM is solved at each step of the sizing optimization using dynamic programming.

The sizing optimization takes into account 4 systemic parameters (maximal power of the ICE, ratios, etc.) and 10 geometrical parameters of the EM. In this study, a multi-objective algorithm NSGA-II is used [5]. The two objectives to be minimized are: the fuel consumption and the battery number.

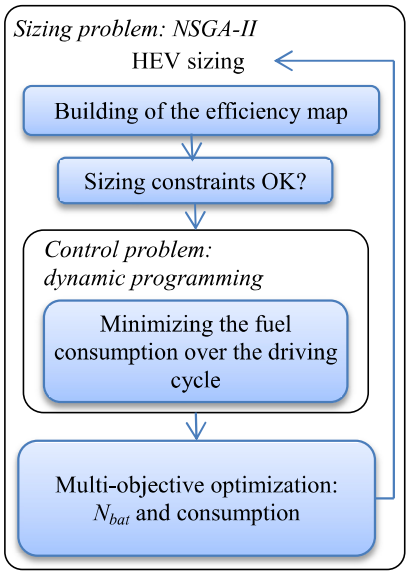

Figure 2. Optimization strategy

RESULTS

The global optimization process has been applied to an urban driving cycle (about 600s). About 27000 simulations are needed. This optimization is performed using parallel computing (8 core and about 8h).

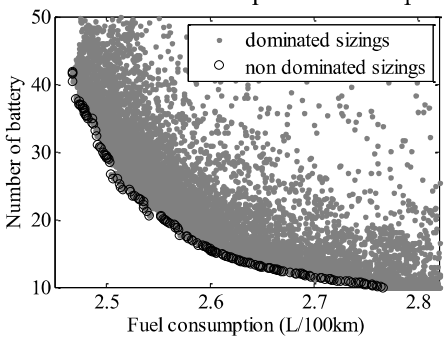

Figure 3. Pareto front for the urban driving cycle

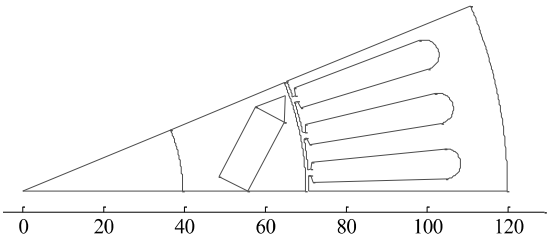

Figure 4. Optimal sizing of the EM for $N_{bat} = 25$

CONCLUSION

In the paper, multi-objective genetic optimization has been applied to a parallel-HEV. This optimization takes into account 15 sizing parameters of the HEV and focuses on the EM geometry. OEM problem is solved using dynamic programming algorithm. The global optimization strategy leads to an optimal Pareto's front (see Fig. 3). Results show fuel saving of 30% depending on the initial sizing and number of battery. Because of the computation time needed (8h) , a complementary article, using SQP algorithm, is being studied in parallel. The final paper will focus on the modelling of the EM and it will develop the optimization strategy and the modelling hypothesis. Additional results, for different driving cycles, will be shown.

ACKNOWLEDGEMENT

Funding for this project was provided by a grant from la Région Rhône-Alpes.

REFERENCES

[1] Scordia, J.; Desbois-Renaudin, M.; Trigui, R.; Jeanneret, B.; Badin, F. & Plasse, C. Global optimization of energy management laws in hybrid vehicles using dynamic programming, International journal of vehicle design, Inderscience, 2005, *39*, 349-367

[2] Reinbold, V.; Vinot, E. & Gerbaud, L. Global optimization of a parallel hybrid vehicle using optimal energy management, IJAEM : International Journal of Applied Electromagnetics and Mechanics, IOS Press, 2013, 43, 115-126.

[3] Kirk, D. E. *Optimal control theory: an introduction,* Courier Dover Publications, 2012

[4] Du Peloux, B.; Gerbaud, L.; Wurtz, F.; Leconte, V. & Dorschner, F. Automatic generation of sizing static models based on reluctance networks for the optimization of electromagnetic devices, IEEE Transactions on Magnetics, 2006, 42, 715-718.

[5] Deb, K.; Pratap, A.; Agarwal, S. & Meyarivan, T. A fast and elitist multiobjective genetic algorithm: NSGA-II Evolutionary Computation, IEEE Transactions on, 2002, *6*, 182-197

JOINT OPTIMIZATION OF CONTROL AND SIZING OF THE PARALLEL HEV USING SQP ALGORITHM

Vincent REINBOLD*, Laurent GERBAUD* and Emmanuel VINOT**

* Univ. Grenoble Alpes, G2eLab (CNRS UMR5269, INPG, UJF), F-38142 Cedex, Grenoble, France
vincent.reinbold@g2elab.grenoble-inp.fr

** IFSTTAR, LTE, 25 av. François Mitterrand, 69675, Bron, France
emmanel.vinot@ifsttar.fr

Abstract. In electromagnetic research, the optimization of electrical machine is a very common issue. The improvement of computational capabilities allows researchers to improve models and complexity of the optimization problem. In transportation applications, electrical machines are subjected to a large panel of operating points. Moreover, for hybrid vehicles, the sizing problem involves a control problem as a sub-optimization problem (power sharing between electric and thermal transmission). Therefore, a joint optimization of the energy management and sizing of the EM over a driving cycle shall be considered. The paper presents the modelling of the electrical machine based on magnetic circuit equivalence.

Keywords: Electrical machine, hybrid electrical vehicle, optimal control, sizing.

INTRODUCTION

Optimization of electrical machine (EM) and modelling hypothesis are always subject to the specifications of the EM: operating points and environment. Usually, some fixed operating points are used to represent the use of the EM. In complex systems, where interactions between the components and the system cannot be neglected, the problem is different (e.g. the operating points of the EM are varying during the optimization process). In order to keep an optimal approach, the environment of the EM (interactions with the system that involves the EM) has to be taken into account.

In this study, hybrid electrical vehicle (HEV) is our study case. In HEV, a common power-train is coupled to at least one electrical machine. A possible configuration of the HEV is a parallel two-clutch architecture [1]. In this architecture, both the internal combustion engine (ICE) and the electrical machine (EM) provide power to the wheels. The energy management determines the propulsion mode (electric, hybrid or thermal) and the power-sharing between the ICE and the EM. The optimal control of the HEV is an optimization problem [2].which leads to the optimal power sharing and propulsion mode (electric, hybrid or thermal) over driving cycle a priori known. The non-optimal energy management (rule-based, fuzzy logic, etc.) depends on the sizing of the vehicle and therefore, cannot be used in a sizing optimization process. In the paper, a joint optimization of control and sizing is proposed.

Firstly, the paper presents the design model of the electrical machine based on the magnetic circuit equivalence. Secondly, the paper presents an optimal control problem applied to a parallel HEV joint to the sizing problem of the EM optimization results for an urban driving cycle will be presented.

MODELLING OF THE ELECTRICAL MACHINE

In this study, an interior permanent magnet synchronous motor such as those usually used in hybrid electrical vehicle is studied. The magnetic model is a reluctance circuit model [3]. As it is a design model, it is based on the knowledge of geometrical parameters, named X (e.g. air-gap, magnet sizes, external radius of the machine, etc.). A geometrical representation of the structure is shown in Fig. 1. A proposed reluctance circuit model is presented in Fig. 2.

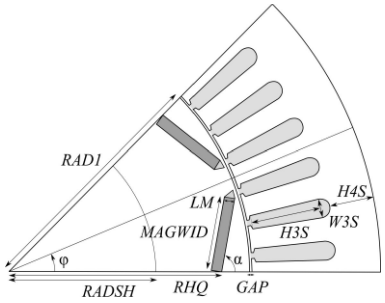

Figure 1. Geometrical representation of the EM

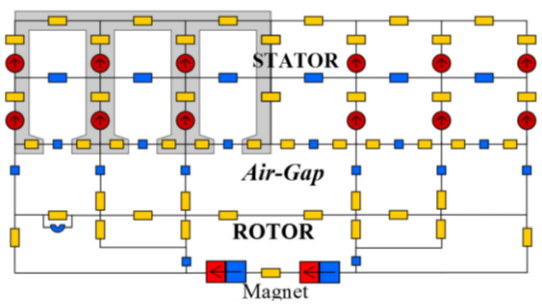

Figure 2. Reluctances circuit model

Magnetic sources depend on the RMS current I_{me} and on the internal electrical angle, ψ_{me}. This is a quasi-static model, built in order to compute the mean torque. The magnetic circuit model is fast to compute (≈100 ms) and it is automatically differentiate, thanks to Reluctool and Cades software tools [3, 4]. It is well adapted to global optimization process because it is compatible with fast gradient optimization algorithms. This model incorporates nonlinear phenomena, iron saturation, and *d-q* cross saturation.

OPTIMIZATION PROBLEM OF THE ELECTRICAL MACHINE

For charge sustaining hybrid vehicles, when the battery only recharges during regenerative braking or when absorbing additional power from the ICE, the global battery discharge is constrained equal to zero over a driving cycle. In the paper, the objective function J is expressed by Eqn. 1:

$$J = \int_{t_0}^{t_f} d_{carb}(I_{me}, \delta_{me}, X)dt \quad (1)$$

where d_{carb} is the instantaneous fuel rate, and t_0, t_f are respectively the initial and the final time of the driving cycle.

The aim of the paper is to optimize the energy management and the sizing of the EM in a joint optimization process. The optimization problem involves the geometrical parameters of the EM named X (see Fig. 1), and the control variables of the vehicle, i.e. I_{me} and ψ_{me}. The entire problem involves about 410 optimization variables and about 1000 constraints (e.g. voltage, torque, speed instantaneous limitations, etc.), depending on the driving cycle length. A SQP algorithm is used to solve the optimization problem [5]. The initialization of the energy management is done by using a dynamic programming algorithm.

RESULTS

The optimization process has been applied to a parallel HEV on the ECE15 driving cycle. For this result, 10 sizing parameters of the EM and 400 control parameters are considered variable. This leads to an optimal solution in 150 iterations (~5s per iteration). The fuel saving is about 10% (from 3.50 initially, to 3.20 L/100km), whereas the other systemic parameters (ratios, nominal power of the ICE, etc.) are fixed. Fig. 4 shows the optimized geometry of the EM.

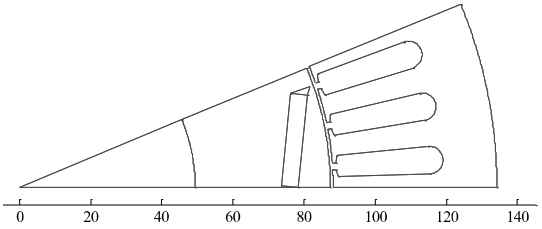

Figure 3. Optimized geometry of the EM (in mm)

CONCLUSION

In this study, a global optimization of the energy management and sizing of the EM has been applied to a parallel HEV architecture for an ECE15 driving cycle, using SQP algorithm. This study focuses on the sizing of the EM and takes into account the optimal energy management. Result shows a fuel saving of 10%. An alternative global strategy, using genetic algorithm, is being studied in parallel of this article. The final paper will present more precisely the reluctance circuit model and hybrid electrical vehicle model. Sizing and instantaneous constraints will be presented in detail. Results over road and highways driving cycle will be also presented.

ACKNOWLEDGEMENT

Funding for this project was provided by a grant from la Région Rhône-Alpes.

REFERENCES

[1] Reinbold, V.; Vinot, E. & Gerbaud, L. Global optimization of a parallel hybrid vehicle using optimal energy management, IJAEM : International Journal of Applied Electromagnetics and Mechanics, IOS Press, 2013, 43, 115-126.

[2] Delprat, S.; Lauber, J.; marie Guerra, T. & Rimaux, J. Control of a parallel hybrid power train : optimal control, IEEE Transactions on Vehicular Technology, 2004, 53.

[3] Du Peloux, B.; Gerbaud, L.; Wurtz, F.; Leconte, V. & Dorschner, F. Automatic generation of sizing static models based on reluctance networks for the optimization of electromagnetic devices, IEEE Transactions on Magnetics, 2006, 42, 715-718.

[4] Enciu, P.; Wurtz, F.; Gerbaud, L. & Delinchant, B. Automatic differentiation for electromagnetic models used in optimization, COMPEL: The International Journal for Computation and Mathematics in Electrical and Electronic Engineering, 2009, 28, 1313-1326

[5] Wright, S. & Nocedal, J. *Numerical optimization*, Springer New York, 1999.

13th International Workshop on Optimization and Inverse Problems in Electromagnetism
September 10 – 12, 2014, Delft, The Netherlands

DESIGN OPTIMIZATION OF ELECTROMAGNETIC DEVICES USING THE LEAGUE CHAMPIONSHIP ALGORITHM

Houssem R.E.H Bouchekara*, Luc Dupré**, Hamza Kherrab* and Rabia Mehasni*

* Constantine Electrical Engineering Laboratory, LEC, Department of Electrical Engineering,

University of Constantine 1, 25000 Constantine, Algeria

E-mail: bouchekara.houssem@gmail.com

E-mail: kherrabhamza25@gmail.com

E-mail: mehasni@yahoo.fr

** Dep. of Electrical Energy, Systems & Automation, Ghent University, Belgium

E-mail: luc.dupre@ugent.be

Abstract. Nowadays, there is an increasing attention to novel evolutionary techniques. A new efficient optimization method, called the League Championship Algorithm (LCA) is proposed in this paper for the optimal design of electromagnetic devices. This method is inspired by the competition of sport teams in an artificial sport league for several weeks and over a number of seasons. The validity of the algorithm is tested on the magnetizer benchmark problem, and results are compared with those found in the recent literature, showing the effectiveness and robustness of the proposed method.

Keywords: Electromagnetic Devices, Optimization, League Championship Algorithm, Metaheuristics.

INTRODUCTION

Optimization of devices is one of the major problems in electrical engineering. It involves choosing from many possible variants the best or optimum one according to one or several criteria [1]. Design optimization of Electromagnetic Devices (EMD) using metaheuristics techniques has been successfully implemented and applied since the development of these techniques in the early 1980's. Some recent examples of the application of metaheuristics in EMD design include, among others, Genetic Algorithms, Evolution Strategies, Tabu Search, Artificial Immune Systems, Particle Swarm Optimization, Electromagnetism-Like Mechanism, Imperialist Competitive Algorithm, and Black-Hole-Based Optimization.

Furthermore, recently, great efforts have been devoted to the development and application of new optimization metaheuristics inspired from nature. In this context, a new developed evolutionary metaheuristic which has not received yet much attention in the electromagnetic optimization community is the league championship algorithm (LCA). The LCA is a novel metaheuristic algorithm inspired from the sport league championships. In LCA the league (population) is composed of teams (individuals) that compete in an artificial league several weeks and for a number of seasons [2][3].

The objective of this paper is to review the basic algorithmic features of the LCA optimizer and then apply it to the optimal design of EMD. The proposed algorithm is tested on the magnetizer benchmark problem.

LEAGUE CHAMPIONSHIP ALGORITHM (LCA)

LCA method which was introduced by Husseinzadeh [2] is a new metaheuristic algorithm to solve continuous optimization problems [4]. Like other nature-inspired algorithms, LCA works with a population of solutions to evolve to the optimal solution. Each team (individual) in the league (population) represents a feasible solution to the problem being solved. These teams compete in an artificial league for several weeks (iterations). Based on the league schedule at each week, teams play in pairs (i.e. team i plays against team j) and the outcome is determined in terms of win or loss based on each team playing strength (corresponding to the fitness value) resultant from a particular team formation (solution). In the recovery period, keeping track of the previous week events, each team devises the required changes in its formation to set up a new formation (a new solution is generated) for the next week contest and the championship goes on for a number of seasons (stopping criterion) [4]. More details about the LCA will be given in the final version of the paper.

APPLICATION TO THE MAGNETIZER PROBLEM

The application of LCA for EMD optimization is illustrated on the magnetizer problem modeled as a linear 2D magnetostatic field analysis using the Finite Element Method (FEM). The geometry of the modeled

part of the magnetizer problem is shown in Figure 1 [5][6]. The objective is to optimize the pole shape of the magnetizer in order to get a predefined profile of the magnetic flux density along chord AB positioned halfway through the width of the magnetized piece [7].

The pole shape is modeled using Uniform Nonrational Cubic B-Splines (UNBS) with n control points P1, P2…Pn corresponding to the radial distances r1, r2… rn and separated by α as shown in Figure 1. UNBS interpolation provides local control of the curve i.e., when a control point is moved, this affects only a small part of the curve. A b-spline curve is confined to the convex hull formed by the control points, and unless a control point is repeated at least 3 times, it does not touch the control points [5][6].

In the FEM model, a low permeability (close to that of the air) is assigned to the object to be magnetized (nonmagnetic material), a permeability of 1000 is assigned to the pole face and the outer shell and a high current is applied to the coil region (5 A/mm2).

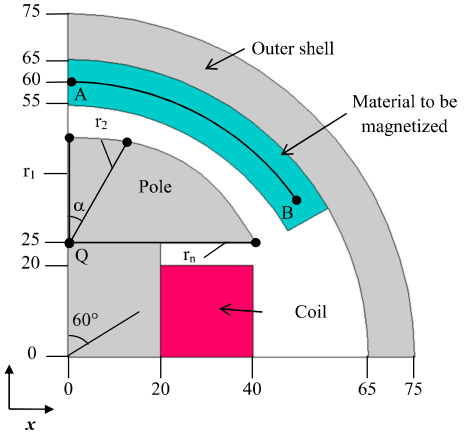

Figure 1. Geometry of the magnetizer.

The distribution of the magnetic flux density is evaluated at N sample points along the chord AB. Based on the desired profile of the magnetic flux density distribution in the chord AB, two cases are proposed and investigated in this paper:

CASE 1: in this case the objective is to get a sinusoidal increasing distribution of B.

CASE 2: in this case the objective is to get a uniform distribution of B.

The results will be presented and detailed in the final version of the paper. Moreover, a comparison with some other techniques will be provided too.

CONCLUSIONS

This paper describes the application of a new nature inspired optimization technique that is the league championship algorithm which is a powerful and easy algorithm for EMD optimal design. One of the major advantages of the proposed LCA technique compared to other optimization techniques is that there is no parameter to tune. In other words, the LCA is a parameterless technique. In order to assess the effectiveness of the proposed technique, it has been applied to the magnetizer problem. Two cases with different number of control points are studied. In both cases the LCA converges rapidly to optimum. The results obtained show that the LCA constitutes a potential and efficient tool for the design and optimization of EMD.

REFERENCES

[1] V.L, Chechurin, N.V. Korovkin, M. Hayakawa, "Inverse Problems in Electric Circuits and Electromagnetics", Springer, ISBN 0-387-33524-2, 2007.

[2] A A. Husseinzadeh Kashan, "League championship algorithm: a new algorithm for numerical function optimization", In: Proceedings of the international conference of soft computing and pattern recognition. SoCPaR 2009, IEEE Computer Society, pp. 43–8, 2009.

[3] A. Husseinzadeh Kashan, "An efficient algorithm for constrained global optimization and application to mechanical engineering design: League championship algorithm (LCA)", Computer-Aided Design, Volume 43, Issue 12, pp. 1769-1792, Dec. 2011.

[4] Z. Pourali, M. Aminnayeri. "A Novel Discrete League Championship Algorithm for Minimizing Earliness/Tardiness Penalties with Distinct Due Dates and Batch Delivery Consideration". In: Advanced Intelligent Computing, Springer, pp. 139-146, 2012.

[5] G.F. Uler, O.A. Mohammed, K. Chang-Seop, "Design optimization of electrical machines using genetic algorithms," IEEE Trans. Magn., vol.31, no.3, pp.2008-2011, May 1995.

[6] O.A. Mohammed, G.F. Uler, "A hybrid technique for the optimal design of electromagnetic devices using direct search and genetic algorithms," IEEE Trans. Magn., vol.33, no.2, pp.1931-1934, Mar 1997.

[7] H.R.E.H. Bouchekara, "Optimal design of electromagnetic devices using a black-hole-based optimization technique", IEEE Trans. Magn., vol. 49, Iss. 12, pp. 5709 – 5714, Dec. 2013.

13th International Workshop on Optimization and Inverse Problems in Electromagnetism
September 10 – 12, 2014, Delft, The Netherlands

Optimization of the control of a doubly fed induction machine

Jules GILLET, Maria Pietrzak–David and Frédéric Messine *

* Université de Toulouse, INPT, UPS, LAPLACE

ENSEEIHT, 2 rue C. Camichel, BP 7122

F31071 Toulouse Cedex 7, France.

E-mail: (jules.gillet) (maria.david) (frederic.messine) @ laplace.univ-tlse.fr

Abstract. This paper focuses on finding an optimal control for a doubly fed induction machine (DFIM) in a motor mode. Our purpose is to develop a numerical method to improve the DFIM efficiency. Thus, we will start with a fixed system made by a DFIM and two ideal 3 phases voltage inverters. Our method will demonstrate its efficiency to improve that control for minimizing the copper loss. This method is based on direct shooting techniques associated with a MATLAB optimization solver: *fmincon*.

Keywords: copper loss; direct shooting method; doubly fed induction machine (DFIM); energetic efficiency; optimization

INTRODUCTION

The Doubly Fed Induction Machine (DIFM) is often used as a Doubly Fed Induction Generator (DFIG). That is why studies are done to optimize the DFIG functioning as in [1]. Controls of DFIM have been developed in [2], but now the goal is to find a method to optimize its functioning, for example by minimizing the copper loss. This paper is a continuation of [3]. A presentation of the studied system, (a DFIM in motor mode fed by two ideal voltage inverters), will be done. Thus, a model of this system will be mentioned. With this model, an optimal control method based on direct shooting will be developed.

SYSTEM PRESENTATION

The system is composed as in Fig. 1:

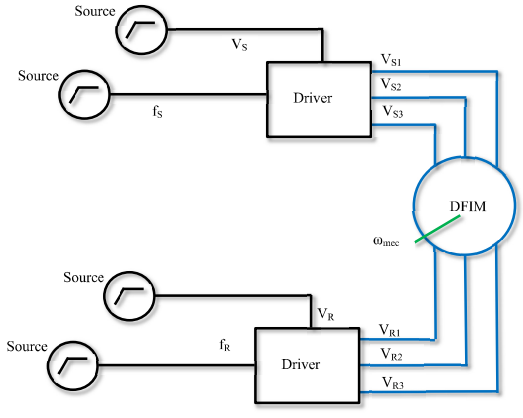

Figure 1. General sketch of DFIM drive.

The different sources give continuous signals which correspond to the amplitudes and frequencies of the two 3 phases tension systems feeding the DFIM. For this transformation, ideals 3 phases voltage inverters are used. They have as inputs, a frequency and amplitude and give an equilibrated tension system at the end to feed the DFIM.The aim in this paper is to optimize these four signals to reduce the copper loss in the machine.

MODELING

The model used in the optimization method will not be described because it is the same than in [3] with the mechanical equation added. The static converter model is not used at the beginning because the goal is to

reduce the copper loss in the motor. It provides a simplified model, to focus on the DFIM, as it is the real purpose. Furthermore, DFIM model used in this paper is developed in François Bonnet's PhD thesis [4].

OPTIMIZATION PROBLEM

The main point developed here is to find a solution to minimize the copper loss:

$$(1)\quad E_J(u) = \int_0^{t_f} 3R_S\left(I_{S\alpha}{}^2 + I_{S\beta}{}^2\right) + 3R_R\left(I_{R\alpha}{}^2 + I_{R\beta}{}^2\right)dt$$

Under various constraints such as start and final speeds, final torque, current limitation etc.

As in [3] the direct shooting optimal control method [5] is used. This method is based on the discretization of the time by small steps h. Hence, this yields to solve a large scale static optimization problem. With the complete model, the problem is too complex to be solved directly. That is why it is cut into two optimization sub problems. First, the electro mechanical part will be solved and then the electrical one as well:

$$(2)\quad \min_{I^i \in \Re^{4*N}} \sum_{i=0}^{N} P_j{}^i \quad \text{That gives the optimal currents : } \mathbf{I}^{*}\cdot \text{.Then:}$$

$$(3)\quad \sum_{i=0}^{N} \min_{V_{1..2}{}^i, f_{1..2}{}^i \in \Re^4} \left(\max_{k=1..4} \left[\left(I_k^* - I_k\left(V_{1..2}, f_{1..2}\right)\right)^2 \right] \right)$$

This separation gives valid results for our problem.

CONCLUSIONS

In this paper, a way to improve the copper loss with a more realistic model is presented. The direct shooting method is used to optimize the current in a DFIM speed drive, then to generate the control to have these currents. This optimization method allows us to adapt the control strategy to the required operation of the system taking into account the formulated constraints.

As in [3], the optimized control is made off line.

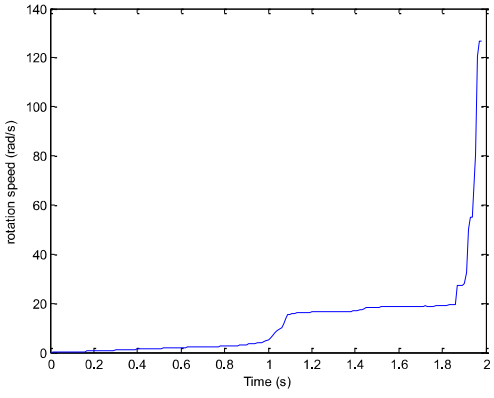

Figure 2. Optimal start of DFIM drive.

As a result the energy lost because of the copper loss is 74% less important than in an open loop static V/f control for a start of the DFIM in 2 seconds. The calculation time is a bit more than 36 min.

REFERENCES

[1] Heng Nian, Jiabing hu, Jia-wen li: "Multi-objective optimization control of DFIG system under distorted grid voltage conditions" IEEE Electrical Machines and Systems (ICEMS), 2011.

[2] M. Abdellatif, M. Pietrzak-David, I. Slama-Belkhodja: "Sensitivity of the currents input-output decoupling vector control of the DFIM versus current sensors fault" IEEE Power Electronics and Motion Control Conference, 2008. EPE-PEMC 2008.

[3] Jules GILLET, Maria Pietrzak–David and Frédéric Messine, "Optimization of the control of a doubly fed induction machine" IEEE Electronics, Control, Measurement, Signals and their application to Mechatronics (ECMSM), 2013.

[4] François Bonnet: « Contribution à l'Optimization de la Commande d'une Machine Asynchrone à Double Alimentation utilisée en mode Moteur » pp. 43-49, Ph-D Thesis, INP-Toulouse.

[5] Emmanuel Trelat: « Contrôle optimal: Théorie et applications » ed Vuibert, Collection "Mathématiques Concrètes", pp. 103-112.

13th International Workshop on Optimization and Inverse Problems in Electromagnetism
September 10 – 12, 2014, Delft, The Netherlands

PARAMETRIC OPTIMIZATION OF THE MAGNETIC CIRCUIT OF A HALL EFFECT THRUSTER

Alberto ROSSI*, Frédéric MESSINE* and Carole HENAUX*

*LAPLACE Laboratory GREM3 Toulouse, INPT, 2, rue Charles Camichel 31071 Toulouse Cedex 7 (France)
E-mail: arossi@laplace.univ-tlse.fr

Abstract. This study presents a design method based on parametric optimization. Knowing that the current average of 80 % of the weight of Hall Effect thrusters is the weight of the magnetic circuit, the two fundamental constraints of dimensioning are respectively the minimization of the mass and the obtaining a specific and given magnetic mapping. The design of Hall Effect thrusters until now was based on empirical models. In this paper, we present some theoretical models and mathematic formulations to find optimal magnetic circuits for those thrusters.

Keywords: Hall Effect thruster, parametric optimization, space propulsion.

INTRODUCTION

Among the technologies of space electric propulsion, Hall Effect thrusters work on the generation of a plasma inside a cylindrical channel. They have already demonstrated their ability to operate on a variety of missions, ranging from control of the orientation and position of orbiting satellites to main propulsion engine for medium-size robotic space vehicles. These thrusters incorporate a magnetic circuit that has to generate a very specific magnetic mapping inside the plasma channel. This magnetic circuit comprises the feature of enclosing the plasma channel which leads to size a very large gap circuit with high leakage rates. Two application examples are presented: the first circuit is dimensioned in order to minimize the mass and the second one to obtain a specific mapping of the magnetic field in the plasma channel.

PAPER ATTRIBUTES

Optimization algorithm

The design of this magnetic structure via optimization based on an analytical model ("reluctances circuit» type) is not appropriate. Indeed, the magnetic circuit comprises a lot of leakage fluxes whose amplitudes are of the same order of magnitude as the useful flux through the channel. Moreover, these flows vary greatly depending on different geometries of ferromagnetic parts. It was therefore chosen to use an optimization method using a finite element model of the structure to assess the relevance of a set of parameters. The developed design method uses a parametric optimization algorithm with a finite elements resolution in order to achieve an optimized geometry. The finite element model takes as input the geometric parameters of the structure and it will output the values of fields for an optimum current configuration. An evaluation criterion for the optimization function is then calculated to assess the correlation between the field values obtained and the initially target set values of the magnetic field. Assumptions conventionally used of azimuthal homogeneity of the field in the thruster channel (invariance of the B field along the circumference of the canal) allow reducing this model to a 2D model, which represents a considerable saving of time in each of the many function called for the evaluation criterion during the optimization procedure. The optimization procedure is started several times with different points. This is because there is a great chance to fall into local minimum points. The optimal solution can be significantly influenced by the starting point that is chosen. This optimization procedure can be applied with several objective functions according to the purpose of the designer. With this optimization algorithm there is the possibility to choose between two optimization criteria: optimization of the magnetic field generated by the structure and optimization (minimization) of the mass of the structure. In the case of the optimization of the magnetic field topology generated by the structure, the objective function to be minimized is represented by the difference between the magnetic field calculated at each iteration in the channel and the required magnetic field. In the case of minimizing the weight of the structure, the objective function of the optimization problem is represented by the surface of the structure (and not the volume because the model used is a 2D model). The criterion of minimization of the mass requires as a constraint the imposition of the magnetic field in the desired points of the channel. In fact the final objective of this last procedure is to minimize the mass of the structure while maintaining unchanged the values of the magnetic field in the channel.

Example

To facilitate subsequent uses and modifications of the optimization tool, it was decided to use commercial numerical codes and solvers. FEMM 4.2 was chosen for the finite element simulations and Matlab ® to drive FEMM and for its optimization procedures. To minimize the objective function the fmincon function of Matlab® was used.

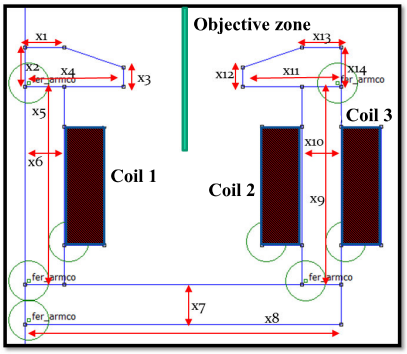

Figure 1: Section of the generic Hall Effect thruster magnetic circuit used for the example.

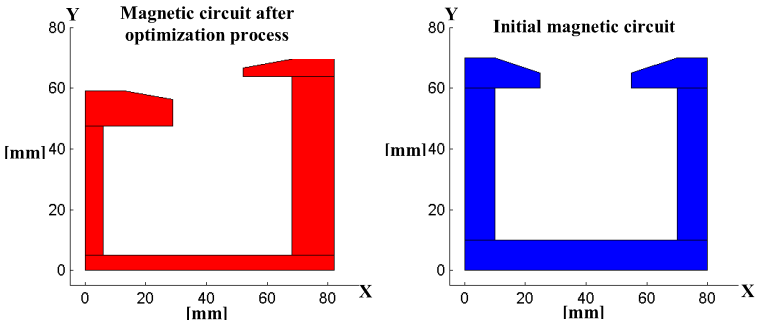

Figure 2: Results of the optimization process.

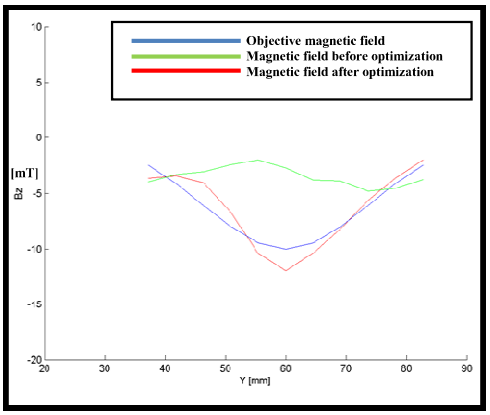

Figure 3 : comparison between the magnetic fields before and after optimization procedure.

In the Fig.2 and Fig.3 is represented an example of the optimization process. The objective of this optimization was to optimize the magnetic field produced in the thruster channel.

CONCLUSIONS

The optimization algorithm developed and named "ATOP^PO" was code and it has demonstrated its efficiency in the first tests whose results are shown in Fig.2. A second phase of this work will consist in associating parametric optimization code with a topological optimization code that has already developed in our laboratory. The set of two codes together can represent a complete design tool for the magnetic circuit dedicated to space propulsion.

REFERENCES

[1] R. G. Jahn, Physics of electric propulsion. McGraw-Hill, 1968.

[2] V. Kim, « Main physical features and processes determining the performance of stationary plasma thrusters », *Journal of Propulsion and Power*, vol. 14, n°. 5, p. 736–743, 1998.

[3] R. R. Hofer et R. S. Jankovsky, « The influence of current density and magnetic field topography in optimizing the performance, divergence, and plasma oscillations of high specific impulse Hall thrusters », in *Internal Electric Propulsion Conference, IEPC-03-142, Toulouse, France*, 2003.

[4] Raphaël Vilamot, « Optimisation de la configuration magnétique d'un propulseur à effet Hall par résolution du problème inverse », PhD thèse, INP-ENSEEIHT Toulouse.

COMPARATIVE ANALYSIS ON VARIABLE SYNRM ACCORDING TO GEOMETRIC STRUCTURE BY NUMERICAL ANALYSIS AND EXPERIMENTATION

Jung Ho Lee*, Jun Ho Lee* and Young Hyun Kim*

* Electrical Engineering Department, Hanbat National University, Daejeon, 305-719 Korea
E-mail: kimyh@hanbat.ac.kr

Abstract. This paper presents the loss and efficiency evaluations for synchronous reluctance motors (SynRM) with permanent magnet assisted (PMA), non-PMA and concentrated winding (CW), distributed winding (DW) by finite element method (FEM) and experiment. In this paper, the performance characteristic is compared according to the stator and rotor types in SynRM. In addition, the efficiency evaluation is also compared including hysteresis loss, copper loss, other loss on the basis of rated load condition.

Keywords: PMA-SynRM, DW-SynRM, CW-SynRM, Loss & Efficiency Evaluations.

INTRODUCTION

Issues such as efficiency, torque/ampere, core loss and torque ripple are important in evaluating the performance of a SynRM [1].

If stator windings of a SynRM are a concentrated type as opposed to a conventional distributed type, a decrease in copper loss and the production cost due to the simplification of winding in factory, is obtained. It is called concentrated winding synchronous reluctance motor (CW-SynRM). On the other hand, Distributed type has advantages that the torque ripple is decreased. It is called distributed winding synchronous reluctance motor (DW-SynRM). By adding a proper quantity of permanent magnets to the SynRM, the torque density and power factor of SynRM can be greatly increased. It is called Permanent Magnet Assisted Synchronous Reluctance Motor (PMA-SynRM).

This paper is, finally, the characteristic comparison relative to torque density, efficiency based on the structure of the stator and rotor in order to select a proper industry application field and production cost problem of each SynRM.

COMBINATION MODELS OF SYNRM

Fig. 1 shows the combination models of PMA-, non PMA-and CW-SynRM, DW-SynRM.

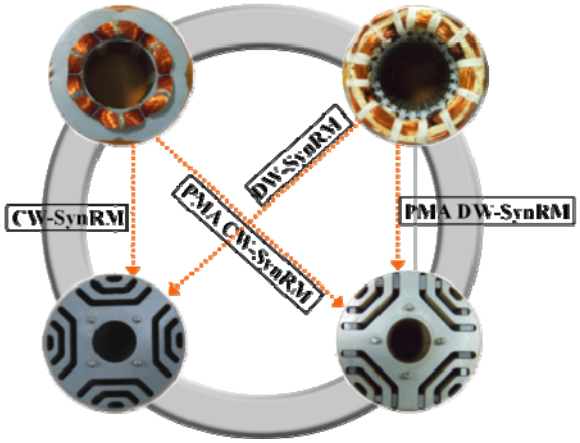

Figure 1. Combinations of SynRM.

Where,
DW-SynRM : Distributed Winding (Stator) + Rotor
CW-SynRM : Concentrated Winding (Stator) + Rotor
DW PMA-SynRM : Distributed Winding (Stator) + Rotor with Permanent Magnet
CW PMA-SynRM : Concentrated Winding (Stator) + Rotor with Permanent Magnet

Formerly, the papers published for optimization of CW-, DW-SynRM [2]-[3]. But these papers deal with optimization according to the rotor shapes only. On the other hand, this paper additionally compared the characteristic of PMA type. The purpose of the inserting PM is to decrease the q-axis inductance. The principle can be illustrated by the following theorem [3].

$$T_{pmr} = \frac{3}{2}\frac{p}{2}[L_d i_q i_d - (L_q i_q - \lambda_{mq(pm)})i_d] . \quad (1)$$

It can be considered that a theoretical maximum torque for a PMA-SynRM is reached if L_q is zero. This possibility can be reached by use of the second-order term of Eqn. 1. It can be assumed that the polarity of the magnets is reversed relative to the positive direction defined by the direction of the stator q-axis mmf.

COMPARISON OF SIMULATION AND EXPERIMENT RESULTS

Table 1 shows the losses, efficiency, and current characteristics of SynRM under the rated output power and the rated speed condition. One should notice that the PMA type can be obtained for same torque values by lower currents than those of non PMA type. The higher currents of the non PMA type for the same torque density, the higher current angle.

Table 2. Comparison of loss in SynRM and PMA-SynRM(3600rpm)

	Torque (N·m)	Efficiency (%)	Core Loss (W)	Copper Loss (W)	Phase current (A)
CW-SynRM	0.90	81.47	36.17	38.07	4.06
PMA-CW SynRM	0.90	83.9	35.70	26.86	3.41
DW-SynRM	0.90	83.53	34.74	29.36	2.93
PMA-DW SynRM	0.90	88.3	21.22	20.69	2.46

The efficiency (close to the efficiency achieved by distributed winding) is obtained and the consequent torque performance approaches state of the art (distributed winding SynRM : 24 slot) at rated wattage and rated speed, as shown in Fig. 2. Even if the stator iron loss of the concentrated SynRM is increased by a lower power factor, due to the simplification of winding carried out in the factory, this still ensures a decrease in both the quantity of copper used (by a half) and the production costs.

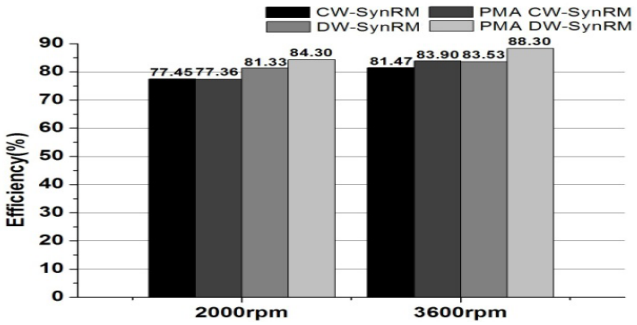

Figure 2. Effcdeiciency of each model.

CONCLUSIONS

In the PMA type, L_q was reduced by inserting permanent magnets in the direction of opposite q axis flux, which results in increased L_d-L_q and L_d/L_q. Also, the increased L_d-L_q and L_d/L_q can help improve torque density and power factor. Therefore, It is confirmed that the PMA type result in high output power performance through experiment. And it is confirmed that the decrease of copper, a similar hysteresis loss characteristic of CW type compared to the state of the art and a decrease of the production cost due to the simplification of winding in factory, obtains the high industrial competitive power. In the near future, SynRM is expected to be generalized in terms of energy-saving, environmental issues and industrial competitiveness.

REFERENCES

[1] L. Xu, X. Xu, T. A. Lipo, and D. W. Novotny, "Vector control of a synchronous reluctance motor including saturation and iron loss", IEEE Trans. Ind. Appl., vol. 27, no. 5, pp. 977–985, Sep./Oct. 1991.

[2] S. J. Park, S. J. Jeon, and J. H. Lee, "Optimum design criteria for a synchronous reluctance motor with concentrated winding using response surface methodology", J. Appl. Phys. (MMM), vol. 99, no. 8, Apr. 2006.

[3] J. M. Park, S. I. Kim, J. P. Hong, and J. H. Lee, "Rotor design on torque ripple reduction for a synchronous reluctance motor with concentrated winding using response surface methodology", IEEE Trans. Magn., vol. 42, no. 10, pp. 3479–3481, Oct. 2006.

OPTIMUM DESIGN CRITERIA OF ALA ROTOR SYNCHRONOUS RELUCTANCE MOTOR FOR THE MAXIMUM TORQUE DENSITY AND POWER FACTOR IMPROVEMENT

Young Hyun Kim*, Jung Ho Lee* and Jin Kyoung Lee*

* Electrical Engineering Department, Hanbat National University, Daejeon, 305-719 Korea
E-mail: kimyh@hanbat.ac.kr

Abstract. This paper deals with the characteristics analysis and optimum design of axially laminated anisotropic (ALA) rotor Synchronous Reluctance Motor (SynRM) considering centrifugal force and the effect on flux path. The rotor core of an ALA type adheres on the shaft axis. Because a rotor rotates at the rated speed as 3000rpm, the rotor is received with the centrifugal force, about 147.16[kN] per one block(diameter of the out rotor : 326.6mm). Because it is dangerous to fix the rotor, which is affected with the centrifugal force into shaft axis, this paper deals with the optimum design of the ALA-type rotor to solve the problem. Therefore, by simulating the structure and electromagnetic field, it is confirmed that the width of rotor core and insulator is set to design variables to reduce the minimum loss and the centrifugal force. In addition, Comparisons are given with characteristics of a same rated wattage traction induction motor and those of ALA-SynRM, respectively.

Keywords: ALA-SynRM, Torque density, Power factor, Centrifugal force, Traction Motor.

INTRODUCTION

In the past, three phase squirrel cage induction motor and synchronous motor are used to apply to electric railway. Generally, the squirrel cage induction motor in terms of operation and maintenance is simple, so it is popular in the industries due to low production cost. Even if industrious small and medium machines are recently improved with high efficiency technology, they still have low efficiency than other machines (SynRM). Also, slip caused by losses has a bad effect on torque in low speed.

On the other hand, Synchronous reluctance motors with the highest saliency ratio are obtained with axially-laminated designs [1]. Also, SynRM has advantages such as high torque and efficiency than induction motor. Therefore, it is advantageous to operate in traction motor or high speed machine. Considering rotor structure, SynRM has segment rotor type and ALA type, as shown in Fig. 1.

(a) Segment type (b) ALA type

Figure 1 Laminated direction of Segment and ALA type.

Segment type has a characteristic of mass production due to simplification of production process but it has low torque [2]. However, ALA type can be higher torque per unit mass because there is no rib. Here, the torque and power factor depends on the two-axis inductance L_d and L_q of the machine. The large difference of (L_d-L_q) and L_d/L_q ratio are improved to the machine's properties [3].

(1) $$T_e = \frac{3}{2} \cdot \frac{P}{2} (L_d - L_q) i_d \cdot i_q \cdot$$

(2) $$\cos\phi = \frac{\xi - 1}{\xi + 1} \text{ with } \tan\gamma = \sqrt{(\xi)} \quad \text{with} \quad \xi = \frac{L_d}{L_q} \cdot$$

The focus of this paper is characteristics analysis and optimum design of ALA-SynRM which makes up for the traction induction motor weakness in electric railway field.

This paper deals with the rotor structure only focuses on the optimum design because the stator of the induction motor is possible to use intactly.

In addition, the structure design of the ALA Rotor considering centrifugal force and the effect of flux path was designed and proved.

OPTIMUM DESIGN AND CHARACTERISTIC ANALYSIS

Decision of the design model

Fig. 2 shows the various rotor shapes of ALA SynRM. The rotor is made up of axial lamination cores(W_c) and the insulation sheets(W_i) which are alternately laminated onto nonmagnetic spider to the axial direction. Table 1 shows inductance values of the each of the rotor shapes. According to the result, model (a) is chosen as the initial model.

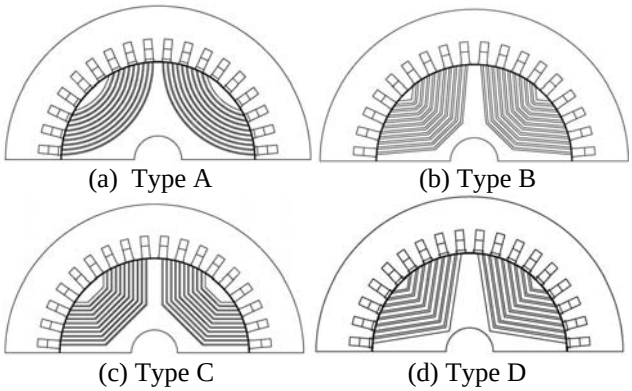

Figure 2. The various rotor shapes of ALA-SynRM.

Table 1. Inductance data of each of the rotor shapes

Shapes	L_d[mH]	L_q[mH]	$L_d - L_q$[mH]	L_d / L_q
(a)	**9.417**	**1.326**	**8.091**	**7.102**
(b)	7.671	1.086	6.585	7.064
(c)	8.540	1.307	7.233	6.534
(d)	5.799	1.127	4.672	5.146

Comparison of induction motor and ALA-SynRM

Table. 2 presents compared analysis result of ALA-SynRM and induction motor. It is confirmed that the output per unit weight of ALA-SynRM is higher than the output of induction motor. But the SynRM has fundamentally some increasing current which is demerit, even if the efficiency is increased by remarkably reducing the loss.

Table 2. Comparison of induction motor and ALA-SynRM

	Induction motor	ALA-SynRM
Torque(kN·m)	0.813	0.819
Current(A)	125.09	147.53
Volt(V)	1350	1350
Input(kW)	266.32	271.23
Output(kW)	249.99	257.39
Efficiency (%)	93.87	94.86
Total Loss(kW)	16.332	8.721
Power factor	0.90	0.77

CONCLUSIONS

In this paper, the magnetic flux distribution of ALA-SynRM is analyzed using Finite Element Method (FEM) considering maximum torque and torque ripple. Also, according to the change of rotor shape, a higher output is obtained by improving flux distribution and torque characteristic.

In future, ALA-SynRM may be considered as low cost and high efficiency model in various industries through improvement on manufacturing technology and process.

REFERENCES

[1]] Wen L. Soong, David A. Staton, Timothy J. E. Miller, “Design of a New Axially-Laminated Interior Permanent Magnet Motor” *IEEE Trans. On Industry Applications*, Vol. 31, No. 2, March/April 1995.

[2] Takayoshi Matsuo, Thomas A. Lipo, "Rotor Design Optimization of Synchronous Reluctance Machine", *IEEE Trans. On Energy Conversion*, Vol. 9, No. 2, June 1994, pp. 359-365.

[3] Staton D.A, Miller T.J.E, Wood S.E, “Maximising the saliency ratio of the synchronous reluctance motor”, *Electric Power Applications, IEEE Proceedings*, Vol. 140, No. 4, July 1993.

OPTIMUM DESIGN OF PMA-SYNRM ACCORDING TO THE RATED WATTAGE FOR POWER IMPROVEMENT

Jung Ho Lee*, Jun Seo* and Young Hyun Kim*

*Electrical Engineering Department, Hanbat National University, Daejeon, 305-719 Korea
E-mail: kimyh@hanbat.ac.kr

Abstract. This paper deals with the optimum design criteria of Permanent Magnet Assisted Synchronous Reluctance Motor (PMA-SynRM) for power improvement. The focus of this paper is found a design solution through the comparison of torque density and d- and q-axes inductances according to the rotor magnet, the number of barriers and dimension variations in various rated wattage.

Keywords: PMA-SynRM, RSM, FEM

INTRODUCTION

The performance of a synchronous reluctance motor (SynRM) in terms of torque and power factor depends on d- and q- axes inductance L_d and L_q of the machine. The large difference of L_d - L_q is good for the machine's properties.

Therefore, Considerable attention has been paid in the past to improve rotor design of SynRM [1]-[2].

By adding a proper quantity of permanent magnets to the rotor, the torque density and power factor of SynRM can be greatly increased. It is called Permanent Magnet Assisted Synchronous Reluctance Motor (PMA-SynRM). And it is important to select an appropriate combination of design parameters to enhance more torque density than an existing PMA-SynRM.

In this paper, the optimum design of PMA-SynRM including rotor structure each rated wattage is proposed by using finite element analysis.

Finally, the focus of this paper is compared with torque density, d- and q-axes inductance of PMA-SynRM according to the rotor magnet, the number of barriers and dimension variations under each rated wattage condition corresponding to the rotor diameters.

MODELING AND PRINCIPLE OF PMA-SYNRM

A SynRM runs at a somewhat poorer power factor than the induction motor.

This problem can be alleviated by inserting permanent magnets to the rotor is to decrease the q-axis inductance. The principle can be illustrated by the following theorem [3].

$$T_{pmr} = \frac{3}{2}\frac{P}{2}[(L_d - L_q) i_q i_d + \Psi_{mq(pm)} i_d] \quad (1)$$

It can be considered that a theoretical maximum torque for a PMA-SynRM is reached if L_q is zero. This possibility can be reached by use of the second term of Eqn. 1.

It can be assumed that the polarity of the magnets are reversed relative to the positive direction defined by direction of the stator q-axis MMF.

Fig. 1 shows Rotor cross-section and a phasor diagram including the effects of a permanent magnet in which the q-axis flux is assumed to be completely canceled.

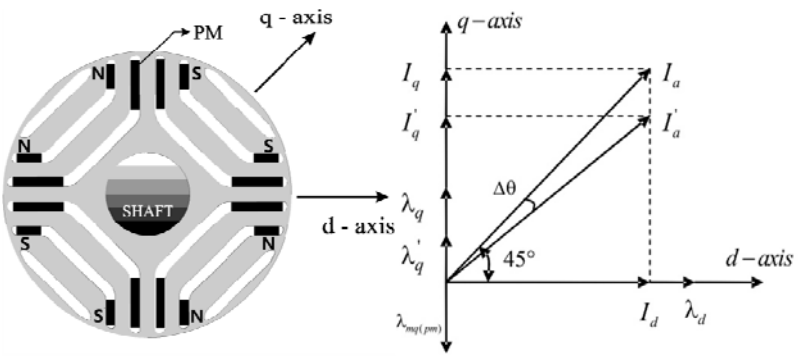

Figure 1. Rotor cross-section and phasor diagram of PMA-SynRM

DESIGN RESULTS AND DISCUSSION

Fig. 2 shows the torque characteristics of initial and optimized PMA-SynRM (3HP) in same torque conditions, respectively.

It can be found that optimized PMA-SynRM is more counteracted q-axis flux than initial model. As a result, the torque density of optimized PMA-SynRM is higher than initial model and the torque ripple of optimized PMA-SynRM is less than initial model, as shown in Fig. 2.

Fig. 3 shows configurations of optimized and initial design model of PMA-SynRM (3HP).

Considering inductance difference and design solutions are shown in Table 1.

One should notice that the design solutions of PMA-SynRM should be related to the rotor design variables dimensions and this will be the important data in motor design of similar specifications. Also, it is confirmed that the value of K_w is decreased by increasing both wattage and diameter.

As a result, the value of K_w is played an important role in the rated wattage selection.

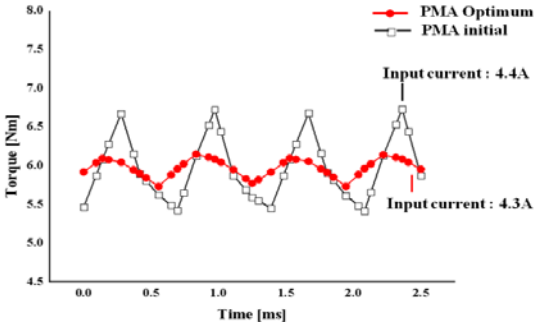

Figure 2. Torque characteristics of initial and optimized PMA-SynRM (3HP)

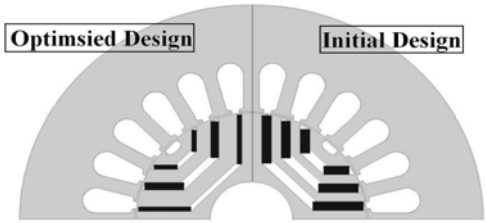

Figure 3. Configurations of optimized and initial design model

Table 1. Design solutions of eachrated watt

Rated Watt	L_d-L_q	K_w	Diameter (mm)	Flux barrier	Rated current(A)
1HP	89.24	0.95	66.8	3	2
3HP	115.84	0.85	71.4	4	6
4HP	71.23	0.78	84.9	5	11
5HP	64.64	0.74	92.1	5	14
6HP	60.46	0.77	101	6	17
7HP	47.76	0.61	109.1	6	20

CONCLUSION

A method of optimum design related to the torque density of PMA-SynRM according to the flux barrier number, K_w and especially, rotor diameter has been proposed.

For rapid design, an automatic pre-process including an automatic CAD file drawing and mesh generation with regard to the rotor shape variations has been developed. Starting from an existing design, the best design solution is selected, and it is confirmed that design solutions of PMA-SynRM should be related to the rotor design variables dimensions.

REFERENCES

[1] J. H. Lee, J. C. Kim, D. S. Hyun, "Effect of Magnet on Ld and Lq Inductance of Permanent Magnet Assisted Synchronous Reluctance Motor", IEEE Transaction on Magnetics, Vol. 35, No. 5, pp. 1199-1202, May 1999.

[2] J. H. Lee, D. S. Hyun, "Hysteresis Analysis for Permanent Magnet Assisted Synchronous Reluctance Motor by Coupled FEM & Preisach Modelling", IEEE Transaction on Magnetics, Vol. 35, No. 5, pp. 1203-1206, May 1999.

[3] J. M. Park, S. I. Kim, J. P. Hong, and J. H. Lee, "Rotor design on torque ripple reduction for a synchronous reluctance motor with concentrated winding using response surface methodology," IEEE Trans. Magn., vol. 42, no. 10, pp. 3479–3481, Oct. 2006.

NONLINEAR MULTIOBJECTIVE TOPOLOGY OPTIMIZATION AND MULTIPHYSICS ANALYSIS OF A PERMANENT-MAGNET EXCITED SYNCHRONOUS MACHINE

Piotr PUTEK*,***, Piotr PAPLICKI**, Roland PULCH***, Jan ter MATEN*, Michael GÜNTHER* and Ryszard PAŁKA**

*Bergische Universität Wuppertal, Chair of Applied Mathematics and Numerical Analysis, Germany

E-mails: {putek, termaten, guenther}@math.uni-wuppertal.de

**West Pomeranian University of Technology, Department of Power Systems and Electrical Drives, Poland

E-mails: {Piotr.Paplicki, Ryszard.Pałka}@zut.edu.pl

***Ernst-Moritz-Arndt-Universität Greifswald, Institute for Mathematics and Computer Science, Germany

E-mails: pulchr@uni-greifswald.de

Abstract. This paper proposes the multiobjective topology optimization of the Electric Controlled Permanent-Magnet Synchronous Machine (ECPMSM) using the level set method and Continuum Design Sensitivity Analysis (CDSA) in order to reduce both the electromagnetic losses and the Cogging Torque (CT). The back-electromotive force (the back EMF) is taken into account in the multiobjective optimization. First, the losses of the ECPMSM such as the stator iron losses, rotor eddy current losses and the hysteresis losses are calculated by the 2D time-harmonic Finite Element (FE) analysis. Next, the temperature distribution is estimated by a coupled heat transfer analysis. During an iterative shape and topology optimization process, the field velocity in the level set method is evaluated using the CDSA approach. Simulation outcomes show that the applied method leads to a significant reduction of both the electromagnetic losses and the CT and additionally minimizes the higher harmonics in the back-EMF.

Keywords: Coupled multiphysics problem, multiobjective topology optimization, level set method, shape optimization, electromagnetic losses, cogging torque, back-EMF, continuum design sensitivity analysis.

INTRODUCTION AND PROBLEM SETTINGS

Permanent-Magnet synchronous machines have several attractive features, particularly the high torque per mass, high power per unit volume, high efficiency and the brush-less design [1]. Thus, the interest in this type of electric machines has been gradually grown over the past decades. This did result in its broad use in the automotive industry, for example, in commercialized hybrid vehicles with different hybridization levels [2]. The resulting pulsating torque, however, causes mechanical vibration and thus, the acoustic noise [3]. Another problem are the eddy current and hysteresis losses in laminated or iron powder stator core in the PM material, which deteriorate the performance such as the maximum torque and the energy efficiency [4].

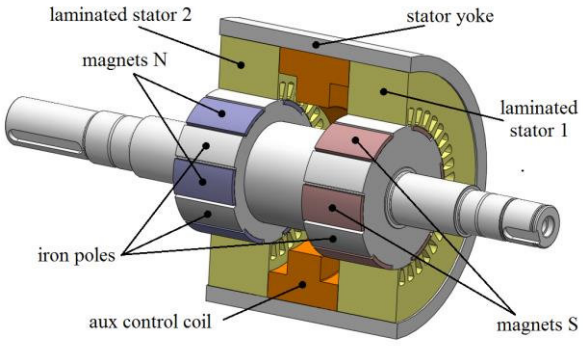

Figure 1. Cross section of the ECPMSM.

Table 1. Main parameters of the ECPMS machine

$2p$: number of poles	12
r_{ostat}: outer radius of the stator	143,5 mm
r_{istat}: inner radius of the stator	87,5 mm
l_{as}: axial length one part of the stator	80 mm
w_{oslot}: width of the slot opening	4,6 mm
ns: number of slots	36
m: number of phases	3
t_m: thickness of magnets made of *NdFeB*, B_r=1,2 T	3,0 mm

These losses, besides the copper losses, are the main heat sources. The rise in the temperature modifies the highly temperature-dependent characteristic of the PM and could lead to the partial demagnetization problem. Therefore, the main objective is to design the rotor poles shape and the teeth of a stator for the minimum of both the Joule losses and the CT by redistributing the iron and the PM over a design domain, while taking the back EMF into account.

NONLINEAR MULTIPHYSICS FORWARD PROBLEM

Let us consider the 2D FE model of the PM machine, which is described by the coupled system of the time-harmonic curl-curl equation and the transient heat equation with suitable boundary conditions

$$(1)\qquad \nabla \times \left(\upsilon \left(|\underline{\mathbf{B}}|^2 \right) \nabla \times \underline{\mathbf{A}} - \upsilon_{PM} \mathbf{B}_r(T) \right) - j\omega\sigma(T)\underline{\mathbf{A}} = \underline{\mathbf{J}}_e,$$

$$(2)\qquad \rho C \frac{\partial T}{\partial t} - \nabla \lambda \nabla T = Q(T, \underline{\mathbf{A}}) = \left[\sigma(T)\right]^{-1} |\underline{\mathbf{J}}_i|^2 = \left[\sigma(T)\right]^{-1} |-j\omega\sigma(T)\underline{\mathbf{A}}|^2 .$$

In (1), $\underline{\mathbf{A}}$ and $\underline{\mathbf{B}} = \nabla \times \underline{\mathbf{A}}$ are the phasors of the magnetic potential $\mathbf{A}$ and of the magnetic flux density $\mathbf{B}$, $\upsilon\left(|\mathbf{B}|^2\right), \upsilon_{PM}$ denote the reluctivity of the soft steel and of the PM, T is the scalar potential – temperature, $\sigma(T)$ describes the temperature-dependent electric conductivity, $\mathbf{B}_r$ is the remanent flux density in the PM, $\underline{\mathbf{J}}_e$ denotes the phasor of the source density $\mathbf{J}_e$ with the angular frequency ω that induces the current density $\mathbf{J}_i$. In (2), ρ is the mass density, C denotes the specific heat capacity, λ is the thermal conductivity, and Q describes the time-average inductive heating [5].

NONLINEAR MULTIOBJECTIVE TOPOLOGY OPTIMIZATION PROBLEM

The multiobjective topology problem is formulated in terms of a cost functional, which after converting into a single-objective problem with the norm defined as $|\underline{\mathbf{W}}| = \sqrt{\underline{\mathbf{W}} \cdot \underline{\mathbf{W}}^*}$ and the weights w_i, takes the form

$$3)\ F(\boldsymbol{\varphi}) = \frac{1}{2}\left(w_1\kappa_1 \int_\Omega |\mathbf{B}(\boldsymbol{\varphi})|^2 dx + w_2\kappa_2 \int_\Omega |\mathbf{J}_i(\boldsymbol{\varphi})|^2 dx + w_3\kappa_3 \oint_l |\nabla \times \underline{\mathbf{A}}(\boldsymbol{\varphi})|^2 dx + w_4\kappa_4 \int_\Omega |\underline{\mathbf{A}}(\boldsymbol{\varphi})|^2 dx \right), \mathbf{w} > [\mathbf{0}], \sum_{i=1}^{4} w_i = 1,$$

where κ_i are prescribed parameters. The representation of the shape of rotor poles and of the base tooth as well as their evolution during the iterative optimization process is obtained by the level set method. In this method, the interface Γ, for example, between two different materials Ω_1 and Ω_2 with the magnetic properties υ_1 and υ_2 is described by a zero level set of φ in such a way that $\Omega_1 = \{\mathbf{x} \in \Gamma \mid \varphi(\mathbf{x}) > 0\}$ and $\Omega_2 = \{\mathbf{x} \in \Gamma \mid \varphi(\mathbf{x}) < 0\}$. Thus, finally $\upsilon(\mathbf{x})$ is represented by $\upsilon(\mathbf{x}) = \upsilon_1 H(\varphi(\mathbf{x})) + \upsilon_2[1 - H(\varphi(\mathbf{x}))]$ in Ω, where $H(\mathbf{x})$ is the Heaviside function. In our work, the CDSA method [6] is used for the calculation of the speed of the zero-level set functions. The level set method, first proposed by [7] has recently found a wide application in electrical engineering, e.g., [3], [6], to address the topology optimization problems.

CONCLUSION

The goal of this research was to minimize the energy consumption and reduce the level of noise and vibrations in the ECPMSM used in modern drives for electro-mobiles. For this purpose, the shapes of both rotor poles and the teeth of stator were investigated. The applied methodology resulted in the reduction of both electromagnetic losses and the CT taking into account the value of the back EMF. This paper also shows the unique design features of the proposed methodology.

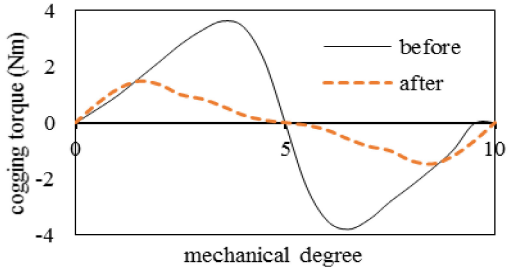

Figure 2. Cogging torque versus rotor position for the initial and optimized 3D FE model of the ECPMSM.

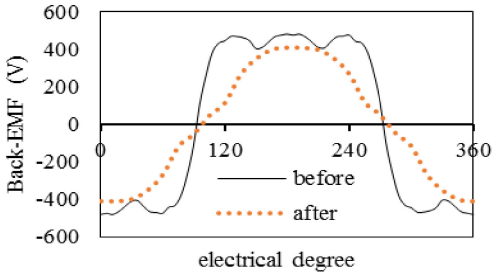

Figure 3. Back EMF waveform versus the electrical degree calculated in 3D FE model before and after optimization.

REFERENCES

[1] F. Gieras, M. Wing, *Permanent magnet motor technology*, John Wiley & Sons Ltd., 2008.

[2] Z. Makni, M. Besbes, and C. Marchand, Multiphysics Design Methodology of Permanent-Magnet Synchronous Motors, IEEE Trans. on Vehic. Techn. vol.56, no. 4, pp. 1524-1530, 2007.

[3] P. Putek, P. Paplicki, and R. Palka, Low Cogging Torque Design of Permanent Magnet Machine Using Modified Multi-Level Set Method With Total Variation Regularization, IEEE Trans. on Magn., vol.50, no. 2, pp. 657-660, 2014.

[4] K. Yamazaki, Y. Fukushima and M. Sato, Loss Analysis of Permanent-Magnet Motors With Concentrated Windings- Variation of Magnet Eddy-Current Loss Due to Stator and Rotor Shapes, IEEE Trans. on Indus. Appli., vol. 45, no 4, pp.1334-1342, 2009.

[5] C. Kaufmann, M. Günther, D. Klagges, M. Knorrenschild, M. Richwin, S. Schöps, J. ter Maten, Efficient Frequency-Transient Co-simulation of Coupled Heat-Electromagnetic Problems, Accepted for publication in Journal of Mathematics in Industry, 2014.

[6] Y.S. Kim; I. H. Park, Topology Optimization of Rotor in Synchronous Reluctance Motor Using Level Set Method and Shape Design Sensitivity, IEEE Trans. on Applied Superconductivity vol.20, pp.1093-1096, 2010.

[7] S.J. Osher, J.A. Sethian, Fronts Propagating With Curvature Dependent Speed: Algorithms Based on Hamilton-Jacobi formulations, Journal of Comput. Phys. vol. 79, pp.12-49, 1988

A PROCEDURE TO IDENTIFY UNIFORM DISTRIBUTION OF CURRENT DENSITY IN MAGNETIZING WINDING USING REGULARIZED SCALAR POTENTIAL FOR EDGE-BASED FEM

Yoshifumi OKAMOTO*, Koji FUJIWARA** and Shuji SATO*

*Utsunomiya University, Department of Electrical and Electronic System Engineering, Tochigi 321-8585, Japan
E-mail: {okamotoy, sato}@cc.utsunomiya-u.ac.jp

**Doshisha University, Department of Electrical Engineering, Kyoto 610-0321, Japan,
E-mail: koji.fujiwara@mail.doshisha.ac.jp

Abstract. The numerical technique to realize the uniform current density vector is required for the modeling of stranded wire in the finite element discretization. This paper presents a technique of being uniform current density using the regularization to achieve the stable convergence of conjugate gradient method with IC factorization (ICCG). The proposed method is mainly composed of two parts, which are the determination of the current density solving Poisson's equation and the regularization to assure div $\boldsymbol{J}_0 = 0$. We verified the effectiveness of proposed method by the application of typical winding structure.

Keywords: current density vector, electric scalar potential, magnetizing winding, regularization, uniform distribution.

INTRODUCTION

It is necessary to accurately estimate the current density vector in the evaluation of various electrical constants. The current density distribution should be uniformly modeled in the stranded winding of finite element analysis. Some effective methods [1], [2] for realizing the uniform current density were developed. The two-scalar method [1] can realize the substantial uniform current distributions. However, the range of use is limited to the winding which shape of current input and output surface is rectangular.

This paper presents a method which can realize the uniform distribution with arbitrary shaped input and output surface. Proposed method is mainly composed of two processes. Firstly, temporary direction of current density is determined by solving Poisson's equation and the normalization. Next, regularization is performed to achieve the stable ICCG convergence. We verify the performance of proposed method in the typical magnetizing winding.

METHODOLOGY TO REALIZE UNIFORM DISTRIBUTION OF CURRENT DENSITY

Governing equation

Firstly, the temporary current density is determined by solving the weak form G of Poisson's equation with respect to the electric scalar potential (ESP) ϕ following as:

$$(1) \qquad G_i = \int_{\Omega_c} (\nabla N_i) \cdot (\sigma \nabla \phi)\, dV + \int_{\Gamma_c} N_i\, (-\sigma \nabla \phi) \cdot \boldsymbol{n}\, dS = 0$$

where N_i is the nodal shape function, σ is the conductivity, $\boldsymbol{n}$ is the external unit normal vector, Ω_c is the microvolume and Γ_c is the its boundary, respectively. The boundary condition for solving (1) is shown in Fig. 1. The Dirichlet condition $\phi = 0$ is imposed on the nodes of the current output surface Γ_{out}, and the unknown equi-potential condition is imposed on the input boundary Γ_{in}. Then, the boundary integration term in (1) on the Γ_{in} corresponds with the input current value I. The resulting residual G_{ep} on Γ_{in} is shown as follows:

$$(2) \qquad G_{ep} = \iiint_V (\nabla N_i) \cdot (\sigma \nabla \phi)\, \mathrm{d}V - I = 0.$$

Simultaneously solving boundary problem (1) and (2), $\boldsymbol{J}_0 = -\sigma \nabla \phi$ is obtained.

Procedure to Make Current Density Uniform

Next, the obtained current density $\boldsymbol{J}_0$ is normalized as $\boldsymbol{J}_{0\_\mathrm{init}} = (I / S_{\Gamma in})\boldsymbol{t}$ where S is the cross-sectional area of input surface Γ_{in}, and $\boldsymbol{t}$ is the unit direction vector which is computed by $\boldsymbol{J}_0^{(e)} / |\boldsymbol{J}_0^{(e)}|$ where $\boldsymbol{J}_0^{(e)}$ shows the current density vector in the gravity center of element e. Because the current density $\boldsymbol{J}_{0\_\mathrm{init}}$ does not satisfy div $\boldsymbol{J}_{0\_\mathrm{init}} = 0$, it is impossible to achieve the stable ICCG convergence. Therefore, the regularization technique is applied to the current density vector $\boldsymbol{J}_{0\_\mathrm{init}}$ by using the correction vector $\boldsymbol{J}_{0c}$ as follows:

$$(3) \qquad \boldsymbol{J}_0 = \boldsymbol{J}_{0\_\mathrm{init}} + \boldsymbol{J}_{0c} \qquad (\because\ \boldsymbol{J}_{0c} \equiv -\nabla \delta\phi)$$

To satisfy the condition div$\boldsymbol{J}_0 = 0$, the weak forms G_i and G_{ep} of (3) about $\delta\phi$ is obtained as follows:

$$G_i = -\int_{\Omega_c} \nabla N_i \cdot (\boldsymbol{J}_{0\_\mathrm{init}} - \nabla\delta\phi)\, dV - \int_{\Gamma_c} N_i\, (\boldsymbol{J}_{0\_\mathrm{init}} - \nabla\delta\phi)\cdot \boldsymbol{n}\, dS$$

$$= \int_{\Omega_c} (\nabla N_i)\cdot(\nabla\delta\phi)\, dV - \int_{\Omega_c} (\nabla N_i)\cdot(\boldsymbol{J}_{0\_\mathrm{init}})\, dV \quad (4)$$

$$= 0$$

$$G_{ep} = \int_{\Omega_c} (\nabla N_i)\cdot(\nabla\delta\phi)\, dV - \int_{\Omega_c} (\nabla N_i)\cdot \boldsymbol{J}_{0\_\mathrm{init}}\, dV - I = 0 \quad (5)$$

NUMERICAL EXAMPLE

Fig. 2 shows the finite element mesh of magnetizing winding which is shaped into the racetrack. The finite element mesh is modeled by 1st order hexahedral elements, and the number of elements, nodes, and unknowns are 268,202, 278,832 and 791,101, respectively. Fig. 3 shows the intensities of current density vector. The uniformity ($|\boldsymbol{J}_0^{(max)}| / |\boldsymbol{J}_0^{(min)}|$) of current density intensity is obtained as ESP: 1.89 and proposed method: 1.07. The inductances evaluated by ESP, proposed method and measurement value are 33.77 mH, 34.10 mH and 34.65 mH, respectively. Furthermore, because the convergence characteristics have almost similar behavior among ESP and proposed method, there is very little difference of the elapsed time between ESP and proposed method. The detailed information will be described in the full-paper, in which further results of iterative implementation of proposed method will be included.

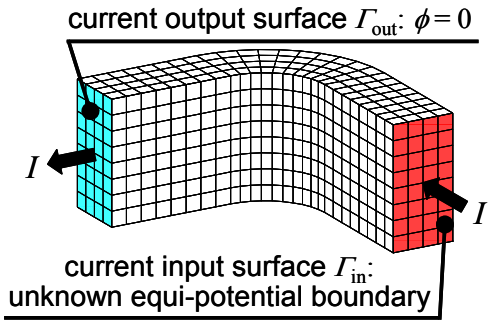

Figure 1. Boundary condition for ESP.

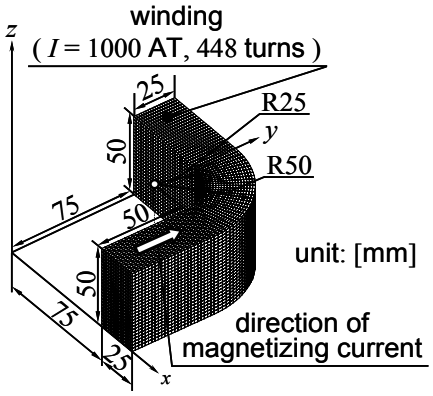

Figure 2. Analysis model.

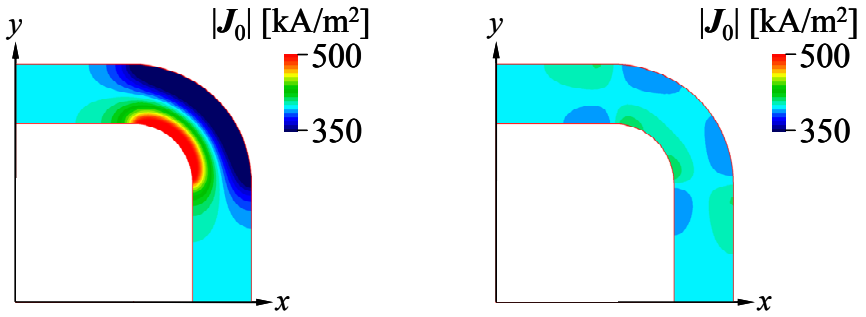

(a) ESP (b) proposed

Figure 3. Intensities of magnetizing current density.

CONCLUSION

Authors proposed a procedure to identify uniform distribution of current density in magnetizing winding using regularized scalar potential for edge-based finite element method. It could be seen that the uniformity performance of proposed method is comparable to the two-scalar method from the view point of the static inductance evaluation of magnetizing winding.

REFERENCES

[1] A. Kameari and K. Koganezawa, "Convergence of ICCG method in FEM using edge elements without gauge condition," *IEEE Trans. Magn.*, Vol. 33, No. 2, pp. 1223-1226, Feb. 1997.

[2] Z. Badics and Z. J. Cendes, "Source field modeling by mesh incidence matrices," *IEEE Trans. Magn.*, Vol. 43, No. 4, pp. 1241-1244, Apr. 2007.

MULTI-LEVEL CONFLICT-FREE SCHEDULING FOR ELECTROPLATING PLANTS

Roland EICHARDT, Uwe GRAICHEN, Alexander HUNOLD and Jens HAUEISEN

Technische Universität Ilmenau, Institute for Biomedical Engineering and Informatics, Ilmenau, Germany
E-mail: Roland.Eichardt@tu-ilmenau.de

Abstract. We present a multi-level optimization method to schedule carriers for an electroplating production process. In our specific application, product carriers with individual processing requests may be available only shortly before their intended start. This limits the optimization time for creating a schedule to a few minutes or less. From the practical perspective, all optimization constraints must be followed, whereas the minimization of the makespan is less critical. We show one scheduling example for eleven carriers, where a conflict-free solution with acceptably low makespan was computed in 0.4s.

Keywords: multi-level optimization, non-linear integer programming, production planning

INTRODUCTION

The application of metallic coatings by electroplating is an important manufacturing process for many products. For medical implants and invasively applied medical articles, these coatings provide biocompatibility or improve the hygienic safety. Medical regulations and requirements necessitate the strict compliance of the manufacturing process with the corresponding specifications. For an optimization of the schedules, these specifications are modelled by constraints, which any result must comply with (conflict-free solutions). Furthermore, the operators of the electroplating plants demand some flexibility when handling the carriers with the products to be processed. In particular, the carriers and their required processing specifications may be available only shortly before the intended start time, which restricts the optimization time to seconds or a few minutes, depending on the production work flow. In this article, we present a new probabilistic multi-level approach, which enables for the considered application the optimization of conflict-free schedules with relatively low computational effort.

METHODS

Optimization problem

A quantity of product carriers (jobs) has to be scheduled. Each carrier holds individual parameters specifying the procedure of electroplating processes, the availability times, possible positions for loading and unloading, and the priority. Carriers with higher priority must be loaded first. The electroplating procedure is represented by a sequence of process tasks, such as electroplating, degreasing, etching and rinsing. For each task, minimal and maximal process times must not be exceeded. Furthermore, the scheduled time should be as close as possible to a predefined optimum (subordinate objective). Preemption is not allowed. Each process task is carried out at a position. One or more positions are available for each task. Subsequent positions may not be identical during processing. The transports of carriers between any two positions are conducted by a hoist. For each transport, specific times for void displacement, carrier displacement, lifts, carrier pick-up, and drop-off have to be respected. A carrier may not be idle after loading, except, it is specified by its procedure. All positions and the hoist transporter can not contain more than one carrier at a time.

Transport and position utilizations describe the scheduled (optimized) transport and processing operations. The total quantity of utilizations represents the operations required for processing all scheduled carriers. Before starting an optimization, several utilizations may already exist, representing previously scheduled or running operations. All optimization variables are represented by positive integers.

The objective is to determine all required transport and position utilizations, such that the makespan describing the total time to process all available carriers is minimal, subject to the constraints stated above. This represents an extension to the unidirectional hybrid flow shop problem [1]. Given that the related Entscheidungsproblem is NP-hard already for simple special cases [2], this optimization problem is intractable and can practically be solved by approximation only.

Algorithm

For the scheduling of the transport and processing operations for all available carriers, we developed a probabilistic three-level optimization approach. In the top level, we use a simplified tabu search algorithm to find an optimal sequence for loading the carriers. For a given sequence of carriers, we optimally select the process positions by a random search on the second level. In the third level, all required position and transport utilizations are scheduled by deterministic decision rules using the current selections of carriers and positions,

and the processing specification described by the procedures. Individual sets for the positions and the transporter store the related utilization items. We use this information in the third optimization level to determine the time slots, at which positions and transporters are available or busy. In the first two levels, several iterations are performed to improve a current solution. If in the third level no compliance with the optimization constraints could be achieved, this scheduling step is repeated by delaying the loading of the carrier. Provided that the model of the electroplating plant and the procedures are consistent, and that the carrier availability times are not too restrictive, the presented scheduling approach always provide solutions that comply with the constraints. Otherwise, the corresponding carrier is rejected from scheduling. The proposed approach is primarily designed to provide valid optimization results within relatively short computation time. Starting form an initial solution, we are able to obtain solutions with smaller makespan by conducting a higher number of iterations in the first two optimization levels.

Example result

We consider a simple but in its setup realistic example. Eleven carriers with unique identifiers between 61 and 90 and with four different electroplating procedures have to be scheduled. Each procedure consists of five to ten process tasks. The positions 2-3 are used for the loading and unloading. The processing is performed at positions >4. The first carriers are available at 4000 s. No previous utilizations existed before the scheduling was started. Figure 1 illustrates the position and transport utilizations that are required to handle these carriers. This schedule results in a makespan of about 2 hours. The computation took 0.4 s on a standard computer.

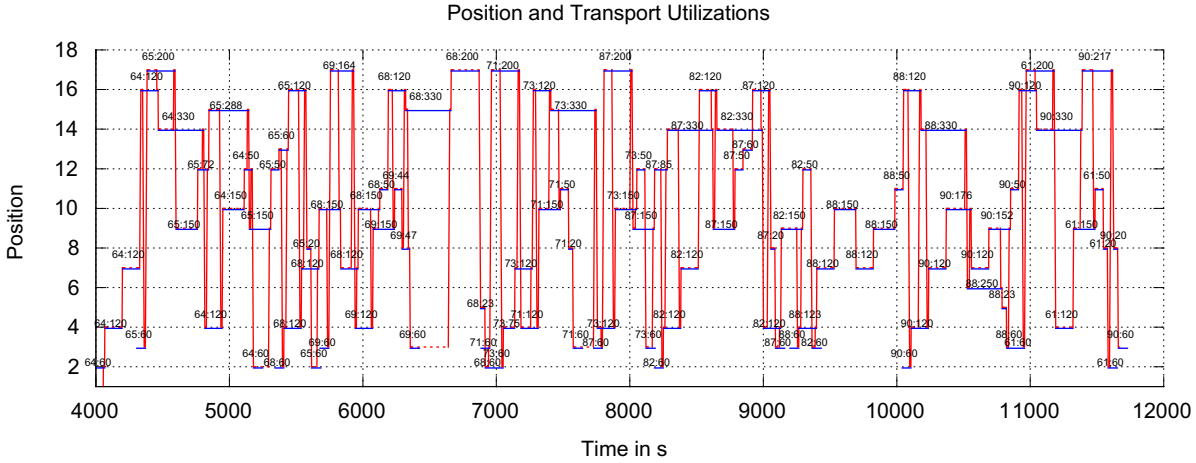

Figure 1. Optimized schedule describing the position (blue) and transport utilizations (red). Eleven carriers are processed. Labels indicate for each position utilization the ID of the carrier and the process time determined by the scheduler (id:time).

DISCUSION AND CONCLUSIONS

Our example result is correct with respect to all existing constraints. The makespan for processing the eleven carriers is acceptably small. However, some time intervals with sparse transport activity and low parallel processing could indicate the possibility for improving the makespan. This might be achieved by increasing the computational effort and by adapting the multi-level optimization strategy. The low computation time results from the small problem size and a minor intricacy.

The deterministic decision rules enable the efficient computation of conflict-free results. However, these rules introduce a solution bias and limit the range of possible solutions that can be generated by the scheduler. Therefore, an adequate and correct definition of the decision rules is vitally important. While the validation of the solution correctness is easy, the evaluation of the optimality is fundamentally difficult, because of the high number of constraints, the NP-hardness, and the multi-objective nature of the optimization problem. Besides the minimal makespan and optimal process times, further objectives, such as the uniform utilization of available positions or the reduction of environmental pollution, may have to be considered in practice, too.

ACKNOWLEDGEMENTS

We thank B. Henfling, H. Fuchs, S. Tellhelm and F. Thron from the ICOM Automation GmbH, Ilmenau, for the discussions of practical requirements and restrictions. This work was supported by the German Federal Ministry for Economic Affairs and Energy (KF2250108WD1).

REFERENCES

[1] R. Ruiz and J.A. Vázquez-Rodríguez. The hybrid flow shop scheduling problem. European Journal of Operational Research, vol. 205, 2010, pp. 1-18.

[2] M.R. Garey and D.S. Johnson. *Computers and Intractability: A Guide to the Theory of NP-Completeness*. W.H. Freeman and Company, New York, 1979, ch. A5.3.

13th International Workshop on Optimization and Inverse Problems in Electromagnetism
September 10 – 12, 2014, Delft, The Netherlands

A SPLINE-BASED SHAPE DERIVATIVE APPROACH FOR THE NONLINEAR MAGNETOSTATIC INTERFACE PROBLEM

Ulrich Römer*, Sebastian Schöps** and Thomas Weiland*

*Technische Universitaet Darmstadt, Institut fuer Theorie Elektromagnetischer Felder, Schloßgartenstr. 8, Darmstadt, D-64289, E-Mail: roemer@temf.tu-darmstadt.de, thomas.weiland@temf.tu-darmstadt.de

**Technische Universitaet Darmstadt, Graduate School of Computational Engineering, Dolivostr. 15, Darmstadt, D-64293, Germany, E-Mail: schoeps@gsc.tu-darmstadt.de

Abstract. This work treats the shape sensitivity analysis of nonlinear magnetostatic interface problems. Based on both well-established and recent results in shape calculus, shape derivatives of fields and quantities of interest will be derived. Numerical results for shape derivatives and applications to magnet design based on a spline representation of geometries, as provided by the isogeometric finite element approach will be given.

Keywords: isogeometric analysis, magnetostatics, shape calculus, velocity method.

INTRODUCTION

Shape sensitivity analysis is a key tool in computational electromagnetics for shape optimization, inverse problems and uncertainty propagation. Unfortunately several difficulties are associated with its realization, most notably the computation of shape derivatives on a continuous level, which is at the core of shape calculus (or continuum sensitivity analysis). Recently, shape calculus has been embedded in a differential form setting [1]. This approach is not only well suited for electromagnetics but also typically simplifies manipulations. Based on these results, as well as shape sensitivity techniques for interface problems [2], this work aims at further simplifying its application to electromagnetics. Thereby, already established results, e.g. [3], will be accompanied by a more detailed treatment of shape derivatives of fields and a rather general, spline-based, shape parameterization. This is appealing for higher order shape calculus and applications to shape optimization as irregular optimal designs can be controlled efficiently. We also note that shape derivatives for the present setting have been rigorously studied in the two-dimensional case in [4].

SETUP AND VELOCITY METHOD

The principal setup is depicted in Figure 1. We consider a ferromagnetic material D^+ within a computational domain D, where the interface will be subject to a deformation. Typically this reflects the situation where iron parts are surrounded by air and coils excite magnetic fields. In an inverse problem setting D^+ represents an object with unknown shape, to be reconstructed, whereas in the context of uncertainty propagation the shape deformations could model manufacturing imperfections.

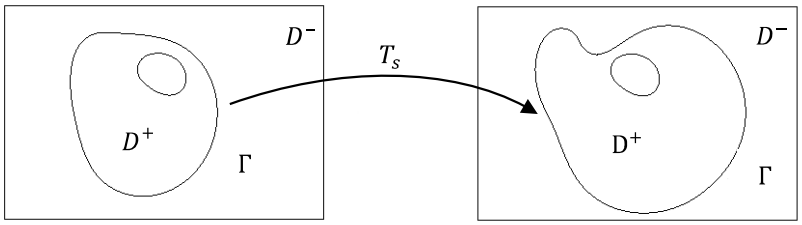

Figure 1. Initial and transformed domain by means of a transformation (1).

A well-established technique to model shape perturbations is given by the velocity method [5]. In this setting, a transformation $T_s(\mathbf{X}) = \mathbf{x}_s(\mathbf{X})$ is defined by the differential equation

(1a) $\frac{d}{ds}\mathbf{x}_s(\mathbf{X}) = \mathbf{V}(\mathbf{X}),\ s \geq 0$

(1b) $\mathbf{x}_0(\mathbf{X}) = \mathbf{X}$

where $\mathbf{V}$ is assumed to be a sufficiently smooth velocity field, satisfying $\mathbf{V}|_{\partial D} = 0$. We then write $D_s^+ := T_s(\mathrm{D}^+)$ for the family of transformed domains. In this rather general framework, derivatives can be defined with respect to the velocity field. To be used within numerical simulations the transformation (1) needs to be parameterized appropriately. We will illustrate how this can be achieved very conveniently in the context of spline representations of the geometry.

SHAPE DERIVATIVES

For a vector field $\mathbf{u}$, we denote with $\mathbf{u}^{\mp}$its restriction to $D^{\mp}$, with outer unit normal $\mathbf{n}^{\mp}$, and with $[\![\mathbf{u}]\!] = \mathbf{u}^{+} \times \mathbf{n}^{+} + \mathbf{u}^{-} \times \mathbf{n}^{-}$ the jump in the tangential component on Γ, respectively. We are concerned with the (un-gauged) nonlinear magnetostatic problem with parametric interface, i.e., the vector potential $\mathbf{A}_s$ is subject to

(2a) $\quad \mathbf{curl}\, \upsilon(\cdot, |\mathbf{curl}\, \mathbf{A}_s|)\, \mathbf{curl}\, \mathbf{A}_s = \mathbf{J}, \;\; \text{in } {D_s}^{+} \cup {D_S}^{-},$

(2b) $\quad [\![\mathbf{A}_s]\!] = 0, \;\; \text{on } \Gamma_s,$

(2c) $\quad [\![\upsilon \mathbf{curl} \mathbf{A}_s]\!] = 0, \;\; \text{on } \Gamma_s,$

(2d) $\quad \mathbf{A}_s \times \mathbf{n} = 0, \;\; \text{on } \partial D.$

The aim of shape calculus is the computation of derivatives of a quantity of interest

(3) $\quad Q_s = \int_{D_{\text{obs}}} f(\mathbf{A}_s, \mathbf{curl}\, \mathbf{A}_s)\, \mathrm{d}\mathbf{x},$

with respect to s, where $D_{\text{obs}} \subset D^{-}$. On a surface (Γ) both a vectorial curl, $\mathbf{curl}_{\Gamma}\, u = \text{grad}\, u \times \mathbf{n}$ and a scalar curl, $\text{curl}_{\Gamma}\, \mathbf{u} = \mathbf{curl}\, \mathbf{u} \cdot \mathbf{n}$ can be defined. Then the shape derivative $\delta\mathbf{A}$ can be characterized as

(4a) $\quad \mathbf{curl}\, \boldsymbol{\upsilon}_{\mathrm{d}} \mathbf{curl}\, \delta\mathbf{A} = 0, \;\; \text{in } D^{+} \cup D^{-},$

(4b) $\quad [\![\delta\mathbf{A}]\!] = V_n [\![\partial_n \mathbf{A}]\!], \;\; \text{on } \Gamma,$

(4c) $\quad [\![\upsilon \mathbf{curl} \delta\mathbf{A}]\!] = \mathbf{curl}_{\Gamma}(V_n(\upsilon^{+} - \upsilon^{-})\text{curl}_{\Gamma}\mathbf{A}), \;\; \text{on } \Gamma,$

(4d) $\quad \delta\mathbf{A} \times \mathbf{n} = 0, \;\; \text{on } \partial D,$

where $\boldsymbol{\upsilon}_{\mathrm{d}}$ is the differential reluctivity and V_n refers to the component in the direction of $\mathbf{n}$. We observe that the tangential component of the shape derivative may exhibit jumps on the moving interface. However, it has been shown, e.g., in [2] that for problems of this type optimally convergent finite element schemes can be constructed. Solving (3) directly is appealing when multiple quantities of interest are studied and in the context of uncertainty propagation when low-rank approximations of stochastic shape representations are available. Alternatively, following an adjoint approach, the gradient is expressed as

(5) $\quad \delta Q = \int_{\Gamma} V_n(\upsilon^{+} - \upsilon^{-})\text{curl}_{\Gamma}\mathbf{A}\, \text{curl}_{\Gamma}\mathbf{P}\, \mathrm{d}\mathbf{x},$

where $\mathbf{P}$ refers to the adjoint solution associated to (2,3). In this work, details of the derivation of (3,4) based on [1,2] and the structure theorem [5] will be given.

NUMERICAL REALIZATION, SPLINE FINITE ELEMENTS

Numerical computations demand for a parameterization of the mapping (1) additionally to the numerical solution of the state, resp. adjoint problem. This can be achieved, e.g., in the iso-parametric finite element context by perturbing the coefficients of the shape functions associated to the geometry representation. Here, we adapt the extension to spline geometry representations, offered in the context of isogeometric analysis [5,6]. In this case, the shapes of the computational domain are represented by means of B-splines or NURBS, offering several benefits. Among others, these are enhanced geometric representation capabilities and the control of the shape's smoothness. Therefore, irregular optimal designs can be avoided. Finally, the shape sensitivity framework is readily embedded into the spline framework. Indeed as $\boldsymbol{D}_s^{+}$ is given by

(6) $\quad \mathbf{F}(\mathbf{X}) = \sum_{ijk} B_{ijk}(\mathbf{X})\mathbf{C}_{ijk}(\mathrm{s})$

with tensor product splines B_{ijk} and control points $\mathbf{C}_{ijk}$, a deformed domain is obtained by simply perturbing the control points with $\mathrm{s}\boldsymbol{\delta}_{ijk}, |\boldsymbol{\delta}_{ijk}| \leq 1$. This yields a velocity field $\mathbf{V}(\mathbf{X}) = \sum_{ijk} B_{ijk}(\mathbf{X})\boldsymbol{\delta}_{ijk}$. We will discuss this modeling step in detail, give numerical results for the shape derivative approach and show applications to shape optimization. Emphasis will be put on applications from magnet design.

REFERENCES

[1] R. Hiptmair, and J. Li, Shape derivatives in differential forms I: an intrinsic perspective, Annali di Matematica Pura ed Applicata, vol. 192, 2013, pp. 1077-1098.

[2] H. Harbrecht, and J. Li, First order second moment analysis for stochastic interface problems based on low-rank approximation, ESAIM: Mathematical Modelling and Numerical Analysis, vol. 47, 2013, pp. 1533–1552.

[3] Il-han Park, J. L. Coulomb, and Song-yop Hahn, Design sensitivity analysis for nonlinear magnetostatic problems by continuum approach, JOURNAL DE PHYSIQUE III, 1992, pp. 2045-2053.

[4] I. Cimrák, Material and shape derivative method for quasi-linear elliptic systems with applications in inverse electromagnetic interface problems, SIAM Journal on Numerical Analysis, vol. 50, 2012, pp. 1086-1110.

[5] M. C. Delfour, and J.-P. Zolésio, *Shapes and geometries: metrics, analysis, differential calculus, and optimization*, Vol. 22, SIAM, 2011.

[6] T. JR Hughes, J. A. Cottrell, and Y. Bazilevs, Isogeometric analysis: CAD, finite elements, NURBS, exact geometry and mesh refinement, Computer methods in applied mechanics and engineering, vol. 194, 2005, pp. 4135-4195.

[7] A. Buffa, J. Rivas, G. Sangalli, and R. Vázquez, Isogeometric discrete differential forms in three dimensions, SIAM Journal on Numerical Analysis, 2011, vol. 49, pp. 818-844.

13th International Workshop on Optimization and Inverse Problems in Electromagnetism
September 10 – 12, 2014, Delft, The Netherlands

ON THE EXTENDED FINITE ELEMENT METHOD USE IN OPTIMISATION OF ELECTRICAL DEVICES

Alexandru AVRAM*, Vasile ȚOPA, Marius PURCAR and Călin MUNTEANU

* Technical University of Cluj-Napoca, Faculty of Electrical Engineering, Cluj-Napoca, 400027 Cluj, Romania
E-mail: alex.avram@ethm.utcluj.ro

Abstract. This paper describes an innovative numerical algorithm specially tailored for optimization of the electrical devices. The proposed numerical algorithm consists in coupling the eXtended Finite Element Method (XFEM) and a stochastic algorithm type in order to handle moving material interfaces in electrical applications. On the one hand, the algorithm proposed benefits from the mesh free approach using XFEM to prevent from mesh distortion situations. On the other hand, the optimization loop based on a stochastic algorithm type is used for generate optimum solutions. The innovation of proposed algorithm consists in applying a mix integration technique in the XFEM numerical scheme in order to reduce computational time. The main value of the proposed approach is a fast, powerful and robust optimization algorithm used in handling topological changes with a high degree of automation in comparison with other methods.

Keywords: Electric structures, Extended finite element method, Moving interfaces, Optimization.

INTRODUCTION

The optimization of electric devices is a very topical issue since trying to obtain more devices producing high performance at minimal costs, timeliness certified by increasing number of contributions in the field in recent years [3, 4]. The computation of the optimal design of these devices is accomplished by inverse problem methodology where series of direct problems are solved. An optimization loop based on inverse problem algorithm usually has two modules that alternate in order to obtain optimum result. The first one is the analysis module and its task is to solve the field equation problem for the submitted device and to provide the relevant parameters to second one which is the optimization module, as shown in Figure 1.When it comes to modeling applications with moving material interfaces, using an optimization scheme based on a stochastic algorithm type, e.g. Genetic Algorithm (GA) then a new geometry is obtained after each optimization step. If the analysis module uses a standard Finite Element (FE) mesh, then a large number of mesh adaptations, or even re-meshes, are required and mesh distortion may occur. Therefore, modeling complex geometries with moving interfaces is a bit difficult and time consuming with standard Finite Element Method (FEM) as the finite element mesh was required to be aligned with the domain boundaries. In order to circumvent the technical difficulties of the moving interface problems, one can use methods which are mesh independent. One of the most common mesh free methods described in the scientific literature is the eXtended Finite Element method (XFEM) specially tailored to simulate problems involving moving interfaces.

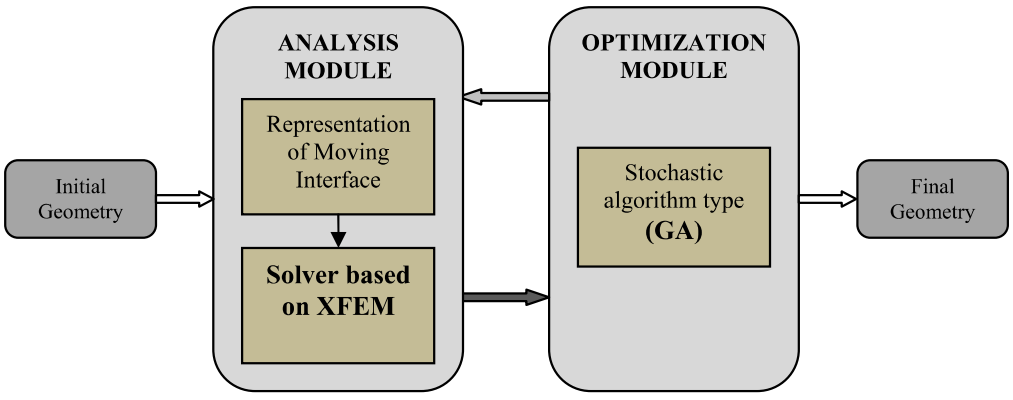

Figure 1. Optimization loop.

This approach offers a very elegant and efficient way of solving the optimal design problem, because the numerical analysis step is done on a single and fixed mesh generated at the beginning of the optimization process. This mesh remains unchanged in size and connectivity throughout the entire optimization process, while the material interfaces are changing their shapes and/or positions within computational domain.

NUMERICAL ASPECTS OF XFEM

Extended finite element method developed by Belytschko and Black [1], is able to incorporate the discontinuous field property into the approximation space within the framework of finite elements. Interfaces can be modeled within an element domain, by a local enrichment as described by the XFEM approximation formulation. The resulting enriched space is then capable of capturing the non-smooth solutions with optimal convergence rate. This becomes possible due to the notion of partition of unity as identified by Melenk and Babuska in [5] and Duarte and Oden in [2].The enriched basis is formed by the combination of the nodal shape functions associated with the mesh and the product of nodal shape functions with discontinuous functions. This construction allows modeling of geometries that are independent of the mesh. Additionally the enrichment is added only locally i.e. where the domain is required to be enriched. The resulting algebraic system of equations consists of two types of unknowns, i.e. classical degrees of freedom and enriched degrees of freedom. Therefore, in XFEM framework two type of mesh elements are used: standard FE elements (uncut elements) and XFEM elements (elements cutted by material interface). The innovation of proposed algorithm consists in applying a mix integration technique in the XFEM numerical scheme in order to reduce computational time. Depending on the type of mesh element used, two ways integration are presented: the first method uses integration by natural coordinates of the element, and the second method uses Gaussian quadrature techniques.

APPLICATIONS AND RESULTS

This section presents the results obtained for the proper optimization an electrochemical application with moving material interface. The example depicted by Figure 2 is found in industry, and represents a 3D application intended to optimize the current density distribution in the manufacturing process of integrated circuits. Within this application, the position of a mobile insulating screen inside a 3D electrochemical reactor to optimize the current density on the cathode surface (2) is intended.

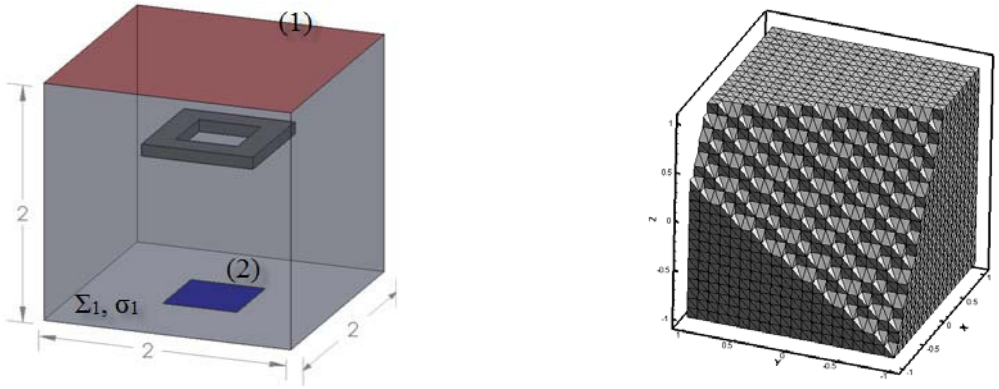

Figure 2. Electrochemical reactor configuration (left) and mesh plot (right): with anode (red), cathode (blue) and moving insulating shield (grey);.

CONCLUSIONS

This paper proposed a generally applicable numerical algorithm for the optimization of moving material interfaces in electric applications. The mathematical model used for optimization consisted in two coupled problems, a field problem and an optimization one. The stochastic type algorithm provides the optimal shape/position of the moving interface. XFEM solves the multiple domains problem governed by a field equation, for every new position of interface. XFEM has the strong feature that it does not need re-meshing of the computational domain after the changing of the interface position. Hence the computational time is highly reduced allowing a higher number of individuals generation if required.

REFERENCES

[1] Belytschko, T. and Black, T., “Elastic crack growth in finite elements with minimal remeshing,” International Journal for Numerical Methods in Engineering, vol. 45 (5), pp. 601-620, 1999.

[2] Duarte, C. A. M. and Oden, J. T., “An hp adaptive method using clouds,” Computer Methods in Applied Mechanics and Engineering, vol. 139, pp. 237-262, 1996.

[3] Ishikawa, T., Tsukui, Y., Matsunami, M., “Optimisation of electromagnetic devices using artificial neural network with quasi-Newton algorithm”, IEEE Transactions on Magnetics, vol. 32, pp.1226-1229, mai 1996.

[4] Koh, Chang-Seop, Hahn, Song-Yop, Chung, Tae-Kyung, Jung, Hyun-Kyo, “A sensitivity analysis using boundary element method for shape optimization of electromagnetic devices”, IEEE Transactions on Magnetics, vol.28, pp.1577-1580, martie 1992.Hoole, S.R.H., Subramaniam, S., Kanaganathan, S., “Two requisite tools in the optimal design of electromagnetic devices”, IEEE Transactions on Magnetics, vol.27, pp.4105-4109, septembrie 1991.

Adaptive Finite Element Method Solution of the Lossless One-Dimensional Westervelt Equation

B. Dirkse[†], D. Lahaye[*] and M. Verweij[**]

[†]Bachelor student Applied Physics & Applied Mathematics, TU Delft.
b.dirkse@student.tudelft.nl

[*]Delft Institute of Applied Mathematics - Faculty of Electrical Engineering, Mathematics and Computer Science
TU Delft, Mekelweg 4, 2628 CD Delft, The Netherlands phone: +31.15.27.87.257 d.j.p.lahaye@tudelft.nl

[**]Department of Imaging Physics - Faculty of Applied Sciences
TU Delft, Lorentzweg 1, 2628 CJ Delft, The Netherlands phone: +31.15.27.81.761 m.d.verweij@tudelft.nl

Abstract. Simulating nonlinear acoustic wave propagation is a problem that arises in medical ultrasound imaging and therapy. The Westervelt equation is the simplest wave equation describing this phenomenon. There are several numerical methods currently in use to solve this equation, but all experience numerical difficulties when the nonlinear propagation leads to shock wave formation. In this work we establish that the Finite Element Method (FEM) is a suitable technique for solving the Westervelt equation. FEM offers a wide variety of adaptive grid techniques, which may be a useful tool in reducing the numerical error caused by the shock wave fronts. In this study we use the a priori knowledge of the wave location to locally refine the grid. Furthermore we investigate an implementation of automated grid refinement, which is calculated simultaneously with the solution.

I Introduction

The accurate simulation of nonlinear acoustic wave propagation has applications in fields such as medical ultrasound imaging and therapy. During the design of ultrasound imaging systems engineers often want to simulate the generated ultrasound field in order to optimize different design parameters [3]. In therapeutic applications it is critical to accurately simulate the nonlinear wave propagation inside the patient to assess, for example, the required dose or potential side effects of each particular treatment.

In this work we use the Westervelt equation to model nonlinear acoustic wave propagation. The nonlinear behavior causes a propagating wave to form a shock wave front, i.e., a point where the derivative of the waveform becomes infinitely large. This occurs after the wave has traveled a certain distance from the source. When solving the wave propagation numerically, these shock wave fronts usually contribute significantly to the error of the numerical estimation. Every numerical method in existence experiences numerical difficulties when the shock wave fronts occur. We will use the Finite Element Method (FEM) to solve the Westervelt equation numerically. Research on solving the Westervelt equation using FEM is valuable since FEM is a powerful method for solving nonlinear problems on complicated and inhomogeneous domains encountered throughout physics and engineering. Our research focuses on the use of adaptive FEM to increase the accuracy of the solution, especially near the shock wave fronts, and possibly reduce computation time.

II Model equations for nonlinear wave propagation

The simplest wave equation for nonlinear wave propagation is the Westervelt equation. Neglecting attenuation due to absorption and scattering, and restricting to one spatial dimension, it is given by

$$\frac{\partial^2 p}{\partial x^2} - \frac{1}{c_0^2}\frac{\partial^2 p}{\partial t^2} = -\frac{\beta}{\rho_0 c_0^4}\frac{\partial^2 p^2}{\partial t^2}, \tag{1}$$

where $p(x,t)$ is the acoustic pressure field as a function of the position x and time t, c_0 is the small signal sound propagation speed, ρ_0 is the ambient density of mass and β is the coefficient of nonlinearity [1]. The latter three quantities are properties of the propagation medium. In case of inhomogeneous media, these quantities may also depend on position. Our goal is to accurately solve this equation using FEM and exploit adaptive methods developed for FEM. We do this for several case studies.

Equation (1) can reduced to the Burgers equation by assuming one preferred direction of propagation and transformation of the time coordinate [1]. This reduction can only be done in one dimension. Burgers Equation is a valuable model since it has a known implicit solution, which can in principle be solved numerically to arbitrary precision. This solution can be used as a benchmark solution for our research.

III FEM formulation of the Westervelt equation

Before we can cast (1) into a FEM formulation, we have to slightly modify the right-hand-side by using $\frac{\partial^2 p^2}{\partial t^2} = 2(\frac{\partial p}{\partial t})^2 + 2p\frac{\partial^2 p}{\partial t^2}$, in order to obtain more convenient discretization matrices for the nonlinear component of the equation. We will divide the domain x into n discrete elements and let $\mathbf{u}(t)$ represent $p(x,t)$ on the nodes of these elements. We can now state the FEM formulation of (1) as

$$\mathbf{K}\mathbf{u} + \mathbf{M}\ddot{\mathbf{u}} = \mathbf{N_1}(\dot{\mathbf{u}})\dot{\mathbf{u}} + \mathbf{N_2}(\mathbf{u})\ddot{\mathbf{u}} + \mathbf{g}, \tag{2}$$

where $\mathbf{K}$ is the stiffness matrix, $\mathbf{M}$ is the mass matrix, $\mathbf{N_1}$ and $\mathbf{N_2}$ are the nonlinear discretization matrices, and $\mathbf{g}$ is a vector containing the boundary conditions. A dot represents a time derivative. Note that $\mathbf{N_1}$ and $\mathbf{N_2}$ depend on $\mathbf{u}$ or its time derivative, making this a nonlinear system of equations. The size m of this system depends on the number of elements n, the order of the basis functions used to represent $\mathbf{u}$ and the type of boundary conditions given. Once those parameters are fixed, $\mathbf{K}$ and $\mathbf{M}$ are constant. This system of equations can be solved using standard techniques, such as finite difference methods. Since the equation is nonlinear, an approximation must be used to solve $\mathbf{u}$ at a certain time t_k, given previous time points $\{\mathbf{u}(t_{k-1}), ..., \mathbf{u}(t_0)\}$. A commonly used method is a Newton-Raphson method. However when small time steps are taken, the easier to implement fixed-point iteration method may converge fast enough. This may be the case when a high frequency wave is modeled.

IV Adaptive FEM techniques

In general, a finer mesh (larger number of elements n) increases the accuracy of the solution at the cost of computation time. In transient problems, this cost in computation time can be significant. The largest error is made around the shock wave fronts, which occur only locally in the domain. Therefore we seek a method to refine the mesh locally, based on some indicator that refinement is needed. Local refinement can be obtained in two distinct manners. The first way is by splitting elements into smaller ones and thus introducing extra nodes (h-refinement). The second way is by moving the existing nodes towards the area of local refinement, therefore adjusting all element sizes but keeping the number elements and nodes constant (r-refinement). Since the spatial derivative becomes extremely large at a shock wave front, the magnitude of the derivative seems to be a good indicator to determine where to refine the mesh. In [2], r-adaptivity algorithms are developed based on this indicator. In all of these algorithms the overall goal is to determine the optimal mesh distribution as function of time. The optimal mesh in this sense is the mesh that equally distributes a certain monitor function, which is a function that 'measures' the magnitude of the derivative. Let Ω_C be the computational domain, for example the closed interval $[1, m]$, which is continuous for now. Let Ω_P be the physical domain, for example the real space interval $[0, L]$ and Ω_T be the time domain, from $[0, T]$. We already introduced $x \in \Omega_P$ and $t \in \Omega_T$ as our physical space and time variables. Let $\xi \in \Omega_C$ denote our spatial computational variable. We seek a function $x(\xi, t) : \ \Omega_C \times \Omega_T \mapsto \Omega_P$, that equally distributes a chosen monitor function and thus represents our optimal mesh. One such map is defined by the equation

$$\epsilon\Big(1 - \gamma\frac{\partial^2}{\partial\xi^2}\Big)\frac{\partial x}{\partial t} = \frac{\partial}{\partial\xi}\Big(M\frac{\partial x}{\partial\xi}\Big), \qquad M = \sqrt{1 + \Big|\frac{\partial u}{\partial x}\Big|^2}, \tag{3}$$

where ϵ and γ are numerical parameters and M is the monitor function. This method is known as MMPDE-6 and has been demonstrated to numerically solve Burgers equation [2], therefore we try to apply it to the Westervelt equation. Discretization of the computational domain, typically of the form $\{1, 2, ..., m\}$, induces a discretization of the real space in x. The derivatives $\frac{\partial x}{\partial\xi}$ and $\frac{\partial^2 x}{\partial\xi^2}$ can be approximated by a finite difference method. The obtained semi-discrete system of (3) can be solved in real physical time simultaneously with (2), resulting is a strongly coupled and stiff system. We encountered several problems when we implemented this algorithm for the Westervelt equation. One of these is that nodes are allowed to move arbitrarily close to each other which causes the time solver to take extremely small time steps in time, in order to maintain certain tolerances. Effectively no progress is time can be made and the algorithm gets stuck. This occurred for both explicit and implicit time solvers. Secondly, we found that moving nodes to fast can cause instability to the system, causing the solution to diverge. We can control the speed of the node movement via the parameter ϵ or the choice of M. A slower movement speed keeps the system stable, but reduces the ability of the algorithm to refine the mesh accordingly.

References

[1] D. T. Blackstock and C. L. Morfrey, Model Equations. In M. F. Hamilton and D. T. Blackstock (eds.) *Nonlinear Acoustics*, p. 41–63. Academic Press, 1998.

[2] C. J. Budd, H. Weizhang and R. Russel. Adaptivity with moving grids. In A. Iserles (eds.) *Acta Numerica, vol. 18*, p. 1–131. Cambridge University Press, 2009.

[3] A. Karamalis, W. Wolfgang and N. Navab, Fast Ultrasound Image Simulation Using the Westervelt Equation. In T. Jiang, N. Navab et al. (eds.) *MICCIA 2010, Part I*, p. 243–250. Springer, 2010.

MONO AND BI LEVEL OPTIMIZATION ARCHITECTURE COMPARISON FOR ELECTRIC VEHICLE POWERTRAIN DESIGN

Pierre CAILLARD*, Frederic GILLON*, Michel HECQUET*, Sid-Ali RANDI**, Noelle JANIAUD**

* ECLille, L2EP, CS 20048 Villeneuve d'Ascq, France, pierre.caillard@ec-lille.fr
** RENAULT, Technocentre, 78288 Guyancourt, France

Abstract. In this paper, an optimization process is used to design an electric vehicle powertrain, including driving cycle and performance constraints. The integration of the machine control is detailed through two optimization architectures: a mono-level formulation where the control variables are added to the design variables and a bi-level method where the control is determined with a nested optimization loop for each operating points. The choice between structures is discussed and the computational time is analyzed in relation with specifications.

Keywords: bi-level optimization, design optimization, electric vehicle, powertrain,

INTRODUCTION

The development of future vehicle concepts deals with the challenge to identify optimized powertrains adapted for each vehicle specifications, to improve range and costs. Instead of sizing charts to design a powertrain, optimization algorithm can be used to explore more possibilities [1]. The formulation of the objective and constraints for the optimization process can lead to several possibilities, resulting in very different computational times and convergence qualities [2][3]. In this paper, the powertrain optimization architecture will be discussed, with two objectives, range on a driving cycle and costs. To deal with the machine control, a mono and a bi level structure where the control is in a nested loop will be studied.

SYSTEM MODEL

An electric vehicle powertrain composed of a battery pack, an inverter, an electric machine and a single gear transmission is modeled to estimate the vehicle range over a driving cycle. This is done by sampling those driving cycles into one second time steps operating points. This static behavior is proven to give enough accuracy for energy estimation [4]. This paper describes the optimization architecture but doesn't detail the full content of the models, just an overview is given to understand clearly the optimization problems. The models calculate the losses for each component, with a specific attention on the electric machine model which is an equivalent circuit of a squirreled cage induction machine. A control (stator frequency f and electromagnetic force E) is needed to calculate a given operating point [5]. The system model has been validated with tests: the obtained ranges on some driving cycles have been compared to test results on a study case (Renault Twizy). A cost model is added to build the bi-objective optimization.

OPTIMIZATION ARCHITECTURES

For the case study, it is not necessary to simulate a whole driving cycle to optimize the design but a few representative operating points (driving points *dp*) are sufficient [6]. A first comparison is done with *dp*=2. In addition to the driving cycle that is used for range calculation, performance constraints are added. Three of them (performance points *pp*=3) have been selected for this work, each one is represented by an operating point: climbing a slope at very low speed, maximum vehicle speed, and mid-speed fastest acceleration. Each operating point has to respect 4 constraints: machine current density J_{max} and voltage Um_{max}, inverter current Im_{max} and battery cell currents Ib_{max}. To maximize the range, the machine control should minimize the whole powertrain losses. A nested optimization can be used for this minimization, resulting in the bi-level architecture [7] (fig 1. left). This initial problem can be transformed into a mono level formulation (fig 1. right) by adding the control variables to the design variables (x) since maximizing the range will necessarily give the control that minimizes the whole losses. A similar bi or mono level structures can be obtained for the constraints by calculating the maximum torque T and will be detailed in the full paper.

Bi level

$$\min_{x} \quad \left(-range\left(x, \min_{f_i} losses(x, f_i)\right), cost(x)\right)$$

$$\text{s.t.} \quad \left[T_{required\,i}\right](x) - \left[\max_{f_i} T(x, f_i, E_i)\right] \leq 0$$

$$i = [1, \dots pp]$$

Mono level

$$\min_{x, f_i} \quad \left(-range(x, f_i), cost(x)\right)$$

$$\text{s.t.} \quad \left[J_i \quad Um_i \quad Im_i \quad Ib_i\right](f_i) - \left[J \quad Um(f_i) \quad Im \quad Ib\right]_{max} \leq 0$$

$$i = [1, \dots dp + pp]$$

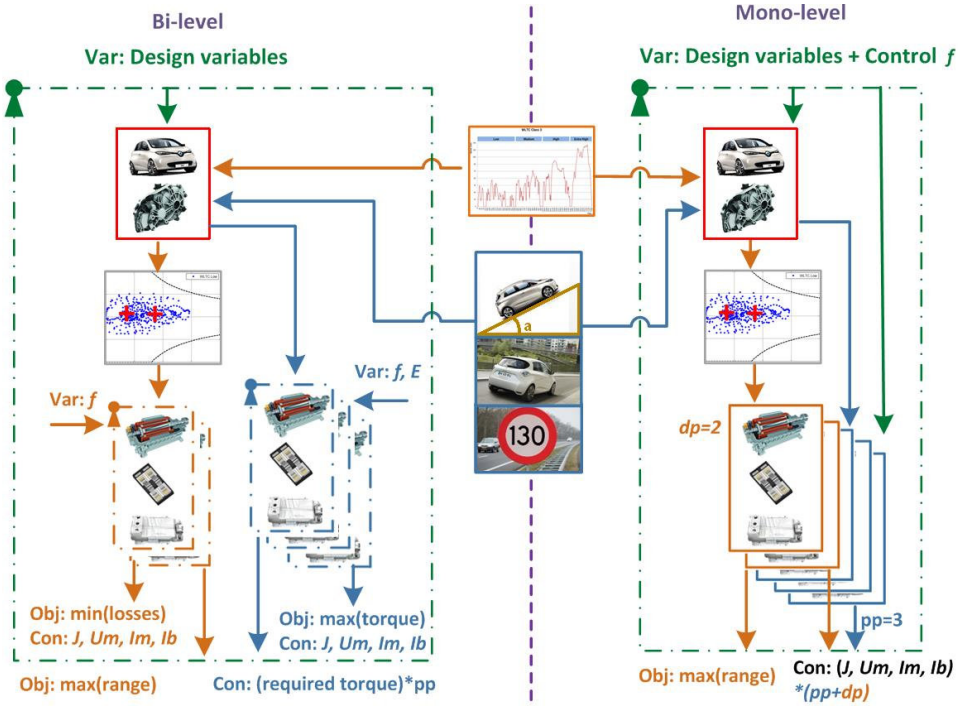

Figure 1. Bi and mono-level optimization architectures

For the study case, 10 electric machine variables have been selected: machine length, slots heights and widths (4), yoke thicknesses (2), number of turns, rotor rings height and width (2). The algorithm for both levels is sequential quadratic programming (SQP) to handle the constraints accurately. The algorithm requires continuous variables so that the number of turns is set continuous. 6 starting points were taken to avoid local optimum for the upper level. One starting point is enough for the lower level, which requires around 20 function evaluations.

Table 1. Computational time comparison

	Number of variables	Average optimization time (s)	Average number of function evaluation	Average time of one function evaluation (s)
Bi-level	10	202	330	0.61
Mono-level	15	17	640	0.027

All 6 starting points converge to the same optimum for both methods. On average, a mono level optimization is 12 times faster than the bi-level formulation despite the increased number of variables, thanks to a much faster model evaluation. Other cases with an increased *dp* and more design variables will be studied in the full paper to analyze the bounds of both optimization architectures.

CONCLUSIONS

Optimization architectures are proposed for designing an electric vehicle powertrain, with two objectives, range and cost, and include driving cycle and performance constraints. The electric machine control which is included as a bi level formulation can be transformed into a mono level architecture, resulting in very different computational time with a significant gain for the mono level on the given example with 10 variables and 5 operating points. Other cases will be studied in the full paper.

REFERENCES

[1] J. Faiz and M. B. B. Sharifian, "Optimum design of a three phase squirrel cage induction motor based on efficiency maximization," *Comput. Electr. Eng.*, vol. 21, no. 5, pp. 367–373, 1995.

[2] S. Cafieri, L. Liberti, F. Messine, and B. Nogare, "Optimal design of electrical machines : mathematical programming formulations," *COMPEL Int. J. Comput. Math. Electr. Electron. Eng.*, vol. 32, no. 3, pp. 977–996, 2013.

[3] A. C. Berbecea, "Approches multi - niveaux pour la conception systémique optimale des chaînes de traction ferroviaire," EC-Lille - USTL, 2012.

[4] T. Letrouvé, A. Bouscayrol, W. Lhomme, N. Dollinger, and F. M. Calvairac, "Different models of a traction drive for An electric vehicle simulation."

[5] P. Caillard, F. Gillon, M. Hecquet, and N. Janiaud, "Influence of machine control strategy on electric vehicle range," in *Ecological Vehicles and Renewable Energies (EVER)*, 2013.

[6] P. Caillard, F. Gillon, M. Hecquet, and N. Janiaud, "Electric machine sizing optimization including control strategy and driving cycle applied to electric vehicle," in *International Symposium on Electromagnetic Fields (ISEF)*, 2013.

[7] L. N. Vicente and P. H. Calamai, "Bilevel and multilevel programming: A bibliography review," *J. Glob. Optim.*, vol. 5, no. 3, pp. 291–306, 1994.

Index